IMPROVING LIQUID CHROMATOGRAPHY PERFORMANCE: NOVEL DEVELOPMENTS IN PRECONCENTRATION, INSTRUMENTATION AND OPTIMIZATION

by

Stephen R. Groskreutz

B.A. Chemistry ACS, Gustavus Adolphus College, 2012

Submitted to the Graduate Faculty of
The Kenneth P. Dietrich School of Arts and Sciences
in partial fulfillment of the requirements for the degree of
Doctor of Philosophy

University of Pittsburgh
2017

UNIVERSITY OF PITTSBURGH

DIETRICH SCHOOL OF ARTS AND SCIENCES

This dissertation was presented

by

Stephen R. Groskreutz

It was defended on

December 13, 2016

and approved by

Adrian C. Michael, Professor, Department of Chemistry

Rena A. S. Robinson, Assistant Professor, Department of Chemistry

Gert Desmet, Professor, Department of Chemical Engineering and Industrial Chemistry,

Vrije Universiteit Brussel, Belgium

Dissertation Advisor: Stephen G. Weber, Professor, Department of Chemistry

IMPROVING LIQUD CHROMATOGRAPHY PERFORMANCE:

NOVEL DEVELOPMENTS IN PRECONCENTRATION,

INSTRUMENTATION AND OPTIMIZATION

Stephen R. Groskreutz, PhD

University of Pittsburgh, 2017

Maximizing performance when using real-world samples and small volume, high sensitivity columns which degrade the native chromatographic separation is a challenge. Loss in column performance is due to precolumn dispersion and volume overload. In this work a series of methods based on novel instrumentation and sound theory is presented to improve a chromatographic result for such samples in both isocratic and gradient elution modes. An approach called temperature-assisted solute focusing (TASF) was developed to improve sample focusing or preconcentration. TASF is designed to address precolumn dispersion in capillary scale LC. Volume overload is a common form of precolumn dispersion and degrades LC performance. TASF works by relying on the temperature dependence of solute retention and high power thermoelectric or Peltier elements (TECs) to actively heat/cool a short segment of the column near its inlet during sample loading. Cooling the head of the column transiently increases retention for solutes during injection, improving focusing and solving the volume overload problem. Following focusing rapid heating decreases retention releasing the compressed injection band to the downstream portion of the column. The TASF approach was assessed using a series of three instruments with well characterized solutes developing it into a robust platform capable of routine, unattended use. Three models for solvent-based on-column focusing in isocratic elution were experimentally

investigated. Solvent-based on-column focusing is a well-known method to increase concentration sensitivity and combat precolumn dispersion by injecting samples made in weak elution solvents. Additionally, solvent-based focusing occurs naturally as a consequence of increased solute retention in the sample solvent and a step gradient generated by the difference between sample and mobile phase composition. Finally, a simple graphical method for rapid chromatographic optimization was developed. This plot was designed specifically to assist practitioners to determine experimental conditions to achieve a desired column efficiency or peak capacity in a defined time in both isocratic and gradient elution modes.

TABLE OF CONTENTS

LIST OF TABLES

LIST OF FIGURES

LIST OF EQUATIONS

PREFACE

First, I must thank my advisor Prof. Stephen Weber. I first met Steve as an undergraduate when he graciously offered me a summer research experience after my junior year. I could not be more thankful for this opportunity. The following year Steve dedicated a significant amount of his time to help me with the graduate application process with no expectation of me returning to him for graduate work. These selfless acts and true generosity of Steve, where he put my interests ahead of his made me want to work with him. Steve is not only a great mentor and researcher, but an even better person. I am thankful every day for the time I have spent working with him and cherish each conversation we had in the hall, break room or standing in the doorway of his office. I will miss these daily conversations. I am lucky to call him a friend. Thank you for a great last five years.

Second, I must acknowledge my first research advisor and the primary reason I am where I am today, Prof. Dwight Stoll of Gustavus Adolphus College. Dwight and I "grew up" together starting at Gustavus at the same time. Just weeks into our first years Dwight took a chance on a naive first year and brought me into his research lab. These experiences sparked my passion for chromatography and working with him changed my career path and ultimately my life. From that point on Dwight has continued to mentor me providing much needed guidance and keeping me grounded. For that I am incredibly grateful. I vividly remember a Skype conversation we had after I finished my graduate classes. The transcript is below:

"I'll tell you the same thing PWC told me ca. 12 years ago.
I asked him what kind of grades were required to 'pass' graduate school.
He said you can get by with B's and even a C here or there,
BUT,

He said, all of the glory goes to the ones on the top of the class.

In hindsight I realize this was incredibly accurate.

And, at the grad school level,

'Glory' is not a pat on the back,

Or recognition at Honors Day,

Glory comes in the form of fame and fortune.

Literally.

It gets you the best papers,

The best post-doc,

The best job,

So, really, there is a lot more incentive than there is at the UG level.

Remember the book,

'Ph.D. is not enough'

You have more freedom now than you will ever have for the rest of your life.

So go get it!"

Dwight Stoll, May 2013

Since, I have had this 'poem' hanging at my desk where I can see it every day and now realize how right Dwight is. It is this kind of advice and true friendship with Dwight I treasure.

I must also acknowledge the support of the Dietrich School of Arts and Sciences Machine and Electronics Shops. Their talent, expertise and patience has been incredibly valuable to make my often crazy ideas a reality. I am also thankful for their willingness to teach me about how these devices are designed, constructed and function. Their efforts have been incredibly valuable to my personal education. A special thanks to Tom Gasmire, Jeff Tomaszewski, Bill Strang, Shawn Artman and Josh Byler in the machine shop and Jim McNerney, Dave Emala and Chuck Fleishaker in the electronics shop.

I would like to recognize the generosity and patience of several external vendors for donating the materials and expertise required to perform my research. Without their support many of these projects just would not exist. First, I would like to thank Andrew Masters at Custom Thermoelectric for providing the necessary expertise regarding Peltier selection and heat sink design for all of our TASF instrumentation. Second, I would like to thank Dr. Ed Bouvier and Dr. Moon Chul Jung from Waters Corporation for providing columns, packing materials and the optical detectors necessary to characterize our instrumentation. I would also like to thank Klaus Witt and Dr. Xiaoli Wang at Agilent Technologies for providing columns, packing materials and valve hardware. In addition, I would like to thank Dr. Dave Bell at Sigma-Aldrich/Supelco for sending countless shipments of columns and stationary phase particles.

Finally, I would like to thank Dr. Kelly Zhang at Genentech, Inc. for the opportunity to conduct a research internship under her guidance. I am very grateful for this opportunity and early exposure to industrial research.

1.0 INTRODUCTION

1.1 LIQUID CHROMATOGRAPHY

Liquid chromatography (LC) is the most commonly used analytical technique where samples composed of mixtures of target solutes are physically separated into their constituent components. The primary advantage to LC comes from its ability to separate, quantify and identify 60-80% of all existing compounds. The near universality of LC makes it a critically important tool for industries from environmental, pharmaceutical and nutritional to forensics, polymers and cosmetics. Column-based LC is the most commonly used type of LC. Modern LC works by introducing a volume of sample much smaller than the volume of the column to the column inlet. Separation of individual components occurs as they pass through the column. Each solute travels down the column with a velocity based on the its partitioning between the moving liquid phase and stationary phase particles that make up the column (the so-called packed bed). At the outlet of the column a detector is placed to "watch" constituents as they exit the column. The signal measured by the detector is called a chromatogram. Chromatograms have axes of time (x-axis) and signal (y-axis). The magnitude of the signal for each constituent or "peak" in the chromatogram is proportional to the amount present. In this work various instrumental and theoretical methods are presented to address several current problems related to column-based LC, all with the goal of increasing its performance.

1.2 METRICS OF CHROMATOGRAPHIC PERFORMANCE

LC performance is characterized by its resolving power or ability to separate individual components of a mixture for each other. The simplest expression to quantify the performance of a

chromatographic separation uses the concept of a theoretical plate from Martin and Synge [1]. Chromatography is fundamentally an equilibration process that can be carried out using a series of "discrete stages"; the efficiency or performance of the column is expressed by the number of theoretical stages or "plates" it contains [2]. More theoretical plates translate to a better separation for the components in a mixture.

Most simply, plate theory states that the efficiency, N, of the separation is a ratio of the column length, L, and the height equivalent to a theoretical plate, H:

$$N = \frac{L}{H} \tag{1.1}$$

where H is equivalent to the spatial variance of the band at the end of the column divided by the column length ($H = \sigma^2/L$). Later, van Deemter et al. developed a method to predict the plate height as a function of mobile phase velocity [3]. In what later became known as the van Deemter equation van Deemter et al. applied the mass balance approach [4, 5] to solving for the chromatographic band width as a function of mobile phase velocity, i.e. the rate at which the fluid passes through the column. The critical conclusion of this work was that the greatest value for N was achieved when operating at a velocity, u_e, such that H is a minimum on the van Deemter curve. This is shown clearly by the form of the van Deemter equation in Eq. 1.2 where the second and third terms both depend on u_e, but with opposing effect. As u_e increases to a maximum H decreases where the B/u_e term dominates, passes through a minimum then increases linearly, Cu_e:

$$H = A + \frac{B}{u_e} + Cu_e \tag{1.2}$$

The A-, B- and C-coefficients of Eq. 1.2 correspond to fitting parameters due to band spreading resulting from eddy dispersion, longitudinal diffusion and resistance to mass transfer, respectively.

Column efficiency is the best metric to evaluate column performance using separation conditions where mobile phase composition and column temperature are held constant throughout the separation. This holds for both isocratic and isothermal separation conditions. Separations may also be performed under changing mobile phase and temperature conditions. Plate theory does not account for the influence changes in column conditions have on a chromatographic band during a run.

The most convenient way to express the resolving power of a separation technique experiencing time varying conditions is peak capacity, n_c. Peak capacity is a theoretical concept developed by Giddings, and defined as the largest number of "peaks" with unit resolution that can be fit into the separation window taken as the time difference between the first and last eluting peak [6]. Eq. 1.3 shows the equation for gradient elution peak capacity [7]:

$$n_c = 1 + \frac{\left(t_{R,2} - t_{R,1}\right)}{W} \tag{1.3}$$

where $t_{R,2}$ and $t_{R,1}$ are the retention times for the first and last eluting solutes in the separation window and W is the average width of the chromatographic bands. W is more-or-less constant throughout gradient elution separation; it can be expressed using Eq. 1.4:

$$W = \frac{4t_0 G\left(1 + k_f\right)}{\sqrt{N}} \tag{1.4}$$

where t_0 is the column void time, N is the isocratic column efficiency (Eq. 1.1), G is a factor related to the gradient conditions and k_f is the retention factor for each solute at elution.

Using Eqs. 1.1-1.4 chromatographic performance can be quantified using the concepts of efficiency, N, and peak capacity, n_c. The goal of this work is to develop methods to adjust chromatographic parameters to maximize N and n_c, under isocratic and gradient elution conditions. Thereby the overall performance of the separation is improved.

1.3 ROLE OF COLUMN DIAMETER IN LC

Chromatographic separation techniques are classified by the scale of the columns used to perform the separation. The majority of the separations are performed using analytical scale columns. Analytical scale columns are defined as those with internal diameters (ID) between 4.6 and 2.1 mm. Figure 1.1 shows the relative column diameters for 4.6 and 2.1 mm ID analytical scale columns and a 100 μm ID capillary column. Each column cross-section is shown as a purple circle. Column volume, V_{col}, and the typical injection volume used with each diameter are also shown. Column length was set at 5 cm for all. Note that injection volume, V_{inj}, for all columns was scaled to represent a value approximately 1% of the column volume, the volume necessary for an efficient separation. Modern sample introduction methods are designed to work best with analytical scale columns and injection volumes from 0.5 to 100 μL. The injection volume required for the 100 μm ID column is only 2.5 nL. Achieving such small injection volumes is not possible with current valve technology.

While sample introduction is a major problem to the use of capillary columns there are a number of important benefits to using capillary columns. These have led to their widespread use in many important biological applications from proteomics [8], metabolomics [9-11], and *in vivo*

neurochemical measurements [12-17]. Chief among them is the improved concentration sensitivity smaller column diameters provide [18]. For a sample with a constant number of moles and column efficiency, capillary scale columns increase detection sensitivity by a factor proportional to the ratio of the column diameter squared. This is a powerful effect. Sensitivity increases are due to the reduction in sample dilution across the column's diameter. Figure 1.1 makes this diameter effect clear. For the column diameters shown, the signal for the 100 μm ID column would be 2100-times that of the 4.6 mm and 440-times the signal for the 2.1 mm ID column. Clearly, the potential for huge increases in detector signal for small, fixed volume samples is the primary reason why capillary scale columns are used in sample limited applications. The sensitivity benefits of capillary columns are exploited throughout this work.

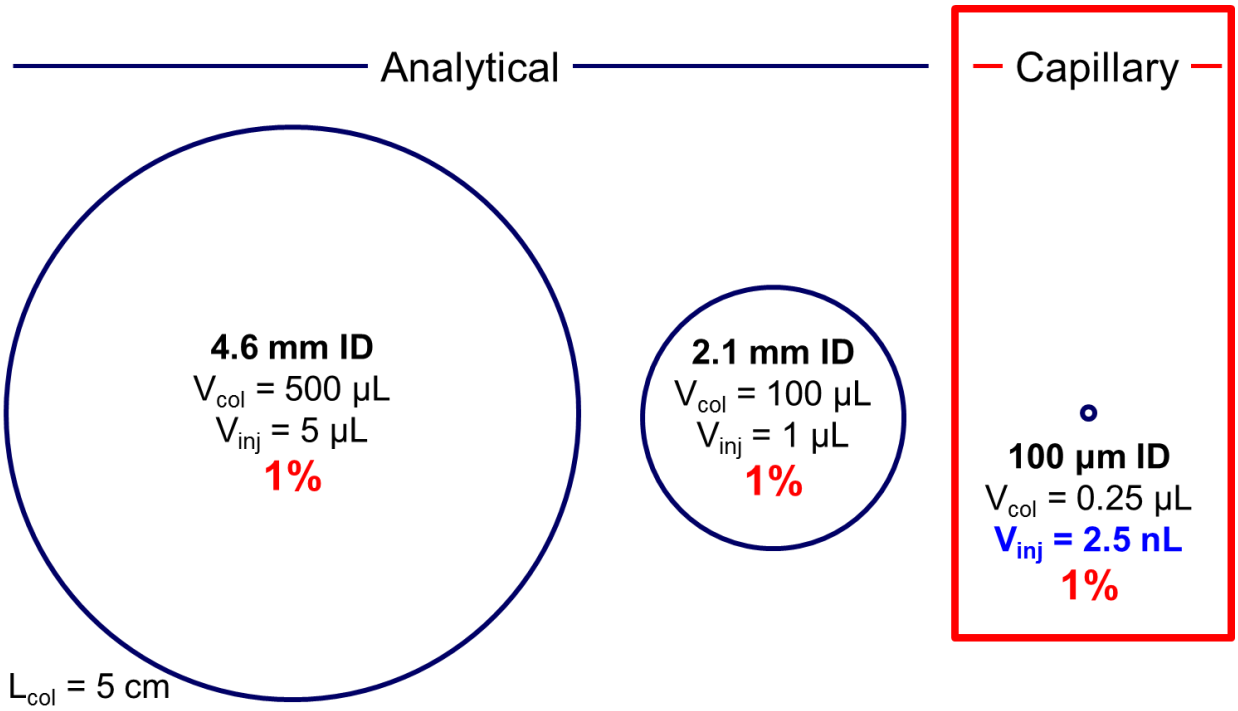

Figure 1.1. Schematic highlighting the commonly used column diameters, column volumes and injection volumes for analytical and capillary scale LC. Circles representing the relative column cross section for each column diameter are drawn to scale. Injection volume required for optimal chromatographic performance is 1% of the column fluid or void volume.

1.4 VOLUME OVERLOAD AND ON-COLUMN FOCUSING

Unfortunately, the sensitivity benefits afforded by small diameter columns is not without cost. The cost is a significant decrease in detector sensitivity, observed efficiency, peak capacity and resolution. This poorer performance occurs when the sample volume is too large for the column and a phenomenon called volume overload. Volume overload is a consequence of the width (volume) of the sample zone injected onto the column contributing significantly to the observed peak shape at the detector [19]. The black trace in Figure 1.2 makes the impact of volume overload on the separation clear for a single component isocratic separation resulting from a 500 nL injection of a lightly retained solute (k' = 5) onto the 100 μm ID column shown in Figure 1.1. The column was operated under conditions to maximize its native efficiency; velocity equals the van Deemter optimum. Obviously, performance was degraded by the large volume injection, so much so that a Gaussian shaped peak is no longer visible. The table-top peak shape for the black trace is characteristic of volume overload. This is an example of unsatisfactory chromatography.

Fortunately, there is a solution to the volume overload problem to allow the use of "larger" samples to enhance sensitivity. The solution is on-column focusing [20, 21]. On-column focusing is a result of generating transient conditions during the injection that result in high retention for sample constituents. The simplest way to induce focusing is to make the sample in a weaker chromatographic solvent than the mobile phase. This is called solvent-based on-column focusing. Solvent-based focusing is achieved by injecting aqueous samples into an organic solvent rich mobile phase (reversed-phase separation). Focusing also happens naturally as a consequence of gradient elution conditions [22]. The blue trace in Figure 1.2 shows the effect of injecting a sample made in a solvent that induced a retention factor corresponding to 200 onto the 100 μm ID column. The sample "focuses" well on the column while the sample solvent acts as the mobile phase. On-

column focusing recovers the native separation performance of the column with the added benefit of significantly improving detector signal. For both signals simulated in Figure 1.2 the signal axis was normalized to that obtained from a 500 nL injection made on a 4.6 mm ID column. While the focused (blue) signal in this simulation does not reach the theoretical sensitivity improvement (2200-fold), on-column focusing was able to increase detection sensitivity by nearly 1600-fold relative to the same injection made on a 4.6 mm ID column. The benefits of on-column focusing have also been shown experimentally quite effective when used with capillary scale columns [23-25].

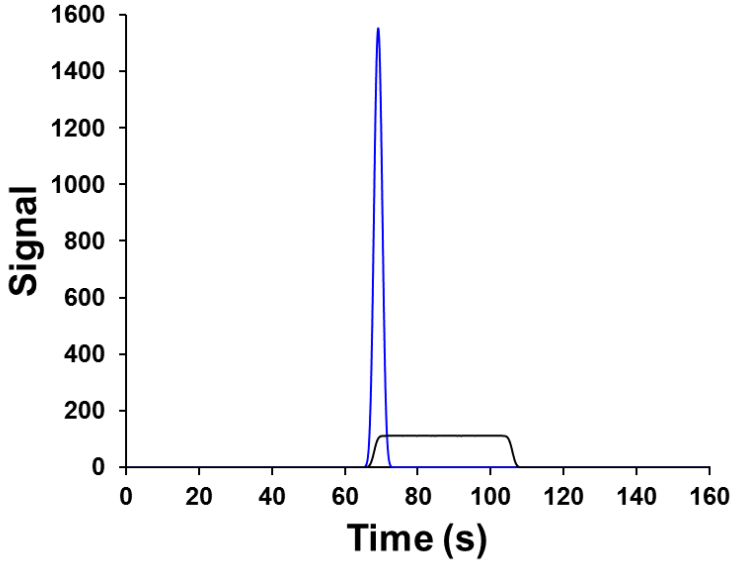

Figure 1.2. Simulated chromatograms for a 500 nL injection of a k' = 5 solute onto a 100 μm ID column. Injection volume was twice the column volume, V_{col} = 250 nL. The black trace shows the signal resulting from the 500 nL injection under conditions where the retention factor in the sample solvent was the same as the elution solvent. The blue trace shows the signal from an injection where on-column focusing was used to transiently increase retention in the sample solvent relative to the elution solvent. The retention factor in the sample solvent was 200. Signal values were normalized to that obtained for a nominally identical injection performed on a 4.6 mm ID column.

1.5 IMPACT OF TEMPERATURE ON RETENTION IN LC

Temperature has long been seen as a useful tool to improve the speed of chromatographic separation through its influence on mobile phase viscosity and analyte diffusivity. Typically, this is achieved by increasing column temperature [26]. Speed improvements are realized with: 1) increased mobile phase velocity allowed with the less viscous mobile phase and 2) increased analyte diffusivity at high temperature resulting in a flatter C-branch of the van Deemter curve. Elevated column temperature allows one to operate the column at an eluent velocity above that normally used at room temperature without the loss in column efficiency typically associated with such high velocities [27-29].

Temperature also influences solute retention because it is fundamentally tied to the thermodynamics of the partitioning (retention) process [30]. Eq. 1.5 shows this relationship between the free energy of transfer for a solute from the mobile phase to the stationary phase:

$$\Delta G^0 = -RT \ln K \tag{1.5}$$

where R is the Ideal Gas constant, T is the temperature in Kelvin and K is the equilibrium constant, equal to ratio k'/φ, where k' is the solute retention factor and φ is the column phase ratio. Substitution of the standard state enthalpy and entropy terms into Eq. 1.5 yields the van`t Hoff equation for the retention factor of a solute as a function of temperature:

$$\ln k = -\frac{\Delta H^0}{RT} + \frac{\Delta S^0}{R} + \ln \varphi \tag{1.6}$$

Plotting Eq. 1.6 on a ln k vs. 1/T (in Kelvin) coordinate system, the enthalpy of transfer can be estimated from the slope of the resulting line (often linear). Differences in enthalpy of transfer values or the so-called retention enthalpy are the key driving force to changes in chromatographic selectivity with temperature. Figure 1.3 shows example van`t Hoff plots for two solutes with different retention enthalpies, $\Delta H^0/R$ = -17.5 (purple) and -27.4 K (red). Lines are plotted from 0-100 °C, points correspond to an experimental temperature range of 25-75 °C. The slopes of these two lines are different; changes in column temperature alter retention for each solute to differing degrees, altering the selectivity of the separation [31-34]. For example, the retention factors for the "red" and "purple" solutes at 25 °C are 21.1 and 238; at 75 °C they are 7.6 and 48.6, respectively. The retention factor for the red solute changed by about a factor of 3 while the purple solute change by nearly a factor of 5 over the same temperature range. While temperatures influence on retention is smaller than that of solvent, temperature-induced changes in retention factor can be substantial. Thus, temperature can be used for more than just fine tuning resolution. This is a cornerstone of the work presented here.

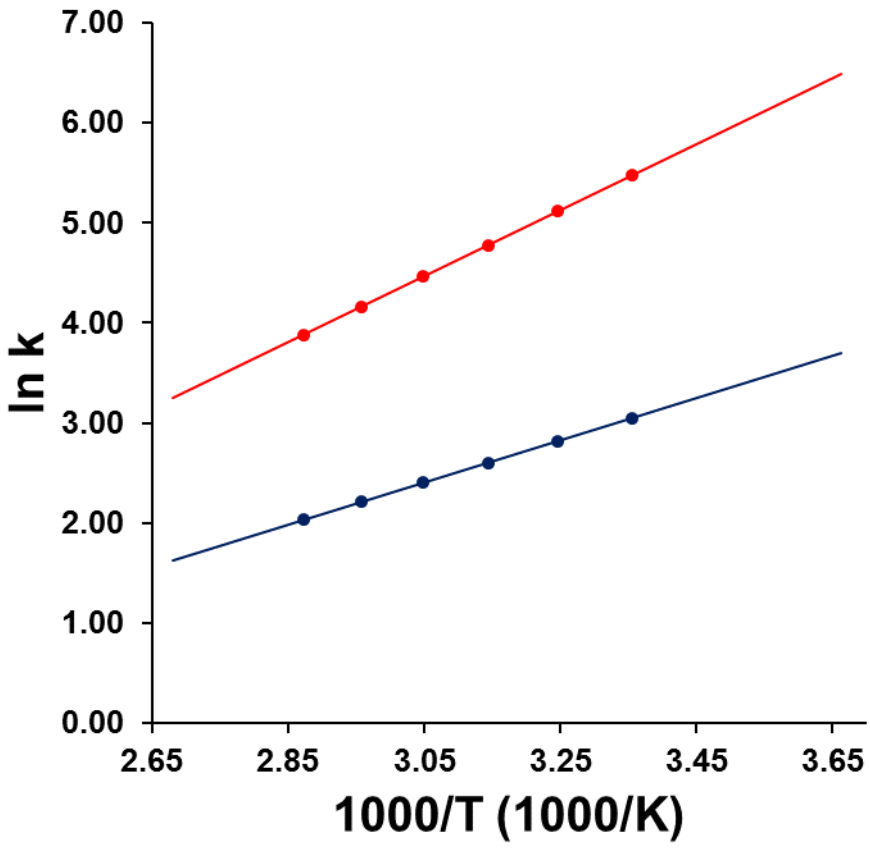

Figure 1.3. van`t Hoff plot for two example solutes, $\Delta H^0/R$ = -17.5 (purple) and -27.4 K (red). Intercepts for each solute were -4 (red) and -5.6 (purple), respectively. Data points correspond to an experimental temperature range from 25 to 75 °C, in 10 °C steps. Lines plotted over a 0-100 °C temperature range.

1.6 SCOPE OF WORK

The objective of this dissertation was to develop a series of independent methods to improve chromatographic figures of merit, namely, resolution, efficiency, peak capacity and concentration sensitivity. Performance has been enhanced through both instrumental and theoretical approaches. In Chapters 2, 3 and 5 we describe *temperature-assisted on-column solute focusing* (TASF), an instrumental approach designed to address the volume overload problem in liquid chromatography. Briefly, TASF works by relying on the temperature dependence of solute retention and high power Peltier or thermoelectric elements (TECs) to rapidly change the temperature of a short portion of the column near its inlet. Prior to injection the TECs actively cool the head of the column to sub-ambient temperatures, increasing solute retention and inducing an additional focusing effect at the column inlet. Following sample loading the cold section of the column is rapidly heated releasing the now focused injection band for separation on the downstream segment of the column. A series of three TASF instruments have been evaluated with test solutes making the approach into a robust system. Further, an accurate simulation procedure was developed to model the effectiveness of TASF and other complex spatial and temporal temperature gradients in both isocratic and solvent gradient elution modes.

Chapter 4 validates a previously developed model to predict the sensitivity enhancements from solvent-based on-column focusing while refuting an often-cited model which predicts widely optimistic preconcentration factors. In Chapter 6 a simple graphical approach to chromatographic optimization is presented, it was designed specifically to assist practitioners. In this approach column efficiency or peak capacity are plotted as constant value contours with linear axes represented by mobile phase velocity (horizontal) and column length (vertical). From this simple

two-dimensional plot, the user can instantly understand LC optimization, i.e. the influence of pressure, particle size, temperature, and time, from a practical level.

Finally, Chapter 7 summarizes the work described here and most importantly outlines the development of a new generation of advanced temperature-based approaches to improving chromatographic performance through *active temperature control* (ATC). ATC means to program temperature in time and space along the columns long axis. Details regarding the development of an ATC system consisting of ten independently controlled, 10 mm long TECs is presented. In addition, a significant advancement to the simulation procedure presented in Chapter 5 is outlined. Now, the procedure can accurately predict the abnormally shaped fronted and tailed peaks resulting from chromatographic bands straddling multiple temperature zones.

2.0 TEMPERATURE-ASSISTED ON-COLUMN SOLUTE FOCUSING: A GENERAL METHOD TO REDUCE PRE-COLUMN DISPERSION IN CAPILLARY HIGH PERFORMANCE LIQUD CHROMATOGRAPHY

The contents of this chapter were previously published in: Groskreutz, S. R. and Weber, S. G. Journal of Chromatography A, **2014**, 1354, 65-74.

Reproduced with permission from Elsevier.

2.1 INTRODUCTION

Small volume samples are commonly encountered in the fields of metabolomics, proteomics, forensics, neurochemistry and single cell analysis [35-38]. The high complexity and mass limited nature of such small samples necessitates the enhanced detection sensitivity offered by reductions in column diameter that limit sample dilution. [39, 40]. The recent significant improvements in column technology, i.e. sub-2 μm fully porous and core-shell particles [41-43], while welcome also create a problem—sensitivity to solute dispersion from pre-column processes including volume overload. Volume overload occurs when the relative contribution of the injection plug width to dispersion is large compared to that produced by on-column convective dispersion [44, 45]. In this work we describe an approach to mitigate the detrimental effects of pre-column dispersion created by volume overload in capillary columns using temperature-assisted on-column solute focusing (TASF).

One potential solution to the volume overload problem is to reduce the injected volume. For example, 5-nL injection volumes are possible in theory with various split- and timed-injection methods [46, 47], but achieving them with currently available instrumentation is non-trivial. Such

a small injection volume with current valve technology is not possible as a reduction in sample volume does not necessarily produce a proportional reduction in the effective volume loaded onto the column due to dispersion contributions by valve passages and all other pre-column volumes [25]. Fortunately, on-column focusing is a simple and effective process that can minimize the effects of volume overload [39, 48]. On-column focusing occurs when injected solute bands are compressed at the head of the column due to high solute retention and their subsequent elution at a much higher velocity by the mobile phase. Upon injection the sample solvent system becomes the mobile phase for the period of time required to flush the loaded sample through the injection zone [45, 49-51]. This solvent-based focusing works particularly well for aqueous samples injected into a reversed phase column. Recently the effect has seen a resurgence as a means to mitigate pre-column dispersion [52, 53] and to counteract the dilution of first dimension analyte bands in online multi-dimensional liquid chromatography [54-60]. Application of solvent-based on-column focusing in capillary scale columns has been more widespread because of their greater susceptibility to volume overload [24, 61-65].

The one fundamental requirement for on-column focusing is the establishment of high retention conditions at the head of the column. The means to attain this retention are not limited to changes in sample solvent composition. The mobile phase has a very strong influence on solute retention; this is why solvent-based focusing works well, but temperature also influences solute retention in LC albeit to a much smaller extent. The effect of temperature on retention is determined by the solute's partial molar enthalpy of retention. Increases in column temperature in RPLC generally decrease solute retention. In fact, high temperature liquid chromatography has exploited elevated temperature's influence on retention, selectivity, solvent viscosity and analyte diffusivity to attain

fast, efficient separations in a wide variety of applications discussed in the following reviews and book [66-69].

Increasing column temperature can decrease the effectiveness of solvent-based focusing in reversed phase chromatography in particular. A significant increase in column temperature generally leads to a decrease in retention which may call for a commensurate reduction in solvent strength to maintain constant retention. [27] Thus, in comparison to near-room temperature separations, high temperature separations may use weaker, more aqueous mobile phases. In such cases, the contrast between retention in water from the sample and retention in the more aqueous mobile phase decreases, thus on-column focusing becomes less powerful.

In contrast, TASF benefits from elevated separation temperatures. TASF is based on the premise that the transient reduction in column temperature for a short column segment, ca. <1 cm, for a short period of time, <1 min., will increase solute retention fostering effective on-column focusing. The freezing point of the mobile phase and pressure limitations of the pumping system set the minimum achievable column temperature to near -20 °C for typical aqueous/organic/reversed-phase systems. [70]

Capillary columns offer low thermal mass and small radial temperature gradients allowing rapid changes in column temperature during the chromatographic run. Temperature programming and various temperature ‘pulsing’ techniques have been successfully used with capillary scale columns. These methods have emphasized the benefits of rapid column heating to generate temperature gradients, increase analysis speed or tune chromatographic selectivity [71-75]. Only the Greibrokk group has explored the potential for sub-ambient column temperatures to focus large injection volumes onto capillary columns. In their work temperature programming initiated at sub-ambient temperatures, ca. 5 °C, was used to focus samples of retinyl esters, polyolefin based

Irganox antioxidants and ceramides made in 80-100% acetonitrile prior to separation using a neat acetonitrile mobile phase and C18 column [76-80]. High hydrophobicity and poor analyte solubility in water, necessary for on-column focusing was common to all of this work.

The primary method used to achieve sub-ambient column temperatures involves the use of programmable column ovens with cooling capabilities where the entire column is cooled via convection. There are two noteworthy limitations to this approach: 1) due to air's low heat capacity, rapid changes in column temperature are difficult to obtain, 2) reduction in column temperature significantly increases mobile phase viscosity. Cooling the entire column to sub-ambient temperatures puts serious restrictions on achievable linear velocities due to maximum pump pressure limitations. For example, cooling a 5 cm long column to 5 °C would increase column pressure by a factor of 3, compared to an identical 60 °C isothermal analysis. Reducing the temperature of only short segments of the column is an effective solution to the pressure problem. Cooling 1 cm of the hypothetical 5 cm column to 5 °C, while holding the remaining 4 cm at 60 °C, does significantly increase backpressure, albeit only by 35% relative to the 60 °C isothermal column. Maximum pump pressure is a limitation to TASF and needs to be considered, although the recent improvements in pump technology and increases in maximum operating pressure have lessened its influence.

To solve the problems associated with convection ovens two alternative cooling methods have been suggested. Holm and coworkers [81] developed a device where a single Peltier type thermoelectric cooler was used to cool an aluminum block through which a short segment of the column passes allowing large volume samples of the same Irganox antioxidants described above to be focused. After focusing, the column was moved manually, in space, from the cold zone to a programmable column oven where the separation was performed. Collins et al. presented another

application of thermoelectric column cooling where an array of ten independently controlled 1.2 cm square Peltier units were aligned allowing precise temperature control for capillary monolith synthesis and temperature programmed separations of alkylbenzene mixtures [82]. In a second approach to temperature assisted focusing Eghabali et al. cooled a 1 cm long section of the column, near its outlet, cryogenically to approximately -20 °C [83]. Heating was achieved using boiling water. What is unique about this focusing method was placement of the cold trap at the column outlet. This was done to trap and re-focus specific analytes (proteins) within regions of interest improving the observed signal-to-noise ratio (S/N).

In this paper, we describe an efficient approach to on-column focusing we refer to as TASF. We view this method as orthogonal to the conventionally used solvent-based on-column focusing methods so it can be employed independently or in conjunction with solvent-based methods. We report on the efficacy of the TASF method applied injection volumes ranging from about 7% to 150% of the column's fluid volume. Samples of solutes were made in mobile phase to avoid solvent focusing. The TASF approach was found to effectively reduce pre-column dispersion for all injection volumes tested. This method is ideal for applications where on-column focusing is required to mitigate volume overload and focus analyte bands, but where sample solvent compositions are fixed and not significantly different from the mobile phase, i.e. where implementation of solvent-based focusing is difficult.

2.2 THEORY

The signal observed in a chromatographic separation is influenced by all the components in the system and their individual contributions to the observed variance of the chromatographic band. The variance of the signal observed by the detector, in time units ($\sigma^2_{t,obs}$) is given by:

$$\sigma_{t,obs}^2 = \sigma_{t,inj}^2 + \sigma_{t,col}^2 + \sigma_{t,det}^2 + \sigma_{t,o}^2$$

(2.1)

where $\sigma_{t,inj}^2$, $\sigma_{t,col}^2$ and $\sigma_{t,det}^2$ are the variances induced by the injector, column and detector; $\sigma_{t,o}^2$ accounts for the sum of all other sources of dispersion in the chromatographic system, i.e. tubing, connections, etc. We note that the formulation shown is based on the assumption of independence of the processes contributing each term and that there is no mass overload (i.e., the system operates where the solute distribution isotherms are linear). In the ideal case the column is the dominant contributor to the observed band variance, but this is not generally true when high efficiency capillary columns are employed. The dispersion resulting from extra-column processes, primarily those related to the injection volume and connection tubing, become more significant.

Figure 2.1 shows that the column consists of three segments. The first is a short segment inside the injector/fitting that is void of packing and held at room temperature. The void ensures analytes reach the cooled focusing segment at the same time, i.e. retention due to the room temperature column inside the injector does not influence results. This simplifies selection of the trapping time although it adds considerably to pre-column bandspreading. The trapping zone is under temperature control by a Peltier thermoelectric device (TEC). It is followed by the remainder of the column at a constant temperature. For more details about the experimental setup, see section 2.3.3.2.

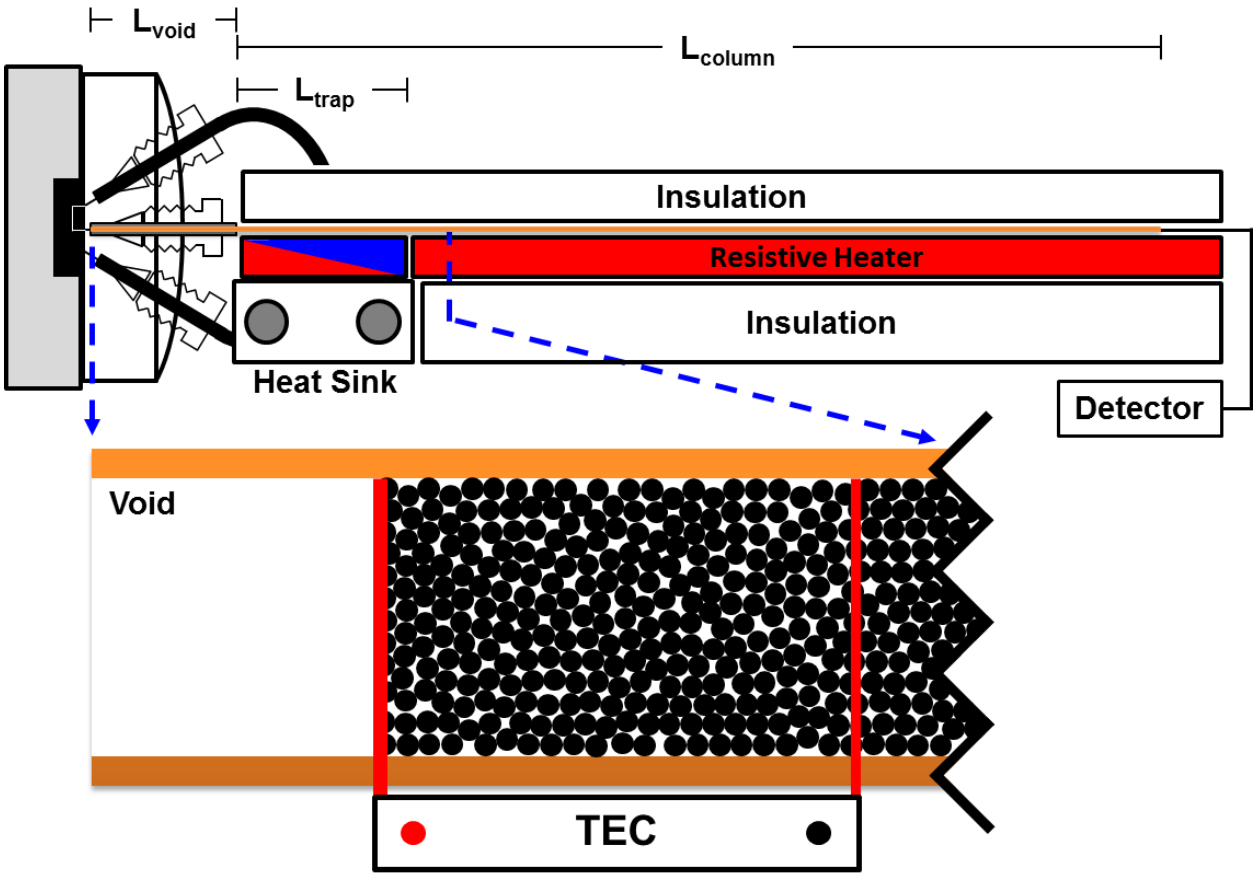

Figure 2.1. Schematic of instrument configuration used to implement the TASF approach. The Peltier cooling element (TEC) is shown in red and blue. The importance of the pre-column void is apparent due to the size of the nut and PEEK sleeve used to connect the column to the injection valve stator. The pop-out at the bottom of the figure highlights how the TEC should be aligned with the top of the packed bed for effective TASF implementation. The size of the TEC dictates the maximum length of the trapping zone; the remainder of the column length was maintained at constant temperature by the resistive heater shown in red.

We can divide the observed peak time variance ($\sigma^2_{t,obs}$) into three segments, the pre-column ($\sigma^2_{t,pre\ col}$), column ($\sigma^2_{t,col}$) and post-column ($\sigma^2_{t,post\ col}$):

$$\sigma^2_{t,obs} = \sigma^2_{t,pre\ col} + \sigma^2_{t,col} + \sigma^2_{t,post\ col} \tag{2.2}$$

The pre-column variance is defined as:

$$\sigma^2_{t,pre\ col} = \sigma^2_{t,inj} + \sigma^2_{t,void} \tag{2.3}$$

where $\sigma^2_{t,inj}$ is the broadening due to the injection time and $\sigma^2_{t,void}$ represents the dispersion in the void section. The importance of this region is described in detail in Appendix A (A1.2.2).

The column variance is composed of two terms: the variance due to the trapping, variable temperature segment ($\sigma^2_{t,1}$) and the isothermal, separation section of the column ($\sigma^2_{t,2}$):

$$\sigma^2_{t,col} = \sigma^2_{t,1} + \sigma^2_{t,2} \tag{2.4}$$

Assuming the largest contribution to $\sigma^2_{t,post\ col}$ is from broadening induced by the Poiseuille flow profile in the connection tubing between the column outlet and the flow cell, $\sigma^2_{t,post\ col}$ can be calculated from Taylor theory as:

$$\sigma^2_{t,post\ col,i} = \frac{r^2 l}{24 D_{m,i,2} v} \tag{2.5}$$

where v is the average linear velocity, r is the radius of the connecting tubing, l is its length, and $D_{m,i,2}$ is the solute diffusion coefficient for solute i in the isothermal section of the column.

The time variance from the injection of a volume V_{inj} onto a column of radius a is given by Eq. 2.6:

$$\sigma_{t,inj,i}^2 = \left[\frac{V_{inj}}{\sqrt{12}\pi a^2 \epsilon_{tot}\left(1 + k'_{i,1}\right)}\right]^2 \frac{\left(1 + k'_{i,2}\right)^2}{v^2} \tag{2.6}$$

where ϵ_{tot}, is the column's total porosity, v, is the interstitial velocity, and $k'_{i,1}$ and $k'_{i,2}$ are the retention factors for solute i on the trapping and separation sections of the column. The term in the square brackets corresponds to the well-known relationship that the length variance of a rectangular concentration profile of width w is $w^2/12$. [19] The width (w) is related to the injection volume (V_{inj}), the liquid filled cross sectional area of the column ($\pi a^2 \epsilon_{tot}$), and a compression factor from retention at the head of the column. The term outside the brackets converts this length variance into a time variance as the band elutes from the isothermal, separation portion of the column.

The contribution to observed bandspreading due to the void at the head of the column ($\sigma_{t,void}^2$) in Eq. 2.3 is difficult to model theoretically due to its short length and relatively wide diameter. Thus, this variance was estimated experimentally. Details are provided in section A1.2.2 of Appendix A. In particular, we estimate the variance for an unretained compound from the void ($\sigma_{t,void,iso}^2$) in an isothermal column (no trapping). This variance is decreased by the factor $\left(1 + k'_{i,1}\right)^2$ in the

trapping zone in a TASF experiment and increased by the factor $\left(1 + k'_{i,2}\right)^2$ at the column outlet as shown in Eq. 2.7.

$$\sigma^2_{t,void,i} = \sigma^2_{t,void,iso}\left[\frac{\left(1 + k'_{i,2}\right)}{\left(1 + k'_{i,1}\right)}\right]^2 \tag{2.7}$$

Thus, combining Eqs. 2.6 and 2.7 we have an expression for the pre-column time variance of:

$$\sigma^2_{t,pre\ col} = \left[\frac{\left(1 + k'_{i,2}\right)}{\left(1 + k'_{i,1}\right)}\right]^2 \left[\left[\frac{V_{inj}}{\sqrt{12}\pi a^2 \epsilon_{tot} v}\right]^2 + \sigma^2_{t,void,iso}\right] \tag{2.8}$$

The primary advantage of TASF is exploited in the first term of Eq. 2.8 as $k'_{i,2}$ is smaller than $k'_{i,1}$.

The column variance can be increased or decreased by cooling a segment of the column. Knox's recent formulation emphasizing the importance of mass transport in the flowing mobile phase [84] was used to determine column variance. From plate theory the length variance due to the column is given by:

$$\sigma^2_{l,col} = HL \tag{2.9}$$

where H is the height equivalent to a theoretical plate and L is the length of the column. Converting to reduced parameters, we obtain the following expression for the length variance in an isothermal column:

$$\sigma_{l,col,i}^2 = Ld_p \left[\frac{B}{v_i} + Cv_i + \frac{1}{\frac{1}{A} + \frac{1}{Dv_i{}^n}} \right]$$

(2.10)

where d_p is the particle diameter, and v_i is the reduced velocity for solute i and n is mobile zone's velocity dependence. The B- and C-coefficients of Eq. 2.10 have their usual meanings related to axial diffusion and mass transfer into and out of the stationary zone. The A- , D-, and n coefficients relate to mobile zone broadening caused by the flow path structure and tortuosity and mass transport among flow paths [84].

Because there are two segments of the column that may be at different temperatures, we must calculate the length variances for the trapping ($\sigma_{l,1}^2$) and separation ($\sigma_{l,2}^2$) segments of the column independently and add the result. Although the physical length of the trapping segment of the column is fixed at L_T, the effective length of the trapping zone experienced by solute i, $L_{i,1}$, depends on its velocity in the trapping zone and the focusing time t_{focus} as shown by Eq. 2.11. Thus,

$$L_{i,1} = \frac{vt_{focus}}{\left(1 + k'_{i,1}\right)}$$

(2.11)

The variance due to the trapping segment of the column ($\sigma_{l,1}^2$) is:

$$\sigma_{l,i,1}^2 = L_{i,1} d_p \left[\frac{B}{\nu_{i,1}} + C\nu_{i,1} + \frac{1}{\frac{1}{A} + \frac{1}{D{\nu_{i,1}}^n}} \right]$$

(2.12)

where $\nu_{i,1}$ is the reduced velocity for solute i in the trapping segment of the column. Analogously the variance due to the remainder of the column ($\sigma_{l,2}^2$) is given by:

$$\sigma_{l,i,2}^2 = \left(L - L_{i,1}\right) d_p \left[\frac{B}{\nu_{i,2}} + C\nu_{i,2} + \frac{1}{\frac{1}{A} + \frac{1}{D{\nu_{i,2}}^n}} \right]$$

(2.13)

where $\nu_{i,2}$ is the reduced velocity for solute i at the column temperature. Adding Eqs. 2.12 and 2.13 yields a column distance variance for TASF separations as:

$$\sigma_{l,col,i}^2 = L_{i,1} d_p \left[\frac{B}{\nu_{i,1}} + C\nu_{i,1} + \frac{1}{\frac{1}{A} + \frac{1}{D{\nu_{i,1}}^n}} \right] + \left(L - L_{i,1}\right) d_p \left[\frac{B}{\nu_{i,2}} + C\nu_{i,2} + \frac{1}{\frac{1}{A} + \frac{1}{D{\nu_{i,2}}^n}} \right]$$

$$= L_{i,1} d_p h_1 + \left(L - L_{i,1}\right) d_p h_2$$

$$= d_p \left[L h_2 + L_{i,1}(h_1 - h_2) \right]$$

(2.14)

It is instructive to point out when the column is not subjected to TASF, i.e. when $\nu_{i,1} = \nu_{i,2}$, and $L_{i,1} = 0$ Eq. 2.14 reduces to Eq. 2.10. Also note that, under the assumptions that the parameters $A, B, C, D,$ and n are independent of k', the temperature dependence resides in the reduced velocities. When the separation is clearly B-term dominated, $h_1 < h_2$, so there is a small decrease

in column variance due to trapping. In the more common situation in which velocity-dependent mass transport is dominant, the opposite is true.

Converting the column variance in length units to time units gives:

$$\sigma_{t,col,i}^2 = d_p\left[Lh_2 + L_{i,1}(h_1 - h_2)\right]\frac{\left(1 + k'_{i,2}\right)^2}{v^2} \tag{2.15}$$

Table 2.1 shows the relevant time variance equations (2.5, 2.6, 2.7, 2.15) which can be substituted into Eq. 2.2 to obtain an observed band variance for isothermal and TASF separations.

Table 2.1. Time variance equations used to calculate individual contributions to observed peak variance due to the injection, pre-column void, and post-column tubing utilizing the TASF approach.

Variance Contribution	**Equation Number**	**Equation**
Injection	2.6	$\sigma_{t,inj,i}^2 = \left[\frac{V_{inj}}{\sqrt{12}\pi a^2 \epsilon_{tot}\left(1 + k'_{i,1}\right)}\right]^2 \frac{\left(1 + k'_{i,2}\right)^2}{v^2}$
Pre-column Void	2.7	$\sigma_{t,void,i}^2 = \sigma_{t,void,iso}^2 \left[\frac{\left(1 + k'_{i,2}\right)}{\left(1 + k'_{i,1}\right)}\right]^2$
Column	2.15	$\sigma_{t,col,i}^2 = d_p\left[Lh_2 + L_{i,1}(h_1 - h_2)\right]\frac{\left(1 + k'_{i,2}\right)^2}{v^2}$
Post-column Tubing	2.5	$\sigma_{t,post\ col,i}^2 = \frac{r^2 l}{24 D_{m,i,2} v}$

2.3 MATERIALS AND METHODS

2.3.1 Reagents and solutions

Methyl, ethyl, *n*-propyl, and *n*-butyl esters of *p*-hydroxybenzoate (parabens) were purchased from Sigma-Aldrich (St. Louis, MO). Standard solutions of each paraben were prepared by first dissolving in acetonitrile, then diluting to the desired concentration and solvent composition with deionized water. DI water was from an in-house Millipore Milli-Q Synthesis A10 water purification system (Billerica, MA) and was used without further treatment. Phosphoric acid was from Fisher Scientific (HPLC grade, Fair Lawn, NJ), and HPLC grade acetonitrile was from Spectrum Chemical (New Brunswick, NJ). All mobile phases were vacuum degassed and filtered twice through 0.45 μm nylon filters (Millipore).

2.3.2 van`t Hoff retention studies

2.3.2.1 Instrumentation

A Jasco X-LC 3000 system consisting of a 3059AS autosampler, dual 3085PU semi-micro pumps, 3080DG degasser, 3080MX high pressure mixer, CO-2060 thermostated column compartment, 3177UV variable wavelength UV absorbance detector, and LC-Net II/ADC from Jasco Inc. (Easton, MD) was used to evaluate the temperature dependence of solute retention. Data analysis and instrument module control was achieved with EZChrom Elite software from Agilent Technologies (version 3.2.1, Santa Clara, CA).

2.3.2.2 Chromatographic conditions

A mixture of 25 μM uracil and 50 μM methylparaben, ethylparaben, propylparaben and butylparaben was made in mobile phase. Samples were injected onto a Waters Acquity BEH C18 column (50 mm x 1.0 mm I.D.; 1.7 μm d_p; Waters Corp., Millford, MA). Isocratic separations were

made at a flow rate of 200 μL/min with a mobile phase consisting of 80% 10 mM H_3PO_4, pH 2.7, 20% acetonitrile. The column temperature was varied from 25 to 75 °C in 10 °C steps, the injection volume was 1.0 μL, and peaks were detected by absorbance of UV light at 210 and 220 nm. Injections at each temperature were performed in triplicate with the order of the subsequent temperature analysis selected at random.

2.3.3 TASF instrumentation and chromatographic conditions

2.3.3.1 Column preparation

Figure 2.1 shows a schematic of the instrument used for TASF separations. Capillary columns were prepared by packing 1.7 μm BEH C18 particles (Waters) into 150 μm I.D. fused-silica capillaries from Polymicro Technologies (Phoenix, AZ). Columns were fritted by sintering 2 μm, solid borosilicate spheres (Thermo Scientific, Fremont, CA) into the end of the column blank using an electrical arc. Particles were slurried in isopropanol (Spectrum) at a concentration of 50 mg/mL, sonicated for 25 minutes and packed using the downward slurry method at 27500 psi using a Model DSHF-302 pneumatic amplification pump from Haskel (Burbank, CA). The packing solvent was acetone (Sigma). Care was taken to pack columns of defined length, ca. 5-6 cm, by limiting the volume of slurry, and subsequent mass of particles, loaded into the packing system. This allowed columns to be packed leaving a 2 cm section free of stationary phase at the head of the column.

2.3.3.2 TASF instrumentation

Packed columns were fitted directly to a Cheminert injection valve (Model 07Y-03BH, VICI Valco, Houston, TX) equipped with a 2 μL sample loop. The sample loop was over-filled with sample. Injection volume was controlled by controlling the injection time. By this means we achieved estimated injection volumes from 45 to 1950 nL. A PeakSimple module and associated

software (Version 393, SRI Instruments, Las Vegas, NV) were used to actuate the valve. An Ultimate 3000 RSLCnano high pressure gradient pump (Thermo Scientific, Sunnyvale, CA) with a an upper pressure limit of 800 bar delivered mobile phase and UV absorbance detection at 210 nm was achieved by a Waters Acquity TUV detector equipped with a 10 nL flow cell (Waters). Data acquisition and export was achieved through connection of the analog output of the Acquity TUV to the Jasco ADC described in the van`t Hoff studies. The ADC sampling frequency was 25 Hz, with analysis performed using PeakFit (v4.12, Systat Software, Inc., San Jose, CA).

As shown in Figure 1.1 two different temperature control assemblies were used to regulate column temperature during the chromatographic run. A Peltier based thermoelectric cooling element (TEC) from Custom Thermoelectic (part number 03111-5L31-03CF, Bishopville, MD) controlled the first 7 mm of the column. Utilization of a TEC allowed first cooling the head of the column to 5 °C for 30 s during the injection process, followed by a rapid heating period to the separation temperature of 60 °C by reversing TEC polarity. To promote rapid heat transfer between the TEC and column a gallium-indium based eutectic was used at the interface between the TEC and column [85, 86]. After the desired focusing time TEC polarity was changed manually using a two position switch. An Agilent 6286A DC power supply powered the TEC, temperature was regulated by manually tuning the current delivered at fixed potential. A Type T thermocouple (COCO-003, Omega, Stamford, CT) and a Eurotherm 2416 temperature controller (Invensys Eurotherm, Ashburn, VA) were used to monitor TEC temperature. Over the course of a day's experiments temperature was found to be relatively stable, ±1 °C. The TEC was fixed to a custom aluminum, water cooled heat sink. A chilled ethylene glycol/water mixture was used to regulate heat sink temperature. The flow rate for the ethylene glycol/water mixture was 1 L/min; it was delivered by a Kryo-Thermostat WK 5 chilled circulator (Lauda-Brinkmann, Delran, NJ).

The second, isothermal section of the column was heated using a Love Model 1500 proportional-integral-derivative (PID) controller (Dwyer Instruments, Michigan City, IN) connected to a Kapton resistive heater (KHLV-103/10-P, Omega). The heater was attached to an aluminum block onto which the column was placed. A temperature sensor (SA1-RTD, Omega) was fitted inside the aluminum block and the signal was fed back to the controller; temperature control precision in the isothermal section of the column was found to be about ±0.1 °C.

2.3.3.3 Injection volume studies

A series of 15 injection volumes from 45 to 1050 nL were performed with and without transiently cooling the head of the column to test the ability of the TASF methodology to alleviate dispersion due to pre-column volumes and volume overload. The column used in all injection volume experiments was 60 mm x 150 μm I.D. and left with a 2 cm void. The flow rate was 3 μL/min, the mobile phase was 80:20 10 mM H_3PO_4/acetonitrile and the UV detection wavelength was 210 nm. Isothermal separations utilized a column temperature of 60 °C. TASF separations employed the same analysis temperature; the focusing temperature was set to 5 °C. The head of the column was held at this temperature for 30 s before manually reversing the polarity on the TEC, heating the column to 60 °C. Isothermal column backpressure was near 330 bar and 470 bar at the 5 °C focusing temperature. Samples were made in mobile phase at concentrations such that the mass of each solute injected onto the column was between 3.5 and 9 ng. Table A2.3 provides details regarding injection volume and sample concentrations used.

2.3.3.4 Limit of quantitation study

Separations were performed with two injection volumes, 60 and 1875 nL. After determining the ethylparaben limit of quantitation for the Acquity TUV detector using the 10σ value for detector noise, solute concentrations for each injection volume were selected. The 60 nL injections were

performed with samples composed of 1.25 μM ethylparaben; the 1875 nL sample was made at 100 nM. The chromatographic conditions for these separations were nominally identical to those used in the injection volume studies described in Section 2.4.3.3 with one notable difference. Focusing conditions were tailored for the separation of ethylparaben to increase usable injection volumes for TASF separations. Ethylparaben optimization was performed by increasing the focusing time from 30 to 45 s for the 1875 nL sample. A detailed description related to selection of this focusing time is reserved for Section 2.4.4.

The following procedure was used to address issues related to carryover between subsequent injections. Two new 2.0 mL glass syringes from Hamilton (Hamilton Company, Reno, NV) were used, the first to flush the injection valve with acetonitrile between samples; the second for the paraben samples. The paraben sample syringe was rinsed three times with acetonitrile before changing to a different concentration sample. Before injection of paraben samples onto the column, 0.5 mL of acetonitrile was flushed through the 2 μL sample loop while the valve was in the load-position. The valve was actuated to the inject-position and mobile phase was passed through the sample loop for five minutes at a flow rate of 3 μL/min. An injection blank consisting of mobile phase was performed to confirm no sample carryover following this cleaning procedure. This procedure was repeated between samples.

2.4 RESULTS AND DISCUSSION

2.4.1 Temperature dependence of retention factors

A series of van`t Hoff studies were performed using a commercially available Acquity BEH C18 column prior to implementation of TASF experiments. Partial molar enthalpies of retention for each solute were determined from van`t Hoff plots (Eq. A1) and retention data over the 25-75 °C

temperature range (Table 2.2). Inspection of residuals indicated there was no significant change in retention enthalpy with temperature. The high degree of linearity allowed extrapolation to the sub-ambient focusing temperature of 5 °C. The ability to predict solute retention factors at specific focusing and separation temperatures was critical to modeling the potential of the TASF approach.

Table 2.2. Partial molar enthalpies of retention for methylparaben through butylparaben obtained from slopes of the van`t Hoff plots (Figure A1.1). Chromatographic conditions can be found in section 2.4.2.2.

Solute	$\Delta H^0/R$ (K)	Error	Intercept	Error
Methylparaben	1999	11	-5.09	0.03
Ethylparaben	2219	15	-4.87	0.05
Propylparaben	2566	21	-4.98	0.07
Butylparaben	2961	26	-5.24	0.08

2.4.2 Simulation of TASF chromatograms

Equations 2.5, 2.6, 2.7 and 2.15 were used to determine the void, column, and post-column variances and assess the relative contribution of experimentally accessible parameters on observed peak variance. To determine the total dispersion of a hypothetical Gaussian peak with no volume overload, $\sigma_{t,G}^2$ combination Eqs. 2.5, 2.7, and 2.15 yield:

$$\sigma_{t,G,i}^2 = \sigma_{t,void,i}^2 + \sigma_{t,col,i}^2 + \sigma_{t,post\ col,i}^2 \tag{2.16}$$

Assuming a rectangular injection plug the variance due to injection was redefined as:

$$\sigma_{t,B,i}^2 = \sigma_{t,inj,i}^2 \tag{2.17}$$

where $\sigma_{t,B,i}^2$ describes the variance of a rectangle.

Solving the convolution integral [19] for a rectangular pulse and a Gaussian distribution yields:

$$C(t) = \frac{C_0}{2\sqrt{12}\sigma_{t,B,i}}\left[\text{erf}\frac{\sqrt{12}\sigma_{t,B,i} - \left(t - t_{R,i}\right)}{\sqrt{2}\sigma_{t,G,i}} + \text{erf}\frac{\left(t - t_{R,i}\right)}{\sqrt{2}\sigma_{t,G,i}}\right] \tag{2.18}$$

upon substitution of Eqs. 2.16 and 2.17 where C_0 is sample concentration and $t_{R,i}$ is the retention time for solute i. The equation used to determine $t_{R,i}$ is provided in section A1.2.2. A total of ten injection volumes were simulated by substitution of the values reported in Table 2.3 into each term of Eqs. 2.16 and 2.17. Injection volumes used in calculations are reported in Table A1.2.

Table 2.3. Parameters involved in isothermal and TASF simulations.

Parameter	**Determination**	**Value**
t_s		0.5 min
V_{inj}		45-1050 nL (See Table A2.2)
F		3 μL/min
T_f		5 °C
T_{sep}		60 °C
van`t Hoff Plot Slope van`t Hoff Plot Intercept	Experiment	See Table 2.2
D_m (310 K)	Literature [70, 87]	See Table A1.1
η(T)	Literature [26, 88]	See Eq. A1.2
ϵ_{tot}	Literature [89]	0.537
A	Literature [84]	20
B		4.5
C		0.01
D		0.42
n		1
d_p	Experiment	1.7 μm
L		6.0 cm
ϕ		0.2
$\sigma^2_{t,void,iso}$		0.000571 min^2
$d_{post\ col}$		25 μm
$l_{post\ col}$		25 cm

Figure 2.2 shows two overlays generated from Eq. 2.18. The blue trace in both panels illustrates the effect of a 5 °C focusing temperature on the observed chromatogram for two injection volumes, 45 and 1050 nL. These injection volumes were selected to mimic experimental results. Using our system the smallest achievable injection volume was 45 nL. The largest sample used in the injection volume studies was 1050 nL. In order of elution, peaks were simulated for uracil, methylparaben, ethylparaben, propylparaben, and butylparaben using appropriate van`t Hoff parameters and diffusion coefficients. In this calculation uracil was used to mark system dead time and was defined to have no retention at either the focusing or separation temperatures. Due to this definition uracil peak shape does not improve when the TASF approach is used at either injection volume. TASF mitigates pre-column induced dispersion. Simulations assumed all pre-column dispersion was due to volume overload and the pre-column void. For the 45 nL injection volume shown in panel A peak heights increased from 15.9 and 15.1 to 34.9 and 30.4 units for methylparaben and ethylparaben when using TASF. To determine the influence of the pre-column void on observed peak width a hypothetical system with no pre-column void, i.e. $\sigma_{t,void,i}^2 = 0$, was simulated. Figure A1.2 demonstrates the influence of the pre-column void with 5 and 45 nL injections. A 5 nL injection volume was also selected because it corresponds to just under 1% of the column volume, analogous to a commonly used 1 μL injection onto a 5 cm x 2.1 mm I.D. column. Under the simulated conditions with a 5 nL injection volume, implementation of TASF actually degrades column efficiency by 22% (methylparaben) due to the reduction in column efficiency at 5 °C. Increasing the injection volume to 45 nL, still without a pre-column void, already shows improvement in observed column efficiency when using TASF. This result indicates that a 45 nL injection volume does correspond to volume overload for this column.

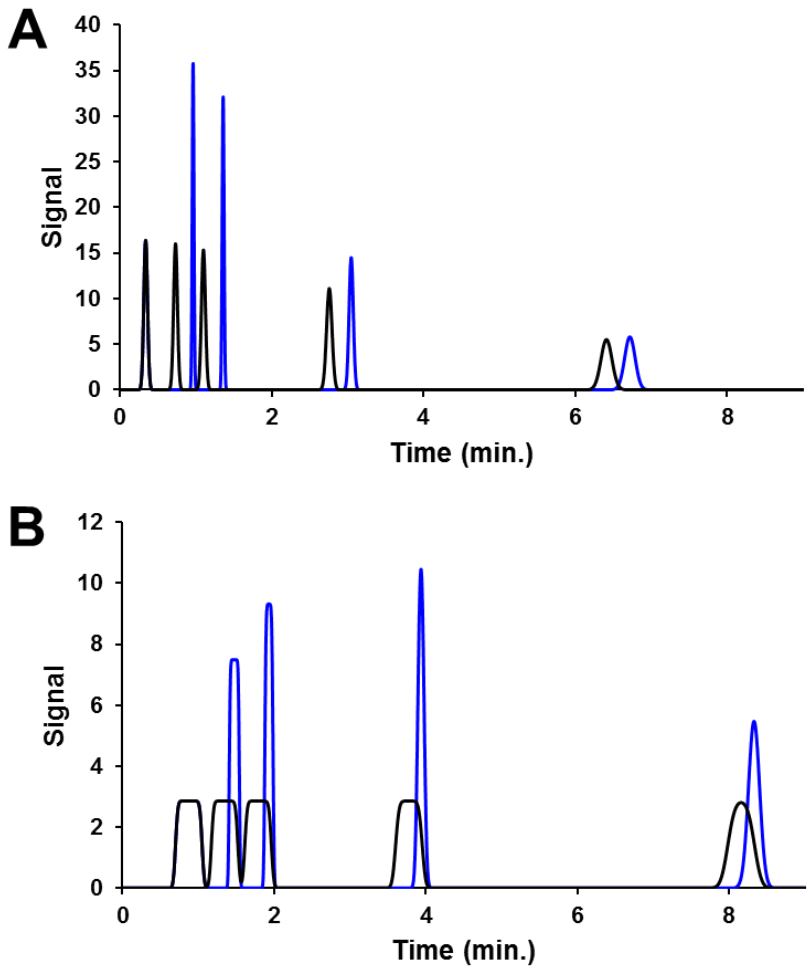

Figure 2.2. Simulated isothermal (——) and TASF (——) separations of paraben mixtures made in mobile phase generated using Eq. 2.17. The first peak in each panel is uracil, the void time marker was defined to have no retention at separation and focusing temperatures. A 45 nL injection is shown in panel A, panel B shows a 1050 nL injection. Peak area for each solute was held constant at both injection volumes to allow easy comparison of peak shape between injection volumes. Values used for simulations can be found in Table 2.3.

Panel B of Figure 2.2 demonstrates the ability of TASF to focus large volume samples onto the head of the column. Defining the liquid volume of the column as the fluid volume of the column ($\pi a^2 L \epsilon_{tot}$) excluding the pre-column void, a 1050 nL injection corresponds to 160% of the column volume. The simulated chromatogram clearly shows significant volume overload. Although TASF with a 5 °C focusing temperature decreased peak width for all solutes, this temperature (5 ˚C) did not suffice to increase retention for methylparaben and ethylparaben to create Gaussian peaks. Retention factors calculated from the van`t Hoff parameters in Table 2.2 are shown in Table A1.1. To solve this problem further reductions focusing temperature would be required for further reductions in peak width for low retention solutes such as methylparaben and ethylparaben.

In order to visualize the effect of TASF over a wide range of injection volumes a metric easily relatable to experimental data was required. The flat-topped peaks obtained at large injection volumes are not well fit by various Gaussian modifications, e.g. exponentially modified Gaussian (EMG) or 5-parameter EMG. However, experimental values for the full width at half maximum (FWHM) can be measured readily. The following approximation was made to allow generation of FWHM vs. V_{inj} plots.

$$FWHM = \left[12\sigma_{t,B}^2 + \left(2\sqrt{2\ln 2}\,\sigma_{t,G}\right)^2\right]^{1/2} \tag{2.19}$$

Equation 2.19 combines the FWHM of a Gaussian peak, $\sigma_{t,G}$, calculated from Eq. 2.16 and adds it to the injection variance width, $\sigma_{t,B}^2$. The square root of the sum accurately estimates the FWHM of peaks from purely Gaussian to purely rectangular over the range of values used here with a maximum error of 12%. Systematic increases in the overestimation values for FWHM values with increased injection value were observed. Figure 2.3 was generated from a series of ten injection

volumes ranging from 45 to 1050 nL and values in Table 2.2. Panels A-D correspond to methylparaben through butylparaben; TASF separations with a 5 °C focusing temperature are shown in blue. Isothermal separations at 60 °C are in black. Red dashed lines indicate a 5% increase in FWHM for 45 nL isothermal injections. A 5% increase in FWHM is approximately equal to a 10% reduction in column efficiency. Benefits obtainable with TASF across all injection volumes are most prominent for low retention solutes at low injection volumes and high retention solutes at large injection volumes. At 5 °C TASF reduces the observed FWHM for a 45 nL injection of methylparaben by a factor of 2.2, speaking to the method's ability to reduce pre-column dispersion. TASF is only able to reduce the width of the observed small injection volume butylparaben band by 5% for a 45 nL injection. This explains why the relative difference between FWHM values for the isothermal and TASF separations show in panels A-D of Figure 2.3 decreases with increasing isothermal retention factor. At injection volumes greater than the column volume TASF is able to limit the rate of increase for observed FWHM values. This effect is most apparent when comparing panels A and D for methylparaben and butylparaben. At an injection volume of 450 nL the TASF FWHM value for methylparaben has risen above the 5% increase line for a 45 nL injection. This does not occur for butylparaben at 5 °C until about 1500 nL.

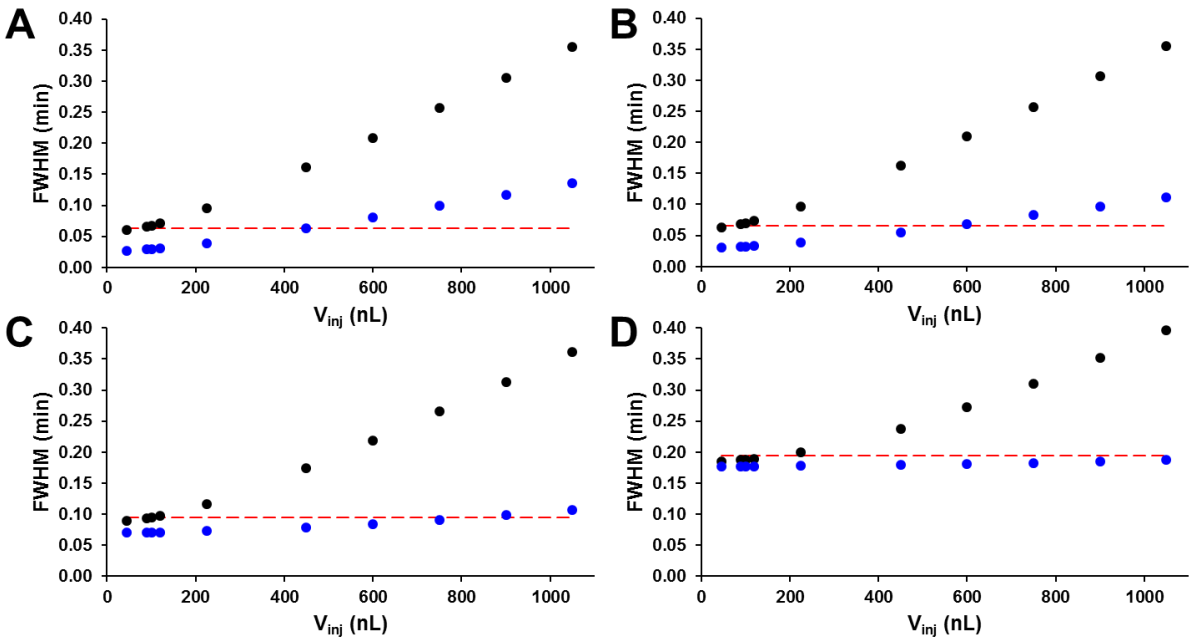

Figure 2.3. Simulated isothermal (●) and TASF (●) separations where the injection volume of paraben samples made in solvent systems identical to the mobile phase was varied from 45 to 1050 nL. Panels A, B, C, and D correspond to simulations for methylparaben through butylparaben, respectively. Red dashed lines represent a 5% increase in the FWHM for a 45 nL isothermal injection for each solute. Increases in simulated FWHM values with increasing in injection volume were due to the pre-column void and volume overload. TASF reduced peak FWHM for all solutes across all injection volumes under the conditions reported in Table 2.3.

2.4.3 Experimental determination of the effect of TASF on peak width

A series of fifteen injection volumes were performed under isothermal and TASF conditions with paraben samples prepared in mobile phase. Example chromatograms are shown in Figure 2.4; both panels display TASF separations with 5 °C focusing temperatures in blue and 60 °C isothermal separations in black. These experimental results mirror the simulated results of Figure 2.2. Panel A corresponds to a 45 nL injection and B a 1050 nL injection. Estimating the column volume to be 640 nL, the 45 nL injection corresponded to 7% of the column volume and the 1050 nL injection 160%. The increase in peak height for TASF analyses was the method's most obvious advantage. The peak height values for methylparaben and ethylparaben in panel A of Figure 2.4 increased by 20% relative to their peaks in the isothermal separation. At both injection volumes, Figure 2.4 panels A and B, methylparaben, ethylparaben, and propylparaben benefitted most from TASF. At the retention factor extremes characterized by uracil, no retention, and butylparaben, $k'_{60\,^{\circ}C} = 38.4$, the influence of TASF was reduced. Uracil, with $k' = 0$, cannot be focused and butylparaben with its large k' is focused without the assistance of reduced temperature. Of course, TASF would improve the butylparaben peak width had larger volumes been injected. These results indicate that under experimental conditions there was an optimal retention factor ratio present between the focusing and separation segments of the column. Panel B of Figure 2.4 demonstrates the potential for TASF to minimize volume overload. The inset in panel B shows the propylparaben peak from an isothermal separation with a 1050 nL injection volume. It shows that flat topped peaks characteristic of volume overload were obtained even for relatively high retention compounds. When TASF was used the large volume sample was effectively focused in the cold trap increasing peak heights for methylparaben, ethylparaben, and propylparaben by factors of 3.2, 4.2 and 3.4, respectively.

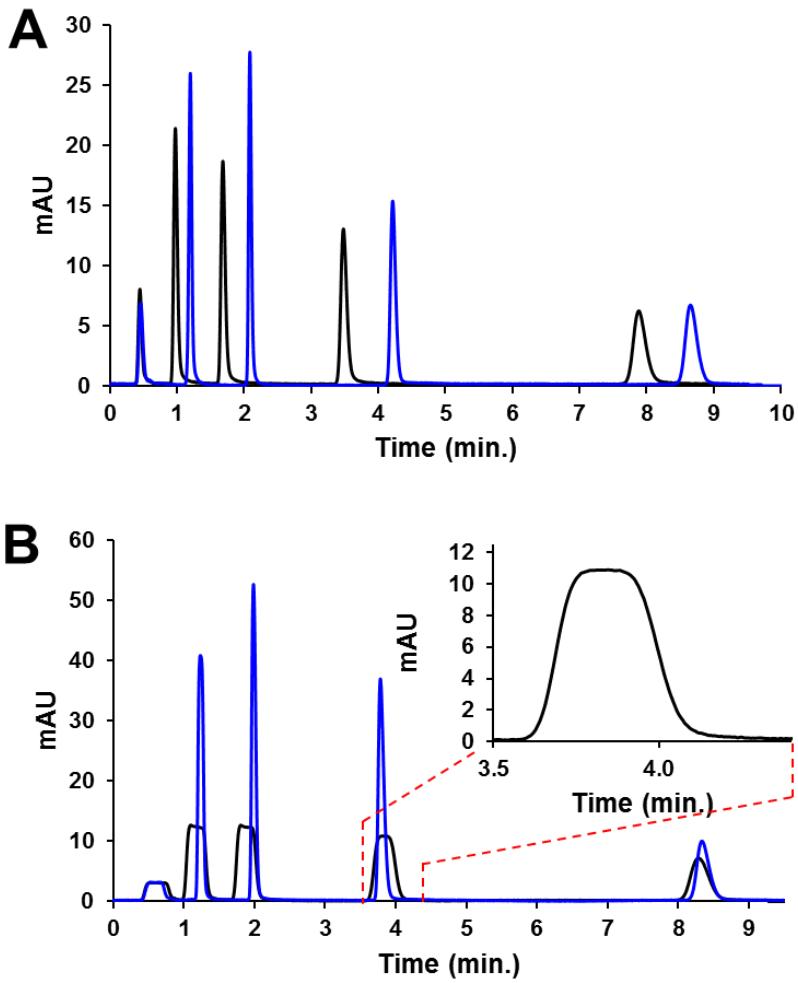

Figure 2.4. Demonstration of the potentiation for the TASF approach to reduce observed peak width for samples made in mobile phase at multiple injection volumes. Isothermal (——) separations were performed at 60 °C. A 5 °C focusing temperature and 30 s focusing time were used with the TASF approach (——). Panel A shows results from a 45 nL injection, panel B a 1050 nL injection. The pop-out in panel B illustrates the flat topped peak profiles observed for the isothermal propylparaben peak.

Figure 2.5 shows measured peak width at half height for each solute as a function of injection volume. These experimental results correspond to the simulated results in Figure 2.3. Panels A, B, C, and D of Figure 2.5 present the results of these experiments for methylparaben, ethylparaben, propylparaben, and butylparaben, respectively. Isothermal separations are plotted as black circles; TASF experiments are blue. Red dashed lines correspond to a 5% increase in FWHM for a 45 nL injection. Error bars were calculated from the standard error for each measured FWHM, with n = 3. Qualitatively, the shape of the plots and relative increase in FWHM between isothermal and TASF experiments mimic the results predicted by the simulations. Low retention solutes are more susceptible to volume overload-related increases in FWHM. The ability of TASF to limit the rate of FWHM increase with increasing injection volume for samples made in mobile phase was impressive. Methylparaben, with an isothermal retention factor of 2.5 was the only solute tested where volume overload induced dispersion increased FWHM values by more than 5% of the value for a 45 nL injection with TASF on. These results demonstrate experimentally the capability of TASF to focus all samples made in mobile phase despite a large pre-column void and modest focusing temperature of 5 °C.

While the guidance from the theory is quite good, there are discrepancies between the predicted and experimental results. For example, the predicted benefit of TASF for small volume injections and low k' solutes is better than we realize experimentally. One factor is our uncertainty about the variance contributed by the void. This variance is most important for low k' compounds. Another factor is our lack of knowledge of the actual temperature inside the column. We model the changes in temperature as a step function, but they are actually not. In addition, the temperature changes are initiated by a manual switch. We are in the process of addressing these limitations.

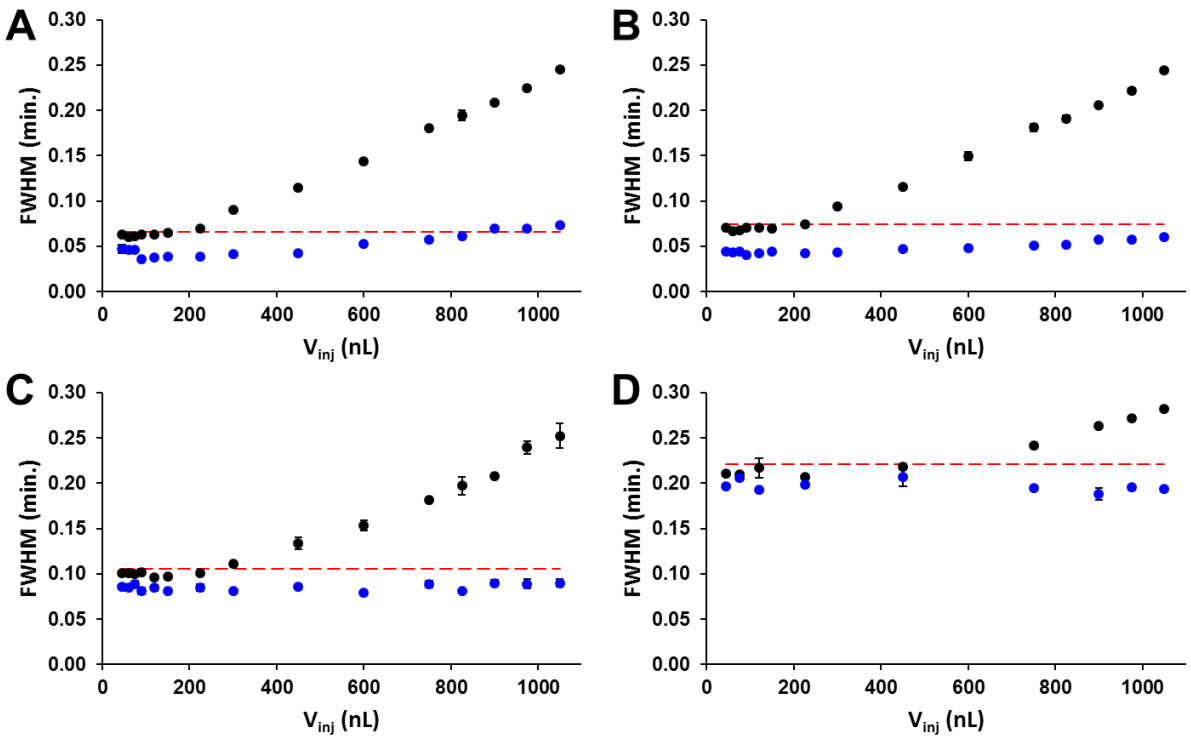

Figure 2.5. Results from volume overload experiments performed under isothermal (●) and TASF (●) conditions with paraben mixtures made in mobile phase. Panels A, B, C, and D correspond to methylparaben through butylparaben peaks, respectively. Red dashed lines represent a 5% increase in the FWHM for a 45 nL injection for each solute. TASF was able to reduce observed FWHM values relative to its isothermal counterpart for every solute at each injection volume.

2.4.4 Improvements in concentration detection limit offered by temperature-assisted solute focusing

As part of our initial assessment of the practical implementation of the TASF approach, we evaluated improvements in the concentration detection limits for the targeted determination of ethylparaben. Assuming constant peak area, reductions in observed peak width due to TASF result in taller peaks with enhanced S/N ratios. To demonstrate our ability to model the effect of TASF and realize the benefits in practice, an experiment was designed to address the following question. Knowing the signal required to be 10-times the standard deviation of the baseline, can you quantitate an injection using TASF to create a narrow peak at the detection limit from a volume overloaded injection at a concentration well below the isothermal detection limit?

In this example the standard state retention enthalpy for the target analyte, ethylparaben, was experimentally determined. Its retention factor and elution velocity in the 5 °C, 7 mm long trapping section at a flow rate of 3 μL/min were calculated to be 18.0 and 0.15 mm/s. For effective focusing, the leading edge of the ethylparaben band must remain within the trapping zone, i.e. not elute from the trap during the focusing time. This condition places a limit on the maximum allowable injection volume given the defined trap length and temperature. Assuming no dispersion from either the leading or trailing edges of the ethylparaben band it will take 7 s for the leading edge of the band to reach the trapping zone and a further 47 s for it to reach the end of the trapping zone. The total injection time is thus 54 s. The presence of dispersion and other nonidealities of our model will cause the band's front edge to reach the end of the trapping zone in a time shorter than 54 s. Experimentally, a focusing time of 45 s was used with an injection time of 37.5 s (1875 nL).

The chromatograms in Figure 2.6 show the results for two injections of ethylparaben under isothermal (black traces) and the optimized ethylparaben TASF conditions (blue traces). Panel A

shows a 60 nL injection of 1.25 μM ethylparaben in mobile phase with a 30 s focusing time. Due to the 1.2 s long injection required to achieve a 60 nL injection volume, increasing the focusing time to 45 s to accommodate larger injection volumes was unnecessary. The red dashed line is at an absorbance value equal to ten times the standard deviation of the baseline noise. The 60 nL injection was designed to act as a control and establish the detection limits for the TASF separations. The detection limit for ethylparaben using the TASF approach and a 60 nL injection was 7.5×10^{-14} moles. Panel B shows a more powerful demonstration of TASF's ability to improve concentration detection limits. To highlight this, the time axes of panels A and B were plotted to roughly center the ethylparaben peaks for isothermal and TASF separations, while the length of each window was held constant at 0.8 minutes. Increasing focusing time and injection volume resulted in an increase in ethylparaben retention time and peak width. Ethylparaben concentration in the 1875 nL sample was 100 nM, 1.9×10^{-13} moles on-column. The most impressive aspect of the TASF methodology came from the comparison of the 1875 nL isothermal and TASF separations. A red arrow is used to highlight what we believe to be the severely broadened ethylparaben peak which is not distinguishable from the baseline noise. The isothermal column is clearly volume overloaded. Only using TASF we were able to focus the large volume sample, nearly three times the fluid volume of the column, to achieve a quantifiable peak. This ability reduced the concentration detection limits for this analysis by a factor of 12.5, relative to the 60 nL injection.

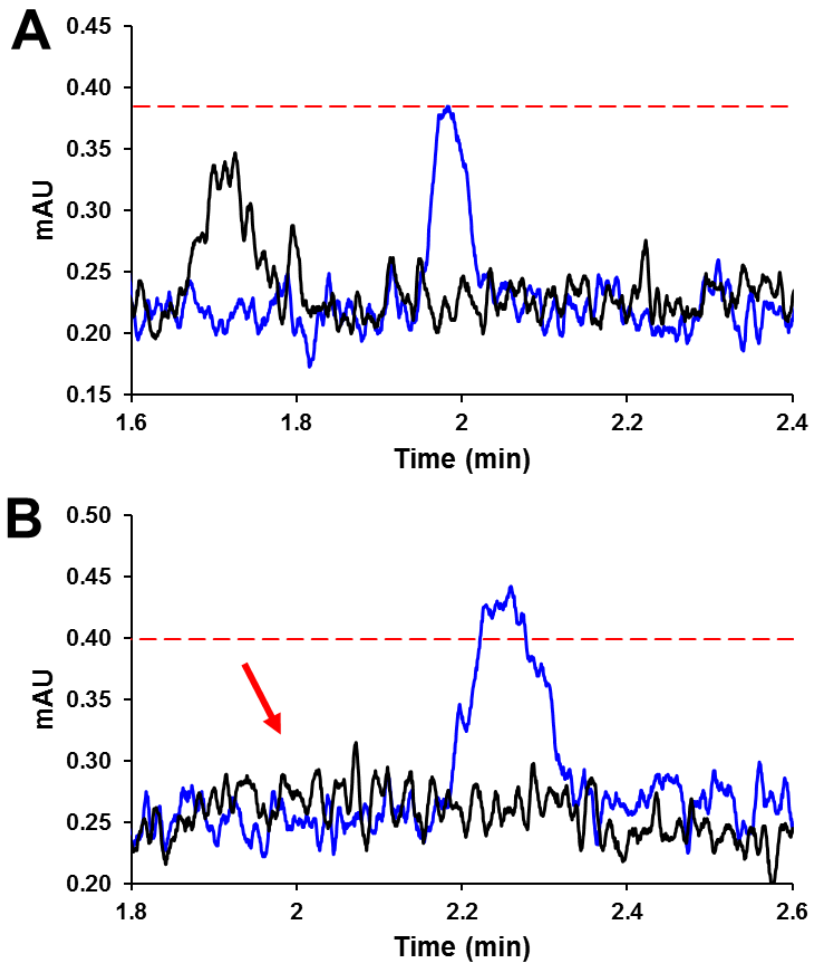

Figure 2.6. Chromatograms from the limit of quantitation study performed following optimization of TASF conditions for the separation of ethylparaben. Ethylparaben concentrations for 60 nL (A) and 1875 nL (B) injections were 1.25 μM and 100 nM. These concentrations were selected to be just above the detector's limit of quantitation, shown by red dashed lines. The TASF approach offered reductions in peak width and increases in peak height making previously unquantifiable isothermal analyses (——) quantifiable when implementing TASF (——). The red arrow in panel B shows what we believe to be the isothermal ethylparaben peak.

2.5 CONCLUSIONS

We have investigated the efficacy of temperature assisted on-column solute focusing to ameliorate all sources of pre-column dispersion and their associated reductions in column efficiency. The primary advantages to TASF for inducing efficient on-column focusing are as follows.

1. The approach effectively mitigates increases in peak width introduced by injecting large volumes of samples dissolved in solvents matching the mobile phase. TASF is orthogonal to solvent-based focusing methods allowing its use to replace or augment solvent-based methods.
2. A variance based model facilitates accurate *in silico* simulation of TASF separations based on solute retention enthalpies, focusing temperature, focusing time, and column parameters.
3. Optimized TASF analyses will decrease the concentration detection limit when large volumes with respect to the void volume are injected.

Potential applications of TASF: 1. continuous, online microdicodialysis sampling of for the rapid quantitation of neurotransmitters [90-92] where large aqueous samples are injected onto a capillary column operated with less than 5% acetonitrile in the mobile phase and 2. re-focusing fractions of first dimension effluent sampled and injected onto the second dimension column in capillary online comprehensive two-dimensional liquid chromatography, LCxLC [93].

3.0 TEMPERATURE-BASED ON-COLUMN SOLUTE FOCUSNG IN CAPILLARY LIQUID CHROMATOGRAPHY REDUCES PEAK BROADENING FROM PRECOLUMN DISPERSION AND VOLUME OVERLOAD WHEN USED ALONE OR WITH SOLVENT-BASED FOCUSING

The contents of this chapter were previously published in: Groskreutz, S. R., Horner, A. R. and Weber, S. G. Journal of Chromatography A, **2015**, 1405, 133-139.

Reproduced with permission from Elsevier.

3.1 INTRODUCTION

When sample volumes are small and quantitative analysis of low-concentration analytes is the goal, it is generally advantageous to use capillary liquid chromatography [35]. The advantage arises from the fact that the use of capillary columns minimizes the dilution of the analytes [18, 94]. With a concentration-sensitive detector, concentration detection limits improve as the injected volume of the sample increases or the column diameter decreases up to a point, however volume overload results when the injection volume contribution to observed bandspreading becomes significant [44, 95]. This contribution of the injected volume to bandspreading is dependent on the solute retention factor in the sample solvent. If retention is low, injection-related band spreading can be significant. Volume overload effects are lower for highly retained solutes. Thus, injecting aqueous samples onto a reversed phase column can be effective at eliminating volume overload as solutes are retained well while the sample solvent is temporarily acting as the mobile phase. This concentration effect is termed solvent-based on-column focusing and is a simple solution to the volume overload problem [48, 94].

Temperature also affects retention. Typically in reversed-phase liquid chromatography retention increases as temperature decreases [68, 96]. Thus, as we have recently shown [97], temperature-based on-column solute focusing (TASF) can be used to minimize the volume overload problem. TASF works by maintaining a temperature of a short segment (e.g., 1 cm) at the head of the column well below the rest of the column temperature for the time period during the injection. Following sample loading and analyte focusing due to increased retention, the temperature of the column (focusing) segment is rapidly heated to match the rest of the column. TASF should be most effective with capillary-scale columns because of their low thermal mass and small radius. The former permits rapid temperature changes while the latter is responsible for rapid relaxation of thermal gradients in the column.

Previously, the Greibrokk group exploited sub-ambient column temperatures to focus large-volume samples of retinyl esters, polyolefin based Irganox antioxidants and ceramides onto the head of capillary columns [76-80]. High solute hydrophobicity and poor solubility in water necessitated the use of neat acetonitrile mobile phases. Temperature was left as the only variable to enhance focusing and control elution. They initiated temperature programs (for the entire column) at sub-ambient temperatures, ca. 5 °C, to focus these solutes in samples made in 80-100% acetonitrile. Later Holm et al. developed a column oven with separate hot and cold zones where a capillary column was moved in-space from the cold zone to a hot zone following temperature-assisted online preconcentration of Irganox samples dissolved in acetonitrile [81]. Eghabali et al. also used temperature to enhance detection sensitivity in capillary LC [83]. In this approach a 1 cm long segment of column near the *outlet* was cooled cryogenically to -20 °C to trap and re-focus specific proteins within defined regions of the chromatogram. Following focusing, boiling water

was used to heat the nitrogen gas flowing around the cooled segment to rapidly release focused bands in targeted regions of the chromatogram.

In our previous work [97], we demonstrated that TASF decreases volume overload significantly when the sample is prepared in a liquid with the same composition (chromatographic strength) as the mobile phase. Here, we demonstrate that TASF is also effective in isocratic elution: 1) when the sample solvent is weaker than the mobile phase, and 2) when the sample solvent is stronger than the mobile phase. In the former case, TASF and solvent together dictate the k' of the solutes during the injection. In the latter case, TASF makes it possible to inject large volumes. Among other technical improvements to the TASF system, we have also automated its control and we demonstrate here its reproducibility in controlling column temperature and focusing for large volume samples.

3.2 MATERIALS AND METHODS

3.2.1 Reagents and solutions

Methyl, ethyl, and *n*-propyl esters of *p*-hydroxybenzoate (parabens) were purchased from Sigma-Aldrich (St. Louis, MO). Standard solutions of each paraben were prepared by first dissolving in acetonitrile (AN), then diluting to the desired concentration and solvent composition with deionized water (DI). Galanin (1-29) (rat) was obtained from Tocris Bioscience (Ellisville, MO). DI water was from an in-house Milli-Q Synthesis A10 purification system (Billerica, MA) and used without further treatment. Phosphoric acid (HPLC grade) and LC/MS grade acetonitrile were from Fisher Scientific (New Brunswick, NJ). Trifluoracetic acid (HPLC grade) and uracil were also from Sigma-Aldrich.

3.2.2 van`t Hoff retention studies using commercial columns

3.2.2.1 Chromatographic instrumentation

A Jasco X-LC system composed of a 3059AS autosampler, dual 3085PU pumps, 3080DG degasser, 3080MX high pressure mixer, CO-2060 thermostated column compartment, 3177UV variable wavelength UV absorbance detector and LC-Net II/ADC from Jasco Inc. (Easton, MD) was used to evaluate the temperature dependence of solute retention. Instrument control and data analysis was achieved using EzChrom Elite software (version 3.2.1, Agilent Technologies, Santa Clara, CA)

3.2.2.2 Chromatographic conditions

A total of three van`t Hoff retention studies using a commercially available 1 mm I.D. Waters Acquity BEH C18 column (50 mm x 1.0 mm I.D.; 1.7 μm d_p; Waters Corp., Millford, MA). were performed for methylparaben, ethylparaben, and propylparaben Solute retention enthalpy values were determined for mobile phases consisting of 70:30, 80:20 and 90:10 (10 mM H_3PO_4, pH 2.7: AN). Column temperature was varied from 25 to 65 °C in 20 °C steps. Samples of 15 μM uracil and 25 μM of each paraben were made at each mobile phase composition. The injection volume was 1.0 μL, flow rate was 0.1 mL/min, and peaks were detected by absorbance of UV light at 220 and 254 nm. Injections were performed at each temperature in triplicate. Extra column time was determined by replacing the column with a zero dead volume union.

3.2.3 Second generation TASF instrumentation and chromatographic conditions

3.2.3.1 Column preparation

Capillary columns used in all TASF experiments were prepared by packing either Acquity BEH C18 or Acquity CSH C18, 1.7 μm particles (Waters) into 100 or 150 μm I.D. fused-silica

capillaries from Polymicro Technologies (Phoenix, AZ). Columns were fritted using an electrical arc to sinter 2 μm solid borosilicate spheres (Thermo Scientific, Fremont, CA) into the end of the column blank. Particles were slurried, 65 mg/mL, in isopropanol and sonicated for 20 minutes prior to packing using the downward slurry method. Fritted blanks were placed into an ultrahigh pressure column packing fitting adapted from that previously described [98]. A model DSF-150 pneumatic amplification pump from Haskel (Burbank, CA) was used to pack columns at 20,000 psi for 20 minutes. Acetone was used as the packing solvent. Defined length columns, ca. 4.5-6.5 cm, were packed by controlling the mass of particles loaded into the packing reservoir. The remainder of the capillary blank was packed with 8 μm solid silica spheres (Thermo) for an additional 20 minutes at 20,000 psi. The silica spheres were slurried at a concentration of 100 mg/mL in a mixture of 50:50 (v/v) isopropanol/water.

3.2.3.2 TASF instrumentation

A 3D rendering of the TASF instrumentation is shown in Figure 3.1. A Thermo Scientific Ultimate 3000 RSLCnano high pressure gradient pump (NCS-3500RS, Germering, Germany) was used to deliver mobile phase. System pressure was monitored using an externally mounted pressure transducer (DF2-SS-01-15000, DJ Instruments, Billerica, MA). The outlet of the pressure transducer was connected to a Cheminert injection valve (C72x-669D, VICI Valco, Houston, TX) via a 75 μm x 35 cm fused silica nanoViper capillary (Thermo). A second 75 μm x 65 cm nanoViper capillary, fluidic volume of 2.9 μL, was used as the sample loop. (Note that all injection volumes were dictated by precisely controlling the period of time the injection loop was in the path of the column.) The sample loop was loaded by flow from the Ultimate ternary loading pump and an HP1050 autosampler (Agilent, Waldbronn, Germany). The autosampler injection volume was set to 75 μL and loading pump flow rate was adjusted to ensure that each sample was introduced

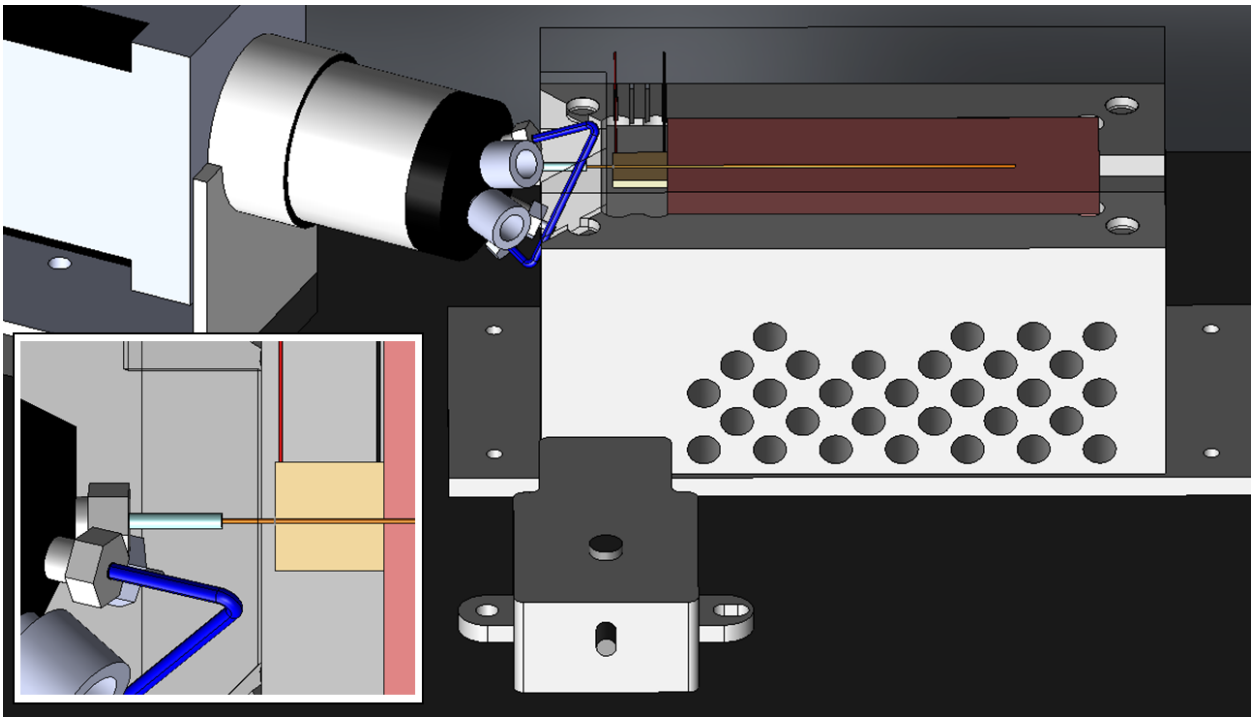

Figure 3.1. Schematic of instrument used to implement the TASF approach. TEC and resistive heaters are shown in gold and red. A loading pump and an autosampler introduced successive samples into a loop connected to the injection valve. Packed void columns were laid on top of the focusing segment and connected directly to the valve. The outlet of the column was connected to the inlet of the detector flow cell using a Teflon sleeve. The insert shows a top- down view of the injection valve and focusing segment of the column.

into the nanoViper injection loop during the previous run. Capillary columns were fitted directly to the injection valve and the column outlet was connected to an Acquity TUV detector fitted with a 10 nL flow cell (Waters). Data acquisition at 25 Hz was achieved via connection of the analog output of the Acquity TUV to the Jasco ADC described in the van`t Hoff studies. Analysis was performed in MATLAB (MathWorks, Natick, MA) using a simple peak finding algorithm to automatically find and measure peak full width at half maximum (FWHM). The MATLAB script used to determine FWHM is provided in Appendix B2.3.

Temperature-based focusing was achieved using a 1.0 x 1.0 cm Peltier thermoelectric cooling element (TEC) from Custom Thermoelectric (part number 04801-9G30-34RB, Bishopville, MD). To enhance heat transfer between the TEC and the column a gallium-indium eutectic was used at the interface between the TEC and column. An Agilent E3646A DC power supply was used to drive the TEC. TEC temperature was set manually by adjusting the current delivered by the power supply at fixed potential. A Type T thermocouple (COCO-003, Omega, Stamford, CT) fixed to the surface of the TEC was connected to a National Instruments 9213 16-channel high speed thermocouple input module (Austin, TX). TEC polarity was changed using a simple electronically controlled relay circuit. The TEC was mounted to a custom aluminum, liquid cooled heat sink. A Kryo-Thermostat WK 5 chilled circulator (Lauda-Brinkmann, Delran, NJ) was used to pump an ethylene glycol/water mixture at 1 L/min through the heat sink.

The isothermal section of the column was heated resistively in a manner similar that used previously [92, 99]. Briefly, a Love Model 1500 proportional-integral-derivative (PID) controller (Dwyer Instruments, Michigan City, IN) was used to control a Kapton resistive heater (KHLV-103/10-P, Omega). The heater was attached to an aluminum block and an SA1-RTD temperature sensor (Omega) was used to monitor temperature.

Instrument control and acquisition of temperature and pressure profiles was collected at 10 Hz using a simple LabVIEW program (National Instruments) written in-house. The injection valve and TEC polarity were also controlled using LabVIEW via an NI 9403 digital I/O module, pressure and HP1050 autosampler remote start signals were monitored using a NI USB-6008 DAQ.

3.2.3.3 TASF reproducibility study

To evaluate the instrumental improvements and assess the speed of column temperature and pressure transients, an eighty-five injection sequence was performed. The column was an 8.9 cm-long, 150 μm I.D capillary packed with 1.7 μm Acquity BEH C18 particles in the downstream 6.5 cm. The 2.4 cm segment of the column at the inlet, which is inside the fitting holding it (see Figure 3.1) to the injection valve and also includes the space between the valve and edge of the TEC, was packed with 8 μm d_p solid silica spheres. We refer to such columns as "packed void" columns. In all subsequent references to column length only the length of the stationary phase is reported; a 2.4 cm packed void segment is assumed. Flow rate was 4.0 μL/min, the mobile phase was 75:25 10 mM H_3PO_4/AN and the detection wavelength was 254 nm. A focusing time of 35 s was used; T_1 and T_2 were set to 0 and 65 °C, respectively. Each run was set to 10 minutes (an 11.5-minute total cycle time including time for 1050AS to perform the injection) with the whole experiment lasting 975 minutes.

3.2.3.4 Injection volume study

To replicate the results of our previous work with the new TASF system a series of ten timed injection volumes in the range of 30 to 750 nL were made in triplicate with and without TASF. The column was an Acquity BEH C18 packed void column, 4.7 cm x 150 μm I.D, 1.7 μm d_p. Flow rate was 4.5 μL/min, the mobile phase was 80:20 10 mM H_3PO_4/AN and the detection wavelength

was 254 nm. Column temperature was 70 °C. TASF separations employed focusing temperatures of 5 °C, focusing times of 15 s. Samples were made in mobile phase. Table B2.2 provides details regarding injection volumes and sample concentrations used.

3.2.3.5 Solvent- and temperature-focusing injection volume study

The complementary nature of solvent- and temperature-based on-column focusing was demonstrated for injection volumes ranging from 100-2000 nL. Isothermal and TASF injections of uracil, methylparaben, ethylparaben, and propylparaben were made in triplicate with sample compositions of 80:20 (matching the mobile phase) and 95:5 10 mM H_3PO_4/AN to evaluate the effect of solvent- and temperature-based focusing when both focusing techniques were used together. An Acquity BEH C18 packed void column as described in Section 3.2.3.3 was used. The fluidic volume of the column, excluding the packed void, was estimated to be 450 nL. The flow rate was 3 μL/min; the mobile phase and detection wavelengths were the same as Section 3.2.3.4. Column and focusing temperatures were reduced to -5 and 62.5 °C to enhance temperature-based focusing. To accommodate the larger injection volumes, the focusing time was increased to 45 s. Table B2.3 provides details about the injection volumes and sample concentrations used.

3.2.3.6 TASF applied to increasing the sensitivity for the peptide galanin

Isothermal and TASF separations were performed on samples of 100 nM galanin prepared in 80:20 water/AN. Injection volumes of 500 nL were made onto a packed void Acquity CSH C18 column (6.0 cm x 100 μm I.D., 1.7 μm d_p) with the mobile phase composition set to 85:15 0.1% trifluoroacetic acid/AN. Flow rate and detection wavelength were 0.85 μL/min and 214 nm, respectively. Isothermal separations were performed at 65 °C. TASF separations utilized focusing temperatures of -10 °C and focusing times of 40 s.

3.3 RESULTS AND DISCUSSION

3.3.1 Temperature dependence of retention factors

A commercially available Acquity BEH C18 column was used to determine retention factors under the various solvent and temperature conditions used in TASF experiments. Retention factors were corrected for extra-column volume using Eq. B2.1 in Appendix B. Partial molar enthalpies (Table B2.1) for each solute were determined from the van`t Hoff plots shown in Figure B2.3 (Eq. B2.2), using retention data collected over the 25-65 °C temperature range. Residual plots showed no evidence of significant curvature, thus there was no substantial change in retention enthalpy with temperature. We took advantage of this linearity to extrapolate retention factors to sub-ambient column temperatures.

3.3.2 TASF instrumentation

We improved the technical capabilities of the TASF system by adding electronic control with data logging, and incorporating the TASF system into the instrument control process of a commercial autosampler. In addition, the physical apparatus is now robust and easily incorporated into a capillary chromatography system. Figure 3.1 is a 3D rendering of the arrangement of the valve, column, TEC, resistive heater, pressure transducer, and other related components of the TASF system. The inset panel shows the placement of the TEC and capillary column. The TEC (1.0 cm x 1.0 cm x 1.6 mm, shown in gold) was mounted to a custom aluminum heat sink fit inside a PVC fixture machined to hold the TEC-heat sink assembly and resistive heater for the downstream separation segment of the column. The resistive heater (shown in red) used to heat the separation segment of the column was maintained at constant temperature (T_2) throughout the run. The TEC changes the column temperature of the focusing segment from T_1 to T_2 and back again. It is clear

from the inset panel of Figure 3.1 that the majority of the thermal mass requiring the temperature change is within the TEC, not the 360 μm O.D. column. Therefore, selection of a thin (low thermal mass), high power TEC is desirable for rapid temperature changes from T_1 to T_2. The TEC is rated at 10.9 W, significantly more powerful than the TEC (6.3 W) used in our previous work [97] and is capable of changing temperatures of the focusing segment by approximately 60-70 ^{o}C (T_2 - T_1). The operator can choose actual T_1 and T_2 values according to the need. For example, to concentrate samples with low retention solutes (at the column temperature and in the sample solvent), a low T_1 would be appropriate to increase focusing and decrease volume overload. However, there is an attendant limitation on how high T_2 can be when T_1 is low. If the desire is for high column temperature, then a higher focusing temperature (T_1) can be used, but this is accompanied by the need to inject smaller volumes to avoid volume overload for the lower retention solutes.

To realize the benefits of TASF, solutes must arrive at the cooled trapping segment at the same time. Thus, in our earlier work we advocated leaving the first ca. 2 cm of capillary – the portion located within the injection valve and fittings – unpacked. The same concept was applied in the work of Holm et al. work using temperature-based focusing with Irganox antioxidants [81]. This void introduced a pre-column volume of more than 350 nL for the 150 um I.D. columns used in our work. The void added significantly to pre-column dispersion and introduced a time delay on the order of 5 s to the separation. To address these problems, we created so-called “packed void” capillary columns. First, the column blank was packed with stationary phase to the desired length. Then the remainder of the capillary was packed with non-interacting solid silica spheres. The silica spheres do not contribute to retention; they act only to fill up the empty space in front of the column. Packing the void reduces the pre-column volume by roughly 65% to 120 nL. Reduced

pre-column volume shortened the time delay, but more importantly the particles significantly reduce pre-column dispersion seen in the absence of temperature- or solvent-based focusing.

To demonstrate the effectiveness of the TASF instrumentation for routine separations and evaluate the speed of column temperature and pressure transients an overnight injection sequence was performed consisting of eighty-five injections. Each run was 10 minutes; cycle time was 11.5 minutes when accounting for the autosampler injection time. The whole sequence lasted just over 16 hours. Figure 3.2 shows overlays of focusing temperature and column pressure. The colored overlays correspond to the first TASF separation performed in the sequence. Black temperature and pressure traces represent traces from the last injection. There are no visible changes in the pressure profile and a minimal deviation between the first and last temperature profiles over the course of the sequence. TEC temperature reached 90% of the set value (58.5 °C) in 5.6 s; this corresponds to a temperature gradient of 625 °C/min. Column pressure transients mirrored those for temperature with minimal time lag. This is due to the low thermal mass and high thermal conductivity of fused silica capillaries [100]. We refer interested readers to Appendix B2.2 for further discussion regarding TASF instrumentation.

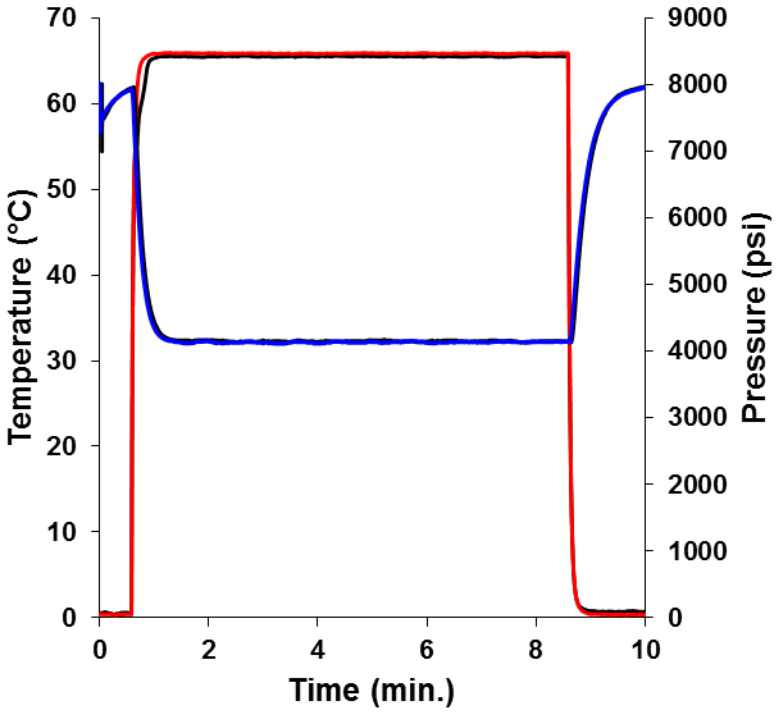

Figure 3.2. Focusing segment temperature profiles are shown in red (——) and column pressure traces in blue (——) for the first TASF separation performed in the 85 injection sequence. Black traces (——) show temperature and pressure profiles for the last TASF separation in the sequence. Column temperature was 65 °C, focusing temperature was 0 °C; the focusing time was 35 s.

3.3.3 Effect of TASF on peak width

Figure B2.4 (see Appendix B) shows representative chromatograms with and without TASF for small (30 nL) and large (750 nL) injections of parabens prepared in mobile phase. Figure B2.5 shows measured peak width at half height for each solute as a function of injection volume. Solute retention factor dictates how susceptible an analyte is to volume overload. Here, we have chosen solutes and conditions to give a range of 3.0 (methylparaben) < *k'* < 17.5 (propylparaben; ethylparaben has a *k'* of 7.1) at T_2 = 70 °C. The data show that for this range of practically useful isocratic retention factors, TASF alone can be effective. At the 5 °C focusing temperature retention factors for each solute are greater: 11.7, 32.0 and 99.4, respectively. (Retention factors were calculated based on the van 't Hoff studies detailed in Section 3.2.1. For further details, see section B2.1 of Appendix B.) Under these conditions, TASF is able to limit the increase in FWHM to 5% for injection volumes up to nearly 100% of the column volume (450 nL) for methylparaben and 165% for ethylparaben and propylparaben. These data are similar to our published data [97] confirming, as expected, that technical changes did not alter the essential function of the TASF device.

3.3.4 Combination of solvent- and temperature-based on-column solute focusing

Figure 3.3 shows results from the large-volume injections performed under isothermal and TASF conditions with paraben samples prepared in 80:20 and 95:5 10 mM H_3PO_4/AN. These experiments were conducted to demonstrate the effectiveness *the combination* of solvent- and temperature-based on-column focusing can have to limit increases in peak FWHM for sample volumes up to 450% of the column volume. Panels A, B, and C present results for methylparaben, ethylparaben, and propylparaben, respectively. Error bars are the standard error for each measured FWHM, with n = 3.

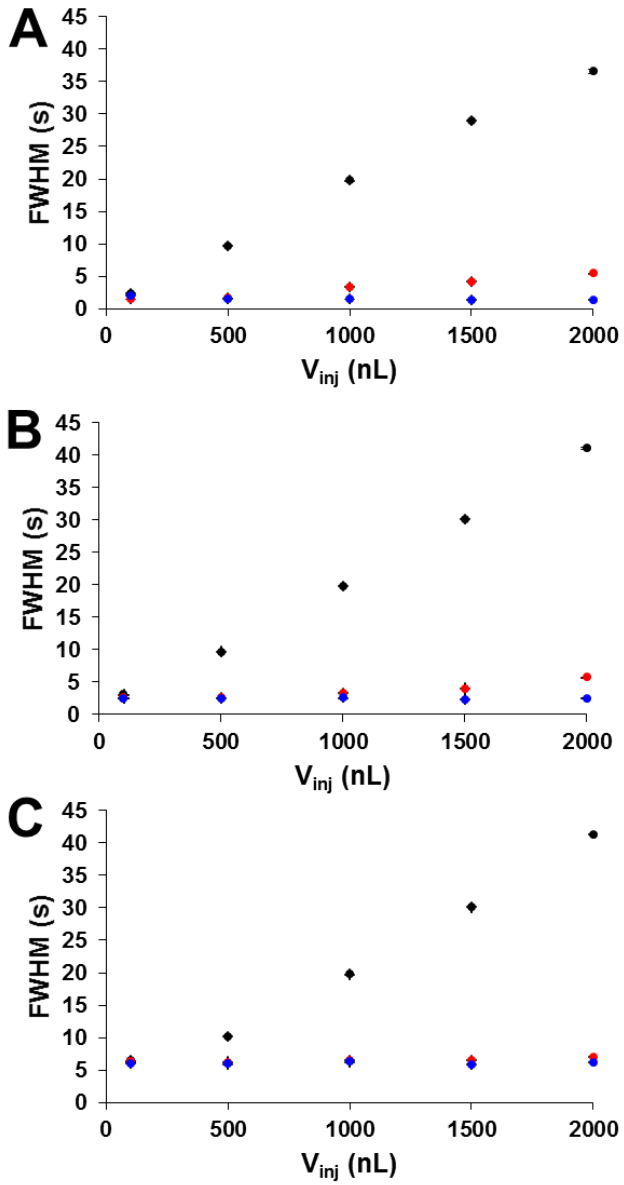

Figure 3.3. Peak width vs. injection volume for solvent- and temperature-based focusing made under isothermal and TASF conditions. Panels A, B, and C correspond to methylparaben through propylparaben peaks, respectively. Black circles represent isothermal separations with sample made in mobile phase. Red, isothermal with samples in 95:5 phosphate/acetonitrile. TASF separations with samples made in 95:5 phosphate/acetonitrile are in blue.

The benefits of solvent-based on-column focusing are clearly evident from each panel of Figure 3.3. Observed peak width is reduced for every injection volume from 100 nL to 2 μL for each solute. For the 2 μL injections, representing a volume 450% of the column volume, peak width values for methylparaben, ethylparaben and propylparaben were reduced from about 40 s (injection width) when no solvent focusing was present to 5.5, 5.8, and 7.1 s, respectively when injecting samples made in 95:5 phosphate/AN. TASF and solvent focusing together reduced the influence of volume overload significantly. FWHM values for the 2 μL injection with solvent- and temperature-based focusing together were reduced to 1.4, 2.5, and 6.2 s.

Figure 3.4 shows an overlay for 2 μL injections under the three conditions described above. The black trace shows the result from injecting the paraben mixture made in mobile phase onto an isothermal column. Clearly, this is unsatisfactory chromatography. The red trace shows the same sample made in 95:5 phosphate/AN. As expected, chromatographic performance improves when using solvent-based focusing. Improvement is due to increased solute retention factors in the sample solvent at the head of the column. Note that injecting a nearly aqueous 2 μL sample onto the column still does not induce enough on-column focusing to generate a Gaussian peak for methylparaben. The ethylparaben peak is also significantly broadened. In principle, a completely aqueous sample would focus more effectively, but not all reversed phase materials perform well with an aqueous mobile phase. Atypical peak shapes may result for large volume aqueous injections. The blue trace shows that TASF augments the on-column focusing from solvent. Using a focusing temperature of -5 °C resulted in peak height increases by factors of 3.4 and 2.2 for methylparaben and ethylparaben relative to the solvent-focusing-only injection. *Better and more sensitive chromatography can result from using solvent- and temperature-based focusing together*.

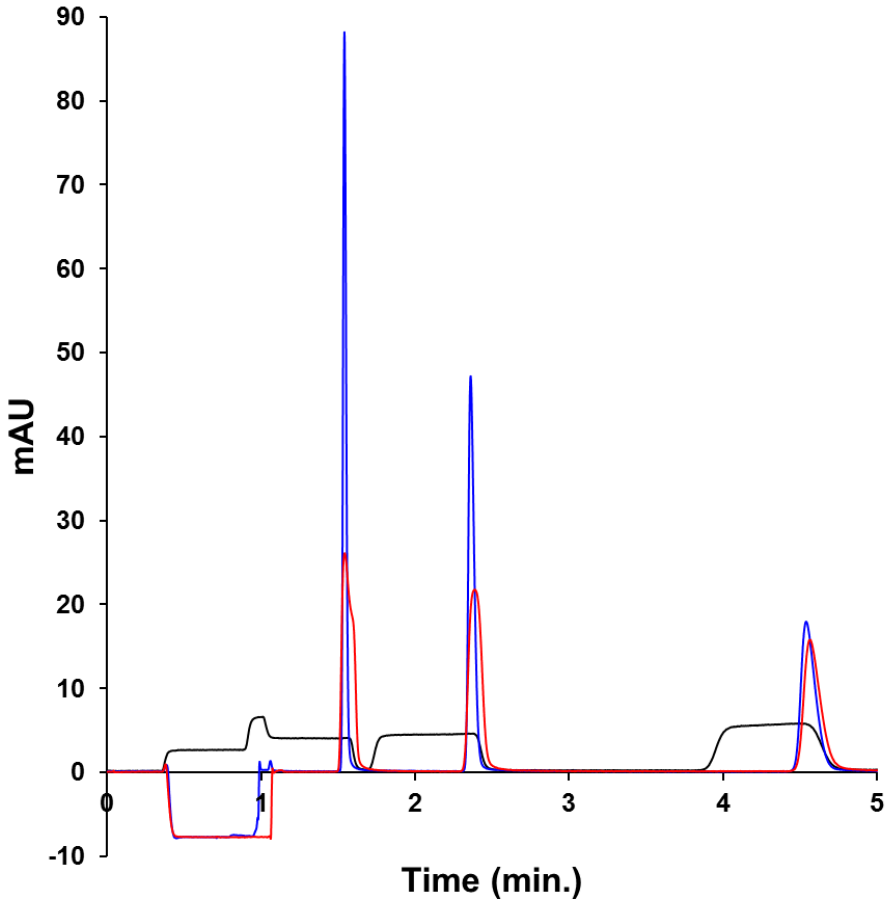

Figure 3.4. Chromatograms from the solvent- and temperature-based comparison. The injection volume was 2 µL. The isothermal no focusing example (——) was made in mobile phase. The solvent-based focusing example (——) was made in 95:5 10 mM H_3PO_4/acetonitrile. The TASF/solvent focusing sample was made in 95:5 (——).

3.3.5 TASF increases sensitivity for samples made in strong elution solvent

The problem of peptide adsorption to containers and other surfaces during analysis is a serious one [101]. Very frequently, a solution of a peptide prepared in an acidic organic/aqueous mixture yields less adsorption than purely aqueous solvents [14, 101-106]. While adsorption may occur within the LC instrument itself [102], here we are concerned with the stability of the solution prior to injection. Maes et al. [102] found that an acidic water/AN (87:13 v/v) solvent was best for a set of neuropeptides. Earlier, Vatansever et al. noted that acidic AN/water solvents were best for a series of peptides but the optimal concentration of acetonitrile, which was as high as 30%, depended on the peptide [103]. Amyloid peptides are best handled in *basic* water/AN 80:20 [104, 105], while calcitonin is stable in water/AN (43:57). Thus, very often analytical determinations of peptides must be carried out with a sample in a solvent with significant elution strength.

We have an interest in the peptide galanin and the products of its hydrolysis in the extracellular space of hippocampal tissue cultures [107, 108]. Our experimental protocol involves the use of electroosmotic flow to perfuse an organotypic hippocampal slice culture with a peptide at high (~300 μM) concentration and variable but low (10 - 25 nL/minute) flow rate. Over a 5-minute sampling time, we collect 50 – 125 nL of the perfusion solution containing peptide and hydrolysis products. This volume is diluted to 10 or 15 μL depending on the application [107-109]. The final concentration of galanin in the injected samples is a few micromolar. Zhou et al. [14] have found that galanin is most stable in an W/AN 80:20 solution. In this example the elution strength of the sample matrix is fixed at this composition and stronger than the 85:15 0.1% TFA/AN mobile phase. In principle, the sample could be diluted with water or an aqueous solution, however the point of using the acetonitrile-based solvent is to avoid losses by adsorption. Thus, dilution with an aqueous solution would be counterproductive.

TASF, on the other hand, should be capable of concentrating the injected peptide despite its relatively high organic content. Figure 3.5 shows the results for isothermal (black) and TASF (blue) separations of a 500 nL injection of 100 nM galanin dissolved in 80:20 W/AN onto a 250 nL volume column. Sensitivity is important to our galanin application. Thus we have selected a sample concentration to clearly demonstrate the potential for TASF-induced improvements in preconcentration. The red dashed line in Figure 3.6 indicates the detector's limit of quantitation calculated for an absorbance value required to be a factor of ten greater than the standard deviation of the baseline noise. The isothermal column temperature was 65 °C and the focusing temperature was -10 °C. Clearly, TASF improves preconcentration and detection limits for trace level peptide samples made in strong elution solvents.

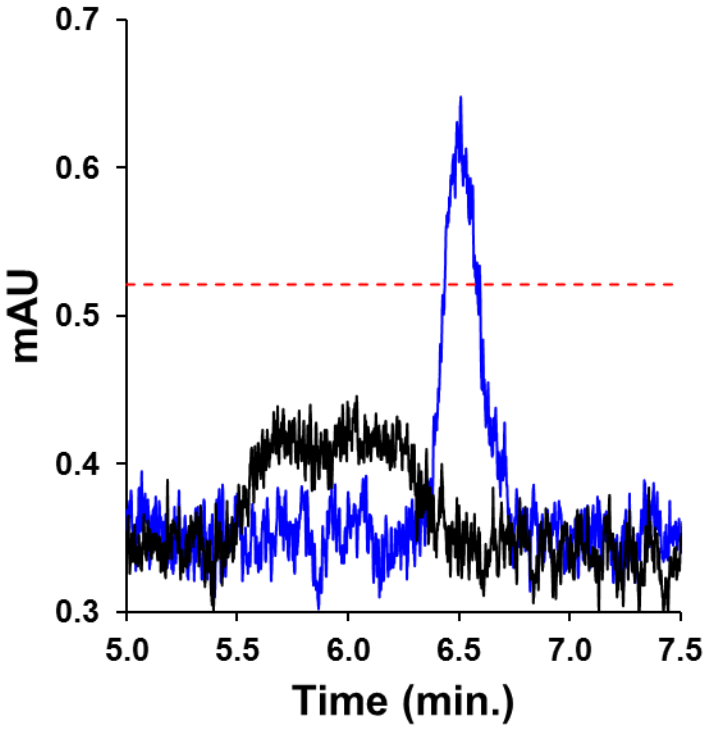

Figure 3.5. Chromatograms resulting from the application of TASF to increasing analysis sensitivity for the peptide galanin. Galanin samples were made in 80:20 water/acetonitrile and 500 nL samples were injected onto a 250 nL volume column operated with a mobile phase composition of 85:15 0.1% TFA/acetonitrile. Isothermal (——) column temperature was 65 °C. TASF (——). The red dashed line represents the detectors limit of quantitation. With a focusing temperature set to -10 °C peak height increased by a factor of 3, relative to an isothermal analysis.

3.4 CONCLUSIONS

This work demonstrates the utility of temperature-based on-column solute focusing to improve peak shape in capillary LC. We can draw the following conclusions:

1. Dispersion and the increase in apparent void time induced by the pre-column void necessary for effective implementation of TASF can be significantly reduced by packing the void with solid non interacting silica spheres.
2. The TASF system is robust; it can be easily incorporated into a modern automated instrument. It is capable of unattended operation for extend periods.
3. The combination of TASF with solvent-based focusing is very effective. The two focusing techniques are complementary, improving peak shape and analysis sensitivity for large volume samples.
4. TASF has the potential to focus large-volume samples made in solvents with elution strength greater than that of the mobile phase.

These results illustrate the potential of temperature to be used as an effective tool to enhance overall separation performance. They clearly demonstrate that TASF can be used independently or in conjunction with solvent-based on-column focusing to enhance analysis sensitivity and separation efficiency in capillary liquid chromatography.

4.0 QUANTITATIVE EVALUATION OF MODELS FOR SOLVENT-BASED ON-COLUMN FOCUSING IN LIQUID CHROMATOGRAPHY

The contents of this chapter were previously published in: Groskreutz, S. R. and Weber, S. G. Journal of Chromatography A, **2015**, 1409, 116-124.

4.1 INTRODUCTION

In most analytical chromatographic analyses, the injected volume of sample is much smaller than the volume of mobile phase carrying a peak out of the column (the peak volume). In this case, the amount of sample injected affects the peak height linearly, but has no effect on the peak width. If the volume of sample injected is increased to enhance concentration detection limits, at some point the eluting peak will become broadened. This phenomenon is now termed volume overload. It is worth noting that a very accurate picture of this phenomenon was published in 1956 by van Deemter et al. using gas chromatography [3]. Sternberg later put this effect into rigorous mathematical terms by explaining that volume overload leads to a peak shape that is a convolution of the peak shape observed with a small-volume injection and the rectangular concentration-distance profile as injected [110]. The former can be determined from a small-volume injection. The latter comes from the fact that the length of the zone of solute on the column once the injection is complete is smaller by the factor $1/(1+k')$ than the length of the column occupied by the injected solvent. Further, Sternberg pointed out that the variance of the resulting peak was the sum of the variances of the two functions. It becomes a simple matter to calculate the maximum injected

volume that leads to an acceptable increase in peak width. Injecting this volume will lead to the highest concentration sensitivity with minimal (tolerable) impact on separation quality.

When the sample liquid is a weaker chromatographic solvent than the mobile phase, analyte retention on the stationary phase is higher, increasing the allowable injected volume in comparison to the allowable volume when the sample liquid is the mobile phase. This phenomenon, often called on-column focusing or preconcentration, is used routinely in capillary LC (cLC) where the injection of low nL-scale volumes is required to avoid volume overload when injecting samples made in mobile phase [23-25, 63]. On-column focusing is not limited to cLC, it can be used to advantage with any size column [95, 111] or application from trace analysis to two-dimensional LC [112-118]. On-column focusing also happens quite often as a natural consequence of gradient elution chromatography because many solutes are highly retained in the relatively weak initial solvent composition as described by Snyder [119]. He described an additional effect that occurs in gradient elution, namely, the peak compression of the already focused band that results because the tail of the injected band moves with the stronger solvent for a longer time than the front of the band. As our current interest is in isocratic elution with on-column focusing followed by peak compression due to the introduction of the stronger mobile phase, we will discuss the problem in the context of a step gradient. Thus, there are two factors to consider in solvent-based on-column focusing: one relates to the retention factor of the solute as it is injected and the other is due to the compression occurring when the mobile phase is stronger than the injected sample's liquid. In the following discussion, we do not consider the case where mass overload contributes to bandspreading.

Several groups have contributed to the understanding of these phenomena. Snyder's work has been mentioned [21, 22]. Later, the Poppe group combined the on-column focusing and the step-

gradient-induced compression in the context of a precolumn trapping column/backflush for analytical work [120, 121]. They arrived at the simple result that the solute elutes from the column in a volume that is a factor k_2/k_1 smaller than the injected volume, where k_1 is the solute retention factor in the sample solvent and k_2 is the retention factor in the mobile phase. Here, for simplicity column dynamics-induced bandspreading was ignored. Hartwick, and subsequently the Desmet group found the same relationship for post-column peak trapping/concentration and elution [122-124]. The same relationship was found for preconcentration in CEC [125].

Mills et al. [48] also derived a factor for preconcentration resulting from the step gradient using a vaguely described function of k_1 and k_2 in Slais et al. [61]. Rather than finding the factor k_2/k_1 they found the factor $\left(\frac{1+k_2}{1+k_1}\right)^2$. This predicts rather large focusing effects. For instance, if $k_1 = 50$ and $k_2 = 5$, the former relationship predicts that the eluted volume would be 10 times smaller than the injected volume while Mills et al.'s relationship predicts that the eluted volume would be 72 times smaller than the injected volume.

Unfortunately, no quantitative evaluation of these relationships exists. The rationale for focusing is to increase sensitivity, so a natural quantitative test is to determine the sensitivity enhancement from these processes. Numerically, the sensitivity enhancement is the inverse of the ratios discussed in the last paragraph. However, peak height is strongly influenced by on-column bandspreading which depends on numerous phenomena. As a result, predicted sensitivity enhancements that do not take into account on-column dynamic bandspreading will be optimistic so they cannot themselves form the basis for a quantitative evaluation of a model. Another approach to testing these predictions is to calculate a volume that can be injected without significant volume overload and then test this experimentally. This approach requires a knowledge

of the number of theoretical plates, N, experienced by each solute in the absence of volume overload, a knowledge of the shape of the injected volume (in order to estimate its variance contribution to the overall peak variance), as well as a quantitative assertion of the fractional loss in N that the chromatographer is willing to accept. Because of these factors, this approach also cannot quantitatively confirm the expected result despite its significant practical significance.

In this work, we first recapitulate the simple theoretical derivation of the k_2/k_1 focusing factor. As described above, there are several extant publications reciting the same result. However, it is important to show clearly how this result occurs as a part of this discussion. We have designed an experiment in which we attempt to experimentally validate this relationship by measuring peak width rather than peak height. As the objective is to determine accurately the ratio of eluted volume to injected volume, we create eluted volumes significantly greater than the natural peak volume. This is in contrast to the work cited above where the objective was to demonstrate the utility of on-column focusing to enhance sensitivity in analytical determinations, not the validity of the model. Using accurately determined experimental retention factors and measurements of the injection band width we comment on the validity of the k_2/k_1 factor and its practical application to increase analysis sensitivity in liquid chromatography.

4.2 THEORY

4.2.1 Derivation of the k_2/k_1 factor

Consider a zone of solute of volume V_{inj} injected into a column. During the injection the relative volumes of the sample and the column suffice to cause the sample liquid itself to be the mobile phase transiently during sample loading. The discussion that follows will consider the on-column length occupied by the injected volume. Figure 4.1 illustrates the process schematically. At *t = 0*

a volume V_{inj} passes from the loop onto the column. The solute will occupy a length $\ell_1$on the column given by Eq. 4.1 in which the injection time, t_{inj} is multiplied by the average zone velocity. The former is V_{inj}/F where F is flow rate, while the latter is the determined by the average mobile phase velocity v_{mp} and k_1 the retention factor for the solute in the sample liquid acting as mobile phase.

$$\ell_1 = \left(\frac{V_{inj}}{F}\right)\frac{v_{mp}}{1+k_1} = t_{inj}\frac{v_{mp}}{1+k_1}$$

(4.1)

As the mobile phase passes through the sample band the step gradient that follows compresses the zone further. Additional compression results because the stronger elution strength mobile phase moves the tail of the zone for a longer time than it moves the front. We will thus determine how far the tail of the zone moves, $\Delta\ell_t$, and how far the front of the zone moves, $\Delta\ell_f$, in the time that it takes for the mobile phase to reach the front of the zone, t_1. Once the mobile phase reaches the front of the zone, there is no further compression by the step gradient. The time, t_1, that the mobile phase requires to reach the moving front of the zone is given by a distance into the column, ℓ_2, and the velocity v_{mp}. The distance ℓ_2 (Figure 4.1) is the initial length of the compressed zone plus the additional distance moved at the front,

$$\ell_2 = t_1 v_{mp} = \ell_1 + \Delta\ell_f$$

(4.2)

During time t_1, the front moves at a velocity $v_{mp}/(1+k_1)$. The distance the front moves in time t_1 is:

$$\Delta \ell_f = t_1 \frac{v_{mp}}{1 + k_1}$$

(4.3)

Replacing ℓ_1 in Eq. 4.2 with Eq. 4.1 and $\Delta \ell_f$ with Eq. 4.3 and rearranging leads to Eq. 4.4.

$$t_1 = \frac{t_{inj}}{k_1}$$

(4.4)

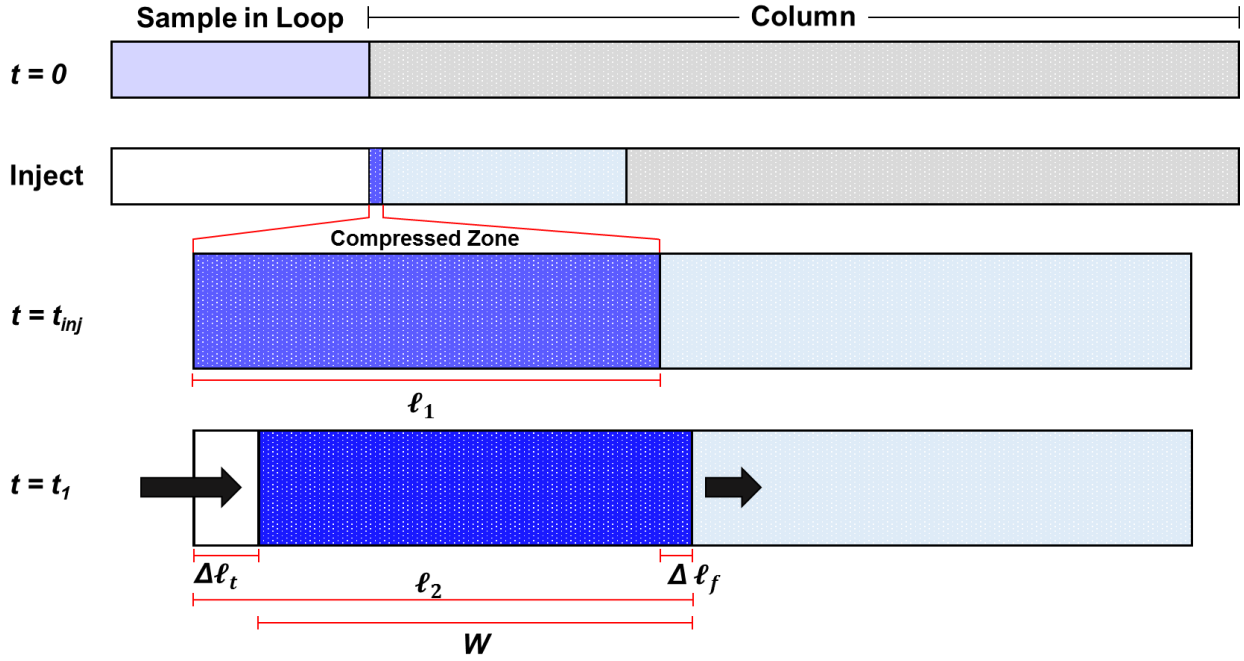

Figure 4.1. Schematic describing the effect of solvent-based on-column focusing. Compression of the injection zone results from the increased retention at the head of the column in the sample solvent and the step-gradient resulting from the higher elution strength mobile phase passing through the injection plug.

During this time, the front moves a distance equal to its velocity multiplied by t_1:

$$\Delta\ell_f = \frac{v_{mp}}{1+k_1}\frac{t_{inj}}{k_1}$$

(4.5)

As the tail moves at a velocity $v_{mp}/(1+k_2)$, the distance that it moves, $\Delta\ell_t$, is t_1 times this velocity:

$$\Delta\ell_t = t_1\ \frac{v_{mp}}{1+k_2} = \frac{v_{mp}}{1+k_2}\frac{t_{inj}}{k_1}$$

(4.6)

The width of the zone on the column is thus the initial width minus the distance traveled by the tail plus the distance traveled by the front:

$$W = \ell_1 - \Delta\ell_t + \Delta\ell_f$$

(4.7)

$$= t_{inj}v_{mp}\left(\frac{1}{1+k_1} - \frac{1}{(1+k_2)k_1} + \frac{1}{(1+k_1)k_1}\right)$$

(4.8)

When eluted, the band expands by the factor $(1 + k_2)$. The width in time of the eluted zone is thus

$$t_{obs} = t_{inj}\left(\frac{1+k_2}{1+k_1} - \frac{1}{k_1} + \frac{1+k_2}{(1+k_1)k_1}\right)$$

(4.9)

Simplification leads to the remarkably simple Eq.4.10, matching the factor derived by the groups mentioned above.

$$t_{obs} = t_{inj}\frac{k_2}{k_1}$$

(4.10)

We can break Eq. 4.10 down into two components, one from the initial focusing of the injected zone as shown in Eq. 4.1 and one from the compression that results. In the absence of this compression effect, the on-column width of the injected solute zone is given by Eq. 4.1. That on-column width remains unchanged in this compression-free model. Of course, bandspreading occurs, but here we just consider the volume overload portion of the problem. In addition, as explained below in Section 4.2.2, the zone width is somewhat independent of mass-transport-based bandspreading. When the zone is eluted, its width in time units, t_{obs}, is the length, ℓ_1, divided by the velocity which is now dependent on k_2.

$$t_{obs} = t_{inj}\frac{v_{mp}}{1+k_1}\frac{1+k_2}{v_{mp}} = t_{inj}\frac{1+k_2}{1+k_1}$$

(4.11)

By comparison of Eqs. 4.10 and 4.11, it can be seen that the effect of compression alone is

$$\frac{k_2}{k_1}\frac{1+k_1}{1+k_2}$$

(4.12)

In summary, the width in time of the eluted zone resulting from an injection large enough to create obvious volume overload is expected to be the factor k_2/k_1 times the injection time. This factor is the product of two factors. One is the initial band focusing due to retention of the solute in the

injected solvent, namely Eq. 4.11. The other is the factor due to compression of this zone by the step gradient, Eq. 4.12.

4.2.2 The eluted peak width is a robust measure of the on-column focusing effect

Our data treatment will compare the eluted width in time of obviously volume-overloaded peaks to the injection width in time. What is the best measure of "eluted width in time"? As Sternberg has explained [110] and Burke showed [126] the injection of a large volume leads to a "peak" that is the convolution of the transfer function of the chromatographic system and the injected concentration profile. This process is shown schematically in Figure 4.2; see figure captions for details. In the simplest case, the latter is a rectangular function, 4.2B. The transfer function of the chromatographic system (Figure 4.2A) is represented by the eluted concentration profile, or peak, resulting from an injection of a volume that is much smaller than the column volume. When the baseline width of the peak is smaller than the width of the rectangle, the eluted concentration profile has a flat top with its leading and trailing edges having a sigmoidal shape, 4.2C. When the peak is also Gaussian, the leading and trailing edges have the shape of an error function complement and error function, respectively (see Figures C3.4 and C3.5 in Appendix C for experimental examples). It is important to note that when the chromatographic transfer function is symmetrical and the eluted concentration profile has a plateau then the peak *width* at half height is independent of the chromatographic system transfer function. Thus, increasing the width of the transfer function, e.g., by greater on-column bandspreading, does not change the width at half height. On the other hand, the *variance* of the eluted band *does* increase as the bandspreading variance increases.

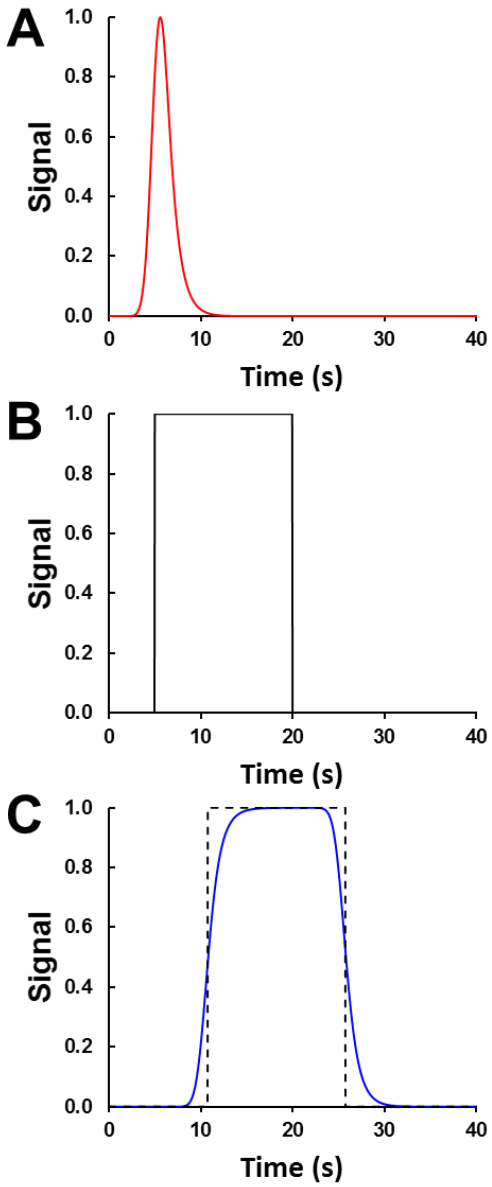

Figure 4.2. Simulated signals for the eluted injection profile corresponding to the convolution of the column transfer function and rectangular injection profile. Panel A shows an exponentially modified Gaussian signal resulting from on-column bandspreading (σ = 0.75 s, τ = 1 s, $\alpha_{5\%}$ = 2.8); panel B a 15 s wide rectangular injection profile. Panel C shows the peak shape resulting from the convolution of the signals in panels A and B in blue. The black dashed trace is used to overlay the 15 s wide injection profile on the convolved signal illustrating the potential utility of the half width metric to quantitatively evaluate the on-column focusing effect.

We demonstrate this in Figure 4.3. We created a series of exponentially modified Gaussians for which the standard deviation of the Gaussian, σ, was 0.75 s and the exponential time constant, τ, varied from 0.001 to 3 s. This led to a range of peaks with asymmetry factors (α) at 5% peak height from 1.00 to 7.6. Each simulated peak was convolved with a 15 s wide injection (as in Figure 4.2). Standard deviation and half width measurements were made on each profile and normalized to the values obtained from the nominally pure Gaussian (τ = 0.001 s), σ/σ_0 (black trace) and $FWHM/FWHM_0$ (red trace), respectively. From this simple demonstration it is clear that an accurate value of the injection width can be obtained for peaks with a flat top by measuring the FWHM. Experimentally, when we use lower V_{inj} or higher k_1, we do not obtain peaks with flat tops, but volume overload is still evident. In these cases, we have deconvolved the transfer function of the chromatographic system from the response to obtain the estimate of the elution profile without on-column bandspreading.

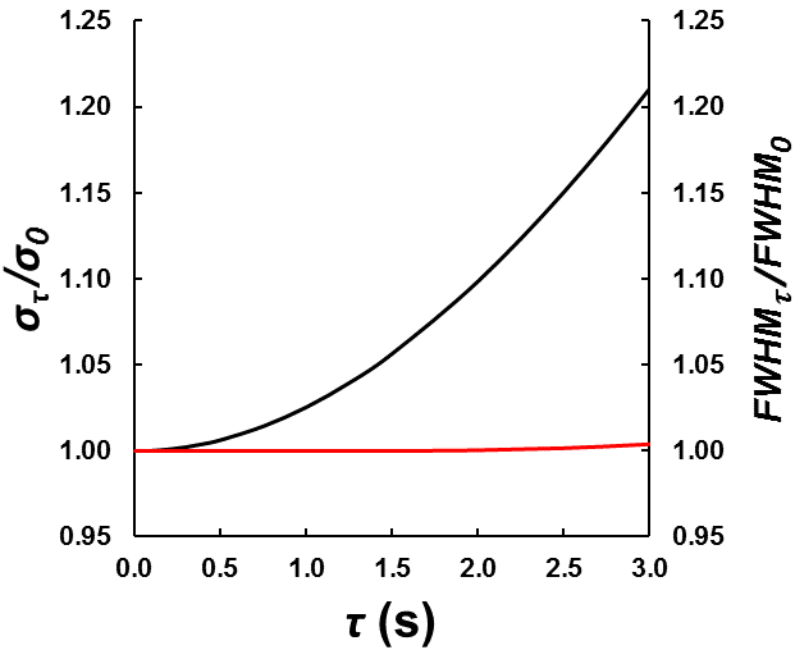

Figure 4.3. Influence of peak asymmetry on peak variance and half width for a series on exponentially modified Gaussians simulated using σ = 0.75 s, τ = 0.001 to 3 s, $\alpha_{5\%}$ = 1.00 to 7.6. Each Gaussian signal was convolved with a 15 s wide injection plug. Peak variances were calculated using the method of moments, half width measurements were made on each profile and each was normalized to the values obtained from the untailed Gaussian injection. The black trace shows the strong influence of peak tailing on the calculated band variance. The red trace highlights the rather small influence of peak tailing on the bands width at half height.

4.3 INSTRUMENTATION AND CHROMATOGRAPHGIC CONDITIONS

4.3.1 Chemicals

Methyl, ethyl, and *n*-propyl esters of *p*-hydroxybenzoate (parabens, notated here after as PB1, PB2, and PB3, respectively) and uracil were purchased from Sigma-Aldrich (St. Louis, MO). Standard solutions for parabens were made by dissolving each individually in acetonitrile. Uracil stocks were made in deionized water. Water was from a Millipore Milli-Q Synthesis A10 water purification system (Billerica, MA) and used without further treatment. Acetonitrile (LC/MS Optima grade), isopropanol (HPLC grade), acetone (HPLC grade) and phosphoric acid (HPLC grade) were from Fisher Scientific (Fair Lawn, NJ)

4.3.2 Instrumentation

Figure 4.4 shows a simple schematic for the instrumentation used. Waters 1.7 μm d_p Acquity BEH C18 particles (Milford, MA) were packed in-house into 150 μm ID x 360 μm OD fused-silica capillaries from Polymicro Technologies (Phoenix, AZ). Column length was 5.5 cm. The remainder of the column was packed with 8 μm solid silica spheres (Thermo). To determine the extra column time a nominally identical fused-silica capillary was packed with 8 μm solid silica spheres. We refer to this column as the *e-column*. For complete details related to column preparation see section C3.1 of Appendix C. The columns packed with stationary phase and 8 μm silica spheres (A) and the *e-column* (B) were connected directly to a 6-port Cheminert injection valve (C72-6676EH, VICI Valco, Houston, TX) using 1/16” OD x 0.015” ID PEEK sleeves (IDEX-Health and Science, Oak Harbor, WA). The additional 3.9 cm segment of each column allowed the unheated, room temperature segment of capillary (2.4 cm) located within the injection valve not to adversely influence the solute retention. In addition, 1.5 cm of the capillary served as

a mobile phase pre-heater. A 75 cm x 75 µm ID nanoViper capillary (volume = 3.3 µL, Thermo) was used as the sample loop. An Ultimate 3000 RSLCnano high pressure gradient pump (NCP-3200, Thermo, Germering, Germany) was used to deliver mobile phase. Detection was achieved using a Waters Acquity TUV detector equipped with a 10 nL flow cell (Waters) set to 254 nm. The column outlet and flow cell were connected by a 30 cm x 25 µm ID fused-silica detection capillary (Polymicro). Data acquisition and export were achieved by connecting the Acquity TUV analog output to an Agilent 1200 UIB (G1390B, Agilent Technologies, Waldbronn, Germany) and Agilent OpenLab ChemStation CDS software (rev. C01.06). Valve actuation was controlled by a National Instruments USB-6008 DAQ and a simple LabVIEW routine written in-house (rev. 2014, National Instruments, Austin, TX). Column temperature was controlled using a simple homemade resistive heating assembly previously described [92, 99]. Further details regarding instrument configuration and control are provided in Appendix C.

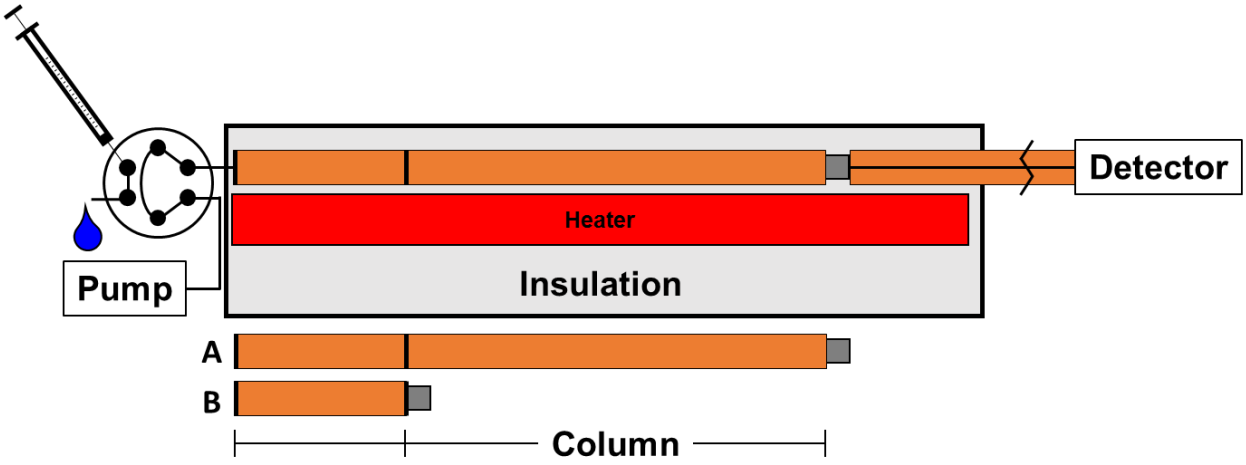

Figure 4.4. Diagram for the instrumentation used in this work. Two-segment capillary columns (A) consisting of non-interacting silica spheres and stationary phase were attached directly to the injection valve and placed inside a resistively heated insulated enclosure. To accurately determine

the extra-column contributions to t_0 injections were made into a so-called *e-column* (B). The *e-column* consisted of all portions of the two-segment column except the stationary phase.

4.3.3 Chromatographic conditions

Precise details related to the preparation of eluents and sample solutions used in this study are critical to interpretation of results. As a result, all samples and eluents were prepared gravimetrically in batches large enough to minimize irregularities in sample preparation and absolute mobile phase composition. Mobile phase was prepared by mixing acetonitrile and 10.0 mM H_3PO_4 in water at 5.0, 10.0, and 20.0% (wt%). The 5.0 and 20.0% acetonitrile mobile phases were made in 1.000 kg batches; the 10.0% solvent was prepared at the 0.500 kg scale. Mobile phase was degassed and filtered using 0.45 µm nylon membrane filters (Millipore) prior to use.

Paraben retention studies used 50 nL timed injections of 250 µM uracil, PB1, PB2, PB3 samples made in each mobile phase. Care was taken to maximize peak height by injecting the highest concentration sample without mass overloading the column. Stock solutions employed for retention studies were made at 200 mM in acetonitrile. Spikes, 125 µL, from each stock were made into 100.0 g volumes of premixed mobile phase to achieve desired solute concentration. For retention studies, differences between sample and mobile phase composition were kept less than 0.5%. This small composition difference was due to the additional acetonitrile present in the sample, from the three 125 µL paraben spikes.

Solvent-based focusing studies used large-volume, timed injections corresponding to 500, 1000, 1500, and 2000 nL. Samples were made using 100.0 g portions of the appropriate premixed mobile phase described above. Paraben concentrations were 10 µM each. Samples were prepared from 50

mM stock solutions made in acetonitrile (20 µL spikes). Thus, differences between sample and eluent composition were less than 0.1%.

The premixed mobile phase for retention and injection volume studies, 80:20 10.0 mM H_3PO_4/acetonitrile (wt%), was used as both solvent A and solvent B in the Ultimate 3000 pump. The flow rate was 4.00 µL/min with eluent composition set to 50:50 channel A/B. Column temperature was maintained at 60.0 ± 0.1 ºC. All retention studies used samples whose composition was nominally identical to the mobile phase and retention measurements were made with n = 4. Focusing studies were performed in duplicate and used samples made in 95:5, 90:10, and 80:20 10 mM H_3PO_4/acetonitrile (wt%) with mobile phase composition maintained at 80:20 10 mM H_3PO_4/acetonitrile (wt%).

4.4 RESULTS AND DISCUSSION

4.4.1 Accurate determination of solute retention factors

To assess the validity of each focusing model we need accurate retention factors. Mobile phase composition and solutes were selected based on our experience to provide a range of k' values that would be a good test for the models. Table 4.1 shows the values of k' determined from solute retention time at the peak maxima for three mobile phase compositions (80.0:20.0, 90.0:10.0, 95.0:5.0 (wt%)) at 60.0 °C for the three solutes PB1, PB2, PB3. PB3 was omitted from the 5.0% acetonitrile sample due to excessive retention. Retention factors were calculated using Eq. C3.1 with n = 4. Retention factors were also calculated based on first central moments for uracil and each paraben (see section C3.4 of Appendix C). No significant difference in focusing results were obtained using either method.

Table 4.1. Experimentally determined retention factors for methylparaben, ethylparaben and propylparaben.

ϕ	**0.20**		**0.10**		**0.05**	
Solute	k'	σ_k	k'	$\sigma_{k'}$	k'	σ_k
PB1	2.06	0.017	7.02	0.019	18.75	0.05
PB2	4.62	0.04	19.62	0.05	59.3	0.19
PB3	10.82	0.08	57.6	0.2	-	-

We note here that evaluation of the models requires accurate measurement of the extent of focusing. This means that injected bands must not be too well-focused or else the natural bandspreading processes will lead to a peak variance that is much larger than the variance of the injected rectangular width. The range of k_1 and k_2 values shown in Table 4.1 reflects this. As we are using capillary liquid chromatography, extra-column volume can be a significant fraction of, or even exceed, the column volume. We paid particular attention to determining accurate values of t_0 and solute retention times, t_R (see Appendix C for details), in order to determine accurate values of k_1 and k_2.

4.4.2 System performance evaluation

As a check on system performance, we performed two control experiments for which the outcome was reliably predictable. In one, a series of timed injections of uracil were made into a 25 μm ID

empty tube. As Figure C3.4 shows, a plot of the full-width of the rectangular zones (in time units) vs. the injection time is linear. From the slope we can calculate the volumetric flow rate (Eq. C3.2). Flow rate calculated from the data in Figure C3.4 was 3.977 ± 0.030 µL/minute. In the second control experiment, a sample of PB1, PB2, and PB3 was prepared in the mobile phase (80:20 (wt%) phosphate/acetonitrile). Injections from 250 to 1500 nL gave wide eluted zones. Plots of the full-width of the observed zone in units of time vs. the injection time give a slope of 0.992 ± 0.006 and an intercept of -0.008 ± 0.002 (means and 95% confidence intervals, Figure C3.5). Full details for performance evaluation experiments are provided in sections C3.4 and C3.5 of Appendix C. We can conclude from results of both control experiments that system performance is satisfactory for the current work.

4.4.3 Quantitative evaluation of solvent-based focusing

4.4.3.1 Solvent-based on-column focusing examples

We made injections of 10.0% (wt%) acetonitrile containing samples of PB1, PB2, and PB3 with V_{inj} = 500 to 2000 nL into a column with 20.0% acetonitrile as the mobile phase. Figure 4.5 shows two example chromatograms in which a small amount of focusing is expected to occur as the composition of the injected solution is weaker than the mobile phase (the full data set is Figure C3.6). Injection volumes for the black and blue traces were 500 and 1500 nL. Qualitatively it is clearly apparent from Figure 4.5 that the 1500 nL injection leads to a volume overloaded peak for PB1 and PB2. Low-retention solutes, particularly PB1 in this demonstration, are most susceptible to volume overload. Under the conditions evaluated, PB1 and PB2 retention factors in the sample solvent and eluent were k_1 = 7.02 and 19.62 with k_2 = 2.06 and 4.62. These factors do not lead to a Gaussian peak shape for the 1500 nL injection.

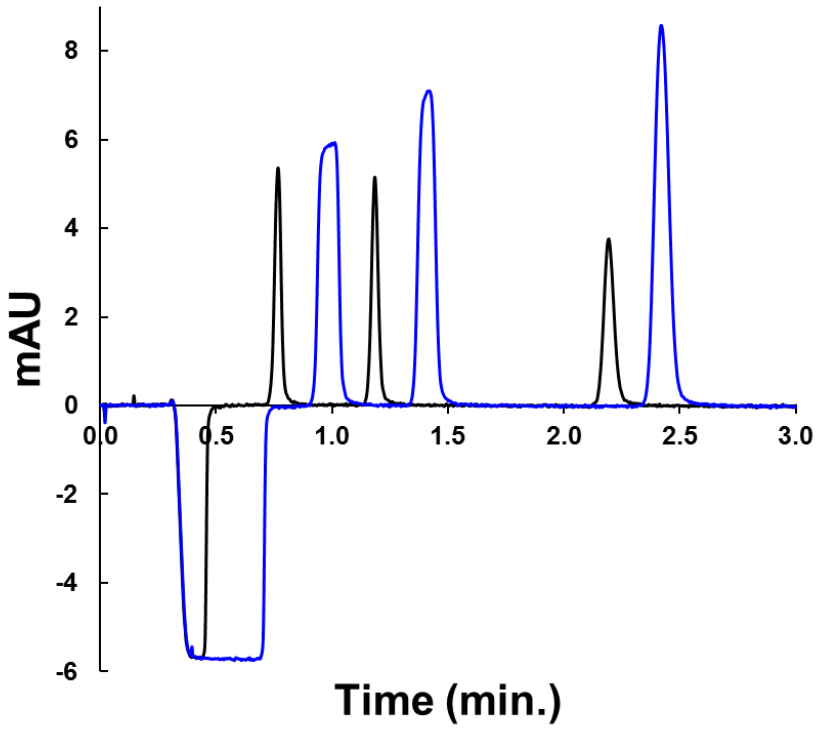

Figure 4.5. Example chromatograms resulting from 500 nL (black) and 1500 nL (blue) injections of paraben samples made in 90:10 wt% 10 mM H_3PO_4/acetonitrile. In each of the two chromatograms, the peaks correspond (in the order of elution) to PB1, PB2, and PB3; mobile phase consisted of 80:20 wt% 10 mM H_3PO_4/acetonitrile. Negative peaks are caused by the injection solvent's refractive index being different from that of the mobile phase. For chromatographic conditions see Section 4.3.3.

Figure 4.6 shows the results for the full range of injection volumes for each solute under all focusing conditions evaluated. Panels A, B and C correspond to PB1, PB2, and PB3 in 10.0% (wt%) acetonitrile. Panels D, E, and F show PB1, PB2, and PB3 in 5.0% (wt%) acetonitrile. After correcting the time axis for the injection time so that the fronts of all zones for a particular solute overlap it can be seen that the peaks get wider as the injection volume increases from 500 to 2000 nL for all solutes. For comparison, a 50 nL injection of 250 μM PB1, PB2, and PB3, 5.0% and 10.0 (wt%) acetonitrile, is shown in each panel as a dashed gray line. The relative effect of the injection width on the peak width, as expected, is smaller for the higher k' compound PB3 than the others. Peak width for each solute in panels D, E, and F is narrower than its analogous injection in panels A, B, and C, as expected, because of the larger values of k_1 in the 5% acetonitrile sample (see Table 4.1). Note that the PB1 and PB2 peaks in panels D and E still exhibit some signs of volume overload for the largest injection volumes, however the peak widths for PB3 in panel F are constant, varying between 3.1 and 3.3 s across the injection volume range tested (50 nL to 2000 nL). The lack of volume overload for the PB3 peak demonstrates the analytical effectiveness of focusing, but as described above does not help to establish the validity of a quantitative model.

As described above, for clearly volume overloaded peaks with flat tops the simple FWHM measurements can be used to evaluate focusing accurately. When on-column focusing is significant as for PB2 and PB3 in panels E and F, deconvolution will be used to remove the contribution from on-column and post-column processes allowing us to determine the width of the injection profile. In cases such as the just-described PB3 peaks, volume overload has virtually no effect on peak width so deconvolution cannot reveal its magnitude.

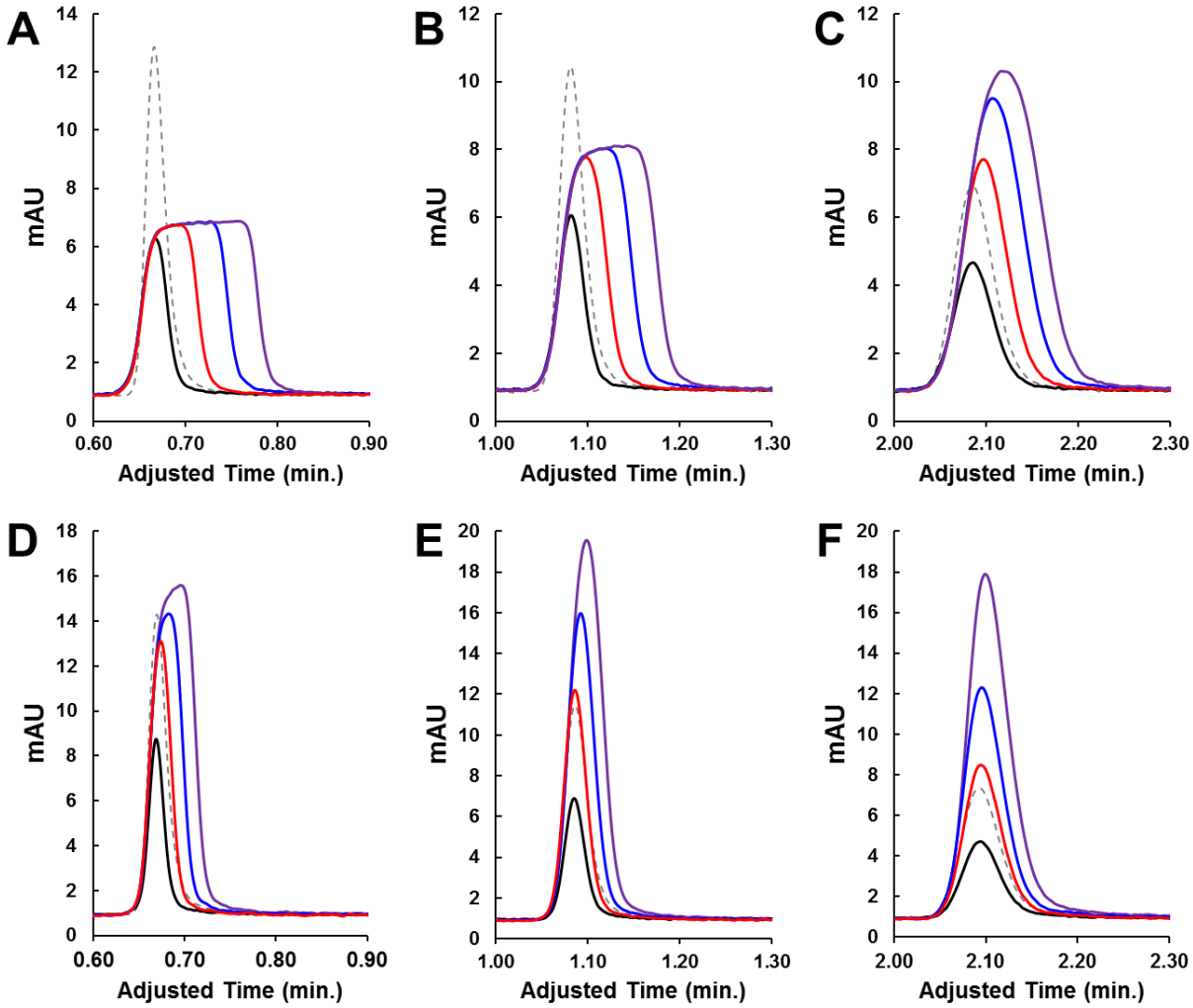

Figure 4.6. Time adjusted chromatograms for 500 (black), 1000 (red), 1500 (blue), and 2000 (purple) nL injections of paraben samples made in 90:10 wt% (A-C) and 95:5 wt% (D-F) 10 mM H_3PO_4/acetonitrile; mobile phase consisted of 80:20 wt% 10 mM H_3PO_4/acetonitrile. Panels A and D correspond to PB1; B and E to PB2, and C and F to PB3. The time axes for each large volume injection were aligned to the leading edge of each injection profile. Analogous 50 nL injections for each solute (- - -) are also provided in each panel. For additional chromatographic conditions see Section 4.3.3. Complete chromatograms for each injection are provided in Figures C3.7 and C3.8.

4.4.3.2 Quantitative comparison of focusing models

Figure 4.7 is a plot of the expected benefit from solvent-based preconcentration for three cases as a function of the single variable k_2/k_1 . The three cases are (red) focusing and compression (Eq. 4.10), the effect of focusing alone (Eq. 4.11, gray), and the prediction of Mills et al. (lavender). The latter two are ranges because neither effect can be expressed as a function of k_2/k_1 only. Thus, the effect at a given value of k_2/k_1 depends on the actual values (magnitude) of each of the two retention factors. Of course, the prediction for Eq. 4.10 is a straight line. The general conclusions are that the step-gradient-induced compression, while small when considering peak capacity in gradient elution [21, 22, 119, 127] is nonetheless significant when considered from the perspective of sensitivity. In addition, for low values of k_2/k_1 , which would be the normal case in practice, the Mills et al. theory predicts dramatically better preconcentration than Eq. 4.10.

With accurate values for k_1 and k_2 for each solute and condition, we can calculate the expected effect from each case as shown in Figure 4.8 which, as Figure 4.7 shows Eq. 4.10 (red), Eq. 4.11 (black) and Mills et al. (blue). Several things are clear. (1) The data describe, within experimental error, a straight line. This supports the idea that Eq. 4.10 most adequately predicts the combined effects of focusing and compression. The experimental slope is 0.90 which is significantly different than the predicted slope, 1.0. We discuss this below. (2) The prediction of the oft-cited work by Mills et al. is not at all accurate. We do not believe that there is justification for using this model to estimate the allowable volume injected or the achievable sensitivity enhancement. (3) As Snyder points out [127] the effect of compression is small, but it is by no means negligible as Figure 4.8 shows by comparing the black and red points for individual k_2/k_1 combinations.

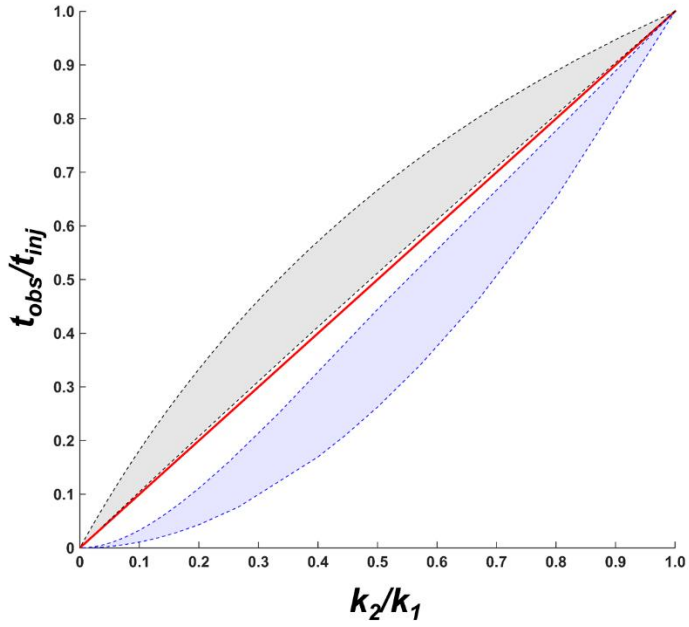

Figure 4.7. Simulations for the apparent on-column focusing (t_{obs}/t_{inj}) resulting from each model were calculated as a function of k_2/k_1. Retention factors were varied from $1 < k_1 < 500$ and $1 < k_2 < 20$; t_{obs}/t_{inj} was calculated for every combination of k_2/k_1 within this range. The lavender and gray bands represent the range of t_{obs}/t_{inj} values obtained when varying the ratio of k_2/k_1 based on the model derived by Mills et al. and Eq. 4.11, respectively. The red line represents the calculated t_{obs}/t_{inj} based on the k_2/k_1 model incorporating the effect of the step gradient. Note that for each of the values of k_1 and k_2 simulated using the k_2/k_1 model only a single value for t_{obs}/t_{inj} is obtained regardless of the magnitude of k_1 and k_2, i.e. only the ratio of k_2/k_1 matters; this is not predicted by the other two models. As expected all three models for on-column focusing converge at both corners of the plot where no focusing and large amounts of focusing are present.

There are several factors that may contribute to the observed deviation from the very simple model. Among the factors to consider are whether values of k' at constant temperature are accurate, whether temperature control is adequate, and whether pressure changes alter the picture. We have made extensive efforts to account for the potential influence of these parameters on the results presented in Figure 4.8. Sections C3.2, C3.3, and C3.4 of Appendix C address potential inaccuracies in k' values. Temperature irregularities on the order of a few degrees, either in the form of viscous heating or local temperature variations in the column heating element could not account for the magnitude of the extra compression observed. The high thermal conductivity of fused silica columns as well as operating them under the moderate linear velocities used here are also not likely to induce viscous heating related changes in k' [100]. Pressurizing the sample in the loop will reduce its volume and thus reduce the initial zone width. The pump pressurizes the loop contents to 425 bar. Sample volume will be decreased less than 2% under these conditions [88]. Thus, it is unlikely that pressure-based compression of the sample either in the loop or at the head of the column can account for the extra compression.

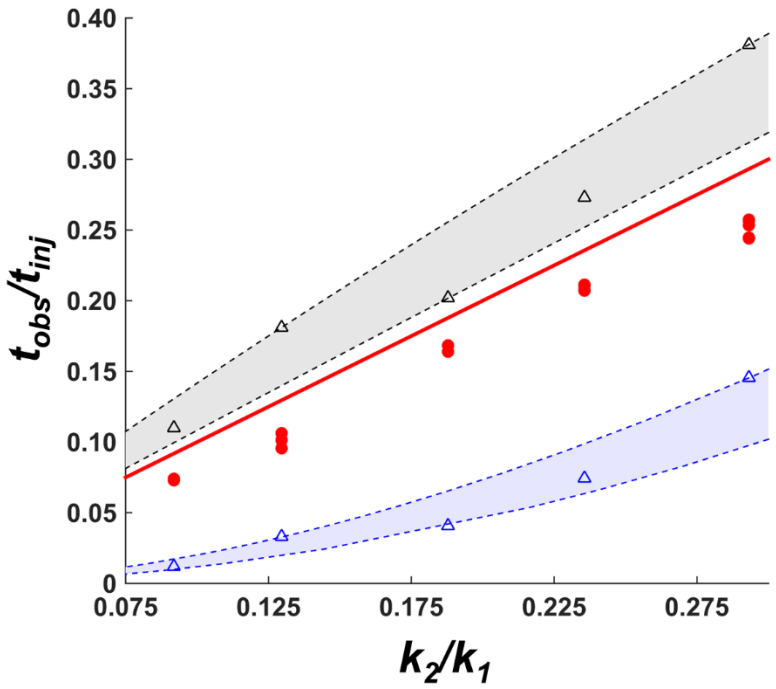

Figure 4.8. Quantitative comparison of on-column focusing models. Experimental data based on deconvoluted injection width measurements and retention factors in Table 4.1 are plotted as red circles. Data points correspond to replicate injections of: 1000, 1500, 2000, and 1500 and 2000 nL injections of methylparaben made in 90:10 and 95:5 wt% 10 mM H_3PO_4/acetonitrile, 1500, 2000, and 2000 nL injections of ethylparaben in 90:10 and 95:5 wt% 10 mM H_3PO_4/acetonitrile, and 2000 nL injections of propylparaben in 90:10 wt% 10 mM H_3PO_4/acetonitrile. A total of 18 data points are plotted corresponding to 5 different k_2/k_1 ratios. The solid red line corresponds to the degree of focusing predicted by the k_2/k_1 model and experimental k' values. Bands calculated based on Eq. 4.11 and the Mills model for the range of k_1 and k_2 values encompassed by the experimental range (see Table 4.1) are plotted as gray and lavender bands, respectively. Individual points based on each experimental k_1 and k_2 value are also plotted for these two models and shown as black and blue circles.

One factor that may explain the extra compression is the actual solvent composition profile on the column when the mobile phase returns to the column behind the injected volume. Consider the simple case in which the solvent front enters the column as a sharp front but spreads as it proceeds down the column. The spreading may be caused by column mass transport dynamics or it may be caused by depletion of organic modifier in the mobile phase at the solvent front as the amount of adsorbed organic modifier increases to equilibrate with the new, modifier-rich mobile phase. Recall that the on-column compression is caused by the fact that the tail of the solute zone moves faster than the front for a particular *time* governed by the zone width and the mobile phase velocity. If the tail is exposed to an abrupt change in solvent strength, but the front is exposed to a relatively gradual change, extra compression will occur. Note that the change in solvent strength is still quite steep at the front when considered in relation to gradient elution chromatography. The extra compression for the injected band arises because it takes a longer time for the front of the zone to be exposed to final composition of the mobile phase when the solvent composition changes over some distance/time.

4.5 CONCLUSIONS

In this work we have evaluated quantitatively the accuracy of a pair of k'-based models designed to predict the effectiveness of on-column focusing in liquid chromatography. We can draw the following conclusions:

1. Quantitative comparisons of models for on-column focusing are best made using metrics based on the peak width at half height for volume overloaded peaks rather than those related to peak height or sensitivity enhancement.
2. The frequently derived k_2/k_1 relationship designed to incorporate focusing due to 1) the higher solute retention in the sample solvent and 2) compression from the resulting step

gradient of the higher elution strength mobile phase is currently the best available analytical model to describe the effect.

3. The oft-cited model derived by Mills et al. is incorrect and significantly overestimates the on-column focusing effect. Thus, we feel it should no longer be used to model the effectiveness of on-column focusing.
4. While the k_2/k_1 model is reasonably accurate and significantly better than its alternatives, the model does not account for the additional compression of the injected band resulting from the steep (but not "step") gradient resulting from the mobile phase passing through the injection band.

This work illustrates the utility of the simple k_2/k_1 relationship for solvent-based on-column focusing. While this model *underestimates* the magnitude of focusing it is easy to use and accurate enough to be practically useful. Experimental results can be expected to be slightly *better* than those predicted by the model.

5.0 TEMPERATURE-ASSISED SOLUTE FOCUSING WITH SEQUENTIAL TRAP/RELEASE ZONES IN ISOCRATIC AND GRADIENT CAPILLARY LIQUID CHROMATOGRAPHY: SIMULATION AND EXPERIMENT

The contents of this chapter were previously published in: Groskreutz, S. R. and Weber, S. G. Journal of Chromatography A, **2016**, 1474, 95-108.

Reproduced with permission from Elsevier.

5.1 INTRODUCTION

To adequately monitor low concentration solutes in small-volume biological samples practitioners turn to gradient elution capillary liquid chromatography (cLC) often coupled to high resolution mass spectrometry. While capillary columns have been effective for proteomics, [8] metabolomics [9-11] and *in vivo* neurochemical measurements [12, 13, 15-17, 128] technological improvements leading to higher concentration solute bands entering the detector are always welcome. Over the last decade major improvements in particle and pump technology have benefitted LC performance [42, 43, 129, 130]. The aforementioned improvements in chromatographic performance are important, but do not address the issues related to the often (relatively) large injection volumes used in cLC. The injection of a large enough volume results in so-called volume overload in which early eluting peaks are broadened as a result of inadequate sample focusing at the head of the column [25, 44, 63, 95, 131]. Pre-column strategies can be particularly effective because they may involve solute-specific, high-affinity focusing [132-136] or fractionation, e.g., in proteomics

(MudPIT [137, 138]). On-column focusing or preconcentration is a consequence of generating transient conditions during the injection that result in high solute retention at the head of the column [20]. For example, focusing can be induced by injecting aqueous samples onto a reversed phase column or application of a solvent gradient [119]. Such on-column focusing may lack the ability to take advantage of solute-specific focusing approaches such as SPE [132-134], but it is very convenient, performed on a single column and widely applicable. On-column focusing at the column head focuses all analytes in the mixture in contrast to post-column trapping and remobilization approaches that enhance single for one or two specific solutes in the mixtures [123, 124, 139, 140]. One process that would be difficult to accomplish using online solvent-based focusing is to amplify the effect by carrying out the focusing process twice, in series, on the same column.

The small size of cLC columns makes them more susceptible to extra column dispersion and volume overload but their low thermal mass makes the application of dynamic temperature changes chromatographically useful [100]. Temperature programming as well as various temperature pulsing techniques are effective for increasing separation speed and tuning chromatographic selectivity in cLC [71, 73, 74, 141-150]. Cooling cLC columns to sub-ambient temperatures is also advantageous. The Greibrokk group has done extensive work in this area with temperature programs initiated near 5 °C [76-80]. Recently, Schoenmakers et al. immersed a capillary monolith in ice water to induce an in-column solvent switch [140]. In addition to our work with temperature-assisted on-column solute focusing (TASF) [97, 151, 152], Holm et al. [81] and Eghbali et al. [83] used segmented column cooling to focus solute bands at specific times and locations along the column, the former the column inlet, the latter the outlet. Dynamic changes in

column temperature can be used effectively to manipulate solute bands on column and address the volume overload and dispersion problems.

In our previous work just mentioned we controlled the temperature of a single, one-cm long zone at the head of a capillary column to focus injected solute bands by cooling. Heating the zone lowers the retention factor, sending the compressed injected band down the column. In principle, this process could be repeated to achieve further focusing in a second, adjacent temperature-controlled zone. Here, we describe the development of this idea. We have termed this approach *two-stage TASF*. Our goal is to understand in detail this two-stage TASF approach. Of critical importance, we have developed a straightforward but powerful simulation of the effect of changing the temperatures in the two zones on retention, band shape, and band spreading. The simulation uses a simple stepwise modeling procedure similar to that of Gilar et al. [153, 154]. The Gilar et al. approach is simpler than the more rigorously formulated approach based on mass balance [155, 156], but it does not calculate on-column dispersion. In the mass balance case, on-column dispersion must be handled in an *ad-hoc* fashion because of the Craig-tube-like spreading that occurs naturally in the computation. We have combined the approach of Gilar et al. in which the front and rear positions of each individual zone are calculated, with a straightforward approach to on-column dispersion. Unlike earlier approaches [153, 155-159] we explicitly include the time- and space-dependence of retention and dispersion. Thus, this simulation is capable of predicting chromatograms resulting from spatial and temporal temperature programs in combination with isocratic and solvent gradient elution.

For simulation of experimental chromatograms, solvent- and temperature-dependent retention data are needed. We determined retention factors at six temperatures in each of twelve mobile phase compositions for a series of *n*-alkyl hydroxylbenzoate esters and *n*-alkyl *p*-hydroxyphenones.

These model solutes were used to assess the instrument's operation in both isocratic and gradient modes. Our understanding of the processes involved was assessed by comparison of simulated chromatograms with no adjustable parameters to actual chromatograms.

5.2 INSTRUMENTATION AND CHROMATOGRAPHIC CONDITIONS

5.2.1 Chemicals

Uracil, methyl, ethyl, *n*-propyl, and *n*-butyl esters of *p*-hydroxybenzoate (parabens, notated here after as PB1, PB2, PB3, and PB4) were purchased from Sigma-Aldrich (St. Louis, MO). *p*-Hydroxy *n*-alkyl phenones, 1-(4-hydroxy phenyl) ethanone, 1-(4-hydroxy phenyl) propanone, and 1-(4-hydroxy phenyl) butanone (HP2, HP3, and HP4) were from TCI America (Philadelphia, PA). Standard solutions for each paraben and hydroxyphenone were made by dissolving each individually in acetonitrile. Uracil stocks were made in deionized water. Water was from a Millipore Milli-Q Synthesis A10 water purification system (Billerica, MA) and used without further treatment. Acetonitrile (LC/MS Optima grade), isopropanol (HPLC grade), acetone (HPLC grade) and phosphoric acid (HPLC grade) were from Fisher Scientific (Fair Lawn, NJ).

5.2.2 Instrumentation

5.2.2.1 Solute retention studies

A Jasco X-LC 3000 system consisting of a 3059AS autosampler, dual 3085PU semi-micro pumps, 3080DG degasser, 3080MX high pressure mixer, CO-2060 thermostated column compartment, 3177UV variable wavelength UV absorbance detector, and LC-Net II/ADC from Jasco Inc. (Easton, MD) was used to evaluate the temperature and solvent composition dependence of solute retention. Data were acquired using ChromNAV version 1.19.3 software. Chromatograms were

exported and analyzed using a peak finding program written in MATLAB 2015a (MathWorks, Natick, MA).

5.2.2.2 Two-stage temperature-assisted solute focusing

A diagram for the instrumentation used for two-stage TASF is shown in Figure 5.1. Hardware was similar to that used for single-stage TASF [151, 152]. In this instrument we constructed an array of three independently controlled 1.0 x 1.0 cm, 10.9 W thermoelectric elements (Peltiers, TECs) from Custom Thermoelectric (04801-9330-34RB, Bishopville, MD). Each TEC, labeled TEC *A, B, C* from the column inlet, was silver soldered to a custom liquid cooled copper heat sink mounted inside a polyvinylchloride housing. Heat sink temperature was controlled using a Thermo Haake K10 (Newington, NH) digital temperature controller pumping an ethylene glycol/water mixture at about 1 L/minute. TECs were separated from each other by a distance of 100 μm. Each TEC's temperature was monitored with a 36-gage Type-T thermocouple (Omega Engineering, Stamford, CT) epoxied to its surface. Care was taken to ensure the tip of each thermocouple rested on the TEC surface with no epoxy at the TEC/thermocouple interface. Temperature measurements were made with a National Instruments 9213 16-channel high speed thermocouple input module (Austin, TX). Each TEC was independently controlled by a Maxim Integrated 1968 electronic TEC driver (V_{max} = 5 V, I_{max} = ± 3 A, Sunnyvale, CA) interfaced with a NI 9264 32-channel analog voltage out module. A simple feedback loop-based LabVIEW program was written in-house to coordinate temperature changes and maintain desired TEC temperature. [152]

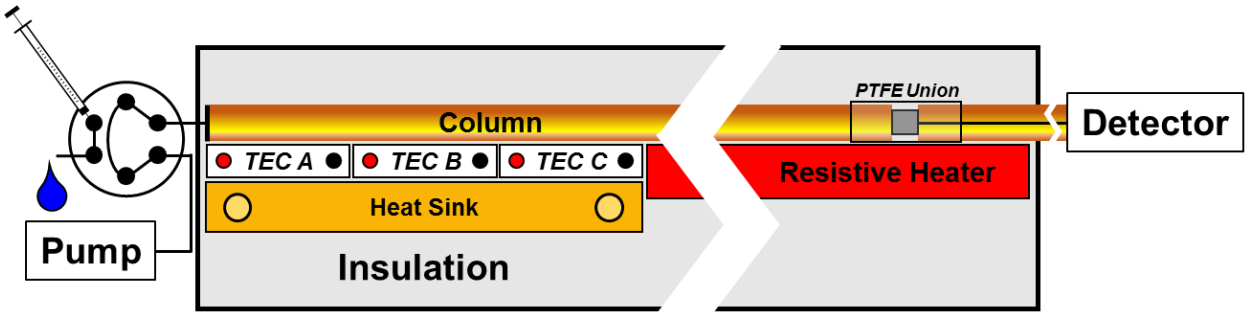

Figure 5.1. Schematic for the column temperature control used for two-stage TASF. Three electronically controlled, one-cm long Peltier elements (TEC A, B, C) were silver soldered to a custom copper liquid cooled heat sink. The remaining segment of the column was heated using a PID-controlled resistive heater.

The downstream, isothermal segment of the column was heated using a 28 V, 3" long Kapton resistive heater (KH-103-10-P, Omega) and a Love Model 1500 proportional-integral-derivative (PID) controller (Dwyer Instruments, Michigan City, IN) as described previously [99].

Mobile phase was delivered by a Thermo/Dionex UltiMate 3000 Nano LC (NCS-3200RS, Germering, Germany) capillary pump. The pump was connected to an externally mounted 6-port two-position Cheminert injection valve (C72x-669D, VICI Valco, Houston, TX) by a 55 cm x 50 µm I.D. nanoViper capillary (Thermo). A second 75 cm x 75 µm I.D. nanoViper capillary (3.3 µL volume) was used as the injection loop. Injected volumes were determined by using timed injections with valve actuation controlled by the same LabVIEW routine used for TEC temperature control. Remote start and valve switching signals were coordinated by an NI USB-6008 DAQ. Fused silica capillary columns (packing described below) were connected directly to the injection valve using 0.015" I.D. x 1/16" O.D. PEEK sleeves from IDEX-Health and Science (Oak Harbor, WA). A Waters Acquity TUV fitted with a 10 nL nano flow cell (Waters Corporation, Milford, MA) was used for detection. A 25 cm long 25 µm I.D. x 360 µm O.D. fused silica detection

capillary was placed between the column outlet and flow cell; connections were made using PTFE unions. Data were acquired at 100 Hz using either an Agilent 1200 Series Universal Interface Box (Agilent Technologies, Waldbronn, Germany) and ChemStation OpenLab CDS (C01.06) software or an Atlas A2D and Chromeleon version 6.8 software (Thermo). All data analysis was performed in MATLAB 2015a using peak evaluation and integration programs written in-house.

5.2.3 Chromatographic conditions

5.2.3.1 van`t Hoff retention studies

Temperature-dependent retention factors for parabens and *p*-hydroxyphenones were determined on a new Waters Acquity BEH C18 (50 mm x 2.1 mm I.D., 1.7 μm d_p) column. Samples were made in mobile phase at concentrations between 100 and 250 μM. Column temperature was varied from 25 to 75 °C in 10 °C steps at each mobile phase composition. Compositions tested were: 0.05, 0.10, 0.15, 0.20, 0.25, 0.30, 0.35, 0.40, 0.45, 0.50, 0.55, and 0.60 (w/w) acetonitrile/10 mM H_3PO_4. Each mobile phase was prepared by weight to improve composition accuracy and minimize inconsistencies in intersystem mobile phase blending. Weight-to-weight aqueous-organic compositions were converted to volume-to-volume units using density data provided by Billen et al. [88]. Detection at 100 Hz used absorbance at 235 and 254 nm; injection volume was 5 μL. Flow rate was set to 0.35 mL/min. Retention times were adjusted for extra column time determined using a Valco zero-dead-volume union in place of the column. Table D4.1 shows the solutes used at each mobile phase composition and conversion of mobile phase composition from w/w to v/v units.

5.2.3.2 Two-stage temperature-assisted solute focusing

5.2.3.2.1 Column preparation

Fused silica capillary columns were packed in-house using a previously described procedure [20, 151, 152]. Briefly, Waters Acquity BEH C18, 1.7 μm d_p, particles were packed into 150 μm diameter fused silica capillaries from Polymicro Technologies (Phoenix, AZ). Column blanks were fritted using electrically sintered 2 μm solid borosilicate spheres (Thermo Scientific, Fremont, CA). Particle suspensions were prepared in isopropanol at 65 mg/mL and sonicated for 20 minutes. Columns were packed via the downward slurry method using a Haskel DSHF-302 pneumatic amplification pump. Acetone was the packing solvent. A maximum packing pressure of 20,000 psi was held for 10 minutes. Following packing, system pressure was allowed to dissipate naturally. After packing the stationary phase bed the remaining length of the capillary was packed with 8 μm solid silica spheres (Thermo) at 21,500 psi for an additional 10 minutes. Columns were flushed with acetonitrile prior to use. The column used for TASF instrument evaluation had dimensions of 78 mm x 0.15 mm I.D. Column fluid volume or dead volume (V_0) was estimated at 750 nL.

5.2.3.2.2 Two-stage TASF: Isocratic elution

Mobile phase was prepared by mixing 800.00 g of 10 mM H_3PO_4 and 200.00 g of acetonitrile. Samples were made to match the mobile phase composition; an approximately 10 μM sample of PB2, PB3 and uracil was prepared by adding 20 μL of 50 mM paraben stocks to 100.00 g of the premixed mobile phase. The difference between the mobile phase and sample solvent was kept under 0.05%. Flow rate was 3.00 μL/min, with the pump delivering 50:50 channel A/B. Detection wavelength was 254 nm. Injection volume was 1500 nL for all isocratic separations. The injection volume corresponded to about 200% of the column void volume.

The 1500 nL injection resulted in a 30 s injection time; TEC *A* focusing time was set to 35 s. This value was in line with the focusing times used in our previous work with single-stage TASF [151,

152]. TEC *B* focusing times were varied systematically from 35 s, corresponding to a single-stage TASF run, to 80 s in 5 s steps up to 70 s. Variable focusing time injections were performed in duplicate. Injections with focusing times for TEC *B* at 35 and 60 s were performed in triplicate. TEC *C* was operated isothermally, maintaining a fixed temperature throughout the run. Heat sink temperature was 25 °C. Focusing and separation temperatures for TECs *A* and *B* were 5 and 70 °C, respectively. TEC *C* and the resistive heater were maintained at 70 °C.

5.2.3.2.3 Two-stage TASF: Gradient elution

Mobile phase for channel A was 10 mM H_3PO_4 in water and channel B was acetonitrile. The linear gradient was initiated at 5% B and increased to 45% B in 16 minutes. Following the gradient, the pump and column were reequilibrated at the initial mobile phase condition for 4 minutes. The flow rate and detection wavelength were 3.00 μL/min and 254 nm. Samples of 5 μM PB1, PB2, PB3, and PB4, 7.5 μM HP2, HP3, and HP4 and 25 μM uracil were made volumetrically in 5% acetonitrile to match the initial composition of the gradient. Injection volume was 3000 nL corresponding to 400% of the column volume. Focusing times for TEC *A* and TEC *B* were 65 s and 65/100 s (single-stage/two-stage TASF). TEC *A* and *B* were reequilibrated for 30 s at the focusing temperature prior to the next run. Focusing and separation temperatures were identical to those used in the isocratic work. Injections were made in triplicate under isothermal, single-stage TASF and two-stage TASF conditions.

5.3 RESULTS AND DISCUSSION

5.3.1 Dependence of retention factors on temperature and solvent composition

Retention was measured at twelve mobile phase compositions between 0.05 and 0.60 w/w 10 mM H_3PO_4/acetonitrile and six column temperatures between 25 and 75 °C at each mobile phase

composition. Retention factors under each condition were calculated using Eq. D4.1 with n = 4. Solute mixtures were selected for each mobile phase composition to have a practical experimental k' range at 25 °C from 1 to 65.

Retention data were assessed using a two-step procedure. First partial molar enthalpies of retention were determined for each solute at each mobile phase composition using van`t Hoff plots (see Figure D4.1 and Table D4.1). Inspection of residuals indicated there was no significant change in retention enthalpy with temperature over the range studied. Linearity allowed extrapolation to the 5 °C focusing temperature and ensured the accuracy of simulation results. Second, we fit a recent equation to predict the influence of changes in solvent composition and column temperature on solute retention [160] to the retention data. This Neue-Kuss equation is shown as Eq. 5.1:

$$\ln k = -\ln k_{0,T} + \frac{D}{T} + 2\ln(1 + a\phi) - \left(1 + \frac{D}{T}\right)\frac{B_T\phi}{1 + a\phi} \tag{5.1}$$

where T is the temperature in Kelvin, φ is the volume-based mobile phase composition, a and D are coefficients to express the influence of solvent and temperature and $k_{0,T}$ and B_T are the coefficients for retention in 100% water and the slope of the retention relationship with solvent composition including temperature effects.

Nonlinear curve fitting was performed using the Solver add-in in Excel. Note that all fitting results used ϕ values that had been converted from w/w to v/v units using the data from Billen et al. [88]. Results from the curve fitting are shown for all solutes in Table 5.1. Fits for the parabens and hydroxyphenones were good with R^2 values in excess of 0.9996 for each solute. Fit quality

compared favorably with the data presented by Neue and Kuss for the four parabens using a methanol/water mobile phase and the same Waters BEH particle.

Table 5.1. Curve fitting results for Neue-Kuss retention equation using the Waters Acquity BEH C18 column as a function of temperature (25-75 °C) and solvent composition.

Analyte	**ln $k_{0,T}$**	**B_T**	**a**	**D**	**Fit (R^2)**	**n[a]**
p-Hydroxyacetophenone	4.60	2.95	2.42	2559	0.9996	144
p-Hydroxypropiophenone	4.26	2.67	2.03	2878	0.9998	192
p-Hydroxybutyrophenone	4.07	2.65	1.95	3260	0.9998	216
Methylparaben	4.62	2.50	1.96	2890	0.9998	192
Ethylparaben	4.30	2.64	1.99	3271	0.9998	216
Propylparaben	4.24	2.70	2.03	3774	0.9997	216
Butylparaben	4.30	2.73	2.07	4323	0.9996	216

[a]Total number of experimental data points used in nonlinear curve fitting.

5.3.2 Characterization of two-stage TASF instrument performance

For effective implementation of two-stage TASF, rapid changes from focusing to separation temperature for multiple, closely spaced TECs is critical. Temperature transients must also be precisely controlled to insure reproducibility. To achieve this, commercially available electronic TEC drivers were used to run, high power, low thermal mass TECs with control software written in-house. Each TEC was operated individually using a self-learning feedback program written in LabVIEW and described previously for a single TEC device [152]. The program was designed to

deliver a reproducible temperature profile to the column with maximum and minimum steady state temperatures of 70 and 5 °C.

To demonstrate the effectiveness of the two-stage TASF instrument an example temperature profile for a two-stage TASF run is shown in panel A of Figure 5.2 for TEC *A* (red), *B* (blue), and *C* (black). In this example the focusing temperature of 5 °C was held for TEC *A* for 35 s and TEC *B* for 60 s. TEC *C* temperature was maintained at 70 °C throughout the run. What is important to observe from this figure is the response of adjacent TECs to the temperature change of their neighbors. (See Figure D4.4 for plots of the transient portions of Figure 5.2.) After 35 s when TEC *A* changed to 70 °C there is a small increase in temperature for TEC *B* of about 2 °C. The temperature control feedback loop for TEC *B* sensed the increase in temperature and pulled TEC *B* temperature back towards 5 °C. A similar temperature rise in TEC *A* and *C* was observed when TEC *B* temperature was raised, but again the feedback loop compensated for this and the 70 °C temperature was recovered quickly.

The time derivatives of the temperatures of the three TECs are plotted in Figure 5.2B. Maximum heating rates for 15 replicate TASF cycles for TEC *A* and *B* were 1091 ± 9 and 1242 ± 10 °C/min (5-70 °C). These values compare favorably to the maximum value of 360 °C/min (25-60 °C) previously reported for a similar array-based TEC setup of Collins et al. [82]. Heating rates for our device translated to a time-to-90% of the set temperature of 7.1 and 6.3 s for TECs *A* and *B*. Higher maximum heating rates for TEC *B* were due to the influence of neighboring TECs and the 25 s delay between heating of TEC *A* and TEC *B*. During this time heat from the 70 °C TECs *A* and *C* diffused to TEC *B* assisting its rate of increase to the separation temperature. TEC *A* did not have this assistance during heating, as it had a cold TEC *B* to one side and room temperature on the other.

One of the advantages to using TECs to control column temperature was their potential for high speed cooling. High speed heating, up to 1800 °C/min (25-125 °C), has been reported using resistive heaters in cLC [73, 74, 143], but these devices are limited in two ways by their lack of cooling capabilities. First, passive cooling restricts the absolute cooling rate to about -150 °C/min (125-25 °C) [73] and second, it does not allow for use of temperatures below ambient. Various other cooling methods such as submerging the column in ice water or blowing compressed gas over it have been reported [140, 144], however these methods are not practical for automated systems necessary for routine use. Using our TEC-based platform, maximum cooling rates of -1485 °C/min (70-5 °C) were achieved for TEC *B*. This value is nearly ten-times as fast as those reported for passive cooling and over four-times faster than that reported by Collins et al. [82] for TECs (60-25 °C). Performance figures of merit for the two TASF TECs and isothermal TEC *C* have been organized in Table 5.2. Data for TEC *C* has been included to indicate the isothermal performance during operation of the two-stage system.

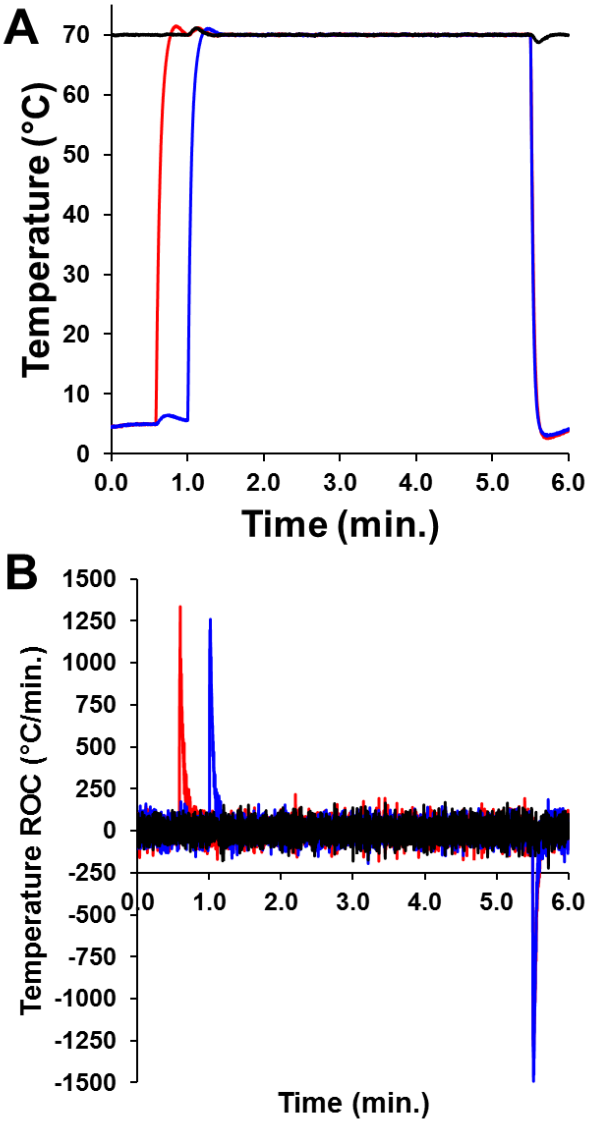

Figure. 5.2. A) Typical temperature profiles for TECs A (red), B (blue), and C (black) for two-stage TASF. Focusing temperature was 5 °C, separation temperature was 70 °C; focusing time for TEC A was 35 s and 60 s for TEC B. Small, ca. 2 °C, temperature transients were observed for each TEC due to the temperature change of the adjacent TEC. B) Plot of time derivative of temperature for TECs A, B, and C. Maximum heating rates were greater than 1000 °C/min (for 5-70 °C) for TECs A and B; maximum cooling rates were nearly -1500 °C/min (for 70-5 °C) for TEC B for the specified temperature range.

Table 5.2. Two-stage TASF instrumental figures of merit for TEC control, maximum TEC heating and cooling rates, and maximum and minimum overshoot values following the temperature change from 5-70 °C.

Figure of Merit	TEC A	TEC B	TEC C
$dT/dt_{Heat,max}$ (°C/min.)[a]	1091 ± 9	1242 ± 10	-
$dT/dt_{Cool,max}$ (°C/min.)[b]	-1287 ± 13	-1485 ± 8	-
$T_{Heat,max}$ (°C)[c]	71.8	71.1	71.2
$T_{Cool,min}$ (°C)[d]	2.1	2.9	68.6

[a,b]Mean from 15 replicates, ± SEM.

[c,d]Maximum and minimum temperatures from 15 separate temperature profiles.

5.3.3 Simulating two-stage temperature-assisted focusing

5.3.3.1 Development of simulation procedure

In our earlier work on TASF [97] we described a simple model to predict separations using single-stage TASF in isocratic elution. Using the same basic idea, here we present a more powerful digital simulation capable of modeling results from instruments with multiple TECs, each subjecting a section of the column to a unique temperature profile during either isocratic or solvent gradient elution. The simulations, 1) validated the effectiveness of two-stage TASF, 2) provided insight into what is actually happening inside the column and 3) can assist in method development for now more complicated experimental setups.

We predict the position(s) and shapes of the leading and trailing edges of a solute band. First, consider their positions on column and the elution profile in time. In two-stage TASF and in

solvent gradient elution these edges have different velocities that are a function of location, *z*, within the column and time, *t*, into the run. First, we create a time- and distance-dependent column temperature profile, *T(t,z)*. Second, we determine a time- and distance-dependent solvent profile, φ*(t,z)*, that incorporates the sample solvent composition, gradient dwell time, initial and final gradient compositions. Local retention factors are calculated at each *t* and *z* based on the Neue-Kuss equation which uses *T(t,z)* and φ*(t,z)*. Eq. 5.2 shows the version of the Neue-Kuss equation used in the simulation:

$$\ln k_{loc,i} = -\ln k_{0,T,i} + \frac{D_i}{T(t,z)} + 2\ln\left(1 + a_i\phi(t,z)\right) - \left(1 + \frac{D_i}{T(t,z)}\right)\frac{B_{T,i}\phi(t,z)}{1 + a_i\phi(t,z)} \tag{5.2}$$

where $k_{loc,i}$ is the local retention factor for solute *i*, *T(t,z)* and φ*(t,z)* are values for temperature and mobile phase composition at specific times and locations within the column, $k_{0,T,i}$, D_i, a_i, and $B_{T,i}$ are solute dependent numerical parameters resulting from the fit of the Neue-Kuss equation to our data (Table 5.1).

From the local retention factors the local elution velocity, $u_{i,loc}$, is determined for each edge of the band:

$$u_{i,loc} = \frac{u}{1 + k_{loc,i}} \tag{5.3}$$

where *u* is the average linear velocity.

Defining a constant time step, *Δt*, we can track the movement of the edges of the hypothetical rectangular band from the product of the local elution velocity in Eq. 5.3 and *Δt* to obtain a distance,

Δz, the band moved during that time. Simulations used a Δt value of 1/15 s. Summing the individual distance and Δt values provided precise time and location information for each edge of a solute band for a predefined experimental setup. When the leading edge reaches the end of the column, the corresponding elution time is simply the number of steps required to proceed all the way down the column multiplied by Δt. The rectangular band width, $w_{i,l}$, in length units is determined from the on column distance between the leading and trailing edges of the band when the leading edge elutes. To convert the on-column width to a time-based width, $w_{i,l}$ is multiplied by the well-known post column expansion term:

$$w_{i,t}^2 = w_{i,l}^2 \frac{\left(1 + k_{eff,i}\right)^2}{u^2} \tag{5.4}$$

where $k_{eff,i}$ is the solute retention factor at elution and u is the average velocity.

Next, consider the shape of the zone. Peak shape depends on injection volume and dispersion. The front and rear edges of the injected zone correspond mathematically to the edges of a rectangle that is the sum of two Heaviside step functions. The width of this rectangle is determined as explained above. Each edge is a convolution of a Heaviside step function and the column transfer function. We use a Gaussian as the column transfer function with length standard deviation, $\sigma_{l,i}$. During each step the band spreads according to its local value for plate height, H_{loc}:

$$H_{loc,i} = H(z,t) = \frac{\Delta\sigma_{l,i}^2}{\Delta z} \tag{5.5}$$

We use $\varphi(t,z)$, $T(t,z)$, values from the solvent and temperature programs to calculate each solutes' local diffusion coefficient, $D_{m,loc,I}$, and reduced velocity, $v_{loc,i}$. Local values for diffusion coefficient were calculated by converting previously reported diffusion coefficients, $D_{m,i,T'}$, at temperature, T', to the local conditions, $\varphi(t,z)$, $T(t,z)$, using the following equation:

$$D_{m,loc,i}\big(\phi(t,z),T(t,z)\big) = D_{m,i,T'}\frac{T(t,z)\eta(T')}{T'\eta\big(T(t,z)\big)}$$

(5.6)

Local values for mobile phase viscosity as a function of temperature and composition were calculated using the correlation of Guillarme et al. [26] fit to viscosity values for acetonitrile water mixtures from Billen et al. [88]:

$$\eta(\phi,T) = 10^{\left[-2.533+{}^{742}/_{T}-0.452\phi+\left({}^{235}/_{T}\right)\phi+1.573\phi^2-\left({}^{691}/_{T}\right)\phi^2\right]}$$

(5.7)

Values calculated for $D_{m,loc,i}$ and $v_{loc,i}$ were inserted into the dimensionless reduced van Deemter equation to determine $\Delta\sigma_{loc,i}^2$ for each particular value of Δz:

$$\Delta\sigma_{loc,i}^2 = \Delta z_i d_p\left[A + \frac{B}{v_{loc,i}} + Cv_{loc,i}\right]$$

(5.8)

where d_p is the particle size and A, B, and C are dimensionless reduced van Deemter coefficients measured by Zhang et al. [89].

Values for $\Delta\sigma_{loc,i}^2$ calculated along the way are summed to determine a variance due to column processes, $\sigma_{l,\,col,i}^2$ when the band elutes from the column. Converting length to time units results in:

$$\sigma_{t,col,i}^2 = \sigma_{l,col,i}^2 \frac{\left(1 + k_{eff,i}\right)^2}{u^2} \tag{5.9}$$

Sternberg solved the convolution integral for a rectangular pulse and Gaussian distribution [161] for the case where there is no focusing. In the presence of focusing, the injection width in time is not the same as the band width at the exit. Incorporation of the focusing effect yields the following equation for the concentration profile of the observed band:

$$C(t) = \frac{C_0 w_{inj,t}}{2w_{i,t}} \left[\mathrm{erf} \frac{w_{i,t} - \left(t - t_{R,i}\right)}{\sqrt{2}\sigma_{t,col,tail,i}} + \mathrm{erf} \frac{\left(t - t_{R,i}\right)}{\sqrt{2}\sigma_{t,col,lead,i}} \right] \tag{5.10}$$

following substitution of values from Eq. 5.4; where C_0 is sample concentration, $w_{inj,t}$, is the injection width in time (the same for all solutes, i), $\sigma_{t,col,lead,i}$ and $\sigma_{t,col,tail,i}$ are the Gaussian standard deviations calculated from Eq. 5.9 for the leading and trailing edges of the band and $t_{R,i}$ is solute retention time. Note that in Eq. 5.10 erf represents the error function.

5.3.3.2 Simulating two-stage TASF with isocratic elution

To judge the effectiveness of two-stage TASF and as an initial validation of our simulation procedure we simulated the separation of a mixture of uracil (void marker), PB2 and PB3 under isocratic conditions. The results from this simulation are shown in Figure 5.3. Panels A, B and C illustrate the distance traveled at any time for the solute band under the three temperature

conditions: isothermal (black), single-stage TASF (blue) and two-stage TASF (red), respectively. An overlay of the simulated chromatograms is in panel D. Column dimensions were 80 mm x 0.15 mm ID, 1.7 μm d_p. Injection volume was 1500 nL, flow rate was 3 μL/min, mobile phase composition was 0.20 (w/w) water/acetonitrile, with focusing and separation temperatures of 5 and 70 °C. Focusing times for TEC *A/B* in the single stage TASF and TECs A/*B* in the two-stage TASF simulations were 35, 35/60 s, respectively. All other chromatographic conditions used in the simulation are in Table D4.2.

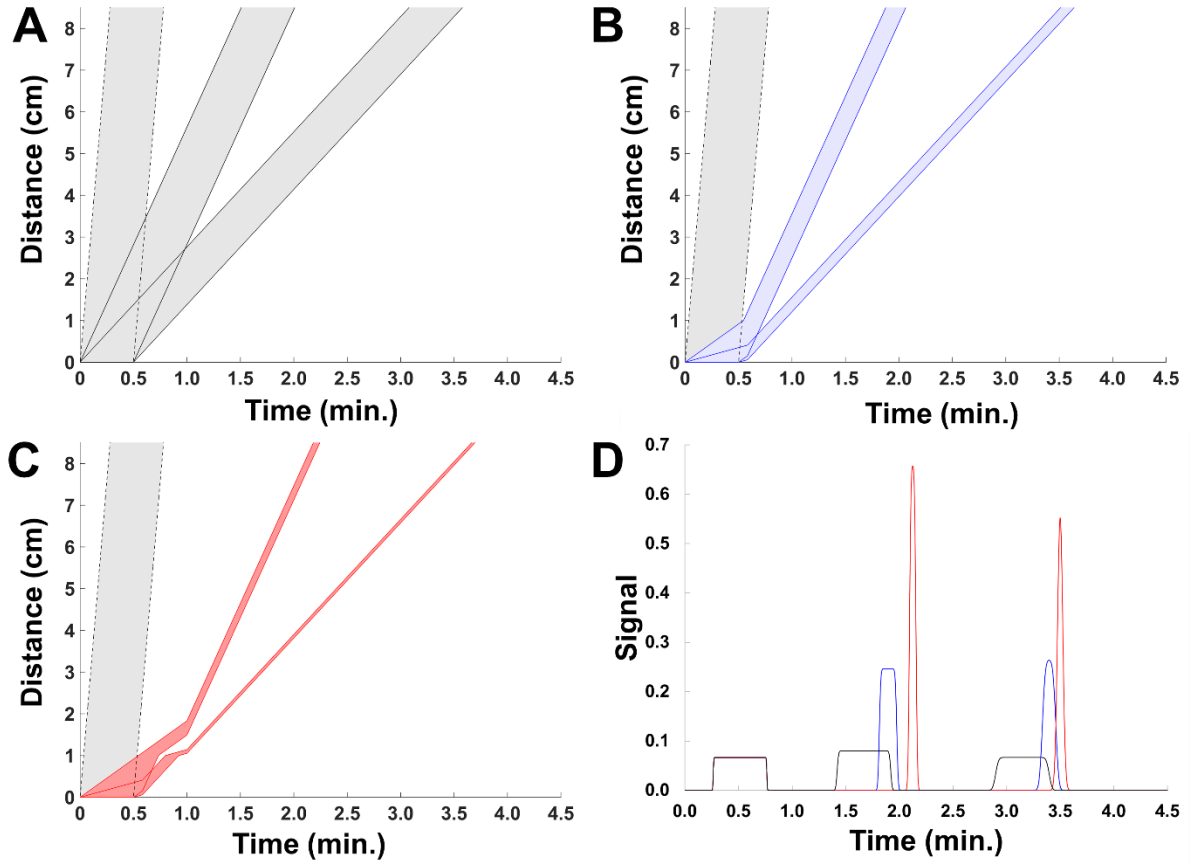

Figure 5.3. A) Spatial representation of isothermal chromatogram for 1500 nL injection of mixture of void marker, ethyl and propylparaben made in mobile phase. B) Same separation under TASF conditions, T_1 = 5 °C for 35 s. C) Two-stage TASF separation demonstrating additional band compression with second focusing stage. D) Simulated chromatogram for isothermal (black), single-stage (blue) and two-stage TASF (red) separations.

From the spatial representations we can clearly see how TASF and particularly two-stage TASF can be used to transiently modulate solute retention in chromatographically beneficial ways. In each spatial representation, sample is injected onto the column from t = 0 until t = 30 s (V_{inj} = 1.5 μL, F = 3.0 μL/min). During the 30 s sample loading time, the leading edge of each solute band traveled down the column at a velocity dictated by its local retention factor. *The width of the injection band on-column is the source of volume overload.* For the simulation the local retention factors for PB2 and PB3 under isothermal conditions were 4.4 and 10.0 at 70 °C. The on-column width of the PB2 and PB3 bands following injection under isothermal conditions were 2.82 and 1.38 cm. In the TASF simulation, column temperature for the first 1.0 cm of the column was set to 5 °C, so local retention factors for PB2 and PB3 increased to 15.5 and 42.3. The increased local retention factors at the head of the column resulted in a reduction of on-column zone width for the injection plug to 0.92 and 0.35 cm for PB2 and PB3. While volume overload was significantly reduced by the first TASF stage the now narrowed injection zones still were not compressed enough to induce a Gaussian shaped peak profile at the outlet of the column (blue trace in Figure 5.3D).

Addition of the second focusing segment in two-stage TASF allowed solute loaded onto segment one (TEC *A)* to be released and focused again on the second 5 °C column segment (TEC *B*). This second focusing effect is clearly visible in Figure 5.3C from about 0.5 to 1.0 min as the trailing edge of both PB2 and PB3 bands velocity increased with respect to the leading edge traveling in the cold second segment. The second focusing stage reduced solute band width further and increased overall peak height for PB2 and PB3 by factors of 2.6 and 2.1 relative to the single-stage TASF separations. Decreased peak width improves the overall peak capacity and resolution of the

separation while increased peak height benefits analysis sensitivity and quantitation figures of merit.

5.3.3.3 Simulating two-stage TASF using solvent gradient elution

Now we extend the scope of our simulation procedure to the more complicated system of solvent gradient elution. Figure 5.4 shows the simulation for the separation of, in order or elution, uracil (void), HP2, PB1, HP3, PB2, HP4, PB3 and PB4 under isothermal, TASF and two-stage TASF conditions. Darker tones in the spatial representations correspond to the paraben homologs, while the lighter fill colors represent the hydroxyphenones. Column dimensions were identical to the isocratic simulations. Injection volume was 3000 nL, flow rate was 3 μL/min, focusing and separation temperatures were again 5 and 70 °C. The solvent program was a sixteen-minute linear gradient of water/acetonitrile from 5-45% acetonitrile. Samples were made in 5% acetonitrile; dwell time was 15 s. The focusing time for the TASF separation was 65 s, with the two-stage separation using 65 and 100 s focusing times for TEC *A* and TEC *B.* All other chromatographic conditions used in the simulation are in Table D4.3.

Figure 5.4A shows the spatial representation for the isothermal separation. Note that even when using solvent gradient elution with its gradient compression effect the large sample volume and relatively low retention factors for the early eluters still generated significant volume overload for the separation. For clarity, retention factors for each solute under the initial gradient conditions, k_1, and at the time of elution, k_{eff}, are provided in Table 5.3. Volume overload is clearly visible for HP2, PB1, HP3, PB3 and HP4 bands as each has a significant width at elution.

Table 5.3. Predicted gradient elution retention factors for each solute under isothermal and two-stage TASF conditions.

	$k_{1,\ \phi = 0.05}$		$k_{eff,\ 70\ °C}$	
Solute	**70 °C**	**5 °C**	**Isothermal**	**Two-Stage TASF**
p-Hydroxyacetophenone	7.2	32.7	5.3	4.0
p-Hydroxypropiophenone	24.1	135	8.0	7.3
p-Hydroxybutyrophenone	77.4	545	9.4	9.0
Methylparaben	18.5	106	7.7	6.7
Ethylparaben	63.9	454	9.1	8.7
Propylparaben	240	2290	9.9	9.7
Butylparaben	910	12000	10.3	10.3

As the most chromatographically interesting section of the representation is located in the first 2.0 cm of the column and initial few minutes of the simulation just the portion within the red square (4 minutes, 2.5 cm) of Figure 5.4A are plotted for the isothermal, TASF and two-stage TASF in panels B, C and D of Figure 5.4. Figure 5.4C clearly shows how the addition of the 5 °C focusing segment benefited the separation by increasing k_1 for all solutes. While still not compressing the HP2 band width enough to create a Gaussian peak, width at the outlet of the column was reduced significantly, now 0.90 cm compared to 3.70 cm under isothermal conditions. Figure 4D highlights the importance of the second focusing segment where the 100 s *TEC B* focusing time was long enough to allow the leading edge of the HP2 and PB1 bands to enter this segment, get refocused and be released as a now narrower band. *Both the HP2 and PB1 bands are focused twice*. Addition of TEC *B* reduced band width at the outlet of the column to 0.22 cm for HP2. Note that two-stage TASF is a somewhat targeted technique as only solute bands moving fast enough to enter the second cold zone prior to TEC *B*'s heating get focused twice. Low velocity bands, like PB3 and PB4 do not encounter the second focusing zone at all. Fortunately, these slow-moving bands focus well enough on their own, due to large k_1 values, and do not need two-stage TASF to produce acceptable results. This is described in more detail in the discussion of experiments below.

Figure 5.4E shows an overlay for the simulated chromatograms under the three temperature conditions. TASF (blue) and specifically two-stage TASF (red) work to improve peak shape, height and overall separation performance for low retention solutes. Using TASF the initial retention factor for HP2 and PB1 were transiently increased from 7.2 and 18.5 at 70 °C to 32.7 and 106 at 5 °C. These relatively small changes and the spatial temperature program introduced using two-stage TASF increased peak height by factors of 19.9 for HP2 and 10.7 for PB1 relative to the isothermal control.

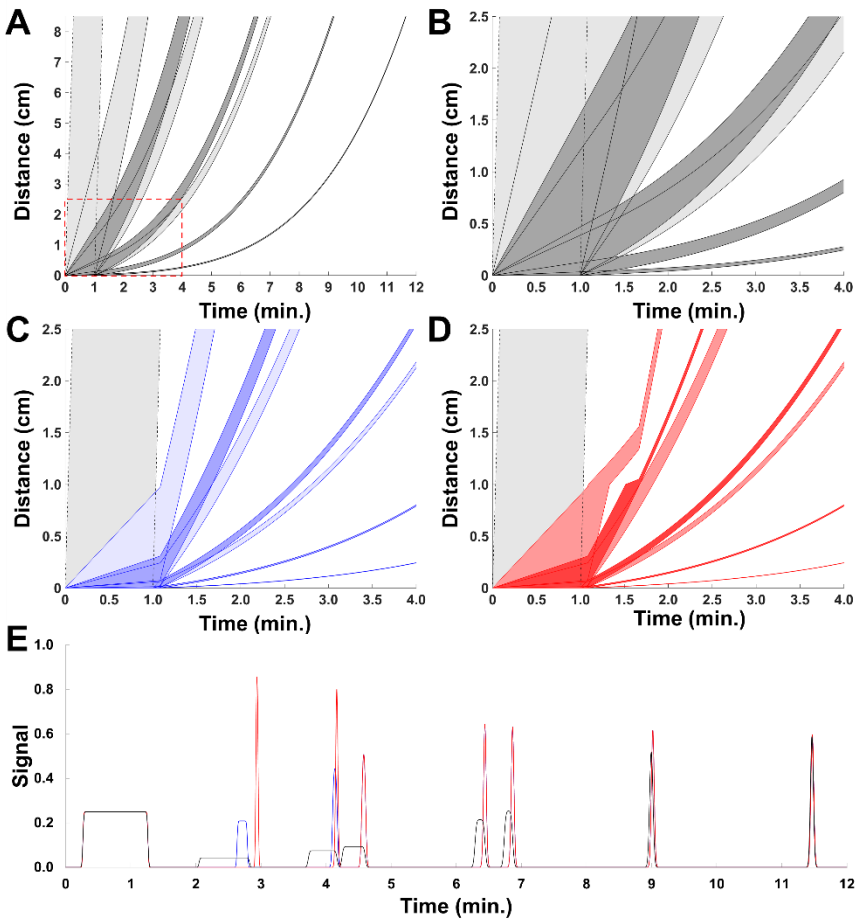

Figure 5.4. Simulations for gradient elution separations of parabens and hydroxyphenones. A) Spatial representation for complete isothermal gradient elution chromatogram. The void maker is bounded by dashed black lines, hydroxyphenones show as light gray bands, parabens as dark gray bands. B) Region of isothermal spatial representation indicated by red box in panel A highlighting segments of column subjected to temperature changes. C) Single-stage TASF spatial representation for the first 4 minutes of the separation. Focusing time was 65 s. Light blue bands correspond to the alkylphenones, dark blue the parabens. Band width was reduced by additional temperature induced focusing at the head of the column. D) Two-stage TASF, alkylphenones are shown as light red bands, parabens in dark red. *p*-hydroxyacetophenone and methylparaben peaks were clearly focused twice using two-stage TASF. E) Simulated chromatograms for isothermal (black), TASF (blue), and two-stage TASF with 100 s $t_{focus,B}$ time (red).

5.3.4 Two-stage TASF experiments: Isocratic elution

A series of 1500 nL injections of PB2 and PB3 was made under isothermal, TASF, and two-stage TASF conditions. Sample volume corresponded to 200% of the column fluid volume; sample composition was fixed such that its composition matched the elution strength of the mobile phase. Thus, any improvement in peak shape, height, or width were due to only single- or two-stage TASF. Focusing and separation temperatures for TECs *A* and *B* were 5 and 70 °C, respectively. TEC *C* and the resistively heated section of the column temperature were maintained at 70 °C. TEC *A* focusing time was 35 s. TEC B focusing times were varied from 35 to 80 s in 5 s steps (up to 70 s).

Panel A of Figure 5.5 shows the signals obtained from the isocratic two-stage TASF runs with the nine different TEC *B* focusing times. What is clearly visible from the overlay is peak height increased for both PB2 and PB3 as TEC B focusing time was increased up to a maximum (55 s, black trace) when peak height began to decrease for PB2. Panels B and C highlight these transitions by plotting the sections of chromatogram corresponding to PB2 and PB3. The primary objective for two-stage TASF was to maximize concentration sensitivity, thus the optimum experimental conditions yielded maximum detector response. Close examination of the 55 s TEC *B* focusing time (black trace) chromatogram in panels B and C show the optimum focusing time for PB2 did not correspond to the optimum focusing time for PB3. The optimal focusing time for PB2 did not provide enough time for the PB3 band to enter TEC *B* prior to heating. The optimum focusing time for PB3 was 70 s (purple trace), a value unacceptable for an analysis including PB2 as portions of the band began exiting the TEC *B* before its temperature rise negating the benefits of TASF. Differences in optimum TEC *B* focusing time for PB2 and PB3 were due to their difference in retention and elution velocity.

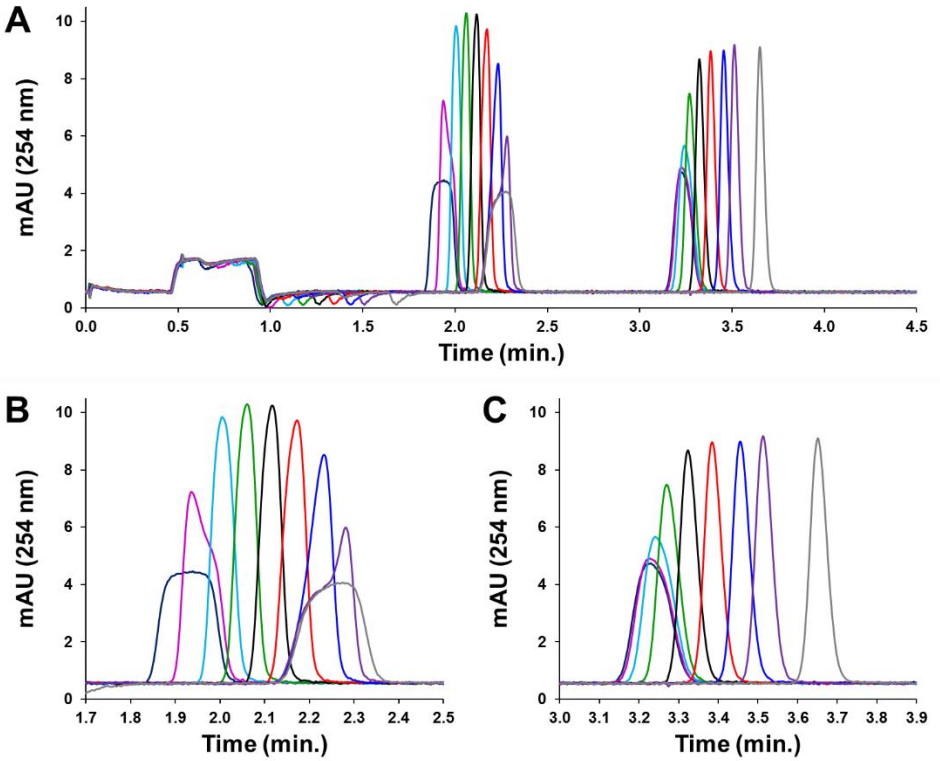

Figure 5.5. A) Example chromatograms from isocratic two-stage TASF study on the optimal TEC B focusing time. TEC A focusing time was fixed at 35 s, TEC B focusing time was systematically increased from 35 s (corresponding to single-stage TASF) to 80 s in 5 s increments. B) Peak profiles for PB2. C) Peak profiles for PB3. See Section 5.2.3.2.2 for chromatographic conditions. Optimal focusing time for TEC *B* represented a compromise between the peak shape for PB2 and PB3. In this example maximum peak height was desired for *both* solutes so a small sacrifice in absolute sensitivity for each was made. Optimal focusing time for the conditions evaluated was determined to be 60 s. For reference this forcing time is shown in red for each chromatogram in Figure 5.5.

Figure 5.6 shows example chromatograms for isothermal (black), TASF (blue), and two-stage TASF (red) using the optimal TEC *B* focusing time for the separation of uracil, PB2, and PB3. Chromatographic conditions were identical to those used in the optimization study. Not surprisingly single-stage TASF increased peak height for PB2 and PB3 by factors of 3.4 and 4.3, relative to isothermal conditions. Note that single-stage TASF also decreased peak width by factors of 3.6 and 4.6. For symmetrical peaks it is expected improvements in peak height be followed by equivalent reductions in peak width. The marginally larger relative improvement in width for TASF peaks was indicative of the potential for TASF to reduce peak tailing and improve peak symmetry. A similar effect was observed in our previous work using single-stage TASF with small volume injections where TASF was shown to significantly reduce tailing relative to isothermal analyses [97]. PB2 peak height was increased by a further factor of 2.3 using two-stage TASF and peak width decreased by an additional factor of 2.4 relative to single-stage TASF separation. Improvements for the PB3 peak using two-stage TASF were similar to those for PB2, peak height increased by a factor of 2.0, peak width decreased by a factor of 2.2. Clearly, when used appropriately a second TASF stage can induce a multiplicative focusing effect compared to single-stage TASF for large volume injections.

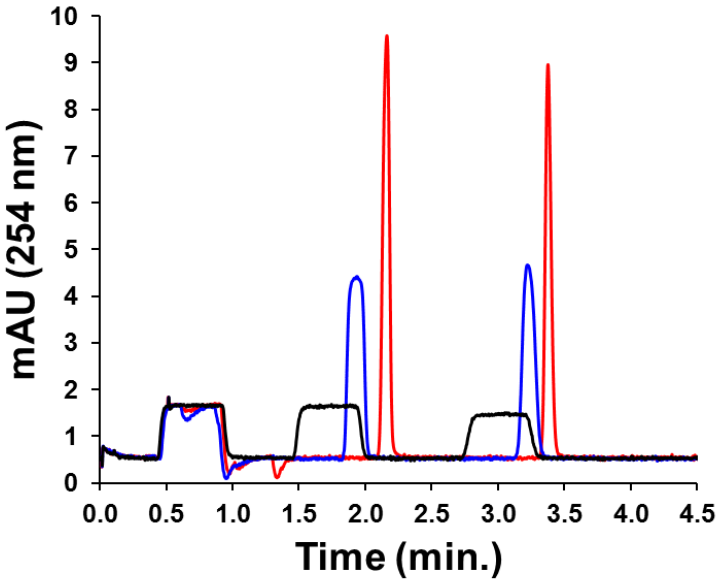

Figure 5.6. Overlay of isocratic chromatograms resulting from 1500 nL injections of uracil, PB2, and PB3 samples under optimal two-stage conditions. Sample composition was made to match the mobile phase composition. Isothermal (black) separations were performed at 70 °C. Single-stage TASF (blue) separations had a focusing time for TEC A and TEC B = 35 s. Two-stage TASF (red) utilized a focusing time for TEC A of 35 s, focusing time for TEC B was 60 s. Focusing and separation temperatures for both TASF modes were 5 and 70 °C.

5.3.5 Two-stage TASF experiments: Gradient elution

To complete our initial assessment of two-stage TASF, we applied the approach to the separation of a 3000 nL sample of three *p*-hydroxyphenones and four parabens using a linear solvent gradient. The sixteen-minute gradient, initiated at 5% acetonitrile, had a final elution strength of 45% acetonitrile. This gradient was performed with samples made in 5% acetonitrile. Separations were conducted under isothermal, TASF, and two-stage TASF conditions. Focusing times for TEC *A* and TEC *B* under TASF conditions were 65 s. Under two-stage TASF conditions, focusing times were 65 and 100 s, respectively. All other chromatographic conditions were identical to those used in the isocratic experiments.

Figure. 5.7 shows an overlay for representative baseline subtracted separations performed under each temperature condition. Isothermal separations are in black, TASF in blue, and two-stage TASF in red. Non-baseline subtracted chromatograms are provided in Figure D4.5. Panel 5.7A shows chromatograms containing all seven retained solutes plus uracil. Uracil was added to make the 1-minute wide injection plug more visible. The isothermal conditions resulted in unsatisfactory chromatography. It was not until the PB3 peak that isothermal conditions yielded peaks similar to those obtained when using either single or two-stage TASF. Most salient was the performance improvement achieved with the addition of the second TASF stage. Two-stage TASF made the early-eluting HP2 peak now the most prominent feature in the chromatogram.

Figure 5.7B shows the first few minutes of the chromatogram containing only HP2. Reducing column temperature from 70 to 5 °C increased k_1 for HP2 from 7.2 to 32.7. Quantitatively, TASF improved peak height for HP2 by a factor of 7.1, relative to the isothermal separation. Addition of the second stage increased peak height further, now by a factor of 22.3 compared to the isothermal separation. Two-stage TASF also outperformed single-stage TASF by a factor of 3.1 for HP2 and

reduced its peak width by a factor of 3.5. Note that HP2 peak width ($w_{1/2}$) for the 3000 nL injection, equal to four-times the column fluid volume, was reduced to only 1.52 s using two-stage TASF.

Figure 5.7C focuses on the most hydrophobic solute in the test mixture, PB4. What is most significant from this overlay is the lack of noticeable difference between the isothermal, TASF, and two-stage TASF separations. Application of either TASF approach did not degrade separation performance for the highly retained solutes.

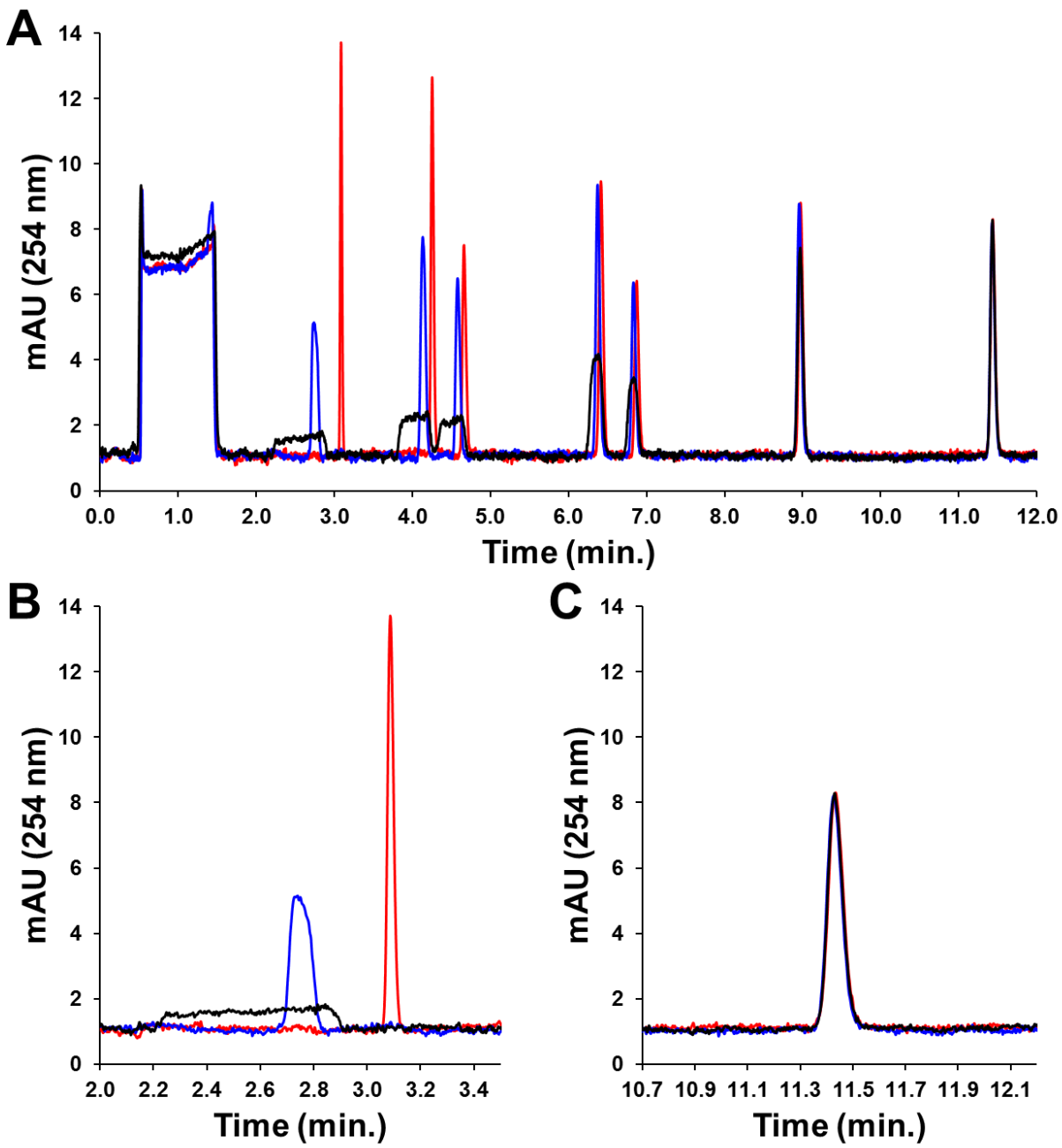

Figure 5.7. A) Overlay of isothermal (black), TASF (blue), and two-stage TASF (red) separations of hydroxyphenones and parabens. B) Excerpt of chromatograms focusing on HP2. Note the significant differences between the isothermal, TASF and two-stage TASF chromatograms. C) Section of the chromatogram containing PB4. Minimal differences between the separation modes is observed indicating the neither TASF approach degraded separation performance.

To evaluate the potential improvement in overall separation performance for two-stage TASF separations, values for peak capacity for the separations shown in Figure 5.7 were calculated under isothermal, TASF, and two-stage TASF conditions. Peak capacity, n_c, was calculated using the formal definition derived by Grushka [162], shown in Eq. 5.11:

$$n_c = \int_{t_{R,1}}^{t_{R,last}} \frac{1}{w_{1/2,i}} dt \tag{5.11}$$

where $t_{R,1}$ is the retention time for the first solute in the chromatogram, HP2 and $t_{R,last}$ is the retention time for the last solute, PB4. For peak width, $w_{1/2,i}$ is the width at half height for each peak in the chromatogram. The advantage to calculating n_c in this fashion is that the calculation does depend on a uniform peak width throughout the chromatogram. We have also adopted the notion of sample peak capacity from Snyder and Dolan to define limits of integration. [163]. Plots of the inverse peak width against retention time are shown in Figure 5.8. The isothermal separation is in black, TASF in blue, and the two-stage separation is in red. The retention time values used for each curve were from those obtained in the isothermal analysis. The single- and two-stage TASF approaches shift early eluting peaks to slightly longer retention times making more space for additional solutes early in the chromatogram, thus the use of retention times from the isothermal analysis was the fairest method for comparison. Trapezoidal integration of the area under each curve yielded peak capacity values of: 75, 146, and 185 for isothermal, TASF, and two-stage TASF separations. Peak capacity improvements were most apparent early in the chromatogram, with curves converging as solute hydrophobicity increased. What is interesting is that under the experimental conditions this convergence does not occur until PB4 demonstrating that TASF would improve peak shape for solutes up to those with hydrophobicity equivalent to PB4.

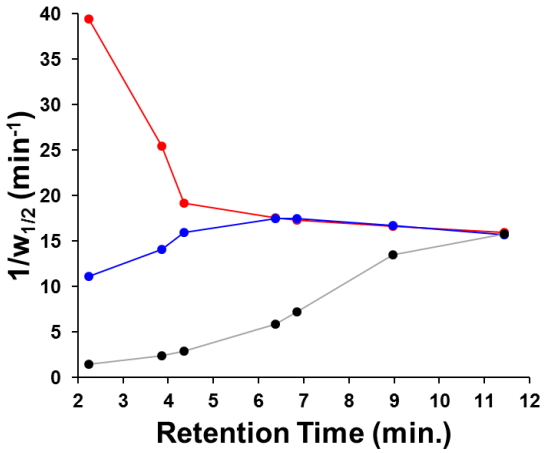

Figure 5.8. Peak capacity for isothermal (black), TASF (blue), and two-stage TASF (red) separations from the example chromatograms shown in Figure 5.7.

5.3.6 Assessment of simulation procedure: Comparison to experimental results

The basis for the simulations is laid out in section 5.3.3.1. It will be helpful to explicitly state here the input parameters required to generate simulated chromatograms. The program requires the following input: injection volume, mobile phase and sample ϕ, TEC temperatures and their related switching times, column length, diameter, porosities, particle diameter, dimensionless van Deemter A, B, C coefficients and mobile phase flow rate. These are all easily specified or controlled except for the van Deemter parameters which we took from the literature [89]. For solutes, we experimentally determined the four parameters of the Neue-Kuss equation that define solute k' as a function of mobile phase composition and temperature, and we used estimates of diffusion coefficients at 37 °C and the temperature-dependence of the mobile phase viscosity to calculate diffusion coefficients at other temperatures. There are no adjustable parameters.

Table 5.4 displays the correspondence between experiment and simulation for the solutes used under all conditions: no TASF, single-stage TASF, and two-stage TASF. The simulated and

experimental retention times are very consistent. From this, we gain considerable confidence in several important aspects of this work. One is the value of the four-parameter Neue-Kuss equation *including extrapolation to temperatures lower than those used in establishing the parameters in the equation*. A second is the confirmation that the temperature control *in the column* is fairly good. It would be difficult to determine the temperature inside the column directly. Even if it were possible with a device like a thermocouple, the presence of the thermocouple itself would be a major perturbation. Thus, the accuracy of the simulation across all of the experimental situations is an indirect indication of the accuracy of the temperature control. In one sense, this should not be surprising. Based on thermal mass, the power used to change a TEC's temperature virtually all goes into changing the TEC's temperature, not the column's. Finally, the third observation is that the overall simulation of retention over different temperatures and solvent strengths is accurate. This provides evidence of an effective simulation.

Table 5.4 also shows experimental and simulated peak half-widths. The agreement is reasonable. Note that we used values of A, B, and C (dimensionless) from the literature which were based on the same stationary phase chemistry and particle, but a different column diameter, 2.1 mm ID, and chromatograph. This undoubtedly leads to some of the differences noted. The most striking difference is for the very lowest k' solute, HP2, in the gradient runs. We suspect that there may be a secondary mechanism for solute focusing. Figures 5.6 and D4.5 show significant "dips" in the baseline of TASF chromatograms which we suspect to be due to the changing acetonitrile concentration in the mobile phase resulting from the change in temperature. This pulse of acetonitrile transiently increases the velocity of the trailing edge, enhancing focusing (band compression), but disperses as it passes down the column. Thus wider zones are more affected, and lower k' species have wider zones at injection than higher k' species.

Table 5.4. Comparison of simulated and experimental retention time and peak width values for test solutes under isothermal, TASF and two-stage TASF conditions using isocratic and solvent gradient elution.

Solute	**$t_{R,exp}$ (min.)**	**$t_{R,sim}$ (min.)**	**$w_{1/2,exp}$ (s)**	**$w_{1/2,sim}$ (s)**
		Isocratic Elution		
Isothermal				
PB2	1.49	1.45	28.8	30.0
PB3	2.82	2.93	28.7	30.0
TASF				
PB2	1.94	1.81	8.1	9.7
PB3	3.22	3.33	6.3	7.6
Two-stage TASF				
PB2	2.16	2.1	3.4	3.6
PB3	3.38	3.5	2.9	2.9
		Solvent Gradient Elution		
Isothermal				
HP2	2.25	2.12	39.7	42.0
PB1	3.85	3.83	24.7	25.2
HP3	4.35	4.36	20.5	21.5
PB2	6.38	6.36	10.1	9.34
HP3	6.84	6.80	8.3	7.80
PB3	8.97	8.99	4.5	3.18
PB4	11.43	11.46	3.8	2.72

Table 5.4 Continued.

TASF				
HP2	2.74	2.70	5.4	9.6
PB1	4.13	4.14	4.3	4.4
HP3	4.58	4.58	3.8	3.7
PB2	6.37	6.44	3.4	2.5
HP3	6.83	6.86	3.4	2.5
PB3	8.95	9.02	3.6	2.6
PB4	11.43	11.47	3.8	2.7
Two-stage TASF				
HP2	3.09	2.94	1.5	2.1
PB1	4.25	4.16	2.4	2.0
HP3	4.66	4.58	3.1	3.7
PB2	6.42	6.44	3.4	2.5
HP3	6.88	6.86	3.5	2.5
PB3	8.97	9.02	3.6	2.6
PB4	11.44	11.47	3.8	2.7

5.3.7 Advantages and limitations

We built a device consisting of three, independently controlled variable temperature segments for use in packed-column cLC. We used this device to improve on our previously developed TASF concept, demonstrating the ability of the new design to focus on-column bands twice using the two-stage TASF approach. The three-TEC system also provides more experimental flexibility than our previous systems composed of a single one-cm long focusing segment. The three TEC system can be operated in the single-stage TASF mode with variable length focusing dimensions, namely one-, two- or three-cm long segments. Longer focusing segments facilitate the use of larger injection volumes improving analysis sensitivity without observing band "leakage" from cold to hot column zones. Leakage degrades TASF performance (see Figure 5.5). Further, the linear array-based TEC configuration allows for dynamic temperature changes in non-TASF applications. For example, TECs can control retention of selected solutes by controlling temperature at *particular locations* along the column at *particular times*. We view the work presented here using two-stage TASF as a first step towards developing the ability to module retention in a *reliable and predictable* way down the entire length of the cLC column.

While the device presented is a significant advance on our previous single TEC devices, it is not without limitations. The current configuration has discrete 1-cm long focusing zones. Systems composed of smaller, ca. 0.5 cm, variable temperature segments offer certain experimental advantages. The primary advantage to smaller TECs is the ability to use *only the required focusing zone length* for the desired solute, injection volume and focusing temperature. Cooling portions of the column not used for actual focusing wastes system pressure making it unavailable to the practitioner to increase column length or analysis speed. (Pressure is directly related to viscosity and viscosity is temperature dependent, usually increasing with reduction in temperature.) A

second limitation of the current design concerns TEC lifetime. TECs in our hands last for hundreds of TASF cycles, but they do wear out eventually becoming unable to change temperature at all. In the current configuration all three TECs are soldered to a single copper heat sink. Repair necessitates the entire heat sink assembly must be disassembled to replace a single malfunctioning TEC. This is the primary limitation of the current design when routine operation is desired. We are in the process of optimizing heat sink design to solve this problem.

5.4 CONCLUSIONS

In this work we have demonstrated through accurate simulation and experiment the potential to focus injection bands *twice on-column* using a process called two-stage TASF. This sequential temperature-based focusing approach presented is not achievable using the more common solvent-based approaches. We have validated its efficacy using simulation and shown experimentally its ability to reduce sample-induced dispersion in isocratic and gradient elution liquid chromatography. We can draw the following conclusions:

1. Linear arrays of closely spaced TECs can be used effectively to modulate solute retention in a space and time dependent way.
2. The simple simulation procedure based on local retention factors accurately predicts experimental band location and shape under isocratic and solvent gradient elution conditions. Simulations match experiments.
3. The addition of a second TASF stage induces a multiplicative focusing effect when used under isocratic conditions. The effect roughly doubles that observed for low retention solutes under single-stage TASF conditions.

4. Solvent gradient elution also sees significant benefit from the two-stage TASF approach, increasing peak capacity for a simple test mixture by a factor of 2.5 relative to an isothermal control.

These results demonstrate the potential for the broader application of dynamic temperature changes in capillary liquid chromatography to modulate solute retention in chromatographically useful ways using simple, reliable and relatively inexpensive hardware.

6.0 GRAPHICAL METHOD FOR CHOOSING OPTIMIZED CONDITIONS GIVEN AN PUMP PRESSURE AND A PARTICLE DIAMETER IN LIQUID CHROMATOGRAPHY

The contents of this chapter were previously published in: Groskreutz, S. R. and Weber, S. G. Analytical Chemistry, **2016**, 88 (23), 11742-11749.

6.1 INTRODUCTION

It takes time to get information about a sample from liquid chromatography. How much depends on the nature of the question and the sample. It also depends upon several parameters related to the liquid chromatographic (LC) system itself. The complexity of chromatographic instruments and the significant number of parameters that control them has spawned many efforts to systematize procedures for optimizing the performance of packed-bed LC which are cited below. Graphical depictions of chromatographic performance as a function of parameters and variables can be useful because they contain a lot of information, however the sheer number of parameters in modern LC confounds efforts to create simple graphics in a two-dimensional format that are easily interpreted. In this work we briefly review previously developed optimization diagrams and present a new graphical approach to determine optimized LC parameters for practitioners wishing to maximize isocratic plate count (N) or peak capacity in gradient elution (n_c) in a given analysis time when using a particular particle diameter and pump pressure.

Most famously, van Deemter et al. developed a plot that continues to guide virtually all reasoning about chromatographic optimization [164]. The van Deemter plot arose from their application of the mass balance approach [4, 5] to solving for a chromatographic band width as a function of mobile phase velocity. Based on earlier work by Klinkenberg and Sjenitzer [165], van Deemter et al. put meat on the bones of the theoretical plate concept of Martin and Synge [1]. What leaps out of the van Deemter plot is the presence of a minimum in theoretical plate height, the change in zone variance (in length units) with a change in zone position as it travels down the column. But, until recently, working at a velocity corresponding to that minimum made for chromatographic run times that were uncomfortably long. Thus, "Ultimately all questions about optimization are related to a compromise between efficiency and time" [28]. Key parameters in realizing a particular chromatographic figure of merit are the available pressure and the particle diameter. The former limits the column length's magnitude, L, and the degree to which particle diameter, d_p, can be decreased. The latter, as well as partly governing the pressure required is also a significant parameter in the van Deemter equation which bounds separating power. These limitations and opportunities have been described in a number of key papers, and interesting plots, in the decades of the '60s – '80s [166-172] some of which we return to below.

Many graphical illustrations of chromatographic performance have been designed to explore the effect of key parameters like particle diameter, pressure, and temperature. The plots that result provide information at three limits: What is the effect of the chosen parameter on the maximum number of theoretical plates? On the highest speed? On the position of the minimum height equivalent to a theoretical plate, H? Giddings's used a so-called kinetic plot to demonstrate the limiting performance of an LC system over long and short timescales in comparison to GC (Figure E5.1 in Appendix E) [167]. The clear conclusion from the plot was that LC will provide more

theoretical plates at long times, but GC will be capable of more theoretical plates with higher speed at short times. The long time limit of the plot is equivalent to about 30 years. While the plot clearly makes its point related to the comparison of GC and LC, it does not provide easily accessible information for practitioners about how to achieve the best performance at reasonable times. Similarly, Knox and Saleem [168] compared LC and GC over a wide range of conditions specifying those required to operate at or near the minimum H while using some or all of the available pressure. Again data are plotted (Figure E5.2) over many orders of magnitude focusing attention at the limits of chromatographic performance. Flow rates near the maximum hypothetical value of ν correspond approximately to filling an Olympic sized swimming pool every 30 minutes with mobile phase passing through a 2.1 mm ID column. Clearly, the point of these early plots is to illustrate broadly the best approach to attain a large number of theoretical plates, or achieve a certain effective number of theoretical plates in a given time.

Poppe reinvigorated the discussion of separation power in a paper comparing various formats for liquid-phase separations including pressure-based chromatography [173]. This work led to another graphical approach to chromatographic optimization that came to be known as the Poppe plot which expresses the plate time (t_0/N) as a function of N (Figure E5.3). More recently, the Desmet group demonstrated the information content in a family of kinetic plots [174-183] (Figure E5.4) developed to expand on the separation impedance concept developed by Knox [184]. These plots speak more directly to practical figures of merit over a very wide range of conditions for different chromatographic supports. The Carr group expanded on that of Poppe to generate a plot for gradient peak capacity production [185]. The same group also clarified the algebraic relationships among the interacting parameters in liquid chromatography [28]. The latter work is quite helpful as it clearly distinguishes two important cases: global optimum (maximum plates per time given a

certain pressure and mobile phase viscosity) which they called the three-parameter problem, and the two-parameter optimization when one additional parameter, usually d_p, is fixed. Although not as crisply articulated, it is noteworthy that Knox and Saleem described the same thing in 1969 [168]. There is no question that plots have great value for understanding in broad strokes how to think about chromatographic optimization.

Both Guiochon [172] and Halasz and Görlitz [186] created nomograms for estimating laboratory conditions (Figures E5.5 and E5.6). While they do cover a rather wide range of conditions they are also useful for determining actual experimental conditions. For example, in Figure E5.5, we illustrate how to find conditions to do a one-minute separation (k' = 3, mobile phase viscosity = 4 x 10^{-4} Pa s) with 600 bar pressure: the particle size should be 1 μm. Similarly, the Halasz and Görlitz plot can be used to deduce similar information. For a k' = 3 and a one-minute separation, t_0 is 15 s. The intersection of that value and P = 600 bar is shown approximately as a dot on Figure E5.6. This guides us to a particle size of about 1.5 μm. Chen and Horvath arrived at similar conclusions for separations of small and large molecules using reasoning analogous to that of Guiochon [187]. Later Meyer extended the Halasz and Görlitz nomogram concept to maximize isocratic and gradient peak capacity [188, 189].

In the process of working on fast neurotransmitter separations, we have realized a need for a plot that illustrates these same concepts, but that also fulfills three other criteria: (1) it is accessible to a non-expert, (2) it is focused on practical parameter ranges over a few powers of 2, not several orders of magnitude, reflecting reality in the lab, and (3) provides experimental parameters of column length and velocity immediately. Here, we explain the plot and demonstrate its value in determining conditions to achieve certain objectives from applications taken from our laboratory under isocratic and gradient elution conditions.

6.2 THEORY

6.2.1. Information needed to construct the plot

Estimates, of the plate height/velocity and pressure/velocity relationships are required to construct optimization graphics. Thus, step one involves selection of the desired solute, mobile phase composition and column temperature. The latter two parameters play a critical role in determining chromatographic performance due to their influence on eluent viscosity and analyte diffusivity. Step two comprises a flow study to measure the kinetic and permeability properties of the column. We used A, B, and C values in the reduced van Deemter equation shown in Eq. 6.1 from Zhang et al. [89] for columns packed with 1.7 μm fully porous particles. Conditions used in the calculation were 25 °C, with a 96:4 water/acetonitrile mobile phase. (Other chromatographic conditions are provided below.)

$$h = \frac{H}{d_p} = A + \frac{BD_m}{u_e d_p} + \frac{Cu_e d_p}{D_m} \tag{6.1}$$

where h is the reduced plate height, H is the dimensioned plate height, d_p is the particle size, D_m is the solute diffusion coefficient in the mobile phase, u_e is the interstitial linear velocity and A, B, and C are the reduced dimensionless van Deemter coefficients.

It requires pressure to force eluent through a chromatographic column. Eq. 6.2 shows a semiemperical equation derived from Darcy's law which relates column parameters to pump pressure, P, under conditions typically experienced when fluids are passed through packed beds.

$$P = \Phi\eta\frac{u_e L}{d_p^2}$$

(6.2)

The plots require the dimensionless flow resistance parameter, Φ, from Eq. 6.2 which can be determined from the slope of pressure vs velocity data. Here, we have used Φ and column porosity values, ε_e and ε_{tot}, reported by Zhang et al.[89] in our calculations.

Numerical values used in subsequent optimization calculations are provided in Table 6.1.

Table 6.1. Parameters used in optimization plots.

Parameter	Source	Value
P_{max} (bar)	Instrument	600, 1000
$D_{m,25\,°C}$ (cm^2/s)	Literature [190]	5.6×10^{-6}
$D_m(\varphi,T)$	Literature [99]	See Eq. E5.1
A	Literature [89]	0.66
B		10.2
C		0.095
d_p (μm)		1.7
Φ		431
ε_e		0.353
ε_{tot}		0.537
T_{col} (°C)	Experience	25
φ		0.04
$\eta(\varphi,T)$ (cP)	Literature [26, 88]	See Eq. E5.2

6.3 RESULTS AND DISCUSSION

6.3.1. Introduction to the plot

Figure 6.1 shows an example of a plot generated from the values in Table 6.1 and equations 6.1, 6.2, and the well-known relationships among average velocity, interstitial velocity and porosity, and among average velocity, length, and time. The vertical axis represents column length (cm); the horizontal axis interstitial velocity, u_e, (cm/s). Dashed lines indicate constant values for t_0, from 1 to 80 s with particular values indicated adjacent to each line. Colored contour lines denote constant values of N. Contours begin with N = 1000 and increase in 1000 plate divisions until N = 10000, where spacing increases to 5000 plates per division up to a maximum of 30000 plates. At any point on the plot, a value of u_e can be chosen which (with data from Table 6.1) provides a plate height. Then a value of L can be chosen which provides a value of N. The values of u_e and L immediately dictate t_0. For example, near the top of the plot, we see that 20000 theoretical plates can be generated (purple line) with a t_0 of 20 s by using approximately a 15 cm long column and a u_e of 1.0 cm/s. Of course, not all lengths and velocities are accessible because the available pumping pressure is a limitation. Black hyperbolas are constant pressure isobars for 600 and 1000 bar. Conditions below and to the left of these hyperbolas are achievable combinations of L and u_e for systems with 600 and 1000 bar limits. Thus, we see that the 20000 theoretical plate/20 s t_0 point is not accessible even with a 1000 bar system (at 25 °C). Optimum conditions occur along an isobar. While one can operate below the isobar, performance is better when the operating point is on the isobar. Values of L, u_e, t_0, and N along the isobar are referred to by Carr et al.[28] with asterisks, e.g., L* etc. To summarize, for a given d_p and T (and other particular attributes of the system as in Table 6.1), each point on this plot represents values of L, u_e, t_0, and N. One cannot operate to the right of an isobar. Operating to the left is permissible. Operating on the isobar is

best. Points along any isobar correspond to the results of Carr at al.'s "two-parameter" optimization [28] for a given P_{max}.

Figure 6.1 presents a significant amount of useful information regarding optimization concepts and chromatographic performance. First, ignore for the time being the need for a particular pressure and focus on the contour lines for N. The constant plate contour lines reflect the shape of the van Deemter curve. This can be understood by following a horizontal, constant L, trajectory across the plot. Consider L = 9 cm. For the lowest interstitial velocity, N is low. As velocity increases, N increases over 10000 then reaches a maximum of about 20000 where the contour line reaches a minimum near u_e = 0.33 cm/s and t_0 about 40 s. The minimum in the contour line for N represents the shortest column at which that number of theoretical plates can be generated. As velocity is increased further, N decreases. This is consistent with the fact that N = L/H (Eq. 6.1 and L is constant). As a vertical trajectory is taken at constant velocity, N increases steadily, again in agreement with N = L/H (and H is constant). The B-term region of the van Deemter curve corresponds to the left side of Figure 6.1 where linear velocity is below the optimum of 0.33 cm/s. This is the long L, long t_0 section of the plot. The C-term dominated portion of Figure 6.1 is in the lower right corner and corresponds to short columns and analysis times.

Now, let us consider the case where we will use the maximum pressure of 600 bar. Under what conditions can we obtain 20000 theoretical plates as we did for L = 9 cm, u_e = 0.33 cm/s, t_0 ~ 40 s at the van Deemter optimum velocity? The 20000 theoretical plate contour crosses the 600 isobar at the point designated by the letter *A*. Operating at 600 bar maintains the plate count but decreases t_0 to about 35 s.

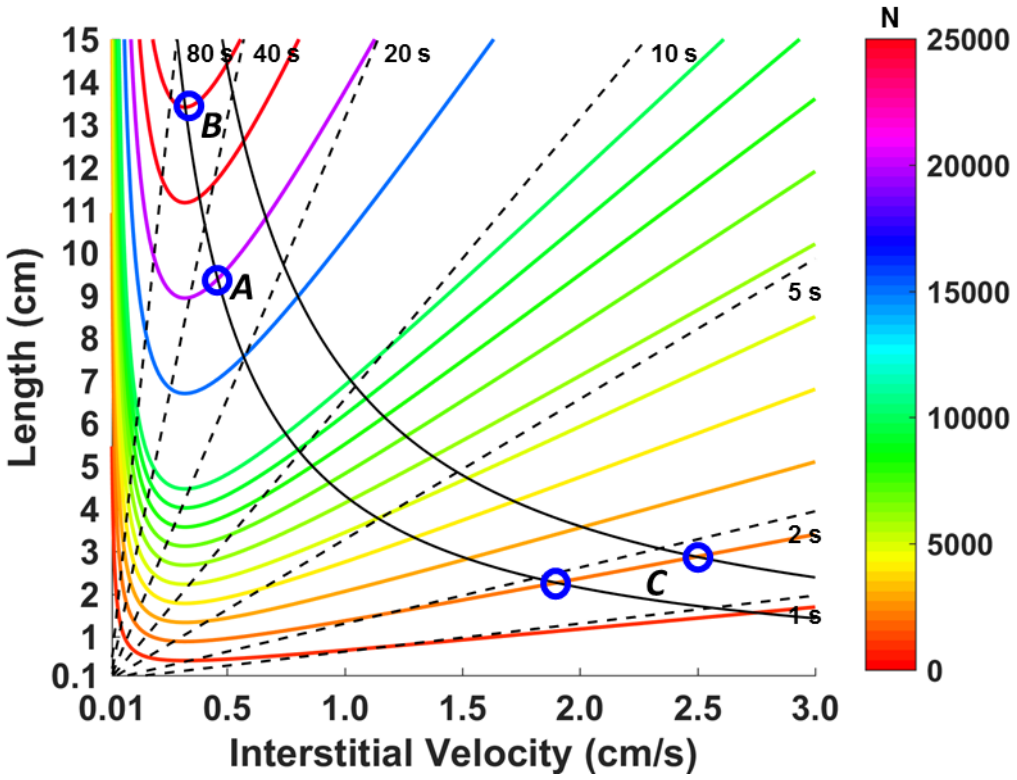

Figure 6.1. Plate count, t_0, and P as a function of u_e and L (given the parameters in Table 6.1). A) Conditions required to generate N = 20000 in the shortest time, t_0 = 35 s, for a pump with a 600 bar pressure limit. B) Conditions that represent the maximum N for t_0 = 63.7 s for the 600 bar system. This point is often referred to as the Knox-Saleem limit where velocity is set to the van Deemter optimum and column length sufficient to operate the system at its pressure maximum. C) Points required to generate 2000 plates for the 600 and 1000 bar systems where the increase in system pressure has little influence on chromatographic speed.

There is one place where the isobar crosses a constant N curve at its minimum indicated by the letter *B*: It is at the van Deemter optimum velocity with column length such that system pressure equals P_{max}. The conditions for point *B* are: P_{max} = 600 bar, u_e = 0.33 cm/s, L = 13.4 cm, t_0 = 63.7 s and N = 30000. Conditions represent the maximum N for t_0 = 63.7 s for the 600 bar system with 1.7 μm particles at 25 °C. This is the *only point* on the isobar that is at the van Deemter optimum velocity. This point is frequently referred to as the Knox-Saleem limit [28, 29, 191].

Supposing we desire a t_0 of 20 s with a 600 bar system pressure limit? From the plot, we can expect that 15000 theoretical plates are generated using a 7.5 cm long column at a linear velocity of 0.57 cm/s. The plot is also useful for a rapid assessment of the consequences of using a particular column length, e.g., 5, 10, or 15 cm.

Further, the plot helps to see whether increasing pressure can aid the chromatographer who is interested in speed, for example, t_0 < 5 s. A system with a 600 bar limit generates 2000 plates for a t_0 = 1.8 s (Figure 6.1 points *C*). Increasing P_{max} to 1000 bar has a negligible impact on speed for the 2000 plate separation, decreasing t_0 only 0.1 s. Clearly increasing system pressure alone is not a viable solution to increase speed under these conditions. Graphically, this information is evident as follows: constant t_0 lines are practically parallel to the constant plate contours. Traveling along a constant t_0 line is achieved by changing pressure while changing L and u_e proportionally. On the other hand, if system pressure is increased with a commensurate decrease in particle size both plate count and separation speed are improved [28]. It is fair to say that, while this plot tells the reader that increasing pressure alone when working on high-speed separations will have minimal effect on separation quality, it does not explain why. Probably the algebraic representation as expressed in Carr et al. [28] (particularly the discussion centered around eqs. 14 – 17) is the best way to understand why this is the case.

6.3.2 Application of the plot to several problems

With this orientation to the plot, we now demonstrate the efficacy of Figure 6.1 based on our laboratory's applications. We have an interest in neurochemistry, specifically the study of monoamine neurotransmitters serotonin (5-HT) and dopamine (DA) *in vivo* by microdialysis coupled online to LC. Changes in 5-HT and DA concentration are measured in response to various chemical and physical stimuli *in vivo* using online LC. The speed of the separation currently limits the time resolution. Better time resolution means we can extract more information.

In our first demonstration of the graphic in Figure 6.1 we require the quantitative determination of 5-HT by LC coupled online to microdialysis with high time resolution. Thus, high speed conditions are required, while the separation must also generate a predetermined number of plates to ensure accurate quantitation. This is a classic two-parameter optimization problem. Temperature, particle diameter, and pressure are the major elements of chromatographic optimization. Thus, we use the plot to assess the role of elevated column temperature and different particle sizes to improve the speed of our neurotransmitter analyses. Our application yields small sample volumes (10 – 500 nL) with low concentrations, thus quantitation is a challenge. Selection of the best column diameter represents a compromise between sample dilution (diameter too large) and volume overload (diameter too small). In a second demonstration we have incorporated the influence of volume overload into the neurotransmitter optimization procedure. Finally, we expand the scope of the plot from purely isocratic elution using the theoretical plate concept to gradient elution to increase the peak capacity production for the analysis of neuropeptide mixtures.

6.3.3 Maximizing isocratic plate count for fixed analysis time

For accurate quantitation neurotransmitter separations require a few thousand theoretical plates – here we specify 5000 theoretical plates. We focus on 5-HT, results are similar for DA. Chromatography uses "ion-pairing" reversed phase LC, with a small portion of acetonitrile in the mobile phase, 96:4 aqueous/acetonitrile, to achieve k' ~ 10 [99]. In Figure 6.2A, the red point is at 5000 theoretical plates and 600 bar. It has been calculated for 5-HT using 1.7 μm fully porous particles and a column temperature of 25 °C (see Table 6.1 for conditions). Under the 5000 plate requirement we see from the light yellow contour, 5000 plates are generated with a t_0 of about 5 s for the 600 bar limit system. 5-HT retention time is 55 s and time resolution is one minute. These results are similar to our previous *in vivo* work with 1-minute temporal resolution separations of 5-HT and DA [92, 192]. Now the question becomes how can we adjust chromatographic parameters to achieve the necessary 5000 plates in less time to improve temporal resolution. Briefly, we again consider what benefit there is to increasing pressure alone as shown by the blue arrows. Blue arrows illustrate the effects. The column's length could be increased to provide more plates, but the chromatographic time increases. The velocity could be increased, decreasing t_0 significantly, but with a concomitant decrease in plates. One could adjust length and velocity to keep N constant, but only a very small increase in speed would be gained. While it cannot be stated that increasing pressure does not help for a t_0 = 5 s separation, it helps very little to increase speed without sacrificing efficiency. Fortunately, there is a simple solution to help increase speed.

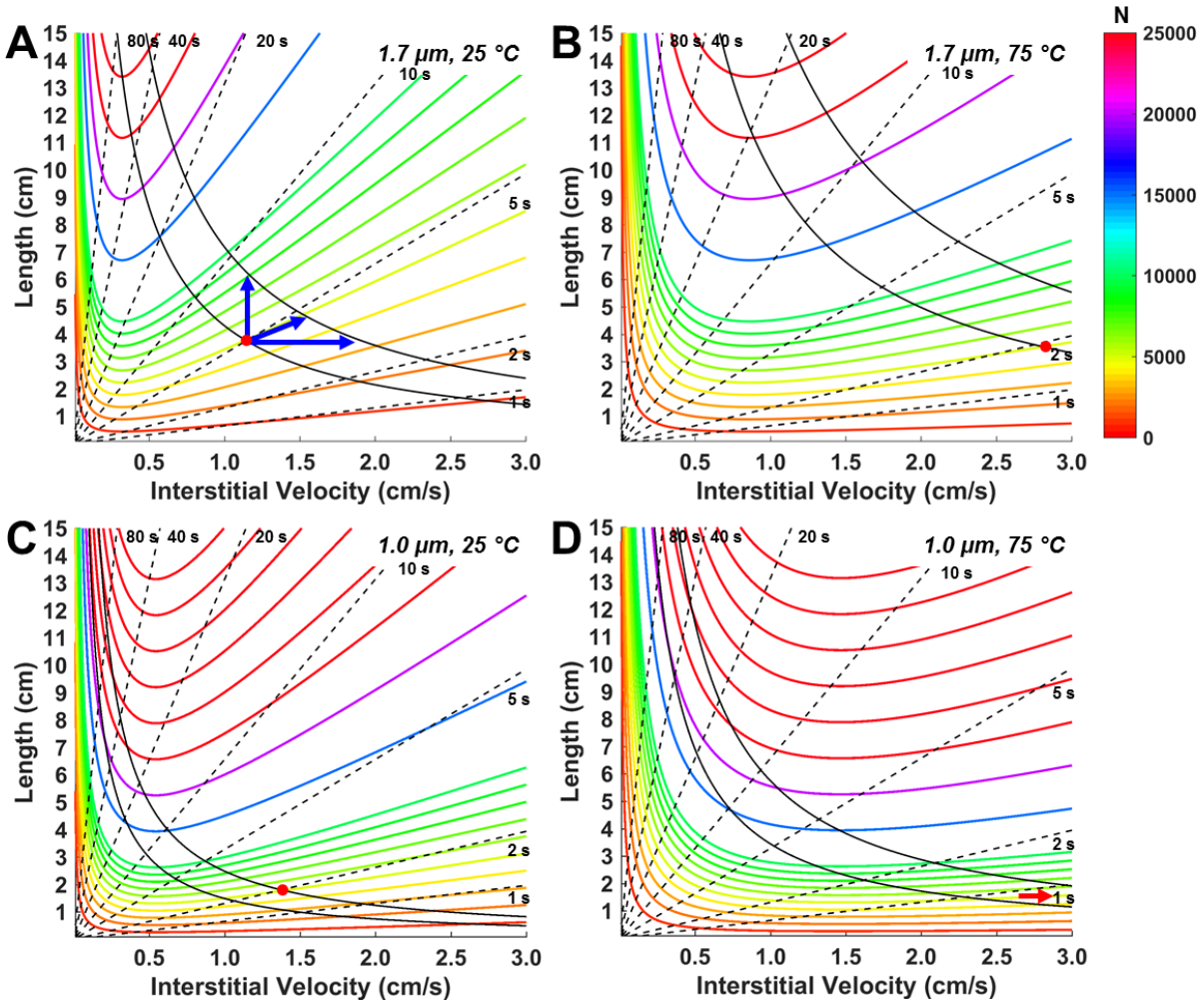

Figure 6.2. Influence of column temperature and particle size on isocratic separation performance. Red dots correspond to the values of L, u_e and N required to achieve 5000 plates in the shortest time with a maximum pressure of 600 bar for the 1.7 µm particles and 1000 bar for the 1.0 µm particles. Blue arrows in A present the series of options to improve performance when increase pressure from 600 to 1000 bar. A) Particle size: 1.7 µm, temperature: 25 °C. B) Particle size: 1.7 µm, temperature: 75 °C. C) Particle size: 1.0 µm, temperature: 25 °C. D) Particle size: 1.0 µm, temperature: 75 °C. All other conditions were identical to Figure 6.1. For clarity axes labels corresponding to linear velocity 0.01 cm/s and column length 0.1 cm have been omitted.

When column temperature is increased the mobile phase viscosity decreases significantly, e.g., $\eta_{75\ ^\circ C}$ = 0.4 cP, $\eta_{25\ ^\circ C}$ = 0.9 cP. This viscosity decrease has the same mechanical effect as increasing the system pressure limit: for the same packed bed, the mobile phase velocity and thus separation time (all else constant) are improved resulting in an increase in speed. At the same time, there is an increase in 5-HT diffusion coefficient, $D_{m,75\ ^\circ C} = 1.4\times10^{-5}$ cm^2/s, $D_{m,25\ ^\circ C} = 0.54\times10^{-5}$ cm^2/s, which is an increase of a factor of 2.6. In high-speed separations where the van Deemter C-term is important we note that the C-term is proportional to the parameter d_p^2 / D_m. Increasing temperature has an effect that is similar to decreasing particle diameter.

Let us return to the 5-HT problem. Increasing the column temperature to 75 °C while maintaining N ≈ 5000 should increase speed. As Figure 6.2A and B show, this is indeed the case. Now, for P_{max} = 600 bar, N = 5000 is achieved with t_0 = 1.9 s, L = 3.5 cm, u_e = 2.81 cm/s (red point, Figure 6.2B). This corresponds to a retention time of 21 s for 5-HT and an analysis time of 25 s. Increasing column temperature would permit 30 s time resolution in the microdialysis experiment. It is interesting to compare the effect of decreasing particle diameter, Figure 6.2C shows the same plot as Figure 6.2A with d_p = 1.0 μm, T = 25 °C. The line for 5000 plates and 600 bar cross at about L = 1.5 cm and u_e = 1.0 cm/s with t_0 = 2.3 s. The decrease in particle size has a similar effect on the separation quality as raising the temperature, although the speed is 20% poorer. Increasing the available pressure to 1000 bar (red dot, Fig. 6.2C) provides virtually equivalent performance to the 75 °C, 600 bar, 1.7 μm particle, case (Fig. 6.2B). Finally, we can see from the red arrow in Figure 6.2D that increasing the temperature from the conditions in Figure 6.2C more than halves t_0 to an impressive 0.8 s with L = 1.7 cm, u_e = 3.4 cm/s and N = 5000 (location of point not shown).

Finally, and briefly, we have been discussing the creation of non-standard length columns. This is not a problem for capillary columns packed in-house, but these plots readily provide useful information about the performance of columns of fixed length at various conditions.

6.3.4 Volume overload and its impact on optimization

Basal 5-HT concentration *in vivo* in the rat striatum is about 1 nM or less, sample volume is 500-1000 nL, consequently accurate quantitation for online neurotransmitter monitoring requires detection limits sufficient to determine quantitatively ~ 1 fmol or less. It is important to minimize the volume of the chromatographic zone that contains that femtomole to achieve the highest possible signal from a concentration sensitive detector. Thus, to avoid significant dilution, capillary columns are used. Column volume is typically 200-500 nL. Under these conditions injection volume often is equivalent to, or may exceed the column fluid or dead volume. Large volume injections can result in a phenomenon known as volume overload. Volume overload occurs when the injection volume contributes significantly to the observed band spreading, decreasing the apparent efficiency of the separation. It is worth noting that this phenomenon was explored by van Deemter et al. in their seminal 1956 paper [164].

The combination of on-column- and volume overload-induced band spreading leads to an observed column efficiency, N_a, shown in Eq. 6.3:

$$N_a = \frac{L}{H_a} = \frac{L}{H + \left(\sigma_{inj}^2 / L\right)} \tag{6.3}$$

where L is column length, H_a is the apparent plate height, H is the non-overload plate height (calculated as above), and σ_{inj}^2 is the injection variance. The injection variance is a function of the injection volume, column volume and solute retention factor in the sample solvent [193]. Figure 6.3 shows the plot with contours of N_a, rather than the column's intrinsic plate count, N. The apparent plate count has been calculated for fixed 125 nL injections into 100 (A), 150 (B) and 250 (C) μm ID columns while the remaining parameters are as in Figure 6.2B. Holding the injection volume constant reflects the situation in online analysis (e.g., microdialysis) in which the fixed time resolution corresponds to a particular, fixed volume of sample from a constant flow rate stream. The solute retention factor in the sample solvent was 10. What is most obvious from Figure 6.3A is the significant loss in observed column efficiency due to the 125 nL injection. Under the same conditions optimized for speed in Figure 6.2B, indicated by the red dot, N = 5000, t_0 = 1.9 s, L = 3.5 cm, u_e = 2.81 cm/s, plate count has decreased from 5000 to 1430.

It is also noteworthy to see the reflection of Eq. 6.3 in Figure 6.3A. The injection variance term is not velocity dependent. As a result, for short columns where the injection variance term is largest for a fixed injection volume and column diameter the N_a contours are flat at sufficiently high velocities.

Apparent column efficiency when injecting 125 nL onto the 100 μm ID column does not yield the required 5000 plates for accurate quantitation. There are several solutions available to regain column efficiency: decrease injection volume, increase column length, increase column diameter, improve focusing. Reducing injection volume increases efficiency by reducing volume overload effects, but a smaller volume injection decreases detector signal as the 5-HT average concentration in the eluting peak will have decreased. This is not a desirable solution. Increasing column length adds plates, improving the separation, but also adds time to the separation. The purple dot in Figure

6.3A shows this, for N_a = 5000, L = 6.9 cm and t_0 = 7.2 s. Improving sample focusing (increase k' in the sample solvent) is the best solution to maintain efficiency with large injection volumes, but is not always simple to implement. Thus we focus on the role of column diameter. Previously we have shown this parameter to be critical to the optimization for speed and sensitivity [99]. Figure 6.3B and 6.3C highlight this importance. As in Figure 6.3A purple dots in 6.3B and 6.3C show the conditions required to achieve N_a = 5000 in the shortest time (operating at P_{max} = 600 bar). Open dashed circles in each panel represent the conditions for the target 1.9 s t_0 and 30 s temporal resolution microdialysis experiments. For the 150 μm ID column in Figure 6.3B 5000 plates are generated using L = 4.4 cm, t_0 = 3.0 s and u_e = 2.24 s. Increasing diameter to 250 μm results in conditions in which L = 3.6 cm, t_0 = 2.0 s and u_e = 2.75 cm/s, virtually identical to the parameters found without volume overload.

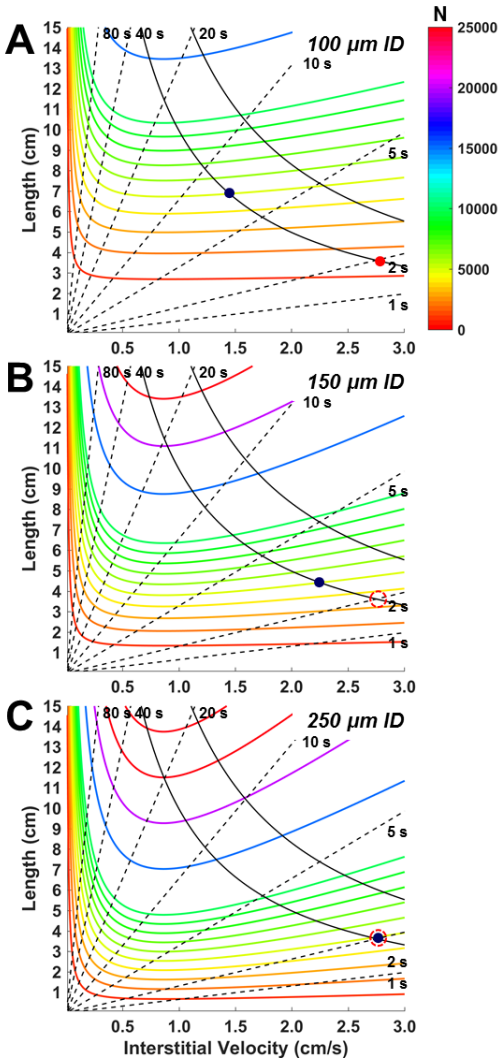

Figure 6.3. Effect of volume overload and column diameter on apparent column efficiency optimization for 1.7 µm diameter particles. A) 100 µm ID column, B) 150 µm ID column, C) 250 µm ID column. The red dot in panel A corresponds to the values of L, u_e, and N required to generate 5000 plates in the shortest time for a 600 bar pressure maximum shown in Figure 6.2B. Open red circles in B and C represent the target conditions indicated by the red dot in A. Purple dots in each panel denote the new conditions required to achieve 5000 plates factoring in volume overload effects. Injection volume was 125 nL, retention factor in the sample solvent was 10, column temperature was 75 °C. All other conditions were identical to Figure 6.1. For clarity axes labels corresponding to linear velocity 0.01 cm/s and column length 0.1 cm have been omitted.

6.3.5 Peak capacity optimization in gradient elution separations

Thus far we have optimized performance of isocratic separations using a series of graphics based on Figure 6.1. Under gradient conditions, peak capacity is the most relevant metric to assess the performance of a separation [7]. In this section we have reformatted Figure 6.1 to optimize separations of neuropeptides by maximizing peak capacity at a given gradient time. Neuropeptides are an important class of signaling molecules in the brain, regulating processes involved with pain and learning [194]. We have a longstanding interest in the fate of neuropeptides in the brain, specifically their hydrolysis by ectopeptidases [195, 196]. To understand the kinetics of neuropeptide hydrolysis, samples must be analyzed using solvent gradient elution to efficiently separate moderately hydrophobic peptides from their often very hydrophilic hydrolysis products. We illustrate this with an example, the quantitative analysis of leucine enkephalin (YGGFL) and its primary hydrolysis product in tissue, GGFL. Inclusion of sampling and LC internal standards yields a relatively simple mixture composed of four solutes accessible with isocratic elution [196]. However, much more biochemical information could be obtained by simultaneously determining other products such as YG, YGG, GFL, and FL. Gradient elution would be the best approach. Furthermore, other neuropeptides and their products span an even greater range of hydrophobicity which requires a gradient method for analysis.

Using an approach similar to that for creating Figure 6.1 we calculated values for peak capacity, n_c, using Neue's formulation [7]:

$$n_c = 1 + \frac{1}{4} N (t_o, L, u_e)^{1/2} \frac{1}{G+1} \ln \left[\frac{G+1}{G} e^{S\Delta\varphi} - \frac{1}{G} \right] \tag{6.4}$$

were N is the column efficiency, a function of t_0, L, and u_e, S is the slope of the log of solute retention factor vs eluent composition from Snyder's linear solvent strength theory [193], $\Delta\varphi$ is the range in eluent composition and $G = S\Delta\varphi t_0/t_G$, t_G is the gradient time.

Figures 6.4A and 6.4B show peak capacity optimization plots similar to Figure 6.1 for the analysis of leucine enkephalin hydrolysis mixtures using short linear gradients. Axes remain L and u_e, dashed lines indicate constant t_0, solid black lines show 600 and 1000 bar system limits. Colored contour lines in Figure 6.4 represent constant values of n_c calculated from Eq. 6.4. Contour spacing in Figures 6.4A and 6.4B are 12.5 peak capacity units. Conditions were: S = 20 (lower limit for small peptides) [197], $\Delta\varphi = 0.5$, t_G = 1 and 3 minutes, d_p = 1.7 μm, T = 25 °C. For simplicity van Deemter coefficients matched those in Table 6.1 and plate height dependence on mobile phase composition was neglected. Column efficiency and pressure were calculated with mobile phase composition set to 0.2 acetonitrile/water. The diffusion coefficient for leucine enkephalin in water is $D_{m,25\,°C} = 4.1\times10^{-6}$ cm^2/s [190]. The diffusion coefficient for leucine enkephalin under specific conditions of mobile phase composition and temperature was calculated using Eqs. E6.1 and E6.2.

What is obvious from Figures 6.4A and 6.4B is the difference in shape for the constant peak capacity contours for each gradient time and presence of a clear n_c maximum which is seemingly independent of column dimensions and system pressure. Unlike the isocratic efficiency plots (Figure 6.2) where characteristic van Deemter-curve shapes are visible under all conditions the peak capacity analogs provide a less consistent general shape, but one which is highly dependent on gradient time. At short gradient times it is particularly obvious that the contours have a shape that is different from the contours of N in the isocratic case. In both the isocratic and gradient plots, for a given length, there is an optimum velocity (reminder: irrespective of pressure limitations). However, only in the gradient plots is there also an optimum length for a given velocity.

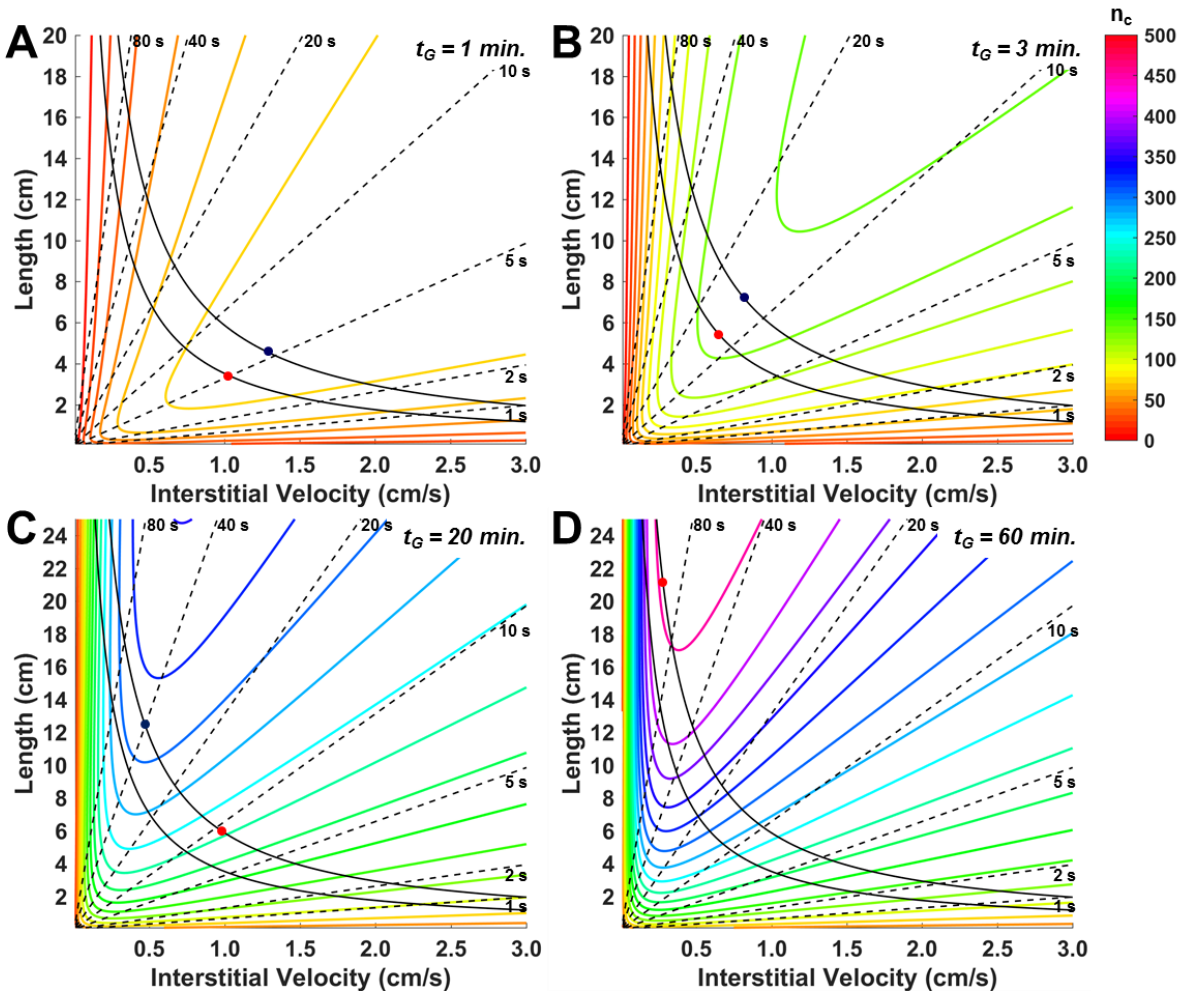

Figure 6.4. Plots for gradient elution peak capacity as a function of u_e, L and t_G for separations of neuropeptides. Gradient times were: A) 1 minute, B) 3 minutes, C) 20 minutes, D) 60 minutes. Particle size and column temperature were 1.7 μm and 25 °C, respectively. See text and Table 6.1 for other chromatographic conditions. For clarity, axis labels corresponding to linear velocity 0.01 cm/s and column length 0.1 cm have been omitted.

Now we return to the enkephalin separation. In Figure 6.4A, with 1000 bar pressure, the maximum value of n_c is 81 (purple dot). However, the contour becomes quite flat in this range of lengths and velocities for short t_G (See Figure E5.8). Thus, lengths from about 3 – 6 cm with appropriate adjustments in velocity yield n_c greater than 75 for the one-minute gradient. Operating at a pressure of 600 bar, where the maximum value of n_c is 80 (red dot), involves no practical sacrifice. As with the isocratic separations, in this regime of speed there is little to be gained from increasing pressure alone.

If we relax the time requirement, Figure 6.4B shows similar general properties at t_G = 3 min but with increased maximum peak capacity: 133 at 1000 bar and 128 at 600 bar. When considering the two upper graphs with reasonably brisk separations, we note that the optimum t_0 hardly changes with changes in pressure. Further, the optimum t_G/t_0 is in the mid-teens.

As mentioned above, we might ask the question, "If we challenge tissue with a small number of neuropeptides, what is the best approach to separation and quantitation of all detectable components in the mixture following hydrolysis in the tissue?". If we were to perfuse tissue with three neuropeptide substrates and expect 3 – 4 quantifiable products from each, the separation would focus on 9 -12 peaks, a rather modest number. Even so, the statistical peak overlap theory [198] tells us that for a 90% likelihood of a clean separation of 12 components we would need a peak capacity of 228; for a 95% probability it would be 468. From Figure 6.4C we see that to achieve a peak capacity of 228 with 1.7 μm particles at 25 °C with a 1000 bar system limit (indicated by the red dot) we need to use a 20-minute linear gradient, a 5.9 cm column and set u_e = 0.9 cm/s yielding t_0 = 9.1 s. We should point out that n_c for the 20-minute gradient can be improved. Moving up and to the left along the 1000 bar pressure contour (to the purple point) leads to a maximum achievable peak capacity of 313. New conditions for the 20-minute gradient are: L

= 12.6 cm, u_e = 0.47 cm/s and t_0 = 40.8 s. Contour spacing in Figure 6.4C and 6.4D is 25 peak capacity units.

In the interest of performing the minimum number of experiments in tissue a second question follows, "What is the maximum number of substrate peptides we can perfuse into tissue while still realizing enough peak capacity to achieve a satisfactory separation in a reasonable time?" We define a 60-minute gradient as a reasonable time. Figure 6.4D shows a maximum peak capacity of about 450 (pink contour) can be reached for the 1000 bar system using a 60-minute gradient. We should point out that further increase in column length does not yield appreciable increases in n_c, data not shown. Conditions to yield a maximum peak capacity of 460 (red point) are as follows: L = 21.5 cm, u_e = 0.27 cm/s, t_0 = 121 s, T = 25 °C. From statistical peak overlap theory and the same 90% likelihood of a clean separation we predict a peak capacity of about 450 could separate 24 peaks from 5-6 neuropeptide substrates.

6.4 CONCLUSIONS

There are several published methods of plotting chromatographic performance vs. controllable conditions (variables) that precede the one(s) presented here. The underlying ideas and quantitative expressions of those ideas are the same in all of them. What distinguishes one plot from another is mostly its intended purpose. Plots of performance have tended to emphasize the big picture and traverse orders of magnitude of variable space. Our intention has been to emphasize what can be done in the lab over a restricted range of parameters. The Carr-Wang-Stoll "two parameter" optimization is easily portrayed in graphical format here. Note that the algebra involved in that optimization is not required; the plots embody the results naturally. In "three parameter" optimization (isocratic), the particle diameter is allowed to vary in a continuous fashion (rather than being limited to commercially available particles which come in discrete sizes). It turns out

that using only commercially available particle diameters will yield a result that is acceptably close to the global optimum [191], as long as changes in diameter are made at the correct t_0, thus a small set of the present plots at commercial particle diameters can provide a pragmatic three-parameter optimization. The application to gradient elution with a similar format to isocratic elution also turns out to be quite informative. This plotting approach is somewhat more limited with gradients because there are other parameters involved such as gradient time and $S\Delta\phi$. In addition, we have not accounted for gradient compression. However, it is still clear that some general properties become evident from observing the plots. And actual laboratory conditions can be estimated for a given gradient time and desired peak capacity.

7.0 SUMMARY AND FUTURE WORK

7.1 IMPORTANT CONCLUSIONS AND SUMMARY

In the course of the work described in this dissertation, a series of tools to improve performance of modern liquid chromatography were developed. We have made significant contributions to the development of column oven technology where temperature can be changed in a *time and space dependent way* with high speed (up to 1250 °C/min, 5-70 °C) and precision (±0.1 °C). The temperature-assisted solute focusing approach has been shown effective for addressing precolumn dispersion and solving the volume overload problem in capillary liquid chromatography improving the most critical figures of merit: resolution, peak capacity and concentration sensitivity. Considerable time was also dedicated to developing an accurate simulation procedure to model TASF and two-stage TASF in isocratic and gradient elution chromatography. Further, a new graphical approach to chromatographic optimization was developed to present key concepts in simple terms for non-experts. Brief summaries of the primary conclusions from each chapter are given below.

Chapter 2 describes the development of the TASF concept, modeling its effectiveness using closed-form theory and proof-of-principle experiments. TASF is an approach designed to combat pre-column dispersion and volume overload in capillary liquid chromatography by generating transient conditions at the head of the column that lead to high retention for solute bands using column cooling. High retention conditions during the injection yields better chromatographic results. Cooling compresses the injection band as retention is higher at lower temperature. In this work a single thermoelectric or Peltier element was used to actively cool/heat the first 7 mm of a 6 cm long 0.15 mm ID fused silica column during injection to 5 °C. Following a 30 s focusing time

the cooled column segment was heated to 60 °C. Heating decreased retention and released solute bands for separation on the downstream section of the column. A simple variance based model is presented to simulate TASF chromatograms based on solute retention enthalpies and chromatographic condition in isocratic elution. The model allowed a systematic study of the effect of sample volume on observed column performance with and without TASF. Experiments were performed with samples made in mobile phase. For all injection volumes evaluated (45-1050 nL) and solutes with retention factors at 60 °C greater than or equal to 2.5, TASF reduced peak width and increased peak height, resolution and sensitivity. As an initial application, TASF was used to improve detection limits for a small molecule test solute, ethylparaben, minimizing the effect of volume overload. Detection limits using TASF were improved by a factor of 12.5 relative to the small volume isothermal control.

Chapter 3 presents a more refined, purpose built, system to implement the TASF approach. Key design improvements were replacing the large precolumn void located between the injection valve with 8 μm non-porous silica spheres and selection of a more powerful 10.9 W/cm^2 TEC to achieve faster temperature changes with electronic control over switching times. Design improvements facilitated sequences for TASF and isothermal runs to be performed unattended for up to 975 minutes (16.25 hours). Isocratic injection volume studies were performed with test solute; samples were made in mobile phase with injection volumes from 30 – 750 nL. Experiments were designed to compare design improvements between Chapter 2 and Chapter 3 devices. Solvent-based on-column focusing is the most common method used to reduce pre-column dispersion and other injection related broadening. A second injection volume study was conducted for volumes up to 3000 nL, 4.5-times the column liquid volume, with samples made in the 80:20 (v/v) mobile phase, 90:10 and 95:5 (v/v) acetonitrile/10 mM H_3PO_4 to evaluate the combination of solvent-based

focusing and the TASF approaches can have to reduce volume overload. The use of TASF and solvent-based focusing together was found very effective at counteracting injection related broadening. Finally, TASF was used to focus the moderately hydrophobic peptide galanin in a sample solvent with elution strength stronger than the mobile phase.

In contrast to the work instrument development work described in Chapters 2 and 3, Chapter 4 is a quantitative evaluation of three models to predict the concentration sensitivity enhancements achievable using solvent-based on-column focusing or preconcentration in isocratic elution. We recapitulate the theory showing the source of the preconcentration phenomena is due to: 1) solute retention by the column; their velocities are lower than the mobile phase velocity and 2) zones are compressed due to the step-gradient resulting from the higher elution strength mobile phase passing through the solute zones. A hypothesis derived by, but not verified by several workers was experimentally evaluated. This hypothesis predicted the extent of solvent-based focusing is simply the ratio of the eluted zone width (in time) to the injection time width is the ratio k_2/k_1, where k_1 is the solute retention factor in the sample solvent and k_2 is the retention factor in the mobile phase. In a second focusing model, Mills et. al derived a different result predicting overly optimistic improvements in preconcentration [48]. After accurately determining retention factors for a homologous series of *n*-alkyl parabens under three different mobile phase conditions we performed large volume injections to induce obvious volume overload. By making accurate measurements of the eluted to injected widths for a range of k_1 and k_2 values it was found the data were in general agreement with the k_2/k_1 model. Focusing was about 10% better than predicted. The Mills model was found not to be correct.

Chapter 5 returns to the TASF approach. In this chapter an improvement to the TASF concept using sequential trap and release zones called two-stage TASF is described. A system consisting

of a linear array of three 1.0-cm long, feedback loop controlled Peltier elements (*A*, *B* and *C*) was built. The two-stage TASF approach has the first two TECs, *A* and *B*, cold during the injection. Following sample loading, TEC *A* is heated; at some time following TEC *A*'s temperature rise TEC *B* is heated to match the temperature of TEC *A*. Using this approach bands get focused twice, first on the cold TEC *A*, then again on TEC *B*. The goal was to study this two-stage focusing effect in detail. powerful digital simulation procedure was developed to predict the impact of the two focusing zones on band shape (width) and band spreading. The simulation is capable of predicting chromatograms for isothermal, single-stage TASF and two-stage TASF under isocratic and gradient elution conditions. The simulation procedure was assessed by comparing simulated chromatograms to experiments with no adjustable parameters. Simulations accurately reflect experiment. Using the two-stage TASF approach a multiplicative focusing effect was induced, increasing signal for a 1500 nL injection of a low retention solute by a factor of 2.2 relative to single-stage TASF in isocratic elution. Two-stage TASF was found to be more effective in gradient elution. For a 3000 nL injection peak height increased by a factor of 3.2 for least retained solute in a test mixture when using two-stage TASF relative to single-stage TASF control. Two-stage TASF outperformed isothermal conditions for the same solute by a factor of 22.3. Further, two-stage TASF increased the peak capacity from 75 under isothermal conditions to 185 for two-stage TASF; analysis time was 12 minutes.

Chapter 6 discusses a simple graphical method to determine optimized chromatographic conditions to achieve the best separation in one's own laboratory. In the plot presented in Chapter 6 a coordinate system is formed with linear axes, column length on the vertical, mobile phase velocity on the horizontal. From the relationship between velocity and plate height, e.g. van Deemter, values for plate count, N, can be calculated for every combination of velocity and column length.

Constant N contours create a two-dimensional plot. Straight lines with intercept zero denote values of t_0. Hyperbolas correspond to constant values of pressure calculated from the product of length and velocity; hyperbolas are overlaid on the constant N contours. Points along hyperbolas represent the best performance, maximum efficiency, one can achieve for given a particle size, solute diffusion coefficient, temperature and pump pressure. We have used these plots to optimize isocratic separations of serotonin, evaluating the impact of d_p, T, d_c and V_{inj} to optimal values of column length and velocity necessary to generate 5000 plates in the shortest time. In the second part of Chapter 6 the plot is extended to maximize peak capacity in gradient elution separations of neuropeptides; peak capacity optimization replaced constant N contours with vales for n_c.

7.2 DIRECTIONS FOR FUTURE WORK

7.2.1 Instrumental advances: Active temperature control

In this section a significant instrumental advancement to that used for the TASF approach is described. This advancement led to an introduction of a broader terminology to describe the application of complex spatial and temporal temperature programs in liquid chromatography. This term is *active temperature control*, ATC. ATC means to change column temperature in a space and time dependent way. A device made of a linear array of ten 1.0 x 1.0 cm, replaceable, high power, PID-controlled Peltiers or TECs has been constructed to realize the benefits of ATC. TECs are the same as those used in Chapters 3 and 5, but controlled using LabVIEW based PID-control algorithms. PID parameters have been tuned to optimize TEC performance and facilitate use of complex multi-segment temperature programs. A schematic of the device is shown in Figure 7.1. TECs are labeled A through J from the column inlet. A 3", 28 V resistive heater is placed downstream of the TEC array. Most significant to the design of the ATC device were the ten individually replaceable TECs. Replaceable TECs solved the critical design limitation of the

device described in Chapter 5, where all three TECs were soldered to the *same* copper heat sink. Briefly, in the ATC device TECs were silver soldered to ten 1.0 cm wide, 3.5 cm long, 1.3 mm thick copper tiles. Tiles were mounted to a custom liquid cooled heat sink using 10 – 32 cap head screws. To improve heat transfer between the heat sink and copper tiles a 0.004" thick aluminum thermal sheet (TS-MF3A4, Custom Thermoelectric, Bishopville, MD) coated with a non-silicon grease was placed between the heat sink and tiles. With the ATC device, up to 10 cm long columns can be subjected to to dynamic temperature changes over about a 75 °C temperature range with 1.0 cm spatial resolution, thereby exploiting the full richness of ATC to improve chromatographic performance.

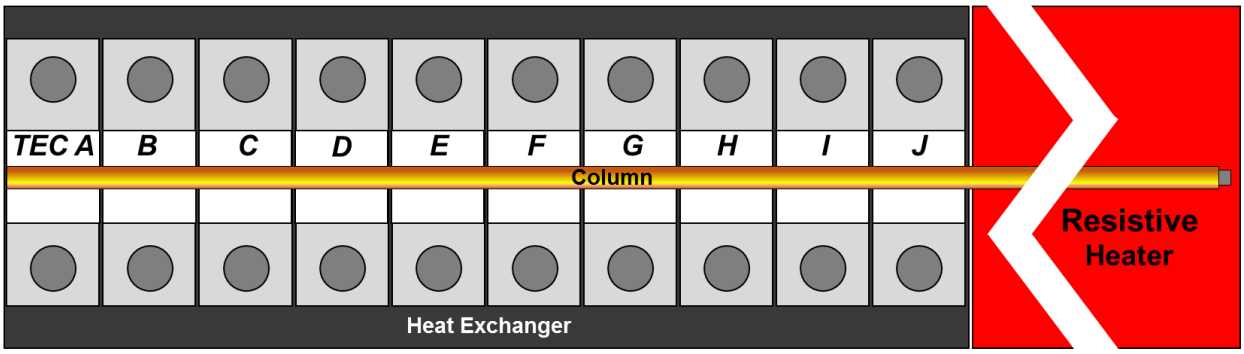

Figure 7.1. Schematic for the ten TEC active temperature control device. Ten independent, electronically controlled (PID-controlled), one-cm long Peltier elements (TEC A, B, C, etc.) were silver soldered to individual copper plates mounted to a sealed copper heat sink. The remaining segment of the column was heated using a PID-controlled resistive heater.

Figure 7.2 shows a series of experimental temperature profiles collected with the ATC device described in Figure 7.1. Panel A of Figure 7.2 shows an overlay of ten temperature profiles for each TEC. TECs had dedicated drivers and individual control programs. To highlight this each TEC performed a simulated TASF experiment where TEC switching times were varied from 10 (TEC A) to 100 s (TEC J) in 10 s divisions. A 5 °C focusing temperature was held until the desired heating time was reached when TEC temperature was stepped to 70 °C. Following heating TECs were set to 70 °C until 570 s into the run when all TECs were cooled to 5 °C to prepare for the subsequent run. Figure 7.2B shows the time derivative of the temperature profiles shown in Figure 7.2A. What is clearly evident from the time derivative plot is the high-speed heating and cooling rates achieved for the current ATC system. Heating rates up to 2460 °C/min (5-70 °C) where observed, with cooling rates in excess of -2000 °C/min (70-5 °C). These values compare favorably with those presented in Chapter 5, 1242 (5-70 °C) and -1485 (70-5 °C) for the two-stage TASF system. Heat sink temperature was 25 °C, the same value used in Chapter 5 with the two-stage TASF instrument. Figures. 7.2C and D show more complicated temperature programs where TEC temperature was stepped from initially cool (25 °C), or cold (5 °C), values to 70 °C. TECs were operated individually or as blocks of small numbers, ca. 5, of TECs. Panels 7.2E and F highlight the flexibility of the control software where temperature programs are shown with the capability to perform a series of temperature steps and linear ramps within the same run, all with individual control over TEC A-J's temperature. See the caption of Figure 7.2 for further details regarding temperature programs used in each panel.

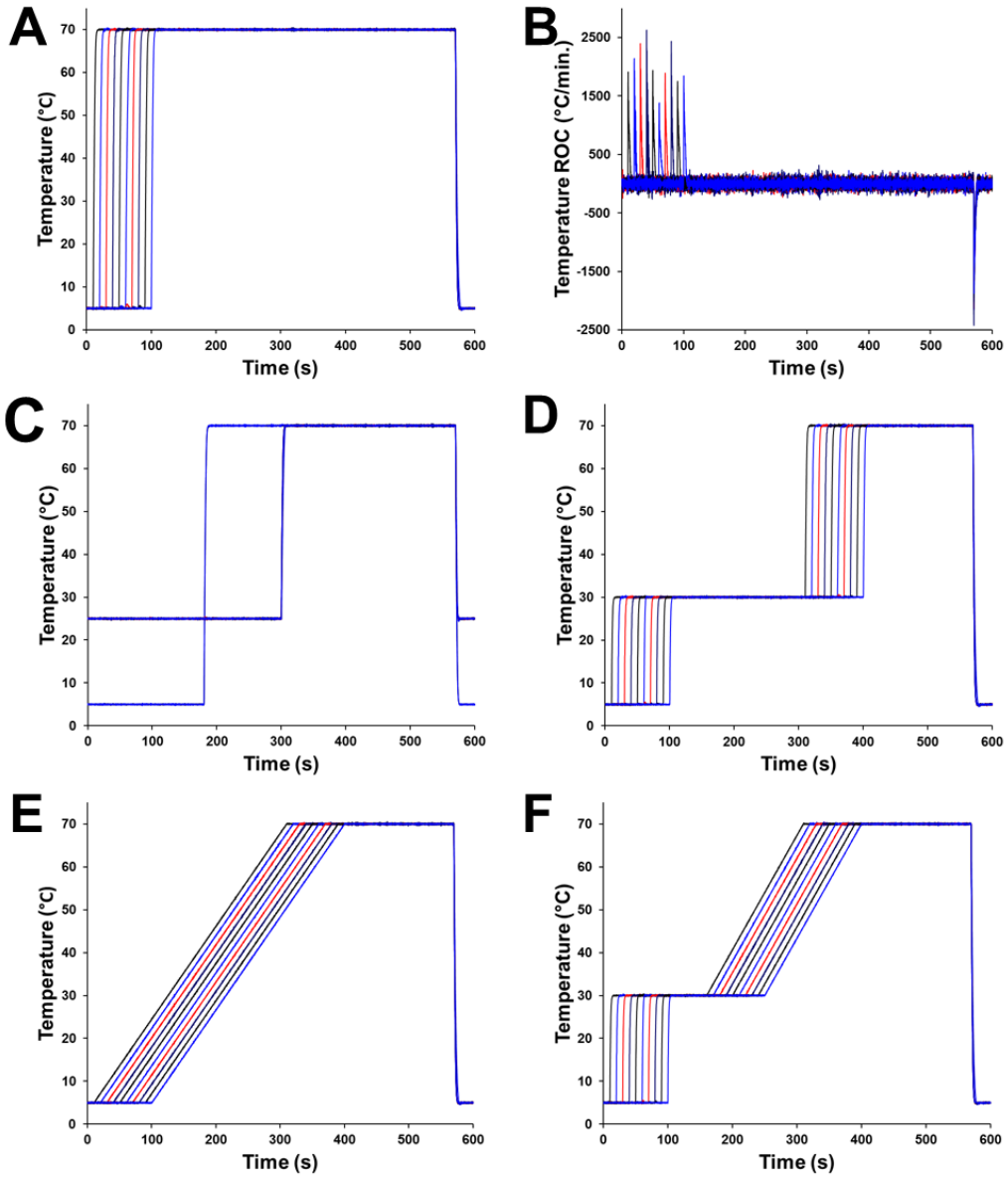

Figure 7.2. Experimental temperature profiles obtained using the ten TEC active temperature control device and PID-controlled drivers. A) TECs A-J were programmed to perform a step gradient from 5 to 70 °C, temperature changes were delayed in 10 s intervals. In all panels the ten TECs were reequilibrated to initial conditions 570 s into the run for subsequent analyses. B) Time derivative of temperature profiles show in panel A. Heating and cooling rates were fast, reaching nearly 2500 °C/min (5-70 °C) when heating and -2500 °C/min (70-5 °C) when cooling. C) Example temperature program where the first five TECs (A-E) were held at 5 °C for 180 s then heated to 70

°C. TECs F-J were maintained at 25 °C until 300 s when they were also heated to 70 °C. D) Time-delayed two-step temperature program. TECs A-J were held at 5 °C and heated to 30 °C every 10 s. The 30 °C temperature was held for 300 s when TEC temperature was again stepped to 70 °C in 10 s intervals. E) Time-delayed temperature programming example. Each TEC was held at 5 °C; every 10 s TEC temperature was increased linearly to 70 °C in 300 s. F) Example multi-segment step/linear temperature program. TEC temperatures were 5 °C, stepped to 30 °C every 10 s, held until 180 s, then increased linearly to 70 °C in 120 s.

7.2.2 Simulating active temperature control

In Chapters 2 and 5 a simple simulation procedures were presented to predict the outcome of TASF experiments. These procedures were critical to assess the performance of instrumentation and understanding of the TASF approach. Only the digital procedure described in Chapter 5 is most relevant to the current discussion. The simple, yet powerful Chapter 5 approach can predict the effect of temperature changes in two zones on retention, band shape (width) and band spreading. The procedure was validated by comparing simulated results to experiment. It was found accurate under the relatively simple conditions tested. Unfortunately, this procedure was only capable of predicting band width contributions to peak shape, as only the locations of the leading and trailing edges of the solute band were calculated directly. While effective, the procedure was unable to model the consequence of temperature changes on band shape for solute zones “straddling” column segments at different temperatures. Experiments show asymmetrical peak shapes often result. For example, in the TEC B focusing time optimization experiments shown in Figure 5.5 fronted and tailed peaks are observed when portions of the solute band begin entering or exiting column segments with different temperature. The Chapter 5 simulation procedure cannot predict

these effects on band shape. Improvements are needed as additional peak shape information is critical for method development/optimization.

7.2.2.1 Discretized simulation procedure

A discretized-convolution simulation procedure has been developed to predict chromatograms with complex, asymmetrical band shapes in liquid chromatography. The simulation procedure functions identically to the digital procedure described in Chapter 5 with one significant change. In Chapter 5 we simulated the movement of only the leading and trailing edges of the solute band as one zone. One solute, one zone. Now we subdivide the solute band into ten discrete zones, tracking the movements of the leading and trailing edges of each as they travel down the column. One solute, ten zones. At elution we calculate an observed signal from the sum of the ten individual signals obtained for the discretized zones. Upon preliminary comparison experiment the accuracy of this new approach is striking.

As an initial demonstration of the discretized-convolution simulation we evaluate its accuracy (qualitatively) for a significantly volume overload isothermal separation. Figure 7.3 shows a simulated isothermal gradient elution separation of uracil, *n*-alkyl parabens and *n*-alkyl *p*-hydroxyphenones. The simulation procedure from Chapter 5 is shown in black, the discretized-convolution program is in red. Dashed red lines in Figure 7.3B and C show the signals calculated for the ten discretized zones. The solid red line is the sum of the ten signals. See the caption of Figure 7.3 for conditions. Figure 7.3A shows the entire 12-minute simulated chromatogram, we begin our discussion here. Most apparent in Figure 7.3A is the difference between the simulated signals for solutes early in the chromatogram. The discretized signal shows narrower bands and a noticeable “tilt” for the early eluters. The Chapter 5 procedure predicts wider zones with flat tops, i.e. no shape information. Also, note that as solute retention increases with the impact of volume

overload and band width are minimized the signals for the two simulation procedures converge to produce identical signals. The accuracy of the procedure under these conditions is good, see Chapter 5 for details.

For comparison to an experimental signal see the black trace of Figure 5.7. The experimental chromatogram was generated under conditions identical to those for both simulations. First, note the same "tilt" in the signal for the early eluting solutes. We believe this is due to an additional gradient compression effect from the trailing edge of the band accelerating relative to the leading edge. Acceleration is due to the higher concentration of strong elution solvent at the rear of the zone and width of the zone over which the acceleration occurs. Figure 7.3A shows this effect for *p*-hydroxy acetophenone, the least retained solute in the mixture, for the discretized signal, the Chapter 5 procedure does not show this effect. In our discussion of the accuracy of the Chapter 5 procedure we observed systematic over-estimations in peak width for the simulation when comparing obviously volume overloaded bands to experiment. In the case of *p*-hydroxy acetopheone the simulation predicted a 42.0 s wide band, the experimental peak was 39.7 s wide. The discretized simulation predicted a narrower zone improving the fit to experiment.

Figure 7.3B focuses on the section of the chromatogram containing *n*-butyparaben. Butylparaben was the most highly retained solute in the mixture and both simulation procedures predict the same result. This is not unexpected. The 3000 nL sample is focused on the column due to high initial retention. Focusing means the only source of band width resulting from on-column convective dispersion (band spreading), not volume overload. Preliminary results with the discretized simulation procedure indicate the potential for the simulation to provide more accurate and informative simulation results.

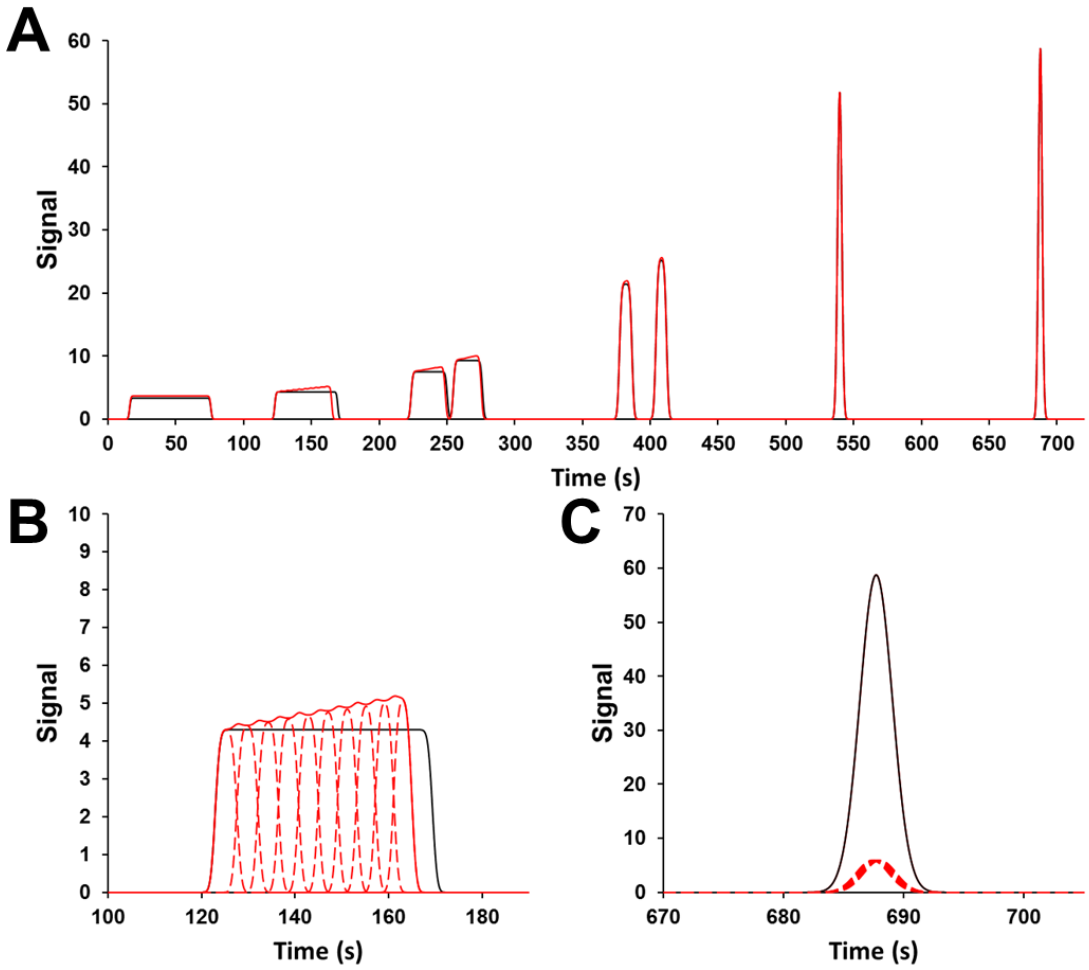

Figure 7.3. A) Simulated gradient separation of uracil, *n*-alkyl parabens and *n*-alkyl *p*-hydroxyphenones using the procedure outlined in Chapter 5 (black) and the discretized sample-convolution summation approach (red). Dashed red lines represent the ten individual chromatograms simulated using the convolution concept. The red trace is the cumulative signal from the ten underlying chromatograms. B) Excerpt of chromatogram focusing on HP2. Note the characteristic tilt in the discretized band. C) Section of the chromatogram containing PB4. No difference is observed between simulation approaches. For comparison, the experimental chromatogram obtained under the *same conditions* is shown as the black trace in Figure 5.7. Conditions: V_{inj} = 3000 nL, l = 8 cm, d_{col} = 150 µm, d_p = 1.7 µm, F = 3 µL/min, T = 70 °C, φ_1 = 0.05, φ_2 = 0.45, t_g = 16 min. For other simulation conditions see Table D4.3.

Now we test the discretized simulation procedure's ability to predict complex peak shape information. Figure 7.4 shows simulated isocratic two-stage TASF separations of ethylparaben under two sets of conditions. We selected simulation conditions to have portions of the ethylparaben bands in two regions of the column at different temperatures simultaneously. Simulation conditions accurately reflect those observed in the TEC B focusing time optimization experiments performed in Chapter 5. (See Figure 5.5 for experimental chromatograms.) Conditions can be found in the caption of Figure 7.4. Fig. 7.4A shows the two-stage TASF experiment where TEC A focusing time is 35 s and TEC B focusing time is 40 s. The discretized simulation is shown in red, the Chapter 5 procedure in black. The 40 s focusing time in Figure 7.4A was chosen to not be sufficient to allow the entire ethylparaben band enter the 5 °C TEC B prior to heating to 70 °C. We expect only a portion of the band to experience a second TASF focusing stage and provide a tailed peak. This is the same result seen in Figure 7.4A; the first six zones of the discretized sample receive the additional focusing of the second TASF stage, the last four do not. A highly tailed band shape results. This is chromatographically undesirable. The Chapter 5 method provides no such peak shape information.

Figure 7.4B shows another two-stage TASF separation of ethylparaben. The discretized method is in blue, the Chapter 5 method in black. In this simulation TEC B focusing time was increased to 70 s, a value long enough to begin letting solute leak from 5 °C TEC B into the 70 °C portion of the column. We would expect to observe a fronted band as solute exiting the focusing zone prior to the focusing time is unaffected by the presence of the focusing zone. Solute that remains in TEC B during heating will be compressed increasing its signal. This is exactly the result the discretized simulation procedure provides. We see the first three discretized segments exiting TEC B prior to heating are not focused twice while the final seven receive the additional focusing. A tailed peak

results; again no such peak asymmetry information is provided by the Chapter 5 method. The additional peak shape information offered by the discretized method is useful in TASF and ATC optimization procedures where TEC switching times for up to ten independently controlled TECs need to be determined.

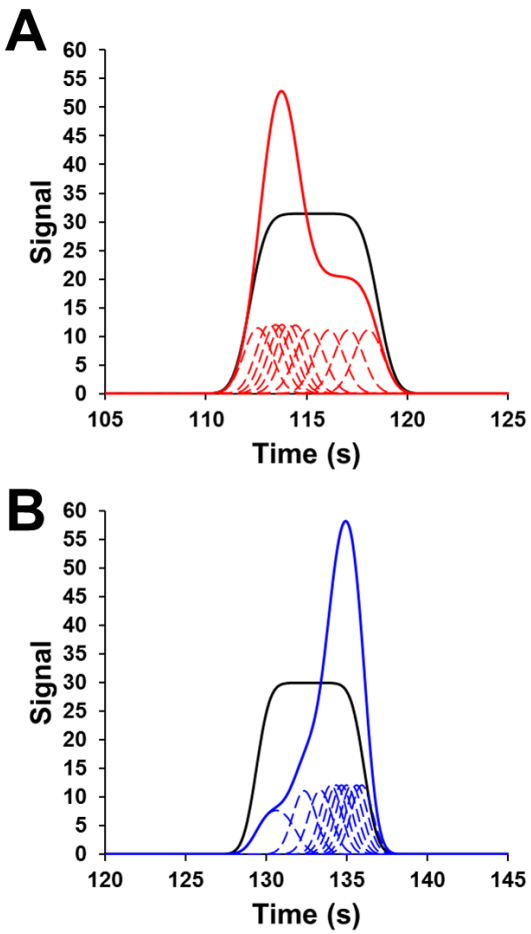

Figure 7.4. Simulated isocratic two-stage TASF separations of PB2 with variable TEC B focusing times. TEC A focusing time was 35 s, TEC B focusing time was 40 s (A) and 70 s (B). Focusing times were selected to ensure bands were in two TECs at two different temperatures during the temperature change. The black traces in both panels represent the signals obtained using the simulation procedure described in Chapter 5. The red and blue traces used the discretized sample-convolution approach. Dashed lines show the ten individual segments of the sample. Conditions: V_{inj} = 1500 nL, l = 8 cm, d_{col} = 150 µm, d_p = 1.7 µm, F = 3 µL/min, T_1 = 5 °C, T_2 = 70 °C φ = 0.2 (w/w). For other simulation conditions see Table D4.2. For comparison to experimental chromatograms see Figure 5.5.

7.2.2.2 Retention enthalpy database

A primary goal of future work is to understand how to fully exploit the ATC concept. To best achieve this, we must first simulate interesting experiments due to the number of experimentally adjustable parameters a device with ten independently controlled TECs, each operating at a different temperature, with different switching times, and solvent gradient elution contains. This is an optimization nightmare. A digital simulation procedure has been developed and validated in Chapter 5; the simulation has been further refined in Section 7.2.2. Now retention data on a large number of more *chemically interesting* solutes is required.

A library of 105 structurally diverse, but related compounds has been assembled; solvent and temperature dependent retention data has been collected for each solute on the Waters Acquity BEH C18 stationary phase. Thus far, retention data has been calculated at 21 mobile phase compositions and a minimum of 5 temperatures at each composition. The retention library contains nearly 24000 individual retention measurements made at 6000 different combinations of solute, temperature and mobile phase composition. Data collection and preliminary analysis has been completed, results are presented below.

7.2.2.2.1 Chemicals

Uracil and all test solutes shown in Table 7.1 were purchased from either Sigma-Aldrich (St. Louis, MO), TCI America (Philadelphia, PA) or Alfa Aesar (Ward Hill, MA). Standard solutions for each solute were made by dissolving each individually in acetonitrile. Uracil and theobromine stocks were made in deionized water. Water was from a Millipore Milli-Q Synthesis A10 water purification system (Billerica, MA) and used without further treatment. Acetonitrile (LC/MS Optima grade) and phosphoric acid (HPLC grade) were from Fisher Scientific (Fair Lawn, NJ).

Table 7.1. Solute names, chemical formula, clog P (calculated using Chemicalize.org) and structures for the retention enthalpy solutes.

Index	Common Name	Abbreviation	Molecular Weight (g/mol)	Formula	clog P	Structure
1	Benzene	Bz	78.11	C_6H_6	1.97	
2	Toluene	1Bz	92.14	C_7H_8	2.49	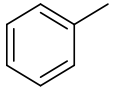
3	Ethylbenzene	2Bz	106.17	C_8H_{10}	2.93	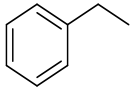
4	n-Propylbenzene	3Bz	120.20	C_9H_{12}	3.38	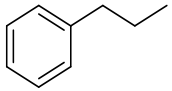
5	n-Butylbenzene	4Bz	134.22	$C_{10}H_{14}$	3.82	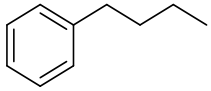
6	n-Pentylbenzene	5Bz	148.25	$C_{11}H_{14}$	4.26	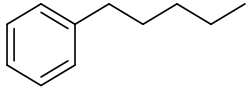
7	Iso-butylbenzene	i3Bz	134.22	C_9H_{12}	3.66	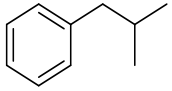
8	Benzaldehyde	BzA	106.12	C_7H_6O	1.69	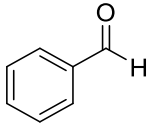
9	Acetophenone	AP2	120.15	C_8H_8O	1.53	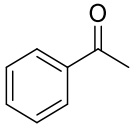

Table 7.1 Continued.

10	Propiophenone	AP3	134.18	$C_9H_{10}O$	2.23	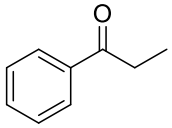
11	Butyrophenone	AP4	148.21	$C_{10}H_{12}O$	2.68	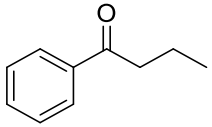
12	Valerophenone	AP5	162.23	$C_{11}H_{14}O$	3.12	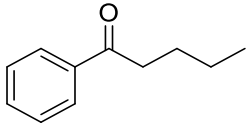
13	Hexanophenone	AP6	176.26	$C_{12}H_{16}O$	3.57	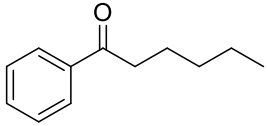
14	Heptanopheone	AP7	190.29	$C_{13}H_{18}O$	4.01	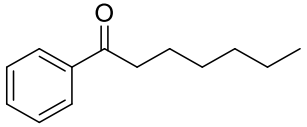
15	Octanophenone	AP8	204.31	$C_{14}H_{20}O$	4.45	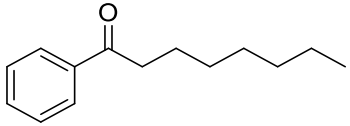
16	Benzoic acid	BA	122.12	$C_7H_6O_2$	1.63	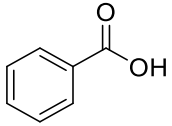
17	Methyl benzoate	Bz1	136.15	$C_8H_8O_2$	1.98	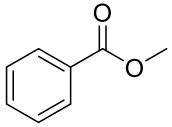

Table 7.1 Continued.

18	Ethyl benzoate	Bz2	150.18	$C_9H_{10}O_2$	2.33	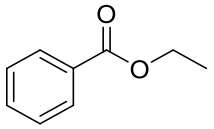
19	n-Propyl benzoate	Bz3	164.20	$C_{10}H_{12}O_2$	2.86	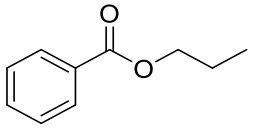
20	n-Butyl benzoate	Bz4	178.23	$C_{11}H_{14}O_2$	3.30	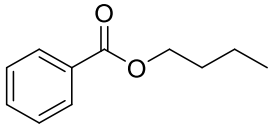
21	p-Hydroxybenzaldehyde	hBzA	122.12	$C_7H_6O_2$	1.38	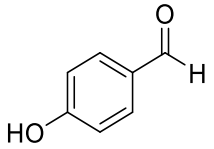
22	p-Hydroxyacetophenone	HP2	136.15	$C_8H_8O_2$	1.23	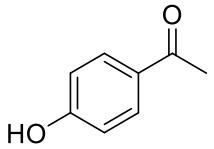
23	p-Hydroxypropiopheone	HP3	150.18	$C_9H_{10}O_2$	1.93	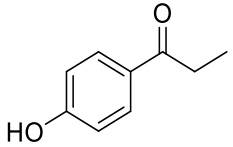
24	p-Hydroxybutyropheone	HP4	164.20	$C_{10}H_{12}O_2$	2.37	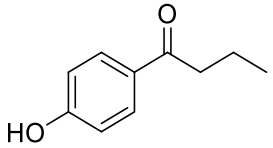

Table 7.1 Continued.

25	p-Hydroxybenzoic acid	hBA	138.12	$C_7H_6O_3$	1.33	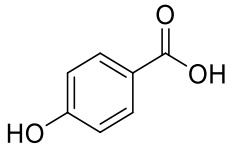
26	Methylparaben	PB1	152.15	$C_8H_8O_3$	1.67	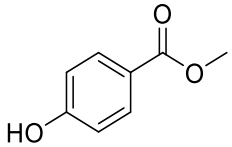
27	Ethylparaben	PB2	166.18	$C_9H_{10}O_3$	2.03	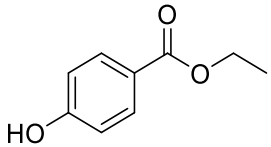
28	n-Propylparaben	PB3	180.20	$C_{10}H_{12}O_3$	2.55	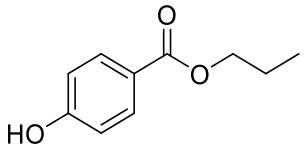
29	n-Butylparaben	PB4	194.23	$C_{11}H_{14}O_3$	3.00	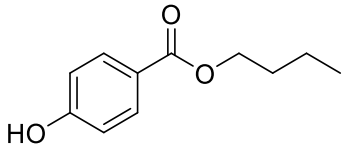
30	Indole	Ind	117.15	C_8H_7N	2.07	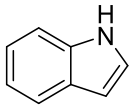
31	Indene	Inde	116.16	C_9H_8	2.70	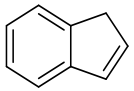
32	Naphthalene	Naph	128.17	$C_{10}H_8$	2.96	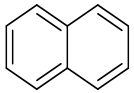
33	Diphenylmethane	DPM	168.24	$C_{13}H_{12}$	4.07	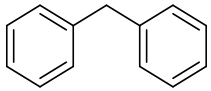

Table 7.1 Continued.

34	Biphenyl	BPh	154.21	$C_{12}H_{10}$	3.62	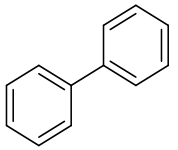
35	Diphenylmethanol	DPol	184.24	$C_{13}H_{12}O$	2.99	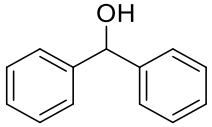
36	Benzophenone	BzP	182.22	$C_{13}H_{10}O$	3.43	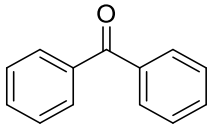
37	Diphenylsulfone	DPS	218.27	$C_{12}H_{10}O_2S$	2.93	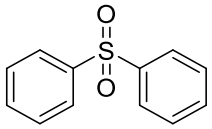
38	Diphenylamine	DPA	169.23	$C_{12}H_{11}N$	3.41	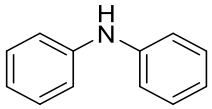
39	Diphenyl ether	DPE	170.21	$C_{12}H_{10}O$	3.47	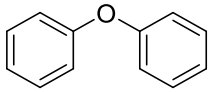
40	Carbazole	Car	167.211	$C_{12}H_9N$	3.09	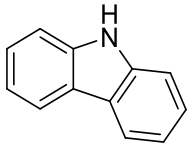
41	Phenyl benzoate	BzPh	198.22	$C_{13}H_{10}O_2$	3.63	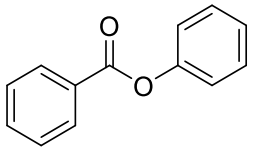

Table 7.1 Continued.

42	Benzoin	BzI	212.25	$C_{14}H_{12}O_2$	2.65	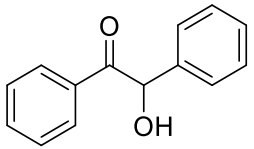
43	Benzanilide	BzTan	197.24	$C_{13}H_{11}NO$	3.07	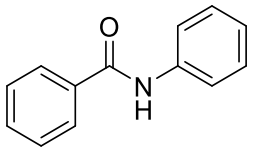
44	Benzamide	BzAd	121.14	C_7H_7NO	0.82	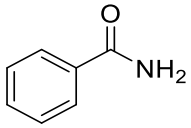
45	N-Methylbenzamide	nBzAd	135.17	C_8H_9NO	1.05	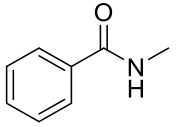
46	Acetanilide	AcTan	135.17	C_8H_9NO	1.21	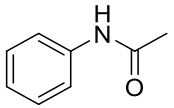
47	α,α,α-Trifluorotoluene	TFT	146.11	$C_7H_5F_3$	2.85	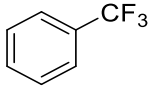
48	Fluorobenzene	FBz	96.10	C_6H_5F	2.12	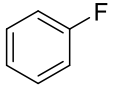
49	1,3-Difluorobenzene	dFBz	114.10	$C_6H_4F_2$	2.26	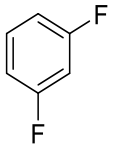
50	2-Fluororbibenyl	FBPh	172.20	$C_{12}H_9F$	3.76	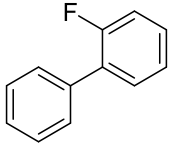

Table 7.1 Continued.

51	Nitrobenzene	NtBz	123.11	$C_6H_5NO_2$	1.91	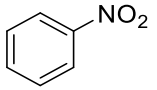
52	Chlorobenzene	ClBz	112.56	C_6H_5Cl	2.58	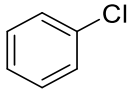
53	1,3-Dichlorobenzene	dClBz	147.0	$C_6H_4Cl_2$	3.18	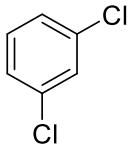
54	Benzenesulfonamide	BzSa	157.19	$C_6H_7NO_2S$	0.58	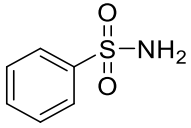
55	Phenol	Phenol	94.11	C_6H_6O	1.67	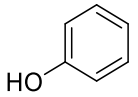
56	4-Methoxypheonol	4MPh	124.14	$C_7H_8O_2$	1.51	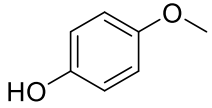
57	Salicylic acid	ScA	138.12	$C_7H_6O_3$	1.98	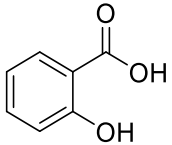
58	Vanillic acid	HVA	168.15	$C_8H_8O_4$	1.17	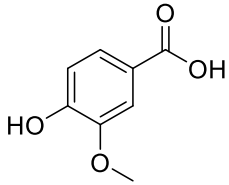
59	Phenylacetic acid	PhAA	136.15	$C_8H_8O_2$	1.61	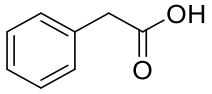

Table 7.1 Continued.

60	p-hydroxyphenylacetic acid	HPhAA	152.15	$C_8H_8O_3$	1.31	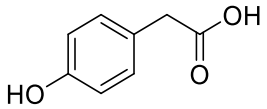
61	2-Phenylpropionic acid	PhAA	150.18	$C_9H_{10}O_2$	2.15	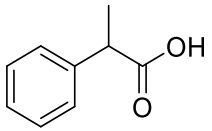
62	4-Methoxybenzonitrile	4MCN	133.15	C_8H_7NO	1.67	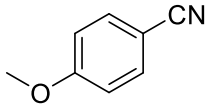
63	Anisole	Ans	108.14	C_7H_8O	1.82	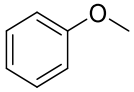
64	Ethoxybenzene	BzO2	122.17	$C_8H_{10}O$	2.17	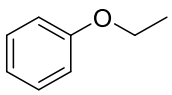
65	2-Methoxynaphthalene	mNap	158.20	$C_{11}H_{10}O$	2.81	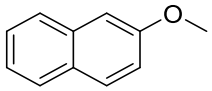
66	2-Naphthalenacetic acid	2NAA	186.21	$C_{12}H_{10}O_2$	2.60	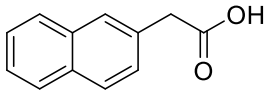
67	Phenyl acetate	PhAc	135.15	$C_8H_8O_2$	1.58	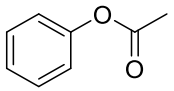
68	3-Indoleacetic acid	InAA	175.19	$C_{10}H_9NO_2$	1.71	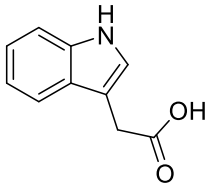
69	5-Hydroxyindole	hInd	133.15	C_8H_7NO	1.77	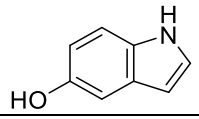

Table 7.1 Continued.

70	2-Methylhippuric acid	2HiP	193.20	$C_{10}H_{11}NO_3$	1.04	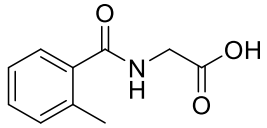
71	4-Methylhippuric acid	4HiP	193.20	$C_{10}H_{11}NO_3$	1.04	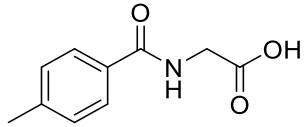
72	Caffeine	Caff	194.19	$C_8H_{10}N_4O_2$	-0.55	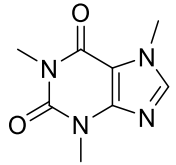
73	Theobromine	The	180.17	$C_7H_8N_4O_2$	-0.77	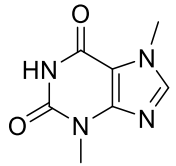
74	2,6-Dichloropyridine	dClPy	147.99	$C_5H_3Cl_2N$	2.40	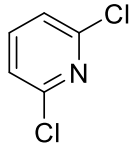
75	2-Chloroquinoline	ClQu	163.6	C_9H_6ClN	2.96	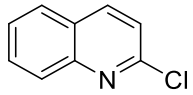
76	6-Methoxy-8-nitroquinoline	mnQu	204.19	$C_{10}H_8N_2O_3$	1.91	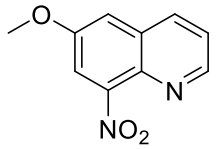
77	N-Phenylanthranilic acid	Pan	213.34	$C_{13}H_{11}NO_2$	4.37	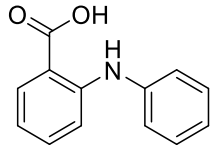

Table 7.1 Continued.

78	Ibuprofen	Ibu	206.29	$C_{13}H_{18}O_2$	3.84	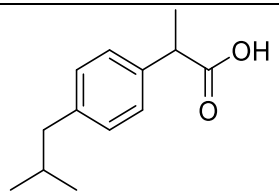
79	Loxoprofen	Lox	246.31	$C_{15}H_{18}O_3$	3.35	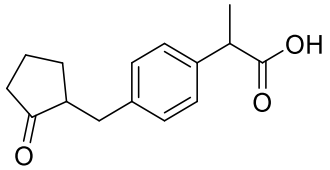
80	Ketoprofen	Ket	254.29	$C_{16}H_{14}O_3$	3.61	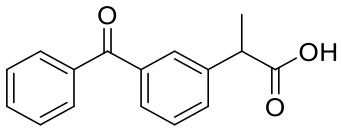
81	Naproxen	Nap	230.36	$C_{14}H_{14}O_3$	2.99	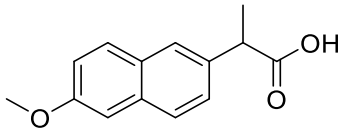
82	Indoprofen	IndP	281.31	$C_{17}H_{15}NO_3$	2.86	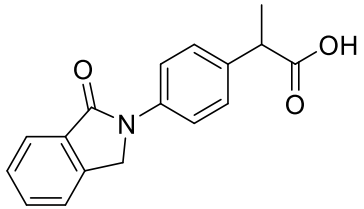
83	Carrprofen	CarP	273.72	$C_{15}H_{12}ClNO_2$	3.88	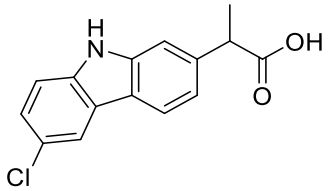

Table 7.1 Continued.

84	Flurbiprofen	FlBp	244.27	$C_{15}H_{13}FO_2$	3.94	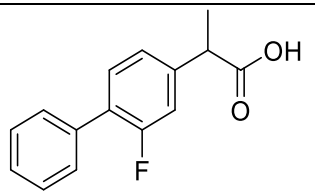
85	Fenoprofen	FenP	242.27	$C_{15}H_{14}O_3$	3.65	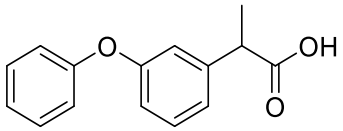
86	Aspirin	Asp	180.16	$C_9H_8O_4$	1.24	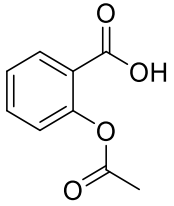
87	Salsalate	Sal	258.23	$C_{14}H_{10}O_5$	3.64	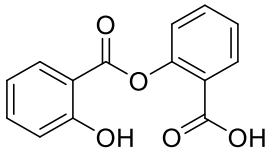
88	Diflunisal	DifS	250.20	$C_{13}H_8F_2O_3$	3.91	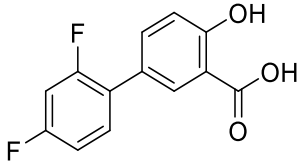
89	Flufenamic acid	FFen	281.23	$C_{14}H_{10}F_3NO_2$	5.25	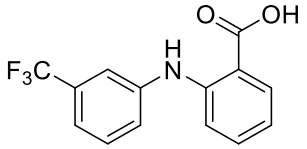
90	Mefenamic acid	MFen	241.29	$C_{15}H_{15}NO_2$	5.40	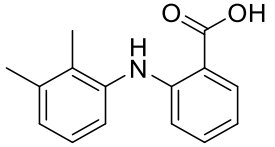

Table 7.1 Continued.

91	Tolfenamic acid	Tof	261.71	$C_{14}H_{12}ClNO_2$	5.49	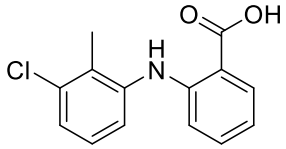
92	Diclofenac acid	DCFen	296.15	$C_{14}H_{11}Cl_2NO_2$	4.26	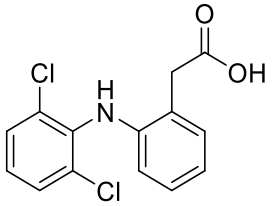
93	Aceclofenac	ACFen	354.18	$C_{16}H_{13}Cl_2NO_4$	3.88	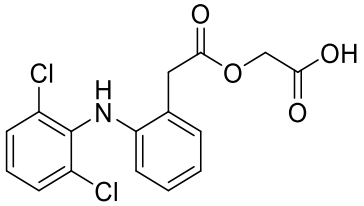
94	Etodolac	EtD	287.36	$C_{17}H_{21}NO_3$	3.44	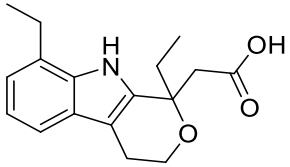
95	Oxaprozin	OxA	293.32	$C_{18}H_{15}NO_3$	3.46	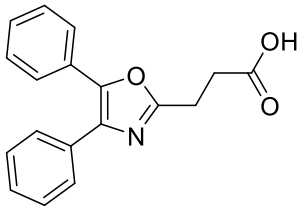
96	Phenylbutazone	PhBtz	308.38	$C_{19}H_{20}N_2O_2$	4.14	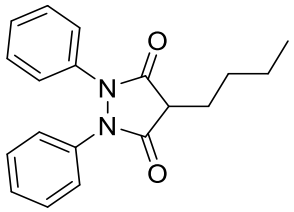

Table 7.1 Continued.

97	Nabumentone	Nab	228.29	$C_{15}H_{16}O_2$	3.22	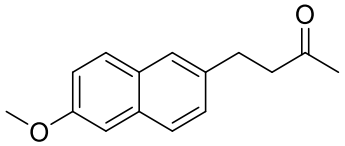
98	Fenbufen	FenB	254.29	$C_{16}H_{14}O_3$	3.00	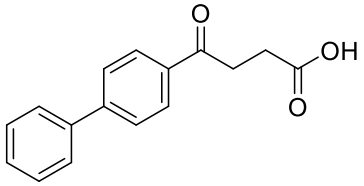
99	Nimesulide	Nim	308.31	$C_{13}H_{12}N_2O_5S$	1.79	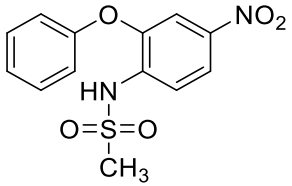
100	Piroxicam	Pir	331.35	$C_{15}H_{13}N_3O_4S$	0.60	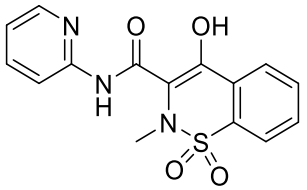
101	Meloxicam	Mel	351.40	$C_{14}H_{13}N_3O_4S_2$	1.60	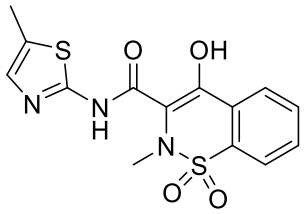

Table 7.1 Continued.

102	Indometacin	IndM	357.79	$C_{19}H_{16}ClNO_4$	3.53	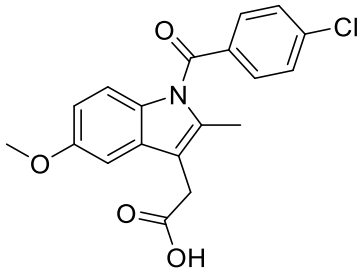
103	Sulindac	Sul	356.41	$C_{20}H_{17}FO_3S$	2.93	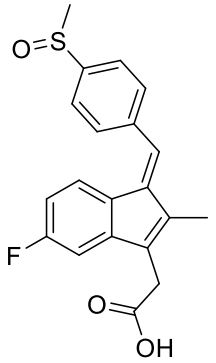
104	Acetaminophen	AcTP	151.17	$C_8H_9NO_2$	0.91	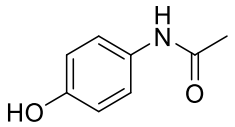
105	Phenacetin	PhAct	179.22	$C_{10}H_{13}NO_2$	1.41	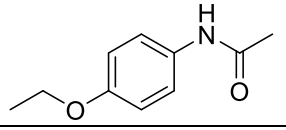

7.2.2.2.2 Instrumentation

A Jasco X-LC 3000 system consisting of a 3059AS autosampler, dual 3085PU semi-micro pumps, 3080DG degasser, 3080MX high pressure mixer, 3177UV variable wavelength UV absorbance detector, and LC-Net II/ADC from Jasco Inc. (Easton, MN) was used to evaluate the temperature and solvent composition dependence of solute retention. Either a CO-2060 or CO-2067 thermostatted column compartments, also from Jasco, were used to regulate column temperature. Data were acquired using ChromNAV version 1.19.3 software. Chromatograms were exported and analyzed using a peak finding program written in MATLAB 2015a (MathWorks, Natick, MA).

7.2.2.2.3 Chromatographic conditions

Temperature-dependent retention factors for all solutes in Table 7.1 were measured on a series of four new Waters Acquity BEH C18 (50 mm x 2.1 mm I.D., 1.7 μm d_p) columns. The 105 solutes were broken into four roughly equivalent groups and screened from 0.975:0.025 to 0.05:0.95 10 mM H_3PO_4/acetonitrile. Care was taken to group solutes from homologous series into the same sample running them on the same column and batch of mobile phase when possible. Samples were made in mobile phase at concentrations between 100 and 500 μM. Column temperature was varied from 25 to 75 °C in 10 °C steps at each mobile phase composition using the CO-2060 oven and 25-65 °C using the CO-2067 oven. The CO-2067 column oven had a temperature maximum of 65 °C, thus the 75 °C runs were omitted. Mobile phase compositions tested ranged from 0.025 to 0.95 (w/w) acetonitrile/10 mM H_3PO_4 in 0.025 (w/w) acetonitrile steps from 0.025 to 0.10, then 0.05 (w/w) steps to 0.95 (w/w) acetonitrile. Each mobile phase was made by weight to improve composition accuracy. Weight-to-weight aqueous-organic compositions were converted to volume-to-volume units using density data provided by Billen et al. [88]. Detection at 100 Hz used absorbance at 220 and 254 nm; injection volume was 5 μL. Flow rate was set to 0.35 mL/min.

Retention times were adjusted for extra column time determined using a Valco zero-dead-volume union in place of the column.

7.2.2.2.4 Preliminary results: Nonlinear fitting to the Neue-Kuss equation

An equation designed by Neue and Kuss to model the influence of changes in solvent composition and column temperature was fit to the raw retention data for all 105 test solutes [160]. This equation is shown as Eq. 7.1:

$$\ln k = -\ln k_{0,T} + \frac{D}{T} + 2\ln(1 + a\phi) - \left(1 + \frac{D}{T}\right)\frac{B_T\phi}{1 + a\phi} \tag{7.1}$$

where T is the temperature in Kelvin, φ is the volume-based mobile phase composition, a and D are coefficients to express the influence of solvent and temperature and $k_{0,T}$ and B_T are the coefficients for retention in 100% water and the slope of the retention relationship with solvent composition including temperature effects. Nonlinear curve fitting for each solute was performed in Excel as described in Section 5.4.1. Results for all solutes are organized in Table 7.2. Fits for all well retained solutes were good, with R^2 values in excess of 0.9990. Fit quality did show a strong correlation with mobile phase composition decreasing for both the high and low acetonitrile compositions. This result was due to the small, but measurable retention of uracil under the highly aqueous, <10% acetonitrile, and organic, >90% acetonitrile, conditions. We are in the process of quantitatively addressing this problem.

Table 7.2. Curve fitting results for Neue-Kuss retention equation using the Waters Acquity BEH C18 column as a function of temperature (25-65 °C) and solvent composition.

Index	Analyte	ln $k_{0,T}$	B_T	a	D	Fit (R^2)	n[a]
1	Bz	2.38	1.14	0.38	2083	0.9993	260
2	1Bz	2.66	1.42	0.70	2674	0.9997	260
3	2Bz	2.87	1.52	0.80	3174	0.9995	280
4	3Bz	3.01	1.37	0.68	3466	0.9989	260
5	4Bz	3.14	1.15	0.47	3609	0.9984	260
6	5Bz	3.27	0.99	0.32	3741	0.9983	240
7	i4Bz	3.51	1.11	0.46	3700	0.9983	312
8	BzA	3.00	1.63	0.93	2054	0.9990	312
9	AP2	2.46	2.26	1.37	2150	0.9994	260
10	AP3	2.50	2.01	1.17	2547	0.9995	260
11	AP4	2.76	1.98	1.20	3059	0.9994	240
12	AP5	3.10	1.93	1.20	3600	0.9993	260
13	AP6	3.41	1.85	1.17	4085	0.9990	260
14	AP7	3.64	1.70	1.04	4418	0.9987	240
15	AP8	3.80	1.49	0.86	4588	0.9984	240
16	BA	4.24	2.20	1.53	2624	0.9993	240
17	Bz1	2.65	2.03	1.22	2542	0.9995	260
18	Bz2	2.78	2.05	1.27	3026	0.9994	240
19	Bz3	3.04	1.98	1.25	3527	0.9993	260
20	Bz4	3.28	1.89	1.20	3974	0.9991	260
21	hBzA	4.71	2.33	1.85	2354	0.9989	160
22	HP2	4.77	2.85	2.37	2605	0.9995	192
23	HP3	4.30	2.66	2.04	2892	0.9998	216
24	HP4	4.07	2.65	1.95	3259	0.9998	216
25	hBA	6.11	2.15	1.67	2639	0.9979	120
26	PB1	4.65	2.50	1.96	2902	0.9998	216
27	PB2	4.30	2.64	1.99	3270	0.9998	216
28	PB3	4.23	2.70	2.02	3770	0.9997	216
29	PB4	4.33	2.59	1.93	4252	0.9995	240
30	Ind	4.35	1.30	0.71	2836	0.9997	240
31	Inde	3.08	1.60	0.91	3116	0.9998	280
32	Naph	3.76	1.59	0.98	3573	0.9995	288
33	DPM	3.33	1.88	1.17	4258	0.9993	260
34	BPh	3.74	1.56	0.92	3936	0.9992	288
35	DPol	3.14	2.57	1.72	3368	0.9998	200
36	BzP	3.76	1.95	1.30	3723	0.9995	288
37	DPS	4.15	2.29	1.64	3629	0.9999	200
38	DPA	4.08	1.87	1.22	4083	0.9998	240

Table 7.2 Continued.

39	DPE	3.48	1.79	1.09	4037	0.9994	260
40	Car	4.60	2.06	1.49	4213	0.9998	220
41	BzPh	3.42	1.99	1.26	3971	0.9995	240
42	BzI	2.90	3.02	2.06	3234	0.9997	200
43	BzTan	3.31	2.09	1.29	3006	0.9997	220
44	BzAd	2.88	2.96	1.43	1647	0.9987	120
45	nBzAd	1.86	4.00	2.10	1510	0.9992	140
46	AcTan	2.66	2.86	1.69	1856	0.9990	160
47	TFT	2.70	1.83	1.03	3224	0.9996	240
48	FBz	2.43	1.31	0.52	2241	0.9994	260
49	dFBz	2.36	1.33	0.52	2320	0.9992	260
50	FBPh	3.32	1.93	1.21	4125	0.9993	260
51	NtBz	2.68	1.14	0.34	2093	0.9984	260
52	ClBz	2.67	1.45	0.71	2724	0.9995	280
53	dClBz	3.10	1.61	0.93	3418	0.9995	280
54	BzSA	4.18	2.20	1.52	2007	0.9977	140
55	Phenol	3.83	2.00	1.45	2185	0.9990	200
56	4MPh	3.78	2.23	1.56	2169	0.9998	180
57	ScA	4.75	1.87	1.33	2841	0.9989	220
58	VA	5.30	3.16	2.61	2638	0.9991	144
59	PhAA	4.06	2.16	1.42	2580	0.9994	240
60	HPhAA	6.63	2.82	2.63	3018	0.9988	144
61	2PhP	4.02	2.52	1.81	3062	0.9998	240
62	4MCN	3.59	1.78	1.11	2621	0.9997	240
63	Ans	3.04	1.33	0.64	2424	0.9996	312
64	BzO2	3.09	1.46	0.77	2847	0.9997	312
65	mNap	3.99	1.65	1.05	3731	0.9995	288
66	2NAA	4.84	2.96	2.36	4151	0.9996	216
67	PhAc	2.86	1.70	0.92	2319	0.9992	288
68	InAA	5.46	2.56	2.05	3303	0.9996	160
69	hInd	5.50	1.46	1.12	2400	0.9998	160
70	2HiP	2.56	3.38	1.77	1855	0.9998	140
71	4HiP	3.15	3.22	1.89	2322	0.9998	160
72	Caff	3.28	4.85	2.67	2084	0.9961	120
73	The	4.40	3.73	0.55	1941	0.9904	80
74	dClPy	1.58	1.39	0.46	1760	0.9986	300
75	ClQu	2.42	2.12	1.28	2624	0.9994	260
76	mnQu	1.78	2.22	1.13	1972	0.9973	260
77	Pan	4.71	2.82	2.20	4948	0.9997	220
78	Ibu	3.94	2.67	1.94	4857	0.9990	264
79	Lox	3.56	4.05	3.05	4239	0.9998	160
80	Ket	4.44	3.32	2.59	4658	0.9995	216
81	NaP	4.68	3.19	2.52	4678	0.9996	216
82	IndP	4.29	4.55	3.64	4867	0.9998	160

Table 7.2 Continued.							
83	CarP	5.10	3.70	3.05	6108	0.9997	200
84	FlBp	4.08	3.44	2.65	5331	0.9997	200
85	FnP	4.13	3.26	2.49	5048	0.9997	200
86	Asp	4.32	2.96	2.24	2828	0.9997	216
87	Sal	4.71	2.94	2.29	4496	0.9999	200
88	DifS	5.14	2.99	2.42	5274	0.9998	220
89	FFen	4.43	2.95	2.24	5810	0.9994	220
90	MFen	4.44	2.71	2.06	5436	0.9992	240
91	Tof	4.53	2.47	1.85	5387	0.9991	220
92	DCFen	4.41	3.03	2.32	5307	0.9996	200
93	ACFen	4.64	3.21	2.50	5782	0.9996	200
94	EtD	3.48	3.30	2.43	4877	0.9994	220
95	OxA	3.61	4.12	3.19	5504	0.9995	200
96	PhBtz	3.26	2.51	1.67	4485	0.9992	220
97	Nab	3.73	2.59	1.85	4243	0.9996	220
98	FenB	4.49	3.58	2.83	5089	0.9998	180
99	Nim	5.04	2.34	1.73	4543	0.9998	200
100	Pir	2.29	4.15	2.90	3066	0.9991	200
101	Mel	4.05	3.37	2.61	4419	0.9996	200
102	IndM	4.39	3.37	2.62	5736	0.9994	200
103	Sul	4.52	6.00	4.92	6364	0.9996	140
104	AcTP	5.43	4.20	3.91	2281	0.9975	96
105	PhAct	2.89	3.39	2.27	2519	0.9998	216

[a]Total number of experimental data points used in nonlinear curve fitting.

Panel A of Figure 7.5 shows simulated ln k versus φ curves using the four Neue-Kuss parameters for each solute in Table 7.2. Column temperature was 70 °C. The degree of chemical diversity and large number of solutes explains the high degree of overlap between all 105 curves. Panel B plots a subset of 29 non-steroidal anti-inflammatory (NSAID) and over the counter pain relievers.

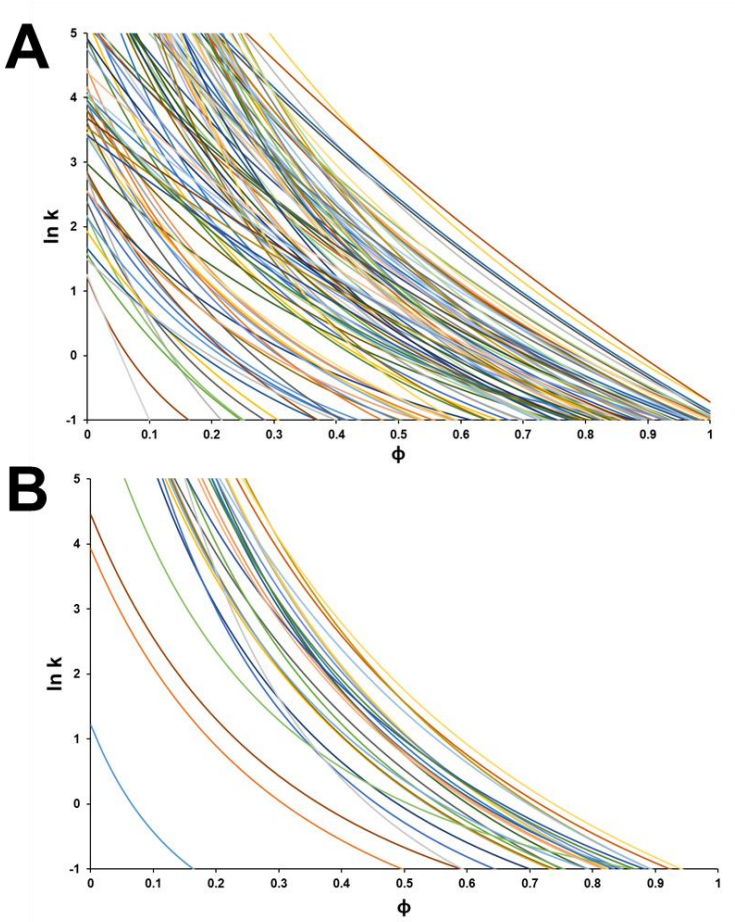

Figure 7.5. A) Simulated ln k versus φ (v/v) plots obtained from the Neue-Kuss fits for the 105 retention enthalpy solutes shown in Table 7.1. B) ln k verses φ (v/v) plot for the subset of 29 non-steroidal anti-inflammatory (NSAID) and pain reliever test solutes. Column temperature in both panels is T = 70 °C. Retention data was collected on four new Waters Acquity BEH C18, 1.7 μm d_p columns from 97.5:0.025 (w/w) to 5:95 (w/w) 10 mM H_3PO_4/acetonitrile. Experimental column temperatures were: 25, 35, 45, 55, 65 and 75 °C.

7.2.2.2.5 Future work

Future work will include: 1) gather more retention data on different stationary phases and 2) determine what additional information resides in the collected dataset. First, we will begin collecting retention data for the same 105 solutes on two additional reversed phase materials. We have selected a polar-embedded amide column (Supelco Ascentis Express RP-Amide) and a pentafluorophenyl propyl phase (Supelco Ascentis Express F5). We have acquired five columns of each phase from their manufacturer. From the data we have we will determine functional group contributions to standard state retention enthalpies. We will apply the extrathermodynamic concept expressed for free energies by the Martin equation. This concept states that retention enthalpy is the sum of the enthalpies of retention from the individual fragments that comprise the molecule. In creation of our 105-solute library we have taken care to select specific solutes that differ by only one or a small number of molecular fragments. Thus, from the solvent and temperature dependent retention data for a small number of test solutes we can elucidate a single molecular fragment's contribution to retention enthalpy. Our hope is to use this information to predict retention enthalpies for compounds for which we have not collected retention data.

APPENDIX A

Supplemental Information for Chapter 2.

A1.1 van`t Hoff retention studies for parabens on Waters BEH C18 phase

Figure A1.1 shows the van't Hoff plot generated for the four parabens tested under the conditions outlined in Section 2.3.2.2. Plots were found to be linear over the temperature range evaluated for samples run in triplicate after inspection of each regression's residuals. Retention factors calculated at 5 and 60 °C from the regression applied to Figure A1.1 are reported in Table A1.1.

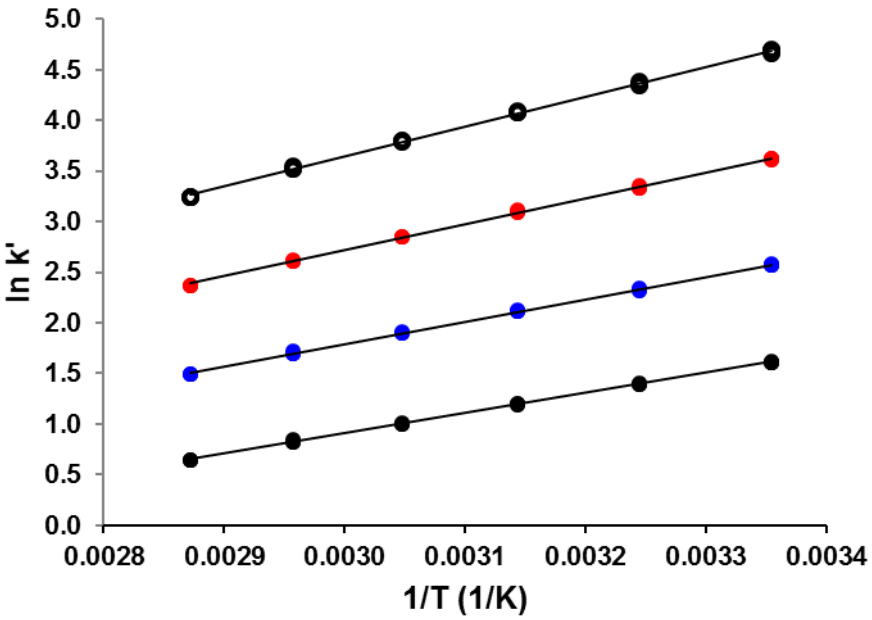

Figure A1.1. van`t Hoff plot for methylparaben (●), ethylparaben (●), propylparaben (●), and butylparaben (○) from 25 to 75 °C. For chromatographic conditions see section 2.3.2.2.

A1.2. TASF simulations, experimental details

A1.2.1 Influence of changes in focusing and separation temperature

The following discussion illustrates the series of relationships used to generate simulated isothermal and TASF separations *in silico*. To model the potential for a hypothetical TASF analysis the influence of column temperature on solute retention factor and reduced velocity must be known accurately. The van`t Hoff equation was used to describe the relationship between solute retention factor and column temperature:

$$\ln k' = -\frac{\Delta H^0}{RT} + \frac{\Delta S^0}{R} + \ln \varphi \qquad \text{(A1.1)}$$

where ΔH^0 is the standard state retention enthalpy, ΔS^0 is the standard state retention entropy, R is the ideal gas constant and φ is the column phase ratio. From experimental plots of ln k' vs. 1/T, so-called van`t Hoff plots (Figure A1.1), retention factors were predicted at specific trapping and separation temperatures.

Temperature's influence on reduced velocity arises from reduced velocity's inverse dependence on solute diffusion coefficient. Diffusion coefficients are dependent on mobile phase viscosity and temperature. An empirical relationship for viscosity as a function of composition and temperature [26] was fit to the apparent integral viscosities at 400 bar for water-acetonitrile mixtures between 20 and 100 °C [88] resulting in:

$$\eta(T) = 10^{\left[-2.533+{}^{742}/_{T}-0.452X_{ACN}+\left({}^{235}/_{T}\right)X_{ACN}+1.573X_{ACN}^2-\left({}^{691}/_{T}\right)X_{ACN}^2\right]} \qquad \text{(A1.2)}$$

Diffusion coefficients at various temperatures and mobile phase compositions were calculated based on the following empirical equation [91]:

$$D_{m,i}(T) = D_{m,i,T'} \times \frac{T \times \eta(T')}{T' \times \eta(T)} \quad \text{(A1.3)}$$

where the diffusion coefficient for solute i at a given temperature (T') is known ($D_{m,i,T'}$). Diffusion coefficients for solutes used in TASF simulations are shown in Table A1.1.

Table A1.1. Experimental diffusion coefficients for each solute in water at 37 °C [87, 199] and retention factors calculated from Table 1.2 at focusing and separation temperatures.

Solute	**$D_{m,37\ °C}$ (cm^2/s)**	**$k'_{5\ °C}$**	**$k'_{60\ °C}$**
Methylparaben	1.09×10^{-5}	8.2	2.5
Ethylparaben	9.80×10^{-6}	18.0	4.5
Propylparaben	9.06×10^{-6}	70.2	15.3
Butylparaben	7.04×10^{-6}	222.5	38.4
Uracil[ı]	9.34×10^{-6}	-	-

[ı]Diffusion coefficient measured at 30 °C and converted to 37 °C here using Eq. A1.3.

A1.2.2 Practical considerations of experimental setup

The physical size of the injection valve stator and associated fittings necessary to connect the column to the valve creates a practical problem. Contained within this 18-20 mm segment of the

room temperature valve is stationary phase. The large size of the valve places a 2 cm long column in front of the Peltier cooled trapping segment. Solutes must first be presented with the cooled trapping segment upon initial interaction with the stationary phase for effective focusing. If not analyte bands begin to separate on this 2 cm pre-column. If retention is high enough solutes may not reach the trap before TEC polarity is reversed negating any potential benefit of the TASF approach. To alleviate this problem experiments effectively removed this pre-column by leaving it void of stationary phase. This exact solution to the problem of uncontrolled column temperature within the injection valve was first proposed by Holm et al. [81] in their application of Peltier based column cooling.

Introduction of the pre-column void is not without practical consequences. The void adds significantly to the pre-column volume, >300 nL for the 150 μm I.D. columns used in this work, introducing additional dispersion and making accurate calculations for solute residence time in the trapping segment (t_{focus}) and observed retention time ($t_{R,i}$) more difficult. Due to the relatively short length, 2 cm, and wide diameter of the pre-column void accurate determination of its contribution to observed dispersion is difficult to model theoretically, i.e. it is not in the Taylor-region. The following method was used to ascertain an approximate value for dispersion introduced by the pre-column void used in TASF simulations. A series of three 45 nL, 60 °C isothermal injections of methylparaben and ethylparaben were made and observed peak variances and retention times were measured. Using the Knox equation the column variance (Eq. 1.10) at reduced velocities of 3, 5 and 10 were estimated from the A, B, C, and n coefficients in Table 2.3. To account for a potentially more poorly packed column two D-coefficients were used in the calculation, 0.42 and 0.6. Post-column dispersion was predicted from Taylor theory. Dispersion due to the column and post-column were subtracted from the observed peak variances for

methylparaben and ethylparaben. A value for the isothermal time variance due to the pre-column void ($\sigma^2_{t,void,iso}$) was estimated from the average of these six values and found to be 0.000571 min^2.

To account for the time delay introduced by the pre-column dead volume the void time (t_{void}) was calculated as:

$$t_{void} = \frac{\pi a^2 L_{void}}{F} \tag{A1.4}$$

where a is the column radius, L_{void} is the length of the void, and F is the volumetric flow rate. The focusing time (t_{focus}) on column 1 is given by:

$$t_{focus} = t_s - t_{void} \tag{A1.5}$$

where t_s is the time when TEC polarity is reversed, heating the focusing segment of the column to the separation temperature. Retention times for retained solutes, $t_{R,i}$, in TASF experiments were calculated by summing the individual times required to progress through the fluidic system:

$$t_{R,i} = t_{inj} + t_{void} + t_{focus} + t_{res,2} + t_{post} \tag{A1.6}$$

where t_{inj} is the injection time, t_{void} is the void time, t_{focus} is the time the solute resides in the trapping segment, $t_{res,2}$ is the time required to the solute to elute from the rest of the column, and t_{post} is the time required to pass through the post column tubing.

Table A1.2 shows the 10 injection volumes used in simulated experiments.

Table A1.2. Values used for injection volume in simulations.

Injection Number	**V_{inj} (nL)**
1	45
2	60
3	90
4	120
5	225
6	450
7	600
8	750
9	900
10	1050

Figure A1.2 shows simulated 5 and 45 nL injections in a hypothetical system without any pre-column void, i.e. $\sigma^2_{t,void,iso} = 0$. Uracil concentration was reduced by a factor of 10 and 5 for the 5 and 45 nL injection simulations.

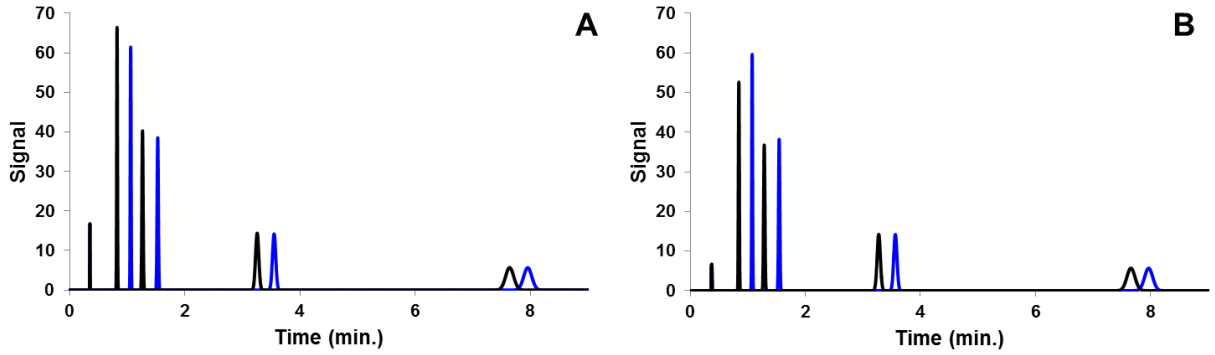

Figure A1.2. Simulated isothermal (——) and TASF (——) separations with 5 °C focusing and 60 °C separation temperatures. Panel A shows a 5 nL injection and panel B a 45 nL; all values used in the simulation were identical to those of Figure 1.2 except for the removal of the pre-column dispersion, $\sigma^2_{t,void,iso} = 0$.

A1.3. Sample information for injection volume experiments

Table S3 shows the 15 injection volumes tested, their sample concentrations and solute mass injected on-column. Due to the high retention factor for butylparaben under the isocratic conditions used it was less susceptible to volume overload. As such it was omitted from the 60, 90, 150, 300, and 825 nL injections.

Table A1.3. Sample information for injection volume experiments.

		Mass On-Column (ng)			
V_{inj} (nL)	**[Sample] (µM)**	**Methylparaben**	**Ethylparaben**	**Propylparaben**	**Butylparaben**
45	500	3.4	3.7	4.1	4.4
60	500	4.6	5.0	5.4	-
75	500	5.7	6.2	6.8	7.3
90	250	3.4	3.7	4.1	-
120	250	4.6	5.0	5.4	5.8
150	250	5.7	6.2	6.8	-
225	100	3.4	3.7	4.1	4.4
300	100	4.6	5.0	5.4	-
450	100	6.8	7.5	8.1	8.7
600	50	4.6	5.0	5.4	-
750	50	5.7	6.2	6.8	7.3
825	50	6.3	6.9	7.4	-
900	25	3.4	3.7	4.1	4.4
975	25	3.7	4.1	4.4	4.7
1050	25	4.0	4.4	4.7	5.1

APPENDIX B

Supplemental Information for Chapter 3.

B2.1. van`t Hoff retention studies for parabens on Waters BEH C18 phase

Solute retention factors were corrected for extra-column contributions to retention time using Eq. B2.1:

$$k' = \left(\frac{t_R - t_0}{t_0 - t_{EC}}\right) \tag{B2.1}$$

where t_R is solute retention time, t_0 is the column void time and t_{EC} is the extra column void time. The van`t Hoff equation was used to describe the relationship between solute retention factor and column temperature:

$$\ln k' = -\frac{\Delta H^0}{RT} + \frac{\Delta S^0}{R} + \ln \varphi \tag{B2.2}$$

where ΔH^0 is the standard state retention enthalpy, ΔS^0 is the standard state retention entropy, R is the ideal gas constant and φ is the column phase ratio. From experimental plots of ln k' vs. 1/T, so-called van`t Hoff plots (Figure. B2.1), retention factors were predicted at specific trapping and separation temperatures.

Figure B2.1 shows the van't Hoff plots generated for the four parabens under the conditions outlined in Section 3.2.2.2. Plots were found to be linear over the evaluated temperature range for

samples run in triplicate after inspection of each regression's residuals. Panels A-C shows results for the 90:10, 80:20 and 70:30 10 mM H_3PO_4/acetonitrile mobile phases, respectively. Table B2.1 shows the results for the linear regressions applied to the van't Hoff plots in Figure B2.1.

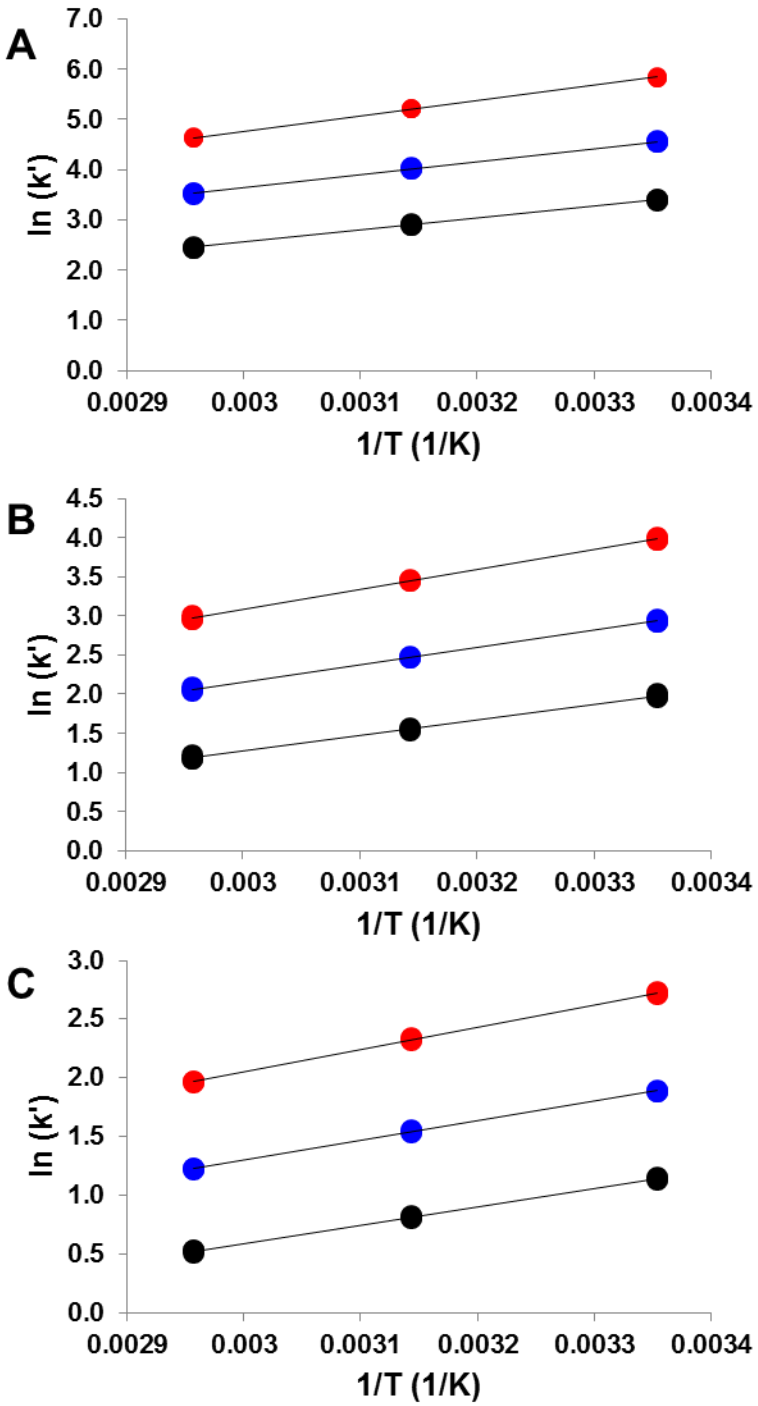

Figure B2.1. van`t Hoff plot for methylparaben (●), ethylparaben (●), and propylparaben (●) from 25 to 65 °C. Panels A-C shows results for the 90:10, 80:20 and 70:30 10 mM H_3PO_4/acetonitrile mobile phases, respectively For chromatographic conditions see Section 3.2.2.2.

Table B2.1. Partial molar enthalpies of retention for methylparaben through propylparaben obtained from slopes of the van`t Hoff plots in Figure B2.1. For chromatographic conditions see Section 3.2.2.2.

ϕ	Solute	-ΔH°/R (K)	Std Error	Intercept	Std Error
	Methylparaben	2394	17	-4.63	0.06
0.1	Ethylparaben	2611	23	-4.20	0.07
	Propylparaben	3036	23	-4.34	0.07
	Methylparaben	2000	35	-4.73	0.11
0.2	Ethylparaben	2205	32	-4.46	0.10
	Propylparaben	2547	33	-4.56	0.10
	Methylparaben	1556	20	-4.08	0.06
0.3	Ethylparaben	1667	21	-3.70	0.07
	Propylparaben	1901	23	-3.65	0.07

B2.2. TASF instrumentation

Figure B2.2 shows plots of temperature and pressure profiles collected from the TASF stability study discussed in Section 3.3.2. The x-axis has been plotted to emphasize the first 90 s of a typical TASF separation. The black dashed line has been placed at 35 s to indicate the focusing time, the time when TEC temperature was changed from T_1 to T_2.

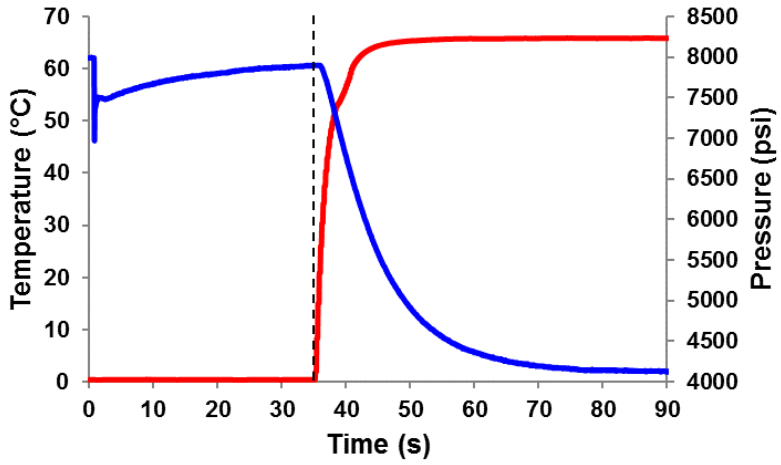

Figure B2.2. Column temperature (——) and pressure (——) profiles from TASF stability study described in Section 3.3.2.

Figure B2.3 shows the long-term stability of the TASF instrumentation. Panel A shows this by plotting the temperature (panel A) and pressure profiles (panel B) collected over the entire 975-minute sequence. Temperature and pressure stability over the course of a 975-minute sequence was good.

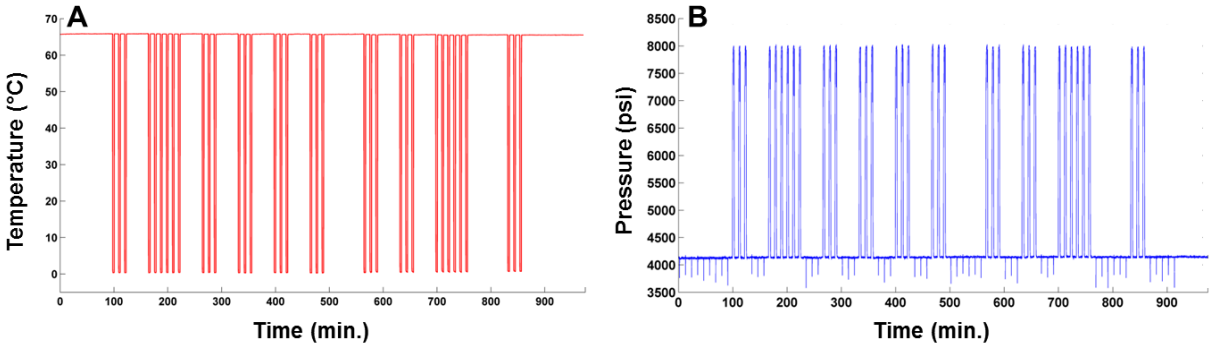

Figure B2.3. Column temperature (——) and pressure (——) profiles from TASF stability study described in Section 3.3.2.

B2.3. Data Analysis

The MATLAB script used to determine peak FWHM values is provided below. The program plotted each run, showing the selected baseline and FWHM for each peak. The file was input into the MATLAB workspace as a single chromatogram containing the series of individual injections. Data was first separated from a sequence of chromatograms into individual runs by factoring in analysis run time. Each run was analyzed for peaks using the "findpeaks" command from the MATLAB Signal Processing Toolbox. This command finds the local maxima within each data set by specifying the minimum peak height and minimum distance between peaks. From the maximum, the algorithm moves down the left and right sides of the peak to determine the baseline. This is done by measuring the slope between two adjacent points 4 seconds apart until the slope reaches or passes zero. The 4 second window was chosen so that algorithm would not stop at noise and the point closest to the peak was used to determine the start of the baseline. The baseline was then averaged on both sides of the peak. Once the baseline of the peak was determined, another algorithm moved down from the peak maximum until it reached peak half height on either side allowing FWHM measurement to be made. The minimum number of data points spanning a FWHM in a single peak was 24 (FWHM = 0.92 s).

Visual inspection allowed for conformation of FWHM values. This program was fairly automated, only requiring optimization of the following parameters: minimum peak height, distance between peaks, length of run, slope thresholds and number of runs. The program allowed rapid analysis of roughly 100 chromatograms containing 5 peaks each in about 20 seconds.

MATLAB Script:

```
clear
clf

hertz = 25;
load 2014-07-17-cgram.mat;
[columnlength,width] = size(cgram2);
```

```
%startingval shifts the window for chopping
startingval = 0;
startrun = 2;
numruns = 70;
%runlentest = 0, analysis; =1, no analysis
runlentest = 0;
%peakstart chooses what peak to start with for outputting the analysis
peakstart = 1;
peakendminus = 0;
runtime = 9.1;

for run = startrun:numruns;
    lenrun = runtime*60*hertz;
    choppeddatatime(:,run) = cgram2(startingval+run*lenrun-lenrun+1:startingval+run*lenrun,1);
    choppeddataabs(:,run) = cgram2(startingval+run*lenrun-lenrun+1:startingval+run*lenrun,2);
    if runlentest == 1
        plot(choppeddatatime(:,run),choppeddataabs(:,run))
        test = run
        pause
        clf
    end
end

for run = startrun:numruns
    %datacollectionrate
    data(:,2) = choppeddataabs(:,run);
    data(:,1) = choppeddatatime(:,run);
    [pks,loc] = findpeaks(data(:,2),'minpeakheight',5,'minpeakdistance',900);
    actualloc = loc/60/25

    %number of peaks
    numpeaks(run,:) = size(loc);

    noisethresh = -0.000001
    distthresh = 100

    %find ends of peaks
    for i=peakstart:numpeaks(run,1)-peakendminus
        lft = loc(i)-800;
        rgt = loc(i)+100;
        while data(lft+distthresh,2) - data(lft,2) > noisethresh
            lft = lft - 1;
        end
        left(i) = lft;
        while data(rgt-distthresh,2) - data(rgt,2) > noisethresh
            rgt = rgt + 1;
        end
        right(i) = rgt;
    end

    %baseline on each side of peaks
    for i=peakstart:numpeaks(run,1)-peakendminus
        leftbaseline = data(left(i)-50:left(i),2);
        rightbaseline = data(right(i):right(i)+50,2);
        peakbaselineavg(i,1) = mean(leftbaseline);
        peakbaselineavg(i,2) = mean(rightbaseline);
    end

    %FWHM
    for step = peakstart:numpeaks(run,1)-peakendminus
        avgbaseline(step,1) = (peakbaselineavg(step,1)+peakbaselineavg(step,2))/2;
        peakheight(step,1) = pks(step,1) - avgbaseline(step,1);
        halfpeakheight(step,1) = peakheight(step,1)/2;
        lft = loc(step)-1;
        rgt = loc(step)+1;
        while halfpeakheight(step,1) < (data(lft,2)-avgbaseline(step,1));
            lft = lft - 1;
        end
        fwhmleft(step,1) = lft;
        while halfpeakheight(step,1) < (data(rgt,2)-avgbaseline(step,1));
```

```
            rgt = rgt + 1;
        end
        fwhmright(step,1) = rgt;
        fwhm(1,step) = (fwhmright(step,1) - fwhmleft(step,1))/hertz/60;
    end


    plot(choppeddatatime(:,run),choppeddataabs(:,run))

    xlabel('Time (min)')
    ylabel('Absorbance (mAu)')
    hold on
    for i = peakstart:numpeaks(run,1)
        p1 = [data(left(i),1),data(left(i),2)];
        p2 = [data(right(i),1), data(right(i),2)];
        plot([p1(1),p2(1)],[p1(2),p2(2)],'Color','r','LineWidth',0.5)
        hold on
        fwhm1 = [data(fwhmleft(i,1),1),data(fwhmleft(i,1),2)];
        fwhm2 = [data(fwhmright(i,1),1),data(fwhmright(i,1),2)];
     plot([fwhm1(1),fwhm2(1)],[fwhm1(2),fwhm1(2)],'Color','r','LineWidth',0.5)
        hold on
    end
    fwhmminutes(run,1:numpeaks(run,1)) = fwhm(1:numpeaks(run,1))
    test = run
    pause
    clf
end
```

B2.4. Second generation TASF instrumentation injection volume control experiments

Table B2.3 shows the 10 injection volumes tested, their sample concentrations and solute mass injected on-column.

Table B2.2. Sample information for injection volume experiments.

		Mass On-Column (ng)		
V_{inj} (nL)	**[Sample] (μM)**	**Methylparaben**	**Ethylparaben**	**Propylparaben**
30	750	3.4	3.7	4.1
75	500	5.7	6.2	6.8
150	250	5.7	6.2	6.8
225	175	6.0	6.5	7.1
300	150	6.8	7.5	8.1
375	125	7.1	7.8	8.4
450	100	6.8	7.5	8.1
525	75	6.0	6.5	7.1
600	50	4.6	5.0	5.4
750	20	3.1	3.1	3.4

Figures B2.4 and B2.5 shows the results from the control experiments used to evaluate the improved TASF system performance. See sections 3.2.3.4 and 3.3.3 for experimental details and further discussion.

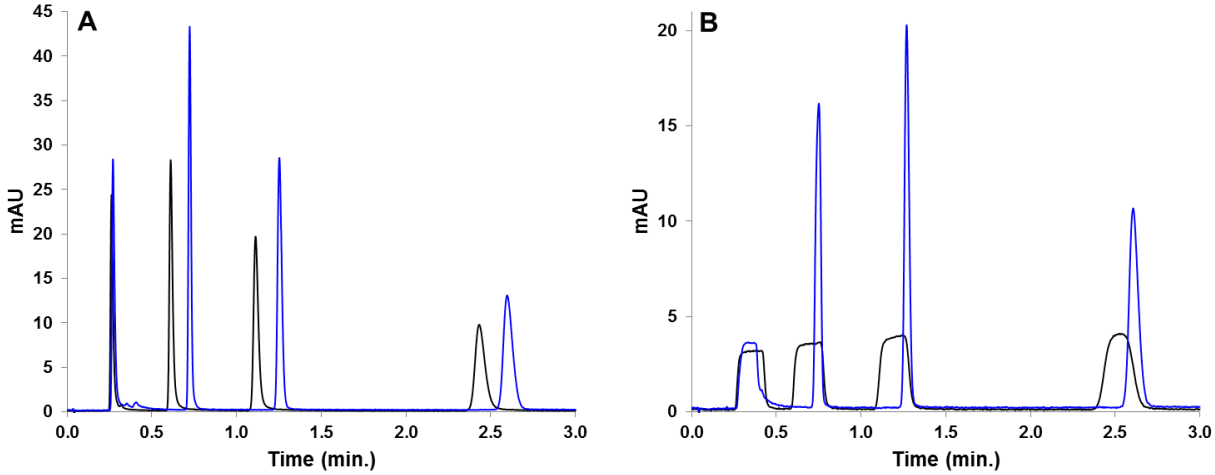

Figure B2.4. Example chromatograms from TASF separations of paraben samples made in mobile phase. Isothermal (——) separations were performed at 70 °C. A 5 °C focusing temperature and 15 s focusing time were used with the TASF approach (——). Panel A shows the 30 nL injection, panel B the 750 nL. For chromatographic conditions see Section 3.2.3.4.

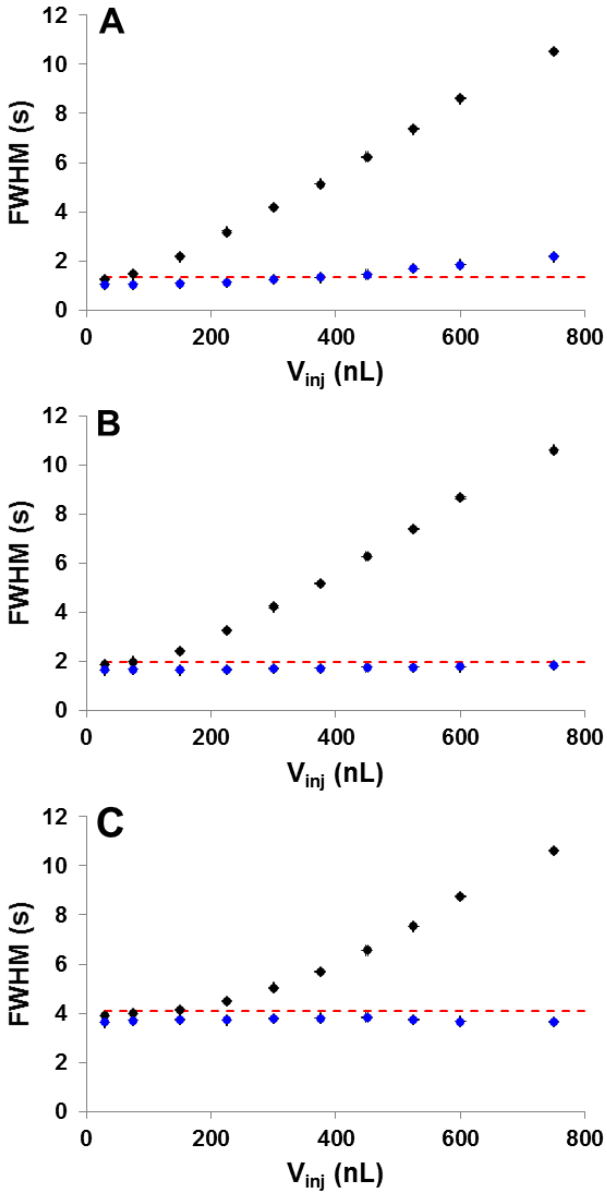

Figure B2.5. Results from the injection volume experiments performed under isothermal (●) and TASF (●) conditions with paraben mixtures made in mobile phase. Panels A, B, and C correspond to methylparaben through propylparaben peaks, respectively. Isothermal separations are in black, TASF in blue. Error bars were calculated using values for the standard error of each measured FWHM, with n = 3. Red dashed lines are used to correspond to a 5% increase in peak width relative to the 30 nL isothermal injection. A 5% increase in FWHM approximates a 10% reduction in column efficiency. For chromatographic conditions see Section 3.2.3.4.

B2.5. Sample information for solvent- and temperature-based focusing injection volume experiments

Table B2.4 shows the 5 injection volumes tested, their sample concentrations and solute mass injected on-column.

Table B2.3. Sample information for injection volume experiments.

		Mass On-Column (ng)		
V_{inj} (nL)	**[Sample] (µM)**	**Methylparaben**	**Ethylparaben**	**Propylparaben**
100	300	4.6	5.0	5.4
500	100	7.6	8.3	9.0
1000	50	7.6	8.3	9.0
1500	35	8.0	8.7	9.5
2000	25	7.6	8.3	9.0

APPENDIX C

Supplemental Information for Chapter 4.

C3.1. Column Preparation

Capillary columns were prepared by packing Waters Acquity BEH C18, 1.7 µm particles (Millford, MA) into 150 µm ID x 360 µm OD fused-silica capillaries from Polymicro Technologies (Phoenix, AZ). Column frits were made by sintering 2 µm solid borosilicate spheres (Thermo Scientific, Fremont, CA) into the end of the 20 cm long column blank. Frits were about 1 mm in length. Fritted column blanks were placed into an ultrahigh pressure column packing fitting described previously [98]. The column packing fitting was connected to a high pressure straight coupler (60-21HF4, High Pressure Equipment, Erie, PA) with an internal volume of about 100 µL. Particles were slurried in isopropanol at a concentration of 65 mg/mL and sonicated for 20 minutes prior to packing using the downward slurry method. A Haskel model DHSF-302 pneumatic amplification pump (Haskel, Burbank, CA) was used to pack the column at 18,500 psi for 10 minutes. Acetone was used as the packing solvent. A defined length column was packed by controlling the mass of particles loaded into the bomb. In this case 30 µL of the particle slurry was used to pack the column blank to a length of 5.5 cm. Following initial packing with stationary phase pump pressure was allowed to dissipate naturally. The remaining section of the column blank was packed with 8 µm solid silica spheres (Thermo). Particles were slurried in a 50:50 (v/v) mixture of isopropanol and water at a concentration of 100 mg/mL. This second section of the

capillary column was packed at 20,000 for an additional 10 minutes. The packed, dual segment column was flushed with acetonitrile and the solid silica section was cut to 3.9 cm prior to use.

To determine extra column time accurately a second nominally identical column blank was packed with only 8 µm solid silica spheres. This column consisted of every portion of the separation column, 8 µm silica spheres, frit, and the connection capillary between the column outlet and the detector. We refer to this column as the *e-column*. The *e-column* was packed at 1,500 psi for 10 minutes using the same procedure described above. Following packing the column was flushed with acetonitrile and cut to 3.9 cm prior to use.

C3.2. Experimental setup

Figure C3.1 shows a block diagram describing how instrument control and timing was achieved. Agilent OpenLab CDS ChemStation (rev. C.01.06) was used to control the instrumentation indirectly and acquire data. ChemStation methods were set to collect data at 100 Hz using the Agilent 1200 UIB (G1390B). The UIB was also used to send a 'remote start' signal via its internal relays to an analog input channel of the National Instruments USB-6008 DAQ. A simple LabVIEW VI was written to interpret this signal and immediately actuate the Valco C72-6676EH 6-port injection valve 'beginning' the chromatographic run. The valve was controlled using TTL logic. The VI was designed to mimic a sequence table where a series of injections of various injection volume (time) could be specified. The table was indexed by the remote signals sent from the Agilent UIB. This configuration meant that a certain amount of discontinuity between the detector time controlled by timers inside ChemStation and the UIB and valve actuation controlled by LabVIEW timers was present. This resulted in a certain time lag between when data collection began and when the injection valve was physically actuated.

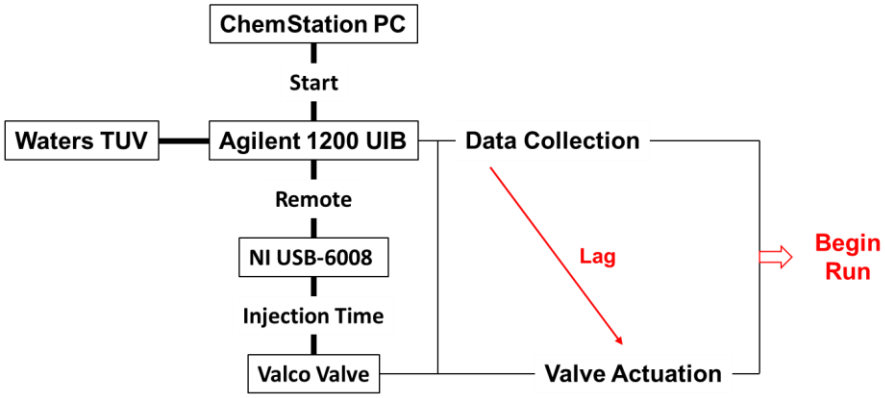

Figure C3.1. Block diagram detailing the configuration for the instrument used in this work.

Figure C3.2 demonstrates the presence of the lag time between data collection and actuation described above for retention experiments under two different mobile phase conditions. Mobile phase composition in panels A and C was 25% (w/w) acetonitrile; B and D was 20% (w/w) acetonitrile. Panels A and B show overlays from four consecutive 50 nL timed injections of 250 µM PB1, PB2, PB3 and uracil made in mobile phase. Panels C and D focus on the UV disturbances introduced by valve actuation at the beginning of the run. UV disturbances, indicated by red arrows, are highly reproducible from run-to-run. Disturbances were found to systematically drift to longer retention times for injections made later in the LabVIEW injection sequence table. Retention times for actuation disturbances for the four runs of panel A occurred at 1.41, 1.37, 1.41, and 1.45 s, respectively. Data for these runs were collected early in the LabVIEW sequence table. Disturbances for panel B occurred at 2.86, 2.88, 2.92, and 2.97 s and were collected later in the injection sequence. To collect accurate k' values the systematic difference (increase) in extra column time for runs must be taken into account. Details regarding the procedure to handle this is described below.

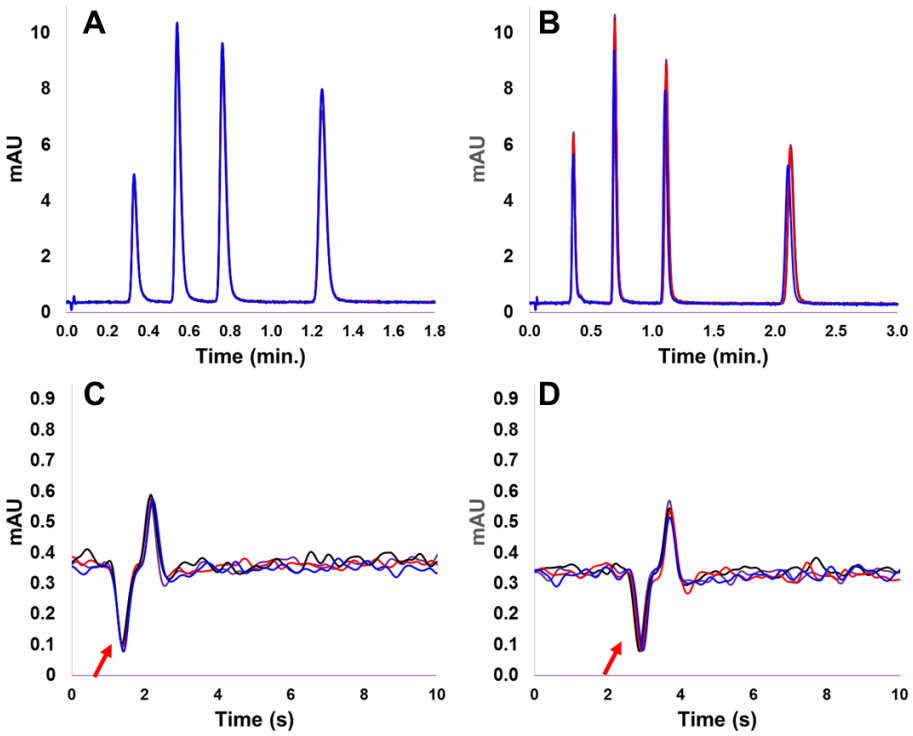

Figure C3.2. Influence of injection delay on observed retention times for UV disturbance peaks due to injection valve actuation.

C3.3. Accurate determination of t_0 and t_{ec}

In capillary liquid chromatography, the extra-column volume can be a significant fraction of the total liquid volume between the injection loop and the optical path of the detector. Thus, the determination of t_0 is not trivial. We determined the extra-column volume by making a column containing only extra-column volume, i.e., it does not have the stationary phase-containing portion of the column. As Figure 4.1 shows, this column has the 8 µm solid silica spheres, the frit, and the connecting tubing between the column outlet and the detector. For convenience, we will refer to this as the *e-column*. Volumes were determined by injecting the unretained (assumed) solute uracil into both the *e-column* and a column with the stationary phase-containing portion. The chromatographic void volume was determined as the difference between the two volumes.

Retention factors, corrected for extra-column volume, were calculated using Eq. C3.1

$$k' = \frac{t_{R,i} - t_0}{t_0 - t_{ec}} \tag{C3.1}$$

where $t_{R,i}$ is the retention time for solute *i*, t_0 is the dead time for the column using uracil and an unretained solute, and t_{ec} is the retention time correction for extra-column volume (extra-column time).

Extra-column time was determined by performing a series of 20 replicate 50 nL injections of uracil into the *e-column*. Mobile phase composition was 80:20 (w/w) 10 mM H_3PO_4/acetonitrile; flow rate was set to 4 µL/min. Figure C3.3 shows the overlay of the 20 injections of 1 mM samples of uracil made in mobile phase. Panel A shows the instrument contributions to the observed peak profile for the 50 nL injections. Panel B focuses on the instrument induced peak tailing due to all extra-column processes. Panel C clearly shows the presence of the UV disturbances produced by valve actuation. Retention time reproducibility for these disturbances is clearly quite good.

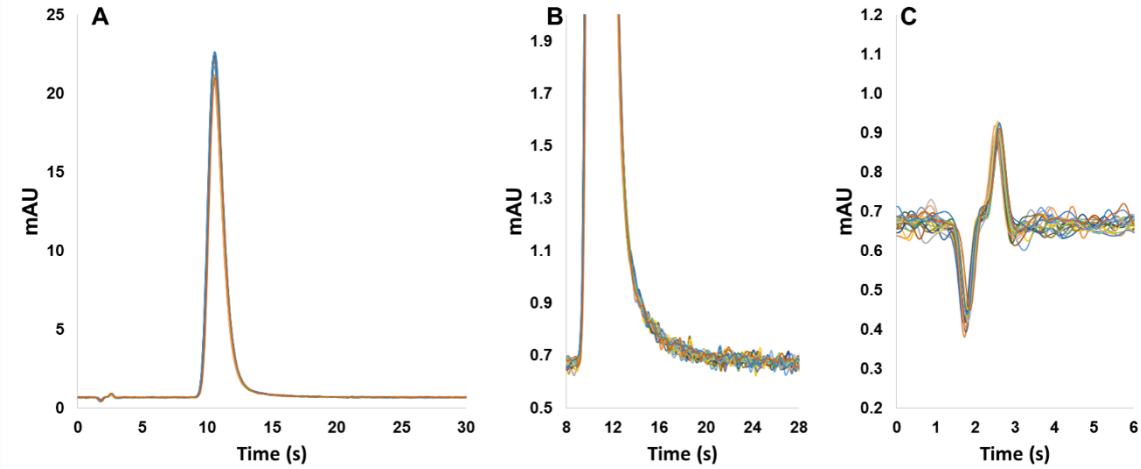

Figure C3.3. Injection profiles for 20 consecutive 50 nL injections of 1 mM uracil onto a 3.9 cm x 150 µm ID column packed with 8 µm solid silica spheres.

Retention factors under each mobile phase composition were calculated using the following procedure. To correct for the time lag between data collection and valve actuation all signals, uracil extra-column time injections and paraben injections under different mobile phase compositions, were aligned using the first UV disturbance induced by valve actuation. A simple MATLAB script (MathWorks, Natick, MA) was written to find the first UV disturbance (valley) then align all signal vectors to the same disturbance in each respective chromatogram. Following alignment, a new time axis beginning at the base of the valley was assigned to the signal vector. The 'findpeaks' function was then used to find the local maxima and retention times for each peak. Finally, retention factors were calculated by substituting the retention times ($t_{R,i}$ and t_0) output by the MATLAB script and a value of 0.147 minutes (the average aligned extra-column time, n = 20, σ_{tec} = 0.0004 min., %RSD = 0.3%) for t_{ec} in Eq C3.1.

C3.4. Accurate calculation of k'

To further address potential inaccuracies in values for k' retention factors were calculated k' based on solute retention time at peak maximum and each peak's first central moment. Table C3.1 shows the results from these calculations (n = 4). While small differences in k' are present under each condition when both datasets are used individual to create Figure 4.8 no significant difference in the magnitude of t_{obs}/t_{inj} or the slope of the t_{obs}/t_{inj} vs k_2/k_1 is observed. Note that retention factors calculated based on moments are smaller, not larger (as expected), than those determined using time at peak maxima. This is due to the first moment calculated for uracil peaks. Uracil retention under experimental conditions is minimal. Thus peak shape is significantly influenced by the injector effects and connections between capillaries. Both combine to increased peak tailing for uracil relative to retained solutes. Increased peak tailing increases the magnitude of the first moment for the void marker leading to a reduction in calculated retention factor.

Table C3.1. Paraben retention factors calculated using time at peak maxima ($t_{R,max}$) and first central moments (μ_1).

φ		**0.2**		**0.1**		**0.05**	
Solute		k'	σ_k	k'	σ_k	k'	σ_k
PB1	$t_{R,max}$	2.06	0.017	7.02	0.02	15.89	0.04
	μ_1	1.93	0.04	6.56	0.13	15.06	0.2
PB2	$t_{R,max}$	4.62	0.032	19.62	0.05	50.28	0.13
	μ_1	4.34	0.07	18.4	0.3	47.6	0.7
PB3	$t_{R,max}$	10.82	0.08	57.56	0.2	-	-
	μ_1	10.18	0.16	54	0.9	-	-

C3.5. Open-tube injection analysis

As an instrument control and to demonstrate the ability to reproducibility for injections up to 2000 nL using the 75 cm x 75 µm ID nanoViper (V = 3.3 uL) injection loop a series of timed injections were made into a 35 cm x 25 µm ID capillary connecting the injection valve directly to the detector flow cell. Mobile phase composition was 80:20 10 mM H_3PO_4/acetonitrile, flow rate was set to 4 µL/min and data was collected at 100 Hz by monitoring UV absorbance at 254 nm. The sample was 1 µM uracil in mobile phase. Injections were made from 250 nL to 2500 nL in 250 nL steps. Order of large volume injections was random and a 50 nL injection of the uracil sample was made between every large volume injection. Figure S4A shows an overlay for all ten injections in black with the 50 nL injection in red.

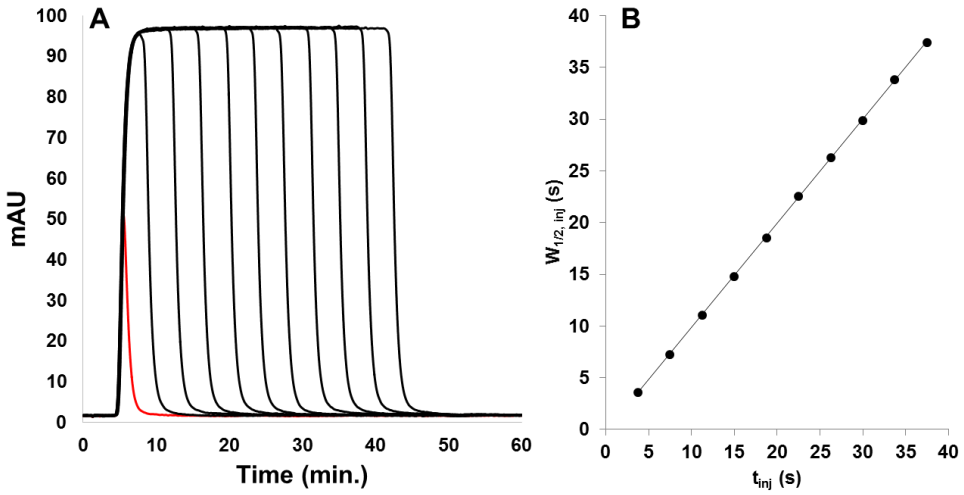

Figure C3.4. Panel A shows injection profiles obtained from time injections from 250 to 2500 nL (black) of 1 µM uracil into a 25 µm ID capillary. The red trace represents the profile obtained when using a 50 nL injection. Panel B shows a plot of injection plug width versus injection volume.

Performing a series of injections into an open tube serves as a good control for the LabVIEW VI, its timers used to control the injection valve, injection time and subsequently the injection volume

delivered to the column. Timed injections were used in all experiments. Thus, as equation C3.2 shows, the width of the injection band in time units, t_{inj}, is the desired injection volume, V_{inj}, over the volumetric flow rate, F, delivered by the pump. If the system (LabVIEW timers, injection valve, and pump) are performing as designed and delivering appropriate length (volume) injections the injection time should equal the width of the injection band at the detector, $w_{1/2}$.

$$t_{inj} = w_{1/2} = \frac{1}{F} V_{inj}$$

C3.2

A plot of measured width versus injection time should be linear and have a slope equal to the one. This plot is show in panel B of Figure C3.4. The equation from the linear regression was y = 1.0058 ± 0.0075x – 0.0039 ± 0.0029 (95% confidence interval). The slope of the linear regression yielded an experimentally determined flow rate of 3.977 ± 0.030 not significantly different from 4 µL/min, the set value at the 95% confidence level. Thermo/Dionex does not provide a specification for flow rate accuracy for the pump used, although we conclude the value of 0.5% to be quite good and will not influence the results of our work.

C3.6. Non on-column focusing instrument control

A second instrument validation test was performed using a series of large volume injections with samples made in mobile phase. For samples made in mobile phase any focusing of the sample band induced by retention at the head of the column due to retention will be reversed as the band expands at the column outlet. For large injections injection time (volume) and measure band width are directly related.

Panel A of Figure C3.5 shows a series of 50 µM paraben injections from 250 to 1500 nL in 250 nL steps onto a 150 µm x 5.5 cm BEH C18, 1.7 µm d_p column. Samples were made in 80:20 (wt%) 10 mM H_3PO_4/acetonitrile. Mobile phase composition was also 80:20 (wt%) 10 mM H_3PO_4/acetonitrile. Flow rate was set to 4 µL/min and column temperature was 60 ºC.

Panel B shows the linear increase in peak width (in time units) with injection volume for all three solutes. The dashed line with slope equal to one has been added to highlight the direct, as expected, relationship between the two variables. Note that only the point for the 250 nL injection for PB3 shows any visible deviation from the linear increase between injection volume and peak width. After performing regression calculations residuals plots clearly showed width values for the 250 nL injections for each solute had significant contributions due to on-column bandspreading. As such the 250 nL points were excluded from the linear regression performed for all three solutes. (Note that for smaller injection volumes on-column convective dispersion begins to contribute a significant fraction of the observed to peak width, i.e. the injection volume is no longer volume overloading the column under the experimental conditions.) The slope and intercept for the linear regression were 0.992 ± 0.006 and -0.008 ± 0.002 (95% confidence interval), respectively. Deviations from the predicted value of 1.0 while significant, are only 2% and represent an acceptable error.

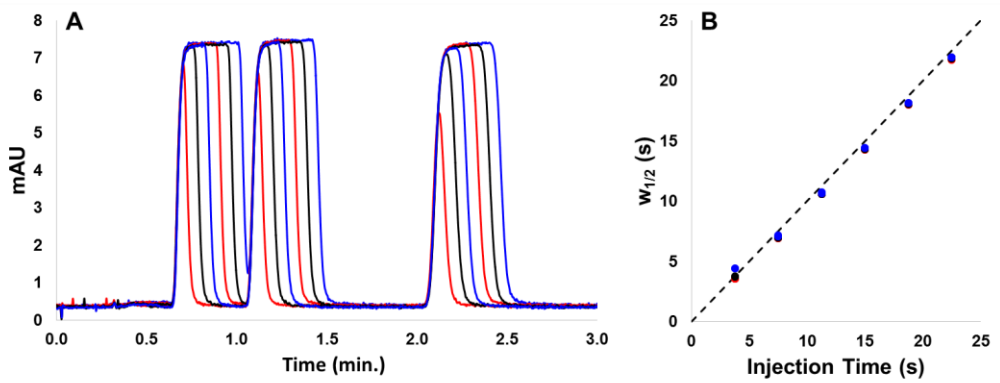

Figure C3.5. Injections of 250 to 1500 nL of 50 mM PB1, PB2, and PB3 made in mobile phase onto 150 μm x 5.5 cm BEH C18 column. Panel B shows a plot of measured peak width versus injection time for PB1 (●), PB2 (●), PB3 (●). To add clarity, the dashed line represents a line with unit slope and intercept at the origin. For chromatographic conditions see Section 4.3.3.

C3.7. Effect of sample solvent composition and volume on peak shape

Figure C3.6 shows the chromatograms obtained from 500 (black), 1000 (red), 1500 (blue), and 2000 nL (purple) injections of PB1, PB2 and PB3 made in 90:10 (wt%) 10 mM H_3PO_4/acetonitrile. These are provided to the reader with the complete chromatograms referenced in Section 4.4.3 and Figure 4.6.

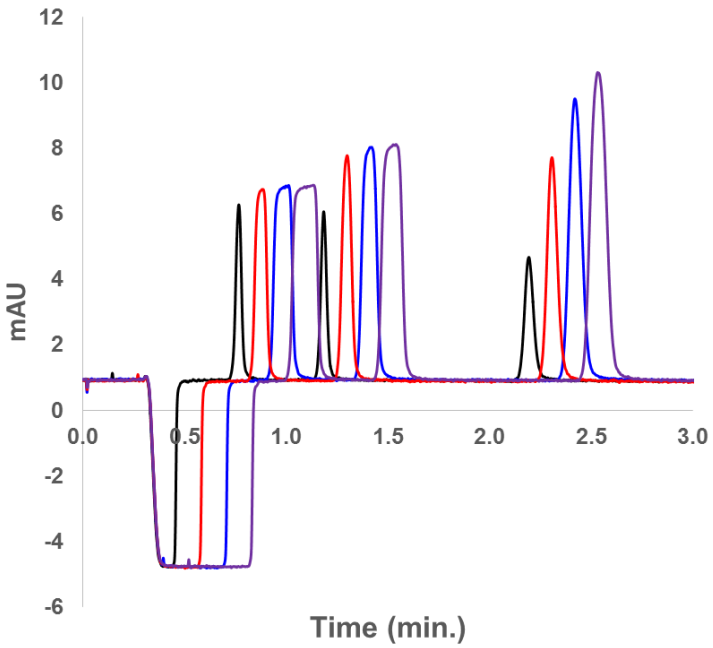

Figure C3.6. Effect of injection volume of peak shape for samples of PB1, PB2, and PB3 made in 90:10 (w/w) 10 mM H3PO4/acetonitrile injected into a mobile phase consisting of 80:20 (w/w) 10 mM H_3PO_4/acetonitrile.

Figure C3.7 shows similar chromatograms obtained from 500 (black), 1000 (red), 1500 (blue), and 2000 nL (purple) injections of PB1, PB2 and PB3 made in 95:5 (wt%) 10 mM H_3PO_4/acetonitrile. These are provided to the reader with the complete chromatograms referenced in Section 4.4.3 and Figure 4.6.

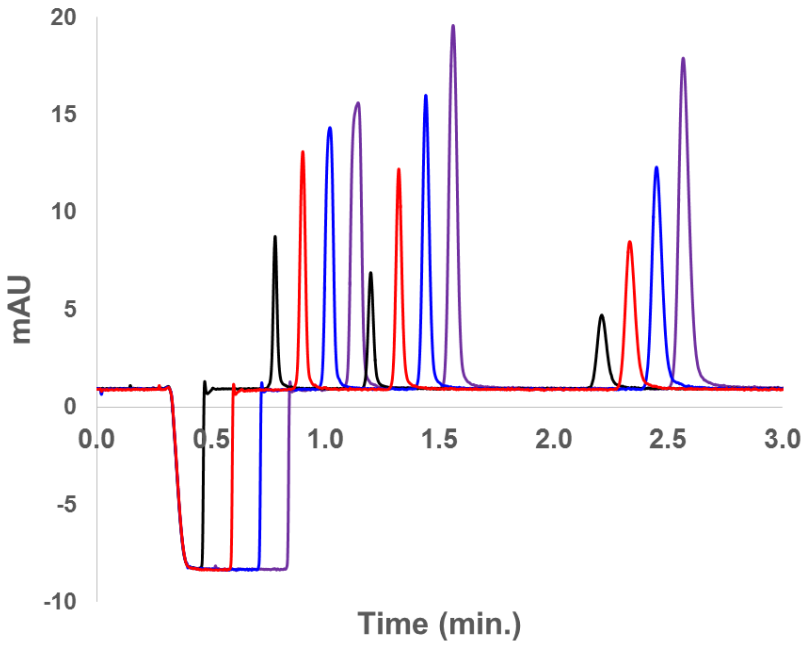

Figure C3.7. Effect of injection volume of peak shape for samples of PB1, PB2, and PB3 made in 95:5 (wt%) 10 mM H3PO4/acetonitrile injected into a mobile phase consisting of 80:20 (wt%) 10 mM H_3PO_4/acetonitrile.

C3.8. Plot of focusing data vs the independent variable $(k_2+1)/(k_1+1)$

A reviewer suggested that we plot the observed focusing factors vs the variable $(k_2+1)/(k_1+1)$. This is equivalent to testing the assumption that there is no step (or "steep") gradient compression of the injected zone. Figure C3.8 shows that the data (red circles): 1) do not lie on a straight line and 2) are consistently lower than the hypothetical result (black line) by significant and variable relative quantities. While the information in Figure C3.8 is the same as that in Figure 4.8, it is perhaps clearer in Figure C3.8 than in Figure 4.8 that on-column compression is a significant factor in the overall focusing phenomenon in solvent-based focusing/isocratic elution.

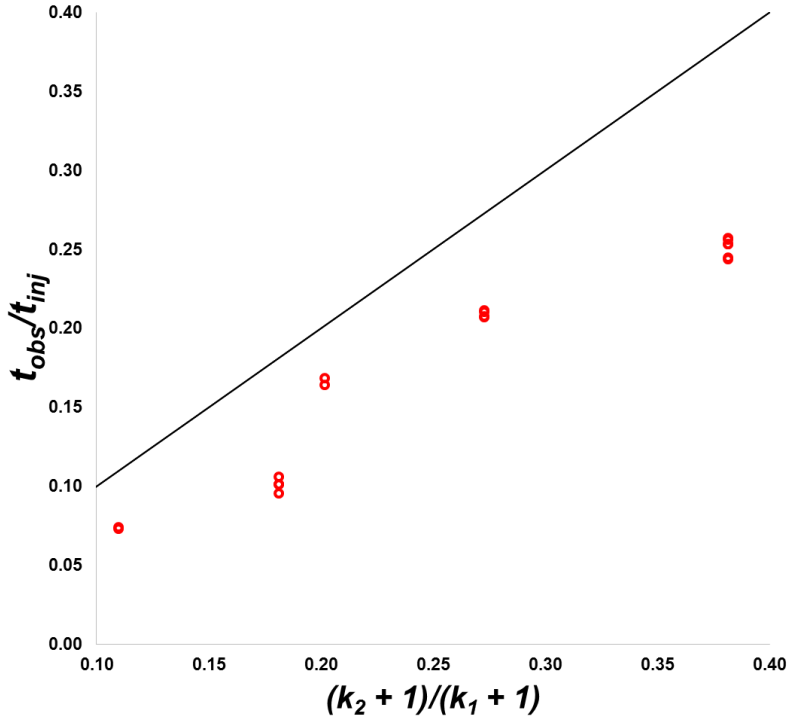

Figure C3.8. Plot of observed focusing vs (k_2+1)/(k_1+1) for experimentally determined k' values (red circles).

APPENDIX D

Supplemental Information for Chapter 5.

D4.1. Temperature and solvent composition dependence of retention factors

Values for retention factors for each solute were calculated based on their retention time and that of uracil to approximate the void time, t_0. Extra column time, t_{ec}, was measured by placing a Valco ZDV union in place of the column. Eq. D4.1 was used to calculate retention factors while accounting for the extra column time:

$$k' = \frac{t_{R,i} - t_0}{t_0 - t_{ec}} \tag{D4.1}$$

The van`t Hoff equation was used to describe the relationship between solute retention factor and column temperature:

$$\ln k' = -\frac{\Delta H^0}{RT} + \frac{\Delta S^0}{R} + \ln \varphi \tag{D4.2}$$

where ΔH^0 is the standard state retention enthalpy, ΔS^0 is the standard state retention entropy, R is the ideal gas constant and φ is the column phase ratio. From experimental plots of ln k' vs. 1/T,

so-called van`t Hoff plots (Figure D4.1), retention factors were predicted at specific trapping and separation temperatures.

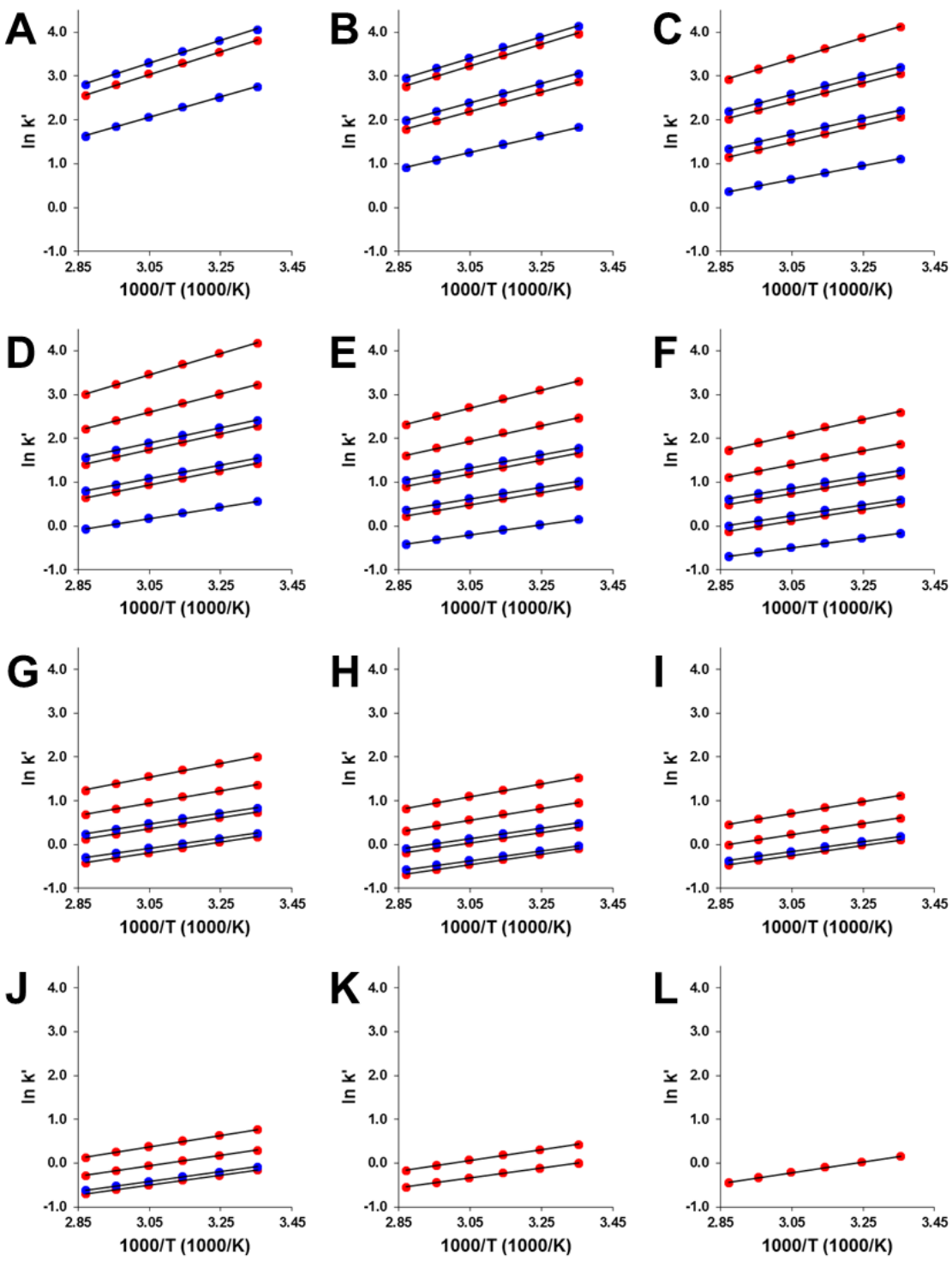

Figure D4.1 van`t Hoff plots for parabens (●) *p*-hydroxyphenones (●). Mobile phase compositions: 0.05 w/w (A), 0.10 (B), 0.15 (C), 0.20 (D), 0.25 (E), 0.30 (F), 0.35 (G), 0.40 (H), 0.45 (I), 0.50 (J), 0.55 (K), 0.60 (L). For chromatographic conditions see section 5.2.3.1.

Table D4.1. Partial molar enthalpies of retention for each solute used in retention studies obtained from slopes of the van`t Hoff plots shown in Figure D4.1.

Solute	φ (w/w)	φ (v/v)	-ΔH°/R (K)	Error	Intercept	Error
***p*-Hydroxyacetophenone**	0.050	0.063	2335	16	-5.07	0.05
	0.100	0.124	1902	9	-4.54	0.03
	0.150	0.184	1555	9	-4.10	0.03
	0.200	0.242	1312	8	-3.83	0.03
	0.250	0.299	1165	9	-3.75	0.03
	0.300	0.354	1095	7	-3.84	0.02
***p*-Hydroxypropiophenone**	0.050	0.063	2602	24	-4.64	0.07
	0.100	0.124	2193	15	-4.30	0.05
	0.150	0.184	1830	14	-3.91	0.04
	0.200	0.242	1543	13	-3.62	0.04
	0.250	0.299	1344	13	-3.48	0.04
	0.300	0.354	1221	11	-3.49	0.03
	0.350	0.407	1149	8	-3.59	0.03
	0.400	0.460	1124	6	-3.79	0.02
***p*-Hydroxybutyrophenone**	0.100	0.124	2459	22	-4.09	0.07
	0.150	0.184	2090	19	-3.80	0.06
	0.200	0.242	1770	17	-3.51	0.05
	0.250	0.299	1522	17	-3.31	0.05
	0.300	0.354	1352	15	-3.26	0.05
	0.350	0.407	1243	13	-3.32	0.04

Table D4.1 Continued.

	0.400	0.460	1190	11	-3.50	0.03
	0.450	0.511	1148	9	-3.66	0.03
	0.500	0.561	1117	7	-3.83	0.02
Methylparaben	0.050	0.063	2599	24	-4.89	0.07
	0.100	0.124	2254	13	-4.69	0.04
	0.150	0.184	1909	11	-4.32	0.03
	0.200	0.242	1624	10	-4.02	0.03
	0.250	0.299	1421	10	-3.85	0.03
	0.300	0.354	1309	9	-3.87	0.03
	0.350	0.407	1233	7	-3.95	0.02
	0.400	0.460	1204	5	-4.13	0.02
Ethylparaben	0.100	0.124	2492	20	-4.37	0.06
	0.150	0.184	2122	17	-4.06	0.05
	0.200	0.242	1794	15	-3.73	0.05
	0.250	0.299	1542	15	-3.51	0.05
	0.300	0.354	1390	14	-3.50	0.04
	0.350	0.407	1275	12	-3.53	0.04
	0.400	0.460	1224	9	-3.70	0.03
	0.450	0.511	1167	7	-3.81	0.02
	0.500	0.561	1139	5	-3.97	0.02
Propylparaben	0.150	0.184	2473	20	-4.16	0.06
	0.200	0.242	2093	18	-3.79	0.06

Table D4.1 Continued.

	0.250	0.299	1780	19	-3.49	0.06
	0.300	0.354	1573	18	-3.40	0.05
	0.350	0.407	1408	17	-3.35	0.05
	0.400	0.460	1328	14	-3.49	0.04
	0.450	0.511	1247	12	-3.58	0.04
	0.500	0.561	1209	10	-3.75	0.03
	0.550	0.609	1141	8	-3.82	0.02
Butylparaben	0.200	0.242	2436	21	-3.98	0.07
	0.250	0.299	2064	22	-3.60	0.07
	0.300	0.354	1803	21	-3.43	0.07
	0.350	0.407	1586	21	-3.30	0.07
	0.400	0.460	1474	19	-3.41	0.06
	0.450	0.511	1367	17	-3.46	0.05
	0.500	0.561	1317	14	-3.65	0.04
	0.550	0.609	1243	12	-3.73	0.04
	0.600	0.657	1237	13	-3.99	0.04

Figure D4.3 shows Neue-Kuss fits to experimental retention data for the parabens and hydroxyphenones in red and blue, respectively. Panels A, B, C, D, E and F correspond to column temperatures of 25, 35, 45, 55, 65 and 75 °C. Fitting parameters are provided in Table 5.1.

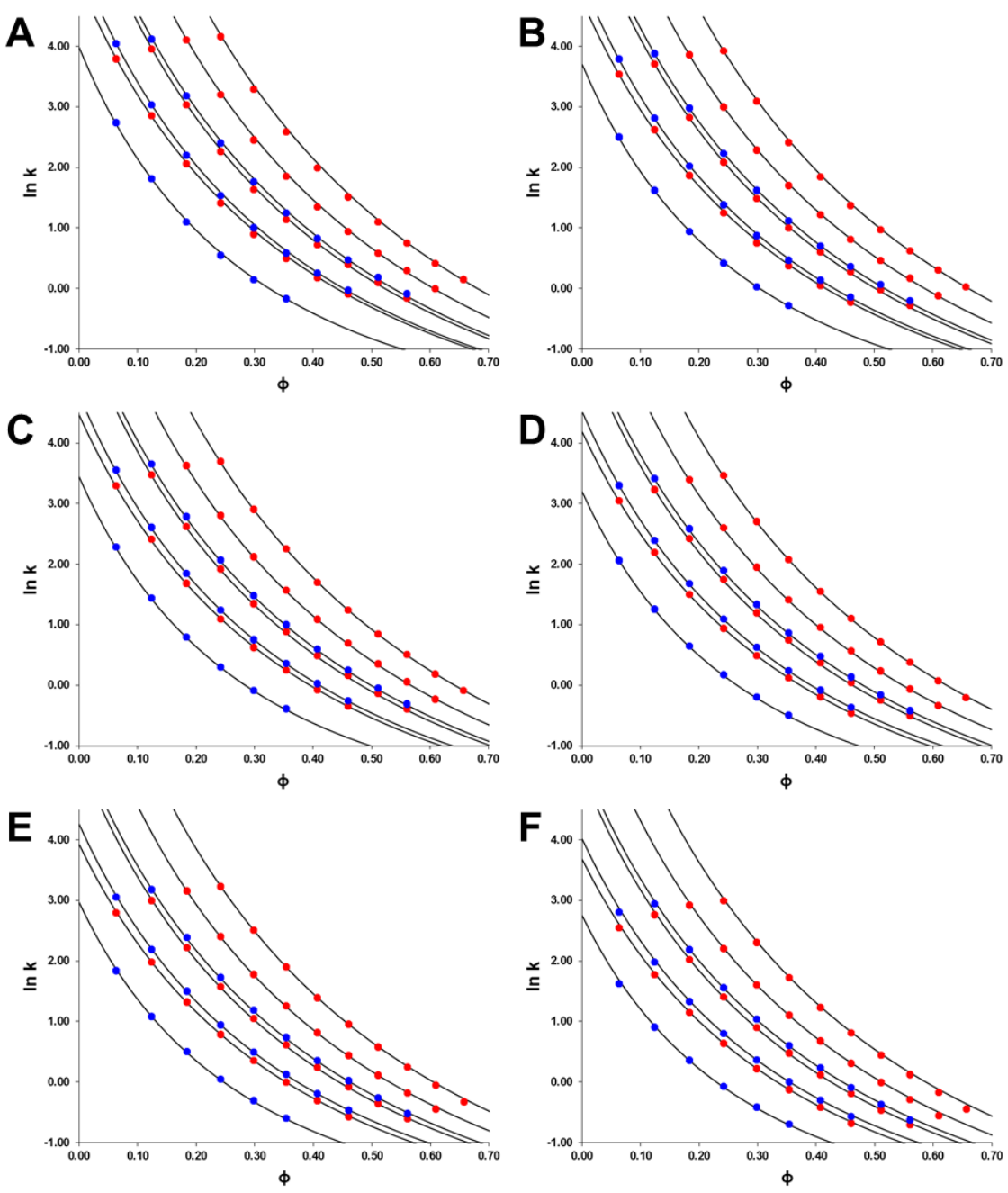

Figure D4.2 Overlay of Neue-Kuss curve fitting results with experimentally determined retention factors for parabens (●) *p*-hydroxyphenones (●). Column temperature: 25 (A), 35 (B), 45 (C), 55 (D), 65 (E), 75 °C (F). For chromatographic conditions see section 5.2.3.1.

D4.2. Characterization of two-stage TASF instrument performance

Figure D4.3 shows temperature profiles for TEC *A (red)*, *B* (blue) and *C* (black) (panels A and B) and temperature rate-of-change profiles (C and D) for the transient portions of Figure 5.2. The temperature change was from 5 to 70 °C.

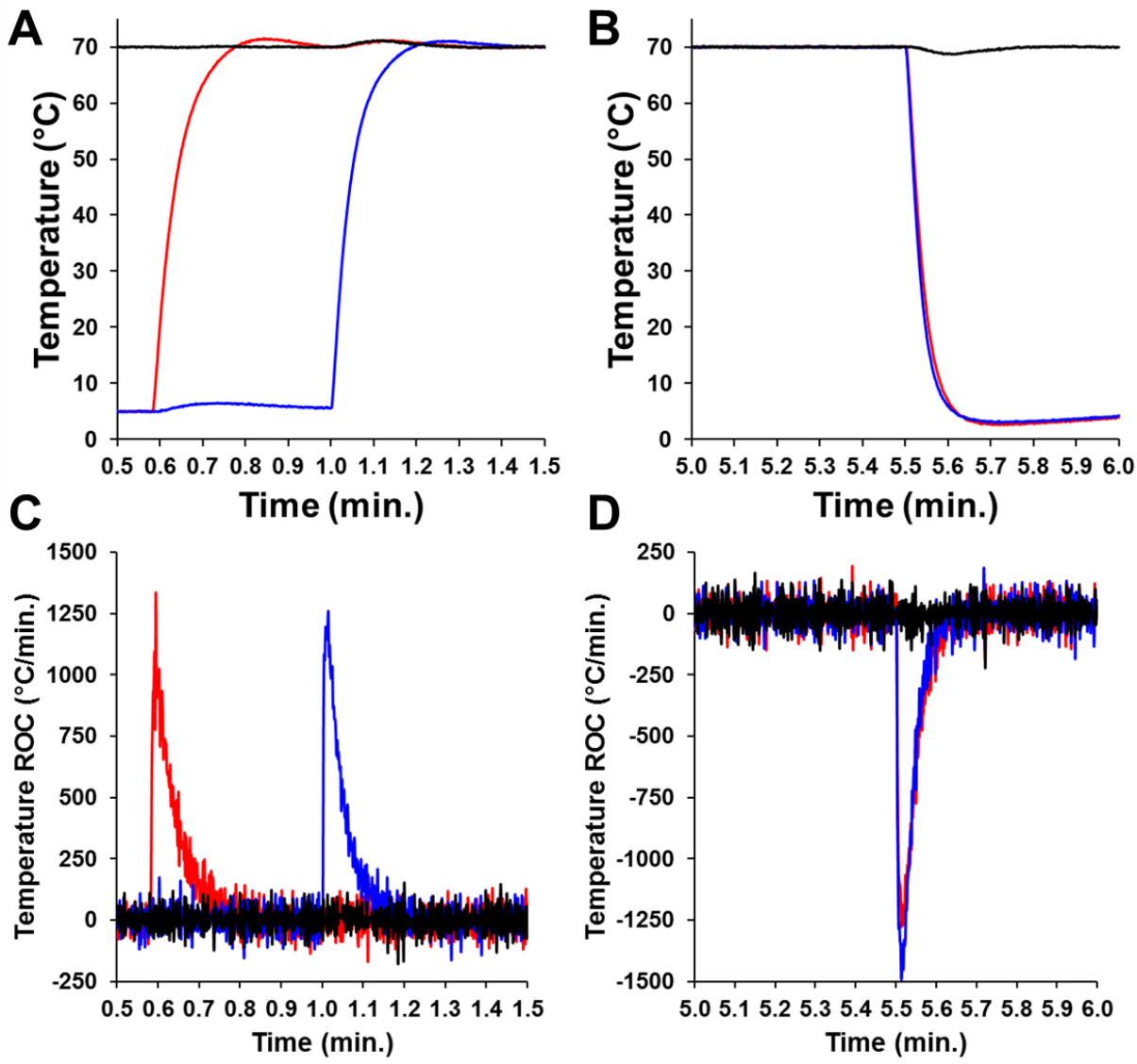

Figure D4.3 Temperature (A, B) and temperature ROC (C, D) profiles for transient heating/cooling sections of Figure 5.2. TEC A is shown in red, TEC B blue, TEC C black.

D4.3. Simulating two-stage temperature-based focusing

Chromatographic conditions not reported in section 5.4.3 for isothermal, TASF and two-stage TASF simulations are provided in Tables D4.2 and D4.3. Table D4.2 lists parameters used in the isocratic simulations, D4.3 gradient elution parameters.

Table D4.2. Parameters used in isocratic isothermal, TASF and two-stage TASF simulations.

Parameter	**Value**
Sample	
V_{inj} (nL)	1500
φ_{sample} (v/v)	0.242 (0.2 w/w)
Temperature Program	
$T_{1,A}$; $T_{1,B}$ (°C)	5, 70
$T_{2,A}$; $T_{2,B}$ (°C)	5, 70
T_{col} (°C)	70
$t_{focus,A}$ (s)	35
$t_{focus,B}$ (s)	35, 60
Column Conditions	
φ	0.242
L (cm)	8.0
d_c (um)	150
F (uL/min.)	3
ε_e	0.38
ε_{tot}	0.56
d_p (μm)	1.7
A (dimensionless van Deemter)	0.66
B	10.2
C	0.095

Table D4.3. Parameters used in gradient elution isothermal, TASF and two-stage TASF simulations.

Parameter	Value
Sample	
V_{inj} (nL)	3000
φ_{sample} (v/v)	0.05
Temperature Program	
$T_{1,A}$; $T_{1,B}$ (°C)	5, 70
$T_{2,A}$; $T_{2,B}$ (°C)	5, 70
T_{col} (°C)	70
$t_{focus,A}$ (s)	65
$t_{focus,B}$ (s)	65, 100
Gradient Conditions	
$\varphi_{initial}$	0.05
φ_{final}	0.45
t_{dwell} (s)	15
t_g (s)	960
L (cm)	8.0
d_c (um)	150
F (uL/min.)	3
ε_e	0.38
ε_{tot}	0.56
d_p (μm)	1.7
A (dimensionless van Deemter)	0.66
B	10.2
C	0.095

D4.4. Two-stage TASF experiments: Gradient elution

Raw, non-baseline subtracted chromatograms are provided in Figure D4.3. Note in the raw signals for the TASF and two-stage TASF runs exhibit large system peaks visible just after 2 minutes in the TASF run and two transient peaks between 2 and 3 minutes in the two-stage experiments. These transients correspond to the changes in column temperature and we believe they are due to additional acetonitrile partitioning into the cold sections of the column. Following heating the

acetonitrile concentration in the stationary phase stabilizes, but heating releases a bolus of ACN rich mobile phase leading to a change in the refractive index observed at the detector.

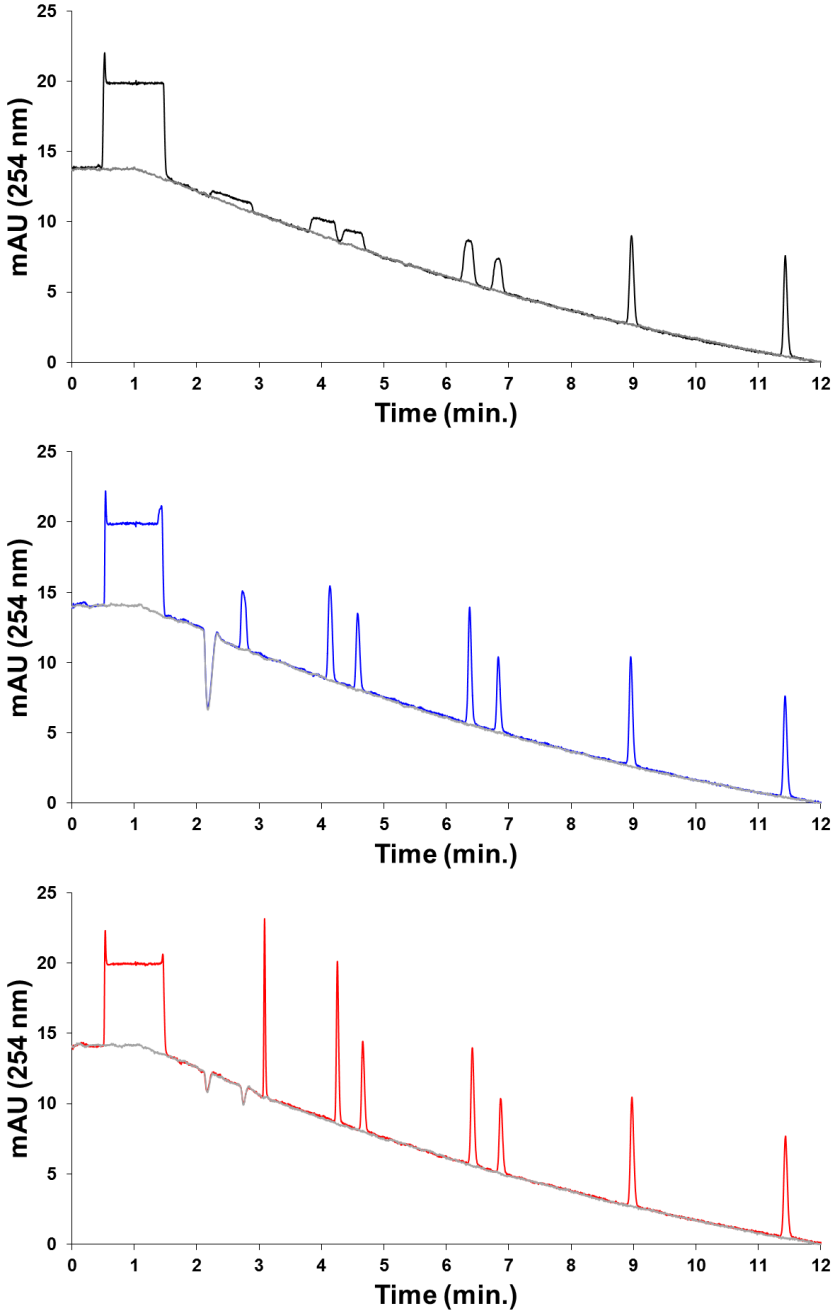

Figure D4.4 Example non-baseline subtracted gradient elution chromatograms under isothermal (black), TASF (blue) and two-stage TASF (red) conditions. Baseline signals under each condition are shown in gray.

D4.5. Simulation/Experiment Comparison

Figures D4.5 and D4.6 show qualitative comparisons of experimental and simulated chromatograms collected under isocratic and gradient elution conditions for each temperature program, isothermal (black), TASF (blue) and two-stage TASF (red).

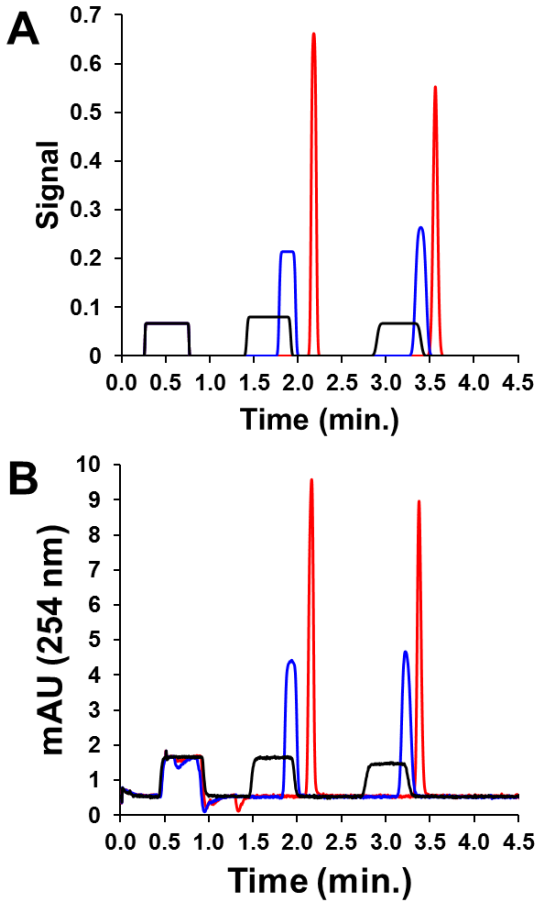

Figure D4.5 Simulated (A) and experimental chromatograms (B) collected for isocratic separations of paraben samples under isothermal (black), TASF (blue) and two-stage TASF (red) conditions.

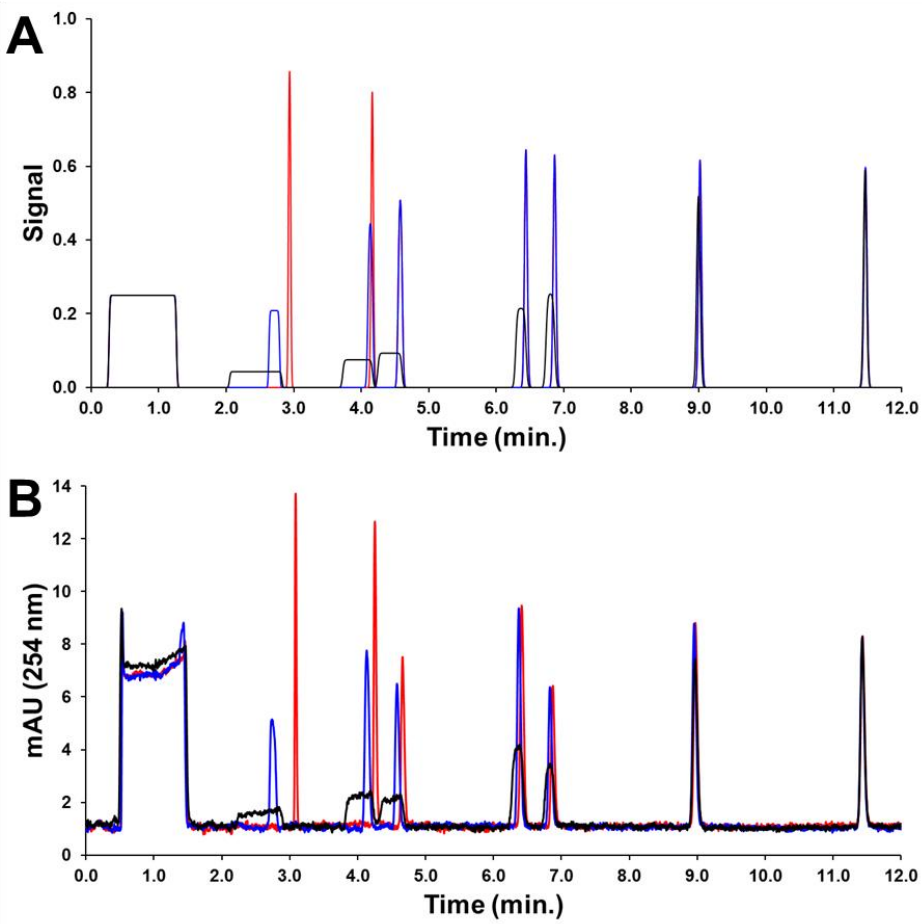

Figure D4.6 Simulated (A) and experimental chromatograms (B) collected using solvent gradient elution conditions for the separation of paraben and *p*-hydroxyphenone samples under isothermal (black), TASF (blue) and two-stage TASF (red) conditions.

APPENDIX E

Supplemental Information for Chapter 6.

E5.1 Historical Plots Used for Chromatographic Optimization

Figure E5.1 shows the initial kinetic plot presented by Giddings to compare the separation time in gas and liquid chromatography [167].

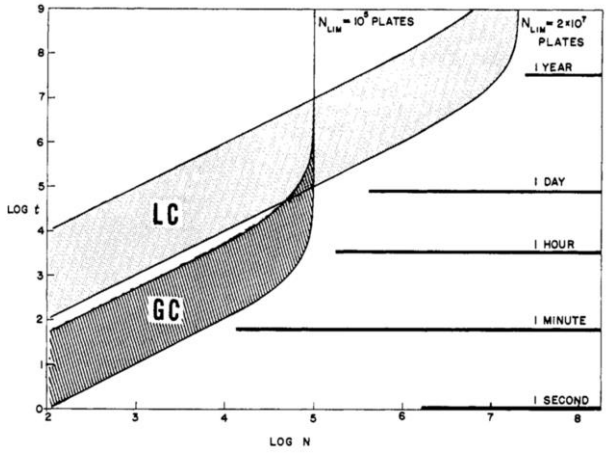

Figure 1. Comparison of separation time in gas and liquid chromatography as a function of the number of required plates

Figure E5.1. Reproduced from Giddings, J. C. Anal. Chem. **1964**, 36, 1890–1892. Copyright 1964 American Chemical Society.

Figure E5.2 is taken from Knox and Saleem to show the range of velocities presented to explore the limits of liquid chromatography [168].

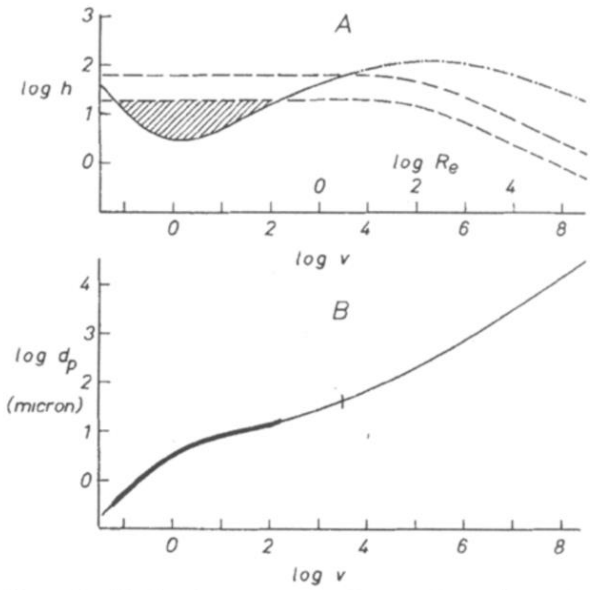

Figure 1. Liquid chromatography. Range of conditions for analysis with S = 30,000 in 1,000 sec.

A. Full line gives dependence of h upon ν; the portion for $\nu > 10^4$ is hypothetical. Broken lines give the maximum allowable h (Equation 40) for P = 30,000 psi (upper) and P = 3,000 psi (lower).

B. Particle diameters required to obtain analysis with S = 30,000 in 1,000 sec (Equation 41). Emphasised section gives range of d_p for P = 3,000 psi; vertical bar gives upper limit of d_p for P = 30,000 psi.

Figure E5.2. Reproduced from Knox, J. H.; Saleem, M. J. Chromatogr. Sci. **1969**, 7, 614–622, Copyright 1969, with permission from Oxford University Press.

Figure E5.3 is the first example of the Poppe plot [173].

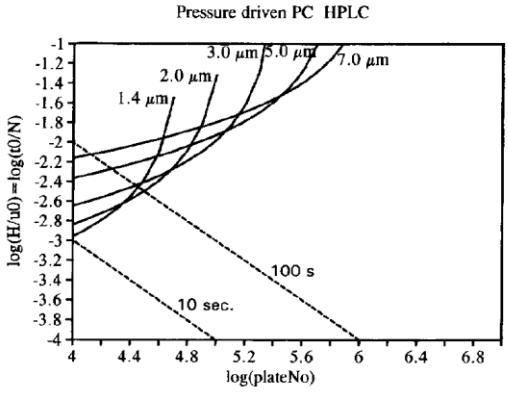

Fig. 3. Plot of plate time, H/u_0 vs. required plate number in conventional HPLC (PD-PCLC) with various particle sizes. Assumed parameters: maximum pressure $\Delta P = 4 \cdot 10^7$ Pa, viscosity $\eta = 0.001$ Pa/s, flow resistance factor $\phi = 1000$, diffusion coefficient $D = 1 \cdot 10^{-9}$ m^2/s, reduced plate height expression Eq. (9) with $A = 1.0$, $B = 1.5$ and $C = 0.05$.

Figure E5.3. Reprinted from the J. Chromatogr. A, Vol. 778, Poppe, H. Some reflections on speed and efficiency of modern chromatographic methods, pp. 3 – 21. Copyright 1997, with permission from Elsevier.

Figure E5.4 is a graphical representation of Kinetic Plot Method from Desmet et al. [183]. The plot in the red square shows the fully transformed H vs u_0 data.

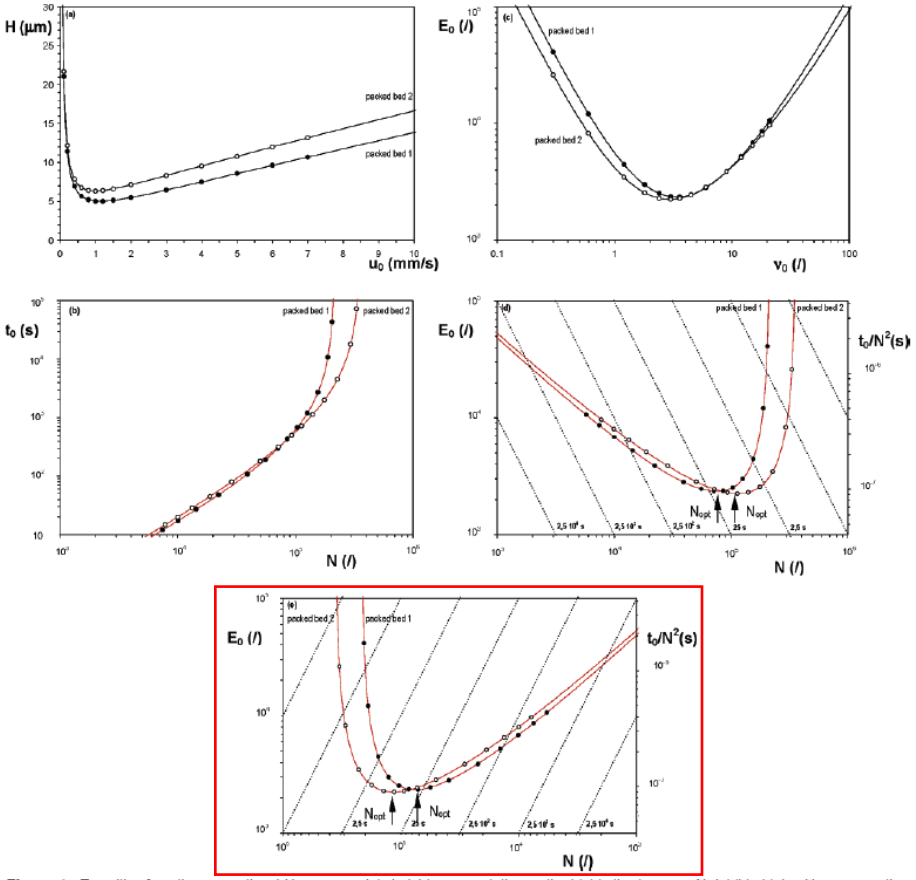

Figure 1. Transition from the conventional H versus u_0 plate height representation method (a) to the t_0 versus N plot (b) obtained by representing the same data sets as a plot of $t_0 = (\Delta P l \eta)[K_v/u_0^2]$ versus $N = (\Delta P l \eta)[K_v/(H u_0)]$. The two data sets were obtained by taking two typical[15] packed bed literature values: packed bed 1, $a = 0.5$ and $\phi = 833$ (●) and packed bed 2, $a = 0.8$ and $\phi = 500$ (○). Other employed parameters: $n = 1/3$, $b = 2$, $c = 0.1$, $d_p = 3$ μm, $D_m = 10^{-9}$ m²/s, $\eta = 10^{-3}$Pa·s, and $\Delta P = 400$ bar. Also shown is the transition of the conventionally used E_0 versus ν_0 plot (c) to the E_0 versus N plots which can be obtained by putting $N = (\Delta P l \eta)[K_v/(H u_0)]$ on the x axis: normal order (d) and inverted order (e). The red lines in (b) and (d) were obtained by using the traditional optimization method,[14] i.e., fitting the a, b, and c parameters of eq 2 to the experimental data points and then using eqs 1−4 in a numerical optimization routine to determine the minimal t_0 time for each considered N. The dashed lines added to (d) represent the cases of constant t_0 times.

Figure E5.4. Reproduced from Desmet, G.; Clicq, D.; Gzil, P. Analytical Chemistry **2005**, 77, 4058–4070. Copyright 2005 American Chemical Society.

Figure E5.5 is the nomogram developed by Guiochon to determine the minimum analysis time to achieve a desired number of theoretical plates [172].

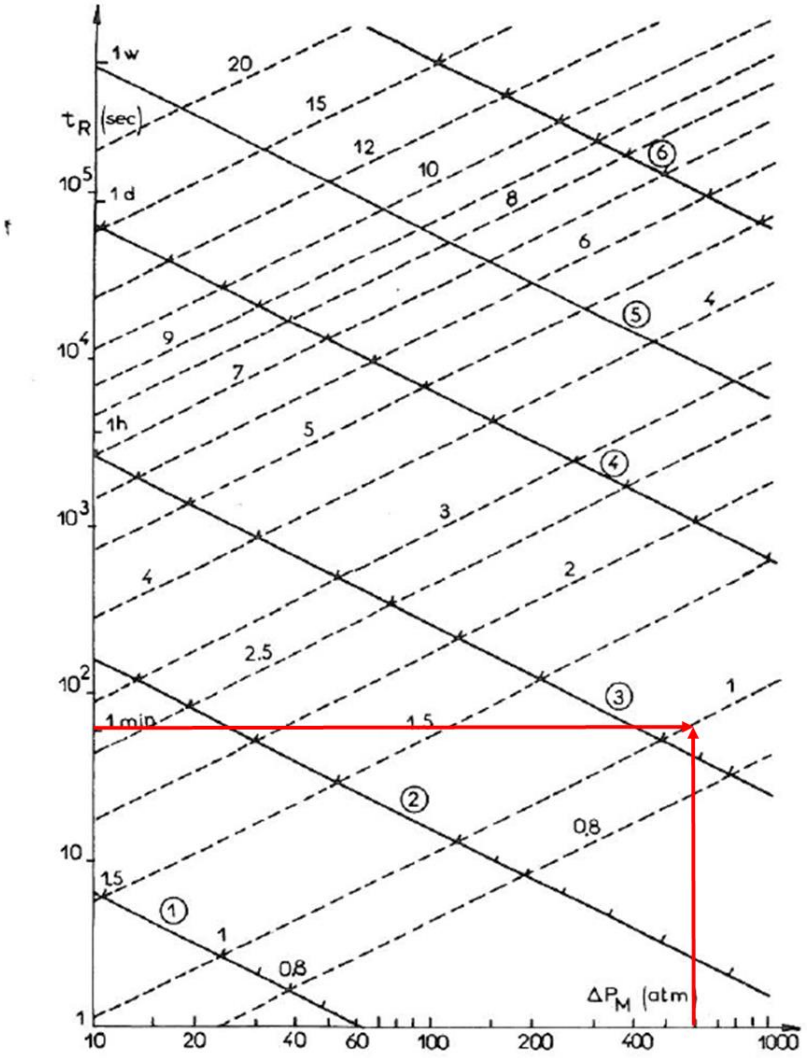

FIG. 11. Minimum analysis time as a function of the maximum available pressure and the particle size. Solid lines represent constant plate numbers: (1) 1000; (2) 5000; (3) 20,000; (4) 100,000; (5) 300,000; (6) 1,000,000; dotted lines represent constant particle size stated in micrometers at each line. The columns are operated at minimum plate height of $h = 2$, and the other conditions are as follows: $\nu = 3$, $k = 3$, $\eta = 0.4$ cP, $k_0 = 1 \times 10^{-3}$, $D_m = 1 \times 10^{-5}$ cm²/sec.

Figure E5.5. Reprinted from High-Performance Liquid Chromatography Advances and Perspectives Vol. 2, Guiochon, G. Optimization in Liquid Chromatography, pp. 1 – 56. Copyright 1980, with permission from Elsevier.

Figure E5.6 is the Halasz and Görlit [186] nomogram to estimate laboratory conditions under similar conditions to Guiochon.

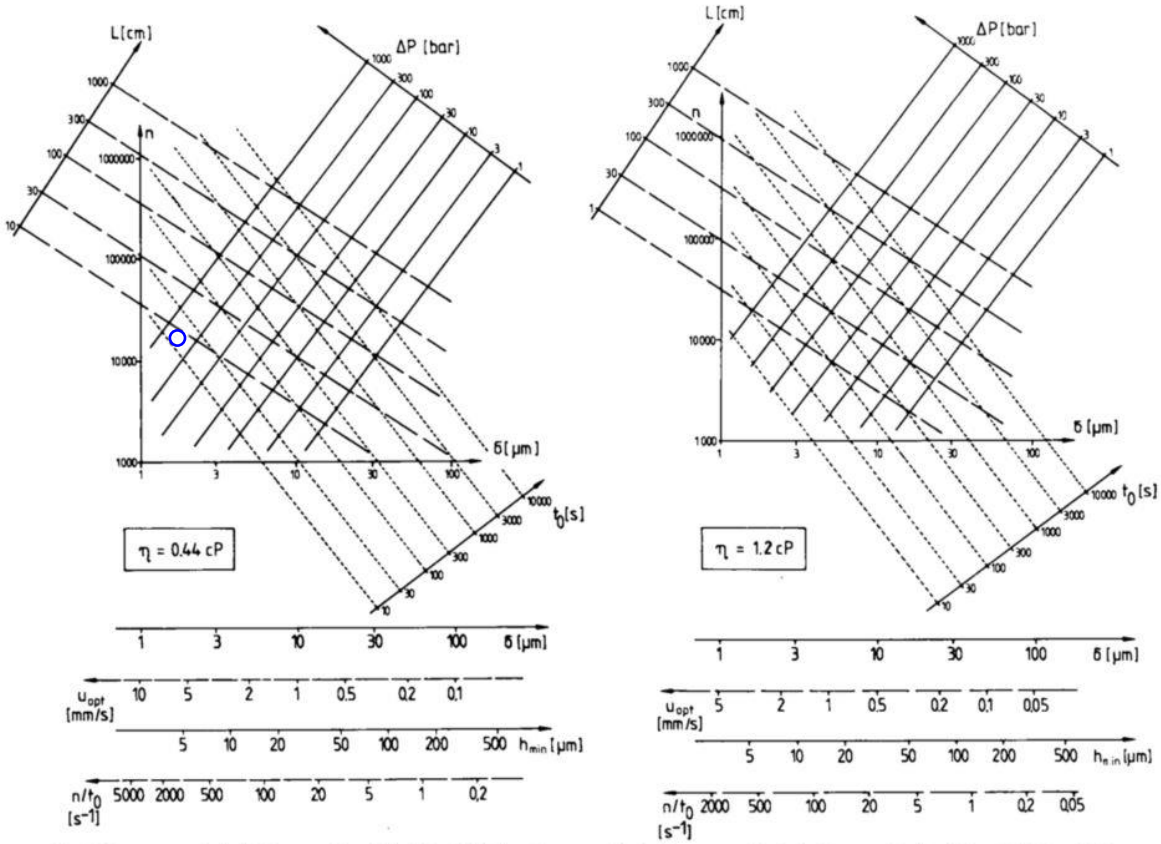

Fig. 7. Nomogramm: Optimale Parameter für „niederviskose" Elutionsmittel, z. B. für das System Silicagel/Dichlormethan.
$h = 1.5\delta + 6/u + \delta^2 u/16$ [Gl. (5)], $\eta = 0.44$ cP, $D_m \approx 3 \cdot 10^{-5}$ cm²/s, $\varepsilon_T = 0.82$.

Fig. 8. Nomogramm: Optimale Parameter für „hochviskose" Elutionsmittel, z. B. für das System C_{18}-Umkehrphase/Methanol-Wasser.
$h = 2\delta + 3/u + \delta^2 u/8$ [Gl. (6)], $\eta = 1.2$ cP, $D_m \approx 1.5 \cdot 10^{-5}$ cm²/s, $\varepsilon_T = 0.70$.

Figure E5.6. Reproduced from Optimale Parameter in der schnellen Fluessigkeitschchromatographie (HPLC), Halász, I.; Görlitz, G. Angew. Chem. **1982**, 94, 50–62 . Copyright 1982 Wiley.

E5.2 Equations Used for Chromatographic Optimization

The value for serotonin's diffusion coefficient measured in water at 25 °C, 5.4×10^{-6} cm^2/s [190], was translated to various temperatures and mobile phase compositions using the following empirical equation [99]:

$$D_{m,i}(T) = D_{m,i,T'} \times \frac{T \times \eta(T')}{T' \times \eta(T)} \quad \text{(E5.1)}$$

where $D_{m,T'}$ is the measured diffusion coefficient at a given temperature (T'), $\eta(T')$ is the viscosity under those conditions, T is the desired temperature, and $\eta(T)$ is the viscosity at the desired composition and temperature.

An empirical relationship for viscosity as a function of composition and temperature was fit to the apparent integral viscosities at 400 bar for water-acetonitrile mixtures between 20 and 100 °C resulting in [26, 88]:

$$\eta(T) = 10^{\left[-2.533+{}^{742}/_{T}-0.452X_{ACN}+\left({}^{235}/_{T}\right)X_{ACN}+1.573X_{ACN}^2-\left({}^{691}/_{T}\right)X_{ACN}^2\right]} \quad \text{(E5.2)}$$

where T is the temperature in Kelvin and X_{ACN} is the volume fraction of acetonitrile and water.

E5.3 Surface plot analog of contour plot optimization graphic

Figure E5.7 is a surface plot of plate count as a function of u_e and L generated under conditions identical to those in Figure 6.1.

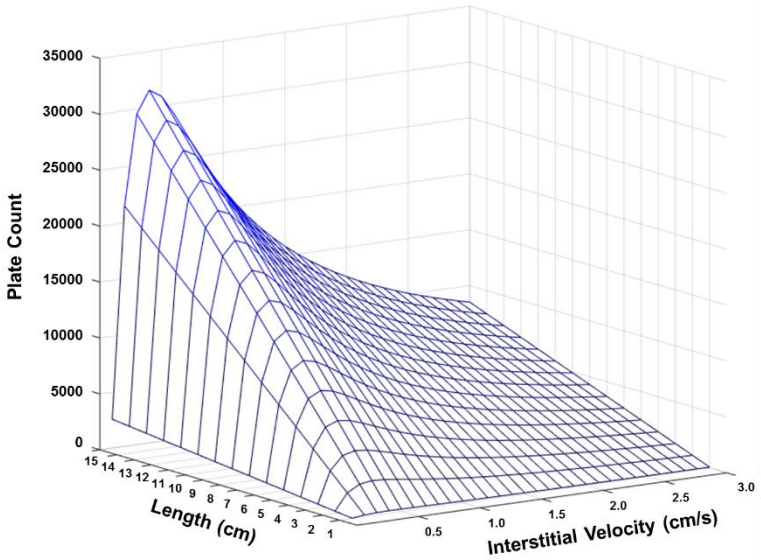

Figure E5.7. Surface plot for plate count as a function of u_e and L. Conditions identical to Figure 5.1. See Table 5.1 for parameters. For clarity axes labels corresponding to linear velocity 0.01 cm/s and column length 0.1 have been omitted.

Figure E5.8 shows surface plots for gradient peak capacity as a function of ue and L. Conditions for each panel of Figure E5.8 were identical to those in the corresponding panels of Figure 6.4.

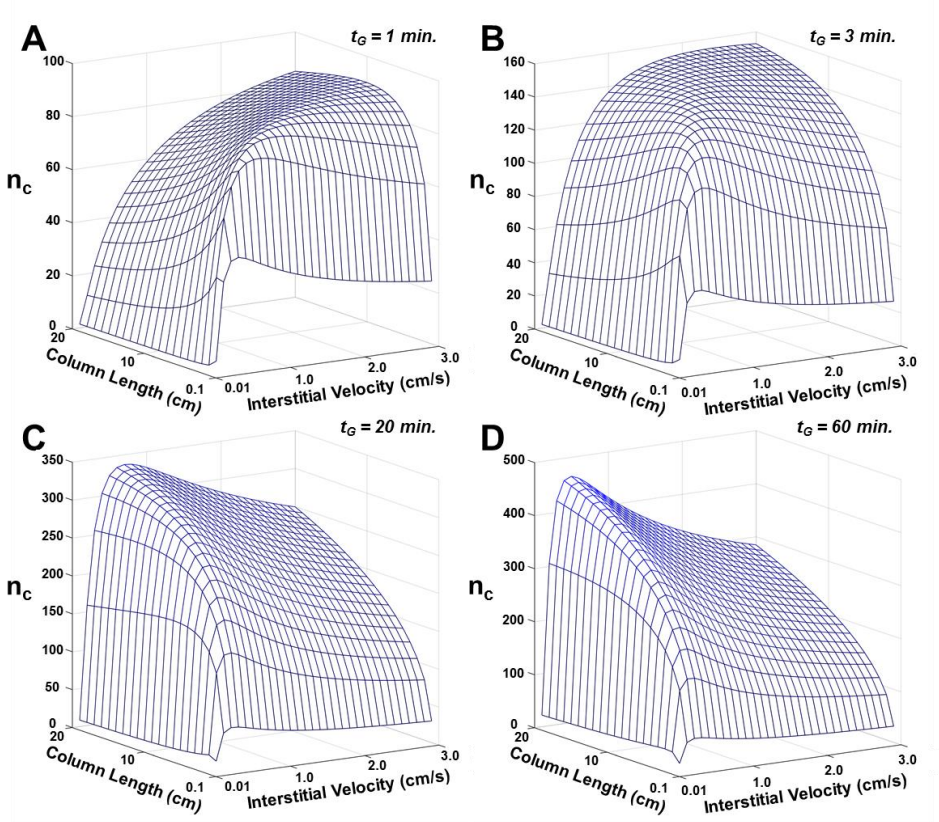

Figure E5.8 Gradient peak capacity surface plots as a function of u_e, t_0 and t_G for gradient times: 1, 3, 20, 60 minutes. Conditions identical to Figure 6.1. For clarity axes labels corresponding to linear velocity 0.01 cm/s and column length 0.1 have been omitted.

E5.3 Statistical peak overlap theory calculations

Values for peak capacity required to resolve a predetermined number of unknown compounds, m, with a desired probability, P_1, of resolution as single component bands were calculated using equation E5.3 [198]:

$$P_1 = \exp\left(\frac{-2m}{n_c}\right) \tag{E5.3}$$

Figure E5.9 shows the peak capacity required to separate m sample constituents with a 90 (blue) and 95% (black) probability of observing pure, single component peaks.

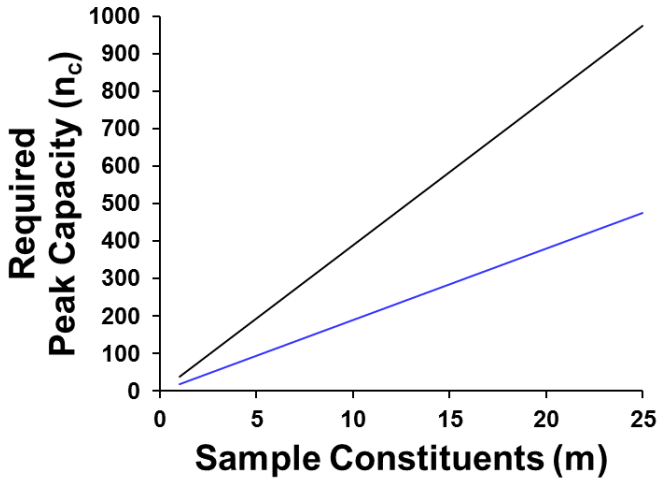

Figure E5.9 Peak capacity required to resolve samples composed of *m* constituents with a 90 (blue) and 95% (black) probability of observing each as a single pure peak.

BIBLIOGRAPHY

[1] A.J.P. Martin, R.L.M. Synge, A new form of chromatogram employing two liquid phases. I. A theory of chromatography. Ii. Application to the microdetermination of the higher monoamino acids in proteins, Biochem. J., 35 (1941) 1358-1368.

[2] B.L. Karger, L.R. Snyder, C. Horváth, An introduction to separation science, Wiley, New York, 1973.

[3] J. van Deemter, F. Zuiderweg, A. Klinkenberg, Longitudinal diffusion and resistance to mass transfer as causes of nonideality in chromatography, Chemical Engineering Science, 5 (1956) 271-289.

[4] P.R. Kasten, L. Lapidus, N.R. Amundson, Mathematics of adsorption in beds. V. Effect of intraparticle diffusion in flow systems in fixed beds, J. Phys. Chem., 56 (1952) 683-688.

[5] L. Lapidus, N.R. Amundson, Mathematics of adsorption in beds. Vi. The effect of longitudinal diffusion in ion-exchange and chromatographic columns, J. Phys. Chem., 56 (1952) 984-988.

[6] J.C. Giddings, Maximum number of components resolvable by gel filtration and other elution chromatographic methods, Analytical Chemistry, 39 (1967) 1027-1028.

[7] U.D. Neue, Theory of peak capacity in gradient elution, Journal of Chromatography A, 1079 (2005) 153-161.

[8] Y. Ishihama, Proteomic lc–ms systems using nanoscale liquid chromatography with tandem mass spectrometry, Journal of Chromatography A, 1067 (2005) 73-83.

[9] G. Theodoridis, H.G. Gika, I.D. Wilson, Lc-ms-based methodology for global metabolite profiling in metabonomics/metabolomics, TrAC Trends in Analytical Chemistry, 27 (2008) 251-260.

[10] L.A. Filla, W. Yuan, E.L. Feldman, S. Li, J.L. Edwards, Global metabolomic and isobaric tagging capillary liquid chromatography–tandem mass spectrometry approaches for uncovering pathway dysfunction in diabetic mouse aorta, Journal of Proteome Research, 13 (2014) 6121-6134.

[11] X. Gao, Q. Zhang, D. Meng, G. Isaac, R. Zhao, T.L. Fillmore, R.K. Chu, J. Zhou, K. Tang, Z. Hu, R.J. Moore, R.D. Smith, M.G. Katze, T.O. Metz, A reversed-phase capillary ultra-performance liquid chromatography–mass spectrometry (uplc-ms) method for comprehensive top-down/bottom-up lipid profiling, Analytical and Bioanalytical Chemistry, 402 (2012) 2923-2933.

[12] W.E. Haskins, Z. Wang, C.J. Watson, R.R. Rostand, S.R. Witowski, D.H. Powell, R.T. Kennedy, Capillary lc−ms ² at the attomole level for monitoring and discovering endogenous peptides in microdialysis samples collected in vivo, Analytical Chemistry, 73 (2001) 5005-5014.

[13] Y. Zhou, O.S. Mabrouk, R.T. Kennedy, Rapid preconcentration for liquid chromatography–mass spectrometry assay of trace level neuropeptides, Journal of The American Society for Mass Spectrometry, 24 (2013) 1700-1709.

[14] Y. Zhou, R.T. Kennedy, Capillary liquid chromatography-mass spectrometry detection of trace level neuropeptides, 41st International Symposium on High Performance Liquid Phase Separations and Related Techniques, (2014).

[15] Y. Zhou, J.-M.T. Wong, O.S. Mabrouk, R.T. Kennedy, Reducing adsorption to improve recovery and in vivo detection of neuropeptides by microdialysis with lc-ms, Analytical Chemistry, 87 (2015) 9802-9809.

[16] K. Maes, G. Béchade, J. Van Schoors, Y. Van Wanseele, J. Van Liefferinge, Y. Michotte, S.N. Harden, E.E. Chambers, J. Claereboudt, I. Smolders, A. Van Eeckhaut, An ultrasensitive nano

uhplc–esi–ms/ms method for the quantification of three neuromedin-like peptides in microdialysates, Bioanalysis, 7 (2015) 605-619.

[17] K. Maes, J. Van Liefferinge, J. Viaene, J. Van Schoors, Y. Van Wanseele, G. Béchade, E.E. Chambers, H. Morren, Y. Michotte, Y. Vander Heyden, J. Claereboudt, I. Smolders, A. Van Eeckhaut, Improved sensitivity of the nano ultra-high performance liquid chromatography-tandem mass spectrometric analysis of low-concentrated neuropeptides by reducing aspecific adsorption and optimizing the injection solvent, Journal of Chromatography A, 1360 (2014) 217-228.

[18] M.V. Novotny, I. Daidō, Microcolumn separations columns, instrumentation, and ancillary techniques, Elsevier ; Distributors for the U.S. and Canada, Elsevier Science Pub. Co., Amsterdam; New York; New York, 1985.

[19] J.C. Sternberg, Advances in chromatography, 2 (1966) 205-270.

[20] S.R. Groskreutz, S.G. Weber, Quantitative evaluation of models for solvent-based, on-column focusing in liquid chromatography, Journal of Chromatography A, 1409 (2015) 116-124.

[21] L.R. Snyder, Principles of gradient elution, Chromatographic Reviews, 7 (1965) 1-51.

[22] L.R. Snyder, D.L. Saunders, Optimized solvent programming for separations of complex samples by liquid-solid adsorption chromatography in columns, Journal of Chromatographic Science, 7 (1969) 195-208.

[23] A. Prüß, C. Kempter, J. Gysler, T. Jira, Extracolumn band broadening in capillary liquid chromatography, Journal of Chromatography A, 1016 (2003) 129-141.

[24] J. Vissers, A. Deru, M. Ursem, J. Chervet, Optimised injection techniques for micro and capillary liquid chromatography, Journal of Chromatography A, 746 (1996) 1-7.

[25] M.D. Foster, M.A. Arnold, J.A. Nichols, S.R. Bakalyar, Performance of experimental sample injectors for high-performance liquid chromatography microcolumns, Journal of Chromatography A, 869 (2000) 231-241.

[26] D. Guillarme, S. Heinisch, J.L. Rocca, Effect of temperature in reversed phase liquid chromatography, Journal of Chromatography A, 1052 (2004) 39-51.

[27] J.D. Thompson, P.W. Carr, High-speed liquid chromatography by simultaneous optimization of temperature and eluent composition, Analytical Chemistry, 74 (2002) 4150-4159.

[28] P.W. Carr, X. Wang, D.R. Stoll, Effect of pressure, particle size, and time on optimizing performance in liquid chromatography, Analytical Chemistry, 81 (2009) 5342-5353.

[29] P.W. Carr, D.R. Stoll, X. Wang, Perspectives on recent advances in the speed of high-performance liquid chromatography, Analytical Chemistry, 83 (2011) 1890-1900.

[30] C.V. McNeff, B. Yan, D.R. Stoll, R.A. Henry, Practice and theory of high temperature liquid chromatography, Journal of Separation Science, 30 (2007) 1672-1685.

[31] P.L. Zhu, L.R. Snyder, J.W. Dolan, N.M. Djordjevic, D.W. Hill, L.C. Sander, T.J. Waeghe, Combined use of temperature and solvent strength in reversed-phase gradient elution i. Predicting separation as a function of temperature and gradient conditions, Journal of Chromatography A, 756 (1996) 21-39.

[32] P.L. Zhu, J.W. Dolan, L.R. Snyder, Combined use of temperature and solvent strength in reversed-phase gradient elution ii. Comparing selectivity for different samples and systems, Journal of Chromatography A, 756 (1996) 41-50.

[33] P.L. Zhu, J.W. Dolan, L.R. Snyder, D.W. Hill, L. Van Heukelem, T.J. Waeghe, Combined use of temperature and solvent strength in reversed-phase gradient elution iii. Selectivity for

ionizable samples as a function of sample type and ph, Journal of Chromatography A, 756 (1996) 51-62.

[34] P.L. Zhu, J.W. Dolan, L.R. Snyder, N.M. Djordjevic, D.W. Hill, J.T. Lin, L.C. Sander, L. Van Heukelem, Combined use of temperature and solvent strength in reversed-phase gradient elution iv. Selectivity for neutral (non-ionized) samples as a function of sample type and other separation conditions, Journal of Chromatography A, 756 (1996) 63-72.

[35] G. Desmet, S. Eeltink, Fundamentals for lc miniaturization, Analytical Chemistry, 85 (2013) 543-556.

[36] E.J. Caliguri, P. Capella, L. Bottari, I.N. Mefford, High-speed microbore liquid chromatography with electrochemical detection using 3-.Mu.M c18 packing material, Analytical Chemistry, 57 (1985) 2423-2425.

[37] I.N. Mefford, E.J. Caliguri, R.K. Grady, P. Capella, T.A. Durkin, P. Chevalier, Microbore hplc of biogenic amines in small biological samples, in: Methods in enzymology, Elsevier, 1986, pp. 402-412.

[38] A.P. Newton, J.B. Justice, Temporal response of microdialysis probes to local perfusion of dopamine and cocaine followed with one-minute sampling, Analytical Chemistry, 66 (1994) 1468-1472.

[39] G.A. Guiochon, H.M. Colin, Microcolumn high-performance liquid chromatography, Elsevier, Amsterdam; New York, 1984.

[40] J.C. Gluckman, M.V. Novotny, Microcolumn separations columns, instrumentation, and ancillary techniques, Elsevier, Amsterdam; New York, 1985.

[41] B. Bobály, D. Guillarme, S. Fekete, Systematic comparison of a new generation of columns packed with sub-2 μm superficially porous particles, Journal of Separation Science, (2014) In press.

[42] S. Fekete, D. Guillarme, Possibilities of new generation columns packed with 1.3μm core–shell particles in gradient elution mode, Journal of Chromatography A, 1320 (2013) 86-95.

[43] A.C. Sanchez, G. Friedlander, S. Fekete, J. Anspach, D. Guillarme, M. Chitty, T. Farkas, Pushing the performance limits of reversed-phase ultra high performance liquid chromatography with 1.3μm core–shell particles, Journal of Chromatography A, 1311 (2013) 90-97.

[44] H. Colin, M. Martin, G. Guiochon, Extra-column effects in high-performance liquid chromatography, Journal of Chromatography A, 185 (1979) 79-95.

[45] S. Bakalyar, C. Phipps, B. Spruce, K. Olsen, Choosing sample volume to achieve maximum detection sensitivity and resolution with high-performance liquid chromatography columns of 1.0, 2.1 and 4.6 mm i.D, Journal of Chromatography A, 762 (1997) 167-185.

[46] T. Tsuda, G. Nakagawa, Open-tubular microcapillary liquid chromatography with 30–40 μm i.D. Columns, Journal of Chromatography A, 199 (1980) 249-258.

[47] V.L. McGuffin, M. Novotny, Nanoliter injection system for microcolumn liquid chromatography, Analytical Chemistry, 55 (1983) 580-583.

[48] M.J. Mills, J. Maltas, W. John Lough, Assessment of injection volume limits when using on-column focusing with microbore liquid chromatography, Journal of Chromatography A, 759 (1997) 1-11.

[49] M. Tsimidou, R. Macrae, Influence of injection solvent on the reversed-phase chromatography of triglycerides, Journal of Chromatography A, 285 (1984) 178-181.

[50] D. Vukmanic, M. Chiba, Effect of organic solvents in sample solutions and injection volumes on chromatographic peak profiles of analytes in reversed-phase high-performance liquid chromatography, Journal of Chromatography A, 483 (1989) 189-196.

[51] J. Layne, T. Farcas, I. Rustamov, F. Ahmed, Volume-load capacity in fast-gradient liquid chromatographyeffect of sample solvent composition and injection volume on chromatographic performance, Journal of Chromatography A, 913 (2001) 233-242.

[52] F. Gritti, C.A. Sanchez, T. Farkas, G. Guiochon, Achieving the full performance of highly efficient columns by optimizing conventional benchmark high-performance liquid chromatography instruments, Journal of Chromatography A, 1217 (2010) 3000-3012.

[53] A.C. Sanchez, J.A. Anspach, T. Farkas, Performance optimizing injection sequence for minimizing injection band broadening contributions in high efficiency liquid chromatographic separations, Journal of Chromatography A, 1228 (2012) 338-348.

[54] J.A. Apffel, T.V. Alfredson, R.E. Majors, Automated on-line multi-dimensional high-performance liquid chromatographic techniques for the clean-up and analysis of water-soluble samples, Journal of Chromatography A, 206 (1981) 43-57.

[55] F. Erni, R. Frei, Two-dimensional column liquid chromatographic technique for resolution of complex mixtures, Journal of Chromatography A, 149 (1978) 561-569.

[56] K. Horváth, J.N. Fairchild, G. Guiochon, Detection issues in two-dimensional on-line chromatography, Journal of Chromatography A, 1216 (2009) 7785-7792.

[57] G. Vivó-Truyols, S. van der Wal, P.J. Schoenmakers, Comprehensive study on the optimization of online two-dimensional liquid chromatographic systems considering losses in theoretical peak capacity in first- and second-dimensions: A pareto-optimality approach, Analytical Chemistry, 82 (2010) 8525-8536.

[58] Y. Oda, N. Asakawa, T. Kajima, Y. Yoshida, T. Sato, On-line determination and resolution of verapamil enantiomers by high-performance liquid chromatography with column switching, Journal of Chromatography A, 541 (1991) 411-418.

[59] S.W. Simpkins, J.W. Bedard, S.R. Groskreutz, M.M. Swenson, T.E. Liskutin, D.R. Stoll, Targeted three-dimensional liquid chromatography: A versatile tool for quantitative trace analysis in complex matrices, Journal of Chromatography A, 1217 (2010) 7648-7660.

[60] S.R. Groskreutz, M.M. Swenson, L.B. Secor, D.R. Stoll, Selective comprehensive multi-dimensional separation for resolution enhancement in high performance liquid chromatography. Part i: Principles and instrumentation, Journal of Chromatography A, 1228 (2012) 31-40.

[61] K. Šlais, D. Kouřilová, M. Krejčí, Trace analysis by peak compression sampling of a large sample volume on microbore columns in liquid chromatography, Journal of Chromatography A, 282 (1983) 363-370.

[62] B.L. Ling, W. Baeyens, C. Dewaele, Comparative study of "on-column focusing" applied to micro-lc and conventional lc, Journal of Microcolumn Separations, 4 (1992) 17-22.

[63] S. Héron, A. Tchapla, J.P. Chervet, Influence of injection parameters on column performance in nanoscale high-performance liquid chromatography, Chromatographia, 51 (2000) 495-499.

[64] M.E. León-González, N. Rosales-Conrado, L.V. Pérez-Arribas, L.M. Polo-Díez, Large injection volumes in capillary liquid chromatography: Study of the effect of focusing on chromatographic performance, Journal of Chromatography A, 1217 (2010) 7507-7513.

[65] G. D'Orazio, S. Fanali, Combination of two different stationary phases for on-line pre-concentration and separation of basic drugs by using nano-liquid chromatography, Journal of Chromatography A, 1285 (2013) 118-123.

[66] G. Vanhoenacker, P. Sandra, Elevated temperature and temperature programming in conventional liquid chromatography – fundamentals and applications, Journal of Separation Science, 29 (2006) 1822-1835.

[67] G. Vanhoenacker, P. Sandra, High temperature and temperature programmed hplc: Possibilities and limitations, Analytical and Bioanalytical Chemistry, 390 (2007) 245-248.

[68] T. Teutenberg, High-temperature liquid chromatography: A user's guide for method development, RSC Pub, Cambridge, 2010.

[69] T. Teutenberg, Potential of high temperature liquid chromatography for the improvement of separation efficiency—a review, Analytica Chimica Acta, 643 (2009) 1-12.

[70] P.K. Zarzycki, E. Wlodarczyk, D.-W. Lou, K. Jinno, Evaluation of methanol-water and acetonitrile-water binary mixtures as eluents for temperature-dependent inclusion chromatography, Analytical Sciences, 22 (2006) 453-456.

[71] O. Nordstrom, P. Molander, T. Greibrokk, R. Blomhoff, E. Lundanes, Evaluation of temperature programming for gradient elution in packed capillary liquid chromatography coupled to electrochemical detection, Journal of Microcolumn Separations, 13 (2001) 179-185.

[72] P. Jandera, L.G. Blomberg, E. Lundanes, Controlling the retention in capillary lc with solvents, temperature, and electric fields, Journal of Separation Science, 27 (2004) 1402-1418.

[73] B. Gu, H. Cortes, J. Luong, M. Pursch, P. Eckerle, R. Mustacich, Low thermal mass liquid chromatography, Analytical Chemistry, 81 (2009) 1488-1495.

[74] T.J. Causon, H.J. Cortes, R.A. Shellie, E.F. Hilder, Temperature pulsing for controlling chromatographic resolution in capillary liquid chromatography, Analytical Chemistry, 84 (2012) 3362-3368.

[75] M. Pursch, P. Eckerle, B. Gu, J. Luong, H.J. Cortes, Selectivity tuning via temperature pulsing using low thermal mass liquid chromatography and monolithic columns, Journal of Separation Science, 36 (2013) 1217-1222.

[76] P. Molander, K. Haugland, D.R. Hegna, E. Ommundsen, E. Lundanes, T. Greibrokk, Determination of low levels of an antioxidant in polyolefins by large-volume injection temperature-programmed packed capillary liquid chromatography, Journal of Chromatography A, 864 (1999) 103-109.

[77] P. Molander, S.J. Thommesen, I.A. Bruheim, R. Trones, T. Greibrokk, E. Lundanes, T.E. Gundersen, Temperature-programmed packed capillary liquid chromatography separation with large volume on-column focusing of retinyl esters, Journal of High Resolution Chromatography, 22 (1999) 490-494.

[78] P. Molander, A. Holm, E. Lundanes, T. Greibrokk, E. Ommundsen, Separation of ceramides by sub-ambient temperature-assisted large volume injection in temperature-programmed packed capillary liquid chromatography, Journal of High Resolution Chromatography, 23 (2000) 653-655.

[79] P. Molander, A. Holm, E. Lundanes, D.R. Hegna, E. Ommundsen, T. Greibrokk, Temperature-promoted large-volume solute enrichment in column-switching miniaturized liquid chromatography: Determination of an antioxidant, The Analyst, 127 (2002) 892-897.

[80] Å. Larsen, P. Molander, Temperature optimization for improved determination of phosphatidylserine species by micro liquid chromatography with electrospray tandem mass spectrometric detection, Journal of Separation Science, 27 (2004) 297-303.

[81] A. Holm, P. Molander, E. Lundanes, T. Greibrokk, Novel column oven concept for cold spot large volume sample enrichment in high throughput temperature gradient capillary liquid chromatography, Journal of Separation Science, 26 (2003) 1147-1153.

[82] D. Collins, E. Nesterenko, D. Connolly, M. Vasquez, M. Macka, D. Brabazon, B. Paull, Versatile capillary column temperature control using a thermoelectric array based platform, Analytical Chemistry, 83 (2011) 4307-4313.

[83] H. Eghbali, K. Sandra, B. Tienpont, S. Eeltink, P. Sandra, G. Desmet, Exploring the possibilities of cryogenic cooling in liquid chromatography for biological applications: A proof of principle, Analytical Chemistry, 84 (2012) 2031-2037.

[84] J.H. Knox, Band dispersion in chromatography—a universal expression for the contribution from the mobile zone, Journal of Chromatography A, 960 (2002) 7-18.

[85] T.J. Anderson, I. Ansara, The ga-in (gallium-indium) system, Journal of Phase Equilibria, 12 (1991) 64-72.

[86] V. Prokhorenko, V. Kotov, Liquid gallium: Potential uses as a heat-transfer agent, High Temperature, 38 (2000) 954-968.

[87] K. Nishida, Y. Ando, H. Kawamura, Diffusion coefficients of anticancer drugs and compounds having a similar structure at 30 c, Colloid & Polymer Science, 261 (1983) 70-73.

[88] J. Billen, K. Broeckhoven, A. Liekens, K. Choikhet, G. Rozing, G. Desmet, Influence of pressure and temperature on the physico-chemical properties of mobile phase mixtures commonly used in high-performance liquid chromatography, Journal of Chromatography A, 1210 (2008) 30-44.

[89] Y. Zhang, X. Wang, P. Mukherjee, P. Petersson, Critical comparison of performances of superficially porous particles and sub-2μm particles under optimized ultra-high pressure conditions, Journal of Chromatography A, 1216 (2009) 4597-4605.

[90] Y. Liu, J. Zhang, X. Xu, M.K. Zhao, A.M. Andrews, S.G. Weber, Capillary ultrahigh performance liquid chromatography with elevated temperature for sub-one minute separations of

basal serotonin in submicroliter brain microdialysate samples, Analytical Chemistry, 82 (2010) 9611-9616.

[91] J. Zhang, Y. Liu, A. Jaquins-Gerstl, Z. Shu, A.C. Michael, S.G. Weber, Optimization for speed and sensitivity in capillary high performance liquid chromatography. The importance of column diameter in online monitoring of serotonin by microdialysis, Journal of Chromatography A, 125 (2012) 54-62.

[92] J. Zhang, A. Jaquins-Gerstl, K.M. Nesbitt, S.C. Rutan, A.C. Michael, S.G. Weber, In vivo monitoring of serotonin in the striatum of freely moving rats with one minute temporal resolution by online microdialysis–capillary high-performance liquid chromatography at elevated temperature and pressure, Analytical Chemistry, 85 (2013) 9889-9897.

[93] J. Haun, J. Leonhardt, C. Portner, T. Hetzel, J. Tuerk, T. Teutenberg, T.C. Schmidt, Online and splitless nanolc × capillarylc with quadrupole/time-of-flight mass spectrometric detection for comprehensive screening analysis of complex samples, Analytical Chemistry, 85 (2013) 10083-10090.

[94] G. Guiochon, H. Colin, Microcolumn high-performance liquid chromatography, Elsevier ; Distributors for the U.S. and Canada, Elsevier Science Pub. Co, Amsterdam ; New York : New York, NY, 1984.

[95] S.R. Bakalyar, C. Phipps, B. Spruce, K. Olsen, Choosing sample volume to achieve maximum detection sensitivity and resolution with high-performance liquid chromatography columns of 1.0, 2.1 and 4.6 mm i.D, Journal of Chromatography A, 762 (1997) 167-185.

[96] L.R. Snyder, J.J. Kirkland, J.W. Dolan, Introduction to modern liquid chromatography, Wiley, Hoboken, N.J., 2010.

[97] S.R. Groskreutz, S.G. Weber, Temperature-assisted on-column solute focusing: A general method to reduce pre-column dispersion in capillary high performance liquid chromatography, Journal of Chromatography A, 1354 (2014) 65-74.

[98] K.D. Patel, A.D. Jerkovich, J.C. Link, J.W. Jorgenson, In-depth characterization of slurry packed capillary columns with 1.0-μm nonporous particles using reversed-phase isocratic ultrahigh-pressure liquid chromatography, Analytical Chemistry, 76 (2004) 5777-5786.

[99] J. Zhang, Y. Liu, A. Jaquins-Gerstl, Z. Shu, A.C. Michael, S.G. Weber, Optimization for speed and sensitivity in capillary high performance liquid chromatography. The importance of column diameter in online monitoring of serotonin by microdialysis, J. Chromatogr. A, 1251 (2012) 54-62.

[100] M. Verstraeten, M. Pursch, P. Eckerle, J. Luong, G. Desmet, Modelling the thermal behaviour of the low-thermal mass liquid chromatography system, Journal of Chromatography A, 1218 (2011) 2252-2263.

[101] K. Maes, I. Smolders, Y. Michotte, A. Van Eeckhaut, Strategies to reduce aspecific adsorption of peptides and proteins in liquid chromatography–mass spectrometry based bioanalyses: An overview, Journal of Chromatography A, 1358 (2014) 1-13.

[102] K. Maes, J. Van Liefferinge, J. Viaene, J. Van Schoors, Y. Van Wanseele, G. Béchade, E.E. Chambers, H. Morren, Y. Michotte, Y.V. Heyden, J. Claereboudt, I. Smolders, A. Van Eeckhaut, Improved sensitivity of the nano ultra-high performance liquid chromatography-tandem mass spectrometric analysis of low-concentrated neuropeptides by reducing aspecific adsorption and optimizing the injection solvent, Journal of Chromatography A, (2014).

[103] B. Vatansever, S.L. Lahrichi, A. Thiocone, N. Salluce, M. Mathieu, E. Grouzmann, B. Rochat, Comparison between a linear ion trap and a triple quadruple ms in the sensitive detection

of large peptides at femtomole amounts on column, Journal of Separation Science, 33 (2010) 2478-2488.

[104] L. Dillen, W. Cools, L. Vereyken, P. Timmerman, A screening uhplc–ms/ms method for the analysis of amyloid peptides in cerebrospinal fluid of preclinical species, Bioanalysis, 3 (2011) 45-55.

[105] T. Oe, B.L. Ackermann, K. Inoue, M.J. Berna, C.O. Garner, V. Gelfanova, R.A. Dean, E.R. Siemers, D.M. Holtzman, M.R. Farlow, I.A. Blair, Quantitative analysis of amyloidβ peptides in cerebrospinal fluid of alzheimer's disease patients by immunoaffinity purification and stable isotope dilution liquid chromatography/negative electrospray ionization tandem mass spectrometry, Rapid Communications in Mass Spectrometry, 20 (2006) 3723-3735.

[106] C.H. Suelter, M. DeLuca, How to prevent losses of protein by adsorption to glass and plastic, Analytical Biochemistry, 135 (1983) 112-119.

[107] A.E. Rupert, Development of electroosmotic sampling for the investigation of galanin-degrading ectopeptidase activity in the hippocampus, in: Dissertation, Department of Chemistry, University of Pittsburgh, 2012, pp. 132 pp.

[108] A.E. Rupert, Y. Ou, M. Sandberg, S.G. Weber, Electroosmotic push–pull perfusion: Description and application to qualitative analysis of the hydrolysis of exogenous galanin in organotypic hippocampal slice cultures, ACS Chemical Neuroscience, 4 (2013) 838-848.

[109] Y. Ou, J. Wu, M. Sandberg, S.G. Weber, Electroosmotic perfusion of tissue: Sampling the extracellular space and quantitative assessment of membrane-bound enzyme activity in organotypic hippocampal slice cultures, Analytical and Bioanalytical Chemistry, 406 (2014) 6455-6468.

[110] J.C. Sternberg, Advances in chromatography, New York, NY, United States, 2 (1966) 205.

[111] H.A. Claessens, M.A.J. Kuyken, A comparative study of large volume injection techniques for microbore columns in hplc, Chromatographia, 23 (1987) 331-336.

[112] J.F.K. Huber, J.A.R.J. Hulsman, C.A.M. Meijers, Quantitative analysis of trace amounts of estrogenic steroids in pregnancy urine by column liquid-liquid chromatography with ultraviolet detection, Journal of Chromatography A, 62 (1971) 79-91.

[113] G. Kamperman, J.C. Kraak, Simple and fast analysis of adrenaline and noradrenaline in plasma on microbore high-performance liquid chromatography columns using fluorimetric detection, Journal of Chromatography B: Biomedical Sciences and Applications, 337 (1985) 384-390.

[114] J.C. Kraak, F. Smedes, J.W.A. Meijer, Application of on-column concentration of deproteinized serum to the hplc-determination of anticonvulsants, Chromatographia, 13 (1980) 673-676.

[115] K. Buonasera, G. D'Orazio, S. Fanali, P. Dugo, L. Mondello, Separation of organophosphorus pesticides by using nano-liquid chromatography, Journal of Chromatography A, 1216 (2009) 3970-3976.

[116] P. Jandera, T. Hájek, P. Česla, Effects of the gradient profile, sample volume and solvent on the separation in very fast gradients, with special attention to the second-dimension gradient in comprehensive two-dimensional liquid chromatography, Journal of Chromatography A, 1218 (2011) 1995-2006.

[117] G. Vivó-Truyols, S. van der Wal, P.J. Schoenmakers, Comprehensive study on the optimization of online two-dimensional liquid chromatographic systems considering losses in theoretical peak capacity in first- and second-dimensions: A pareto-optimality approach, Analytical Chemistry, 82 (2010) 8525-8536.

[118] D.R. Stoll, E.S. Talus, D.C. Harmes, K. Zhang, Evaluation of detection sensitivity in comprehensive two-dimensional liquid chromatography separations of an active pharmaceutical ingredient and its degradants, Analytical and Bioanalytical Chemistry, (2014).

[119] L.R. Snyder, Linear elution adsorption chromatography, Journal of Chromatography A, 13 (1964) 415-434.

[120] J. Lankelma, H. Poppe, Determination of methotrexate in plasma by on-column concentration and ion-exchange chromatography, Journal of Chromatography A, 149 (1978) 587-598.

[121] H. Poppe, J. Paanakker, M. Bronckhorst, Peak width in solvent-programmed chromatography, Journal of Chromatography A, 204 (1981) 77-84.

[122] S.-H. Hsu, T. Raglione, S.A. Tomellini, T.R. Floyd, N. Sagliano Jr, R.A. Hartwick, Zone compressesion effects in high-performance liquid chromatography, Journal of Chromatography A, 367 (1986) 293-300.

[123] J. De Vos, G. Desmet, S. Eeltink, A generic approach to post-column refocusing in liquid chromatography, Journal of Chromatography A, 1360 (2014) 164-171.

[124] J. De Vos, S. Eeltink, G. Desmet, Peak refocusing using subsequent retentive trapping and strong eluent remobilization in liquid chromatography: A theoretical optimization study, Journal of Chromatography A, 1381 (2015) 74-86.

[125] M.J. Hilhorst, G.W. Somsen, G.J. de Jong, Sensitivity enhancement in capillary electrochromatography by on-column preconcentration, Chromatographia, 53 (2000) 190-196.

[126] N.A. Wright, D.C. Villalanti, M.F. Burke, Fourier transform deconvolution of instrument and column band broadening in liquid chromatography, Analytical Chemistry, 54 (1982) 1735-1738.

[127] L.R. Snyder, High-performance gradient elution: The practical application of the linear-solvent-strength model, John Wiley, Hoboken, NJ, 2007.

[128] Z. Zhang, C. Jia, L. Li, Neuropeptide analysis with liquid chromatography-capillary electrophoresis-mass spectrometric imaging: Sample preparation, Journal of Separation Science, 35 (2012) 1779-1784.

[129] B. Bobály, D. Guillarme, S. Fekete, Systematic comparison of a new generation of columns packed with sub-2 μm superficially porous particles: Liquid chromatography, Journal of Separation Science, 37 (2014) 189-197.

[130] J. De Vos, M. De Pra, G. Desmet, R. Swart, T. Edge, F. Steiner, S. Eeltink, High-speed isocratic and gradient liquid-chromatography separations at 1500 bar, Journal of Chromatography A, 1409 (2015) 138-145.

[131] M. Gilar, T.S. McDonald, J.S. Johnson, J.P. Murphy, J.W. Jorgenson, Wide injection zone compression in gradient reversed-phase liquid chromatography, Journal of Chromatography A, 1390 (2015) 86-94.

[132] J. Plotka-Wasylka, N. Szczepanska, M. de la Guardia, J. Namiesnik, Modern trends in solid phase extraction: New sorbent media, TrAC, Trends Anal. Chem., 77 (2016) 23-43.

[133] J. Wackerlig, R. Schirhagl, Applications of molecularly imprinted polymer nanoparticles and their advances toward industrial use: A review, Anal. Chem. (Washington, DC, U. S.), (2015) Ahead of Print.

[134] D. Wei, M. Li, K.W. King, L. Yang, Online and automated sample extraction, Bioanalysis, 7 (2015) 2227-2233.

[135] S. Tang, H. Zhang, H.K. Lee, Advances in sample extraction, Anal. Chem. (Washington, DC, U. S.), (2015) Ahead of Print.

[136] D. Gode, M.M. Martin, F. Steiner, C.G. Huber, D.A. Volmer, Rapid narrow band elution for on-line spe using a novel solvent plug injection technique, Anal. Bioanal. Chem., 404 (2012) 433-445.

[137] M.P. Washburn, D. Wolters, J.R. Yates, Large-scale analysis of the yeast proteome by multidimensional protein identification technology, Nat. Biotechnol., 19 (2001) 242-247.

[138] D.A. Wolters, M.P. Washburn, J.R. Yates, III, An automated multidimensional protein identification technology for shotgun proteomics, Anal. Chem., 73 (2001) 5683-5690.

[139] J. De Vos, G. Desmet, S. Eeltink, Enhancing detection sensitivity in gradient liquid chromatography via post-column refocusing and strong-solvent remobilization, Journal of Chromatography A, 1455 (2016) 86-92.

[140] H.C. van de Ven, A.F.G. Gargano, S. van der Wal, P.J. Schoenmakers, Switching solvent and enhancing analyte concentrations in small effluent fractions using in-column focusing, Journal of Chromatography A, 1427 (2016) 90-95.

[141] T. Greibrokk, T. Andersen, Temperature programming in liquid chromatography, Journal of Separation Science, 24 (2001) 899-909.

[142] T. Andersen, P. Molander, R. Trones, D.R. Hegna, T. Greibrokk, Separation of polyethylene glycol oligomers using inverse temperature programming in packed capillary liquid chromatography, Journal of Chromatography A, 918 (2001) 221-226.

[143] M. Pursch, P. Eckerle, B. Gu, J. Luong, H.J. Cortes, Selectivity tuning via temperature pulsing using low thermal mass liquid chromatography and monolithic columns: Liquid chromatography, Journal of Separation Science, 36 (2013) 1217-1222.

[144] M. Verstraeten, M. Pursch, P. Eckerle, J. Luong, G. Desmet, Thermal modulation for multidimensional liquid chromatography separations using low-thermal-mass liquid chromatography (lc), Analytical Chemistry, 83 (2011) 7053-7060.

[145] J. Bowermaster, H. McNair, Microbore high-performance liquid chromatographic columns: Speed, efficiency, sensitivity and temperature programming, Journal of Chromatography A, 279 (1983) 431-438.

[146] J. Bowermaster, H.M. McNair, Temperature programmed microbore hplc--part i, Journal of Chromatographic Science, 22 (1984) 165-170.

[147] M.H. Chen, C. Horváth, Temperature programming and gradient elution in reversed-phase chromatography with packed capillary columns, Journal of Chromatography A, 788 (1997) 51-61.

[148] K. Ryan, N.M. Djordjevic, F. Erni, Temperature programming in open tubular liquid chromatography, Journal of Liquid Chromatography & Related Technologies, 19 (1996) 2089-2099.

[149] S. Wiese, T. Teutenberg, T.C. Schmidt, General strategy for performing temperature programming in high performance liquid chromatography: Prediction of linear temperature gradients, Analytical Chemistry, 83 (2011) 2227-2233.

[150] R. De Pauw, M. Pursch, G. Desmet, Using the column wall itself as resistive heater for fast temperature gradients in liquid chromatography, Journal of Chromatography A, 1420 (2015) 129-134.

[151] S.R. Groskreutz, A.R. Horner, S.G. Weber, Temperature-based on-column solute focusing in capillary liquid chromatography reduces peak broadening from pre-column dispersion and volume overload when used alone or with solvent-based focusing, Journal of Chromatography A, 1405 (2015) 133-139.

[152] R.E. Wilson, S.R. Groskreutz, S.G. Weber, Improving the sensitivity, resolution, and peak capacity of gradient elution in capillary liquid chromatography with large-volume injections by using temperature-assisted on-column solute focusing, Analytical Chemistry, 88 (2016) 5112-5121.

[153] M. Gilar, T.S. McDonald, J.S. Johnson, J.P. Murphy, J.W. Jorgenson, Wide injection zone compression in gradient reversed-phase liquid chromatography, J. Chromatogr. A, 1390 (2015) 86-94.

[154] M. Gilar, T.S. McDonald, G. Roman, J.S. Johnson, J.P. Murphy, J.W. Jorgenson, Repetitive injection method: A tool for investigation of injection zone formation and its compression in microfluidic liquid chromatography, J. Chromatogr. A, 1381 (2015) 110-117.

[155] L.N. Jeong, R. Sajulga, S.G. Forte, D.R. Stoll, S.C. Rutan, Simulation of elution profiles in liquid chromatography-i: Gradient elution conditions, and with mismatched injection and mobile phase solvents, J. Chromatogr. A, 1457 (2016) 41-49.

[156] M. Czok, G. Guiochon, The physical sense of simulation models of liquid chromatography: Propagation through a grid or solution of the mass balance equation, Anal. Chem., 62 (1990) 189-200.

[157] A. Felinger, G. Guiochon, Rapid simulation of chromatographic band profiles on personal computers, J. Chromatogr. A, 658 (1994) 511-515.

[158] Z. Ma, G. Guiochon, Application of orthogonal collocation on finite elements in the simulation of nonlinear chromatography, Comput. Chem. Eng., 15 (1991) 415-426.

[159] M.Z. El Fallah, G. Guiochon, Gradient elution chromatography at very high column loading: Effect of the deviation from the langmuir model on the band profile of a single component, Anal. Chem., 63 (1991) 2244-2252.

[160] U.D. Neue, H.-J. Kuss, Improved reversed-phase gradient retention modeling, Journal of Chromatography A, 1217 (2010) 3794-3803.

[161] J.C. Sternberg, Advances in chromatography, New York, NY, United States, 1966.

[162] E. Grushka, Chromatographic peak capacity and the factors influencing it, Analytical Chemistry, 42 (1970) 1142-1147.

[163] J. Dolan, L. Snyder, N. Djordjevic, D. Hill, T. Waeghe, Reversed-phase liquid chromatographic separation of complex samples by optimizing temperature and gradient timei. Peak capacity limitations, Journal of Chromatography A, 857 (1999) 1-20.

[164] J.J. van Deemter, F.J. Zuiderweg, A. Klinkenberg, Longitudinal diffusion and resistance to mass transfer as causes of nonideality in chromatography, Chemical Engineering Science, 5 (1956) 271-289.

[165] A. Klinkenberg, F. Sjenitzer, Holding-time distributions of the gaussian type, Chem. Eng. Sci., 5 (1956) 258-270.

[166] J.H. Knox, The speed of analysis by gas chromatography, J. Chem. Soc., (1961) 433-441.

[167] J.C. Giddings, Comparison of theoretical limit of separating speed in gas and liquid chromatography, Analytical Chemistry, 37 (1965) 60-63.

[168] J.H. Knox, M. Saleem, Kinetic conditions for optimum speed and resolution in column chromatography, Journal of Chromatographic Science, 7 (1969) 614-622.

[169] J.H. Knox, High speed liquid chromatography, Annual Review of Physical Chemistry, 24 (1973) 29-49.

[170] I. Halász, R. Endele, J. Asshauer, Ultimate limits in high-pressure liquid chromatography, Journal of Chromatography A, 112 (1975) 37-60.

[171] M. Martin, C. Eon, G. Guiochon, Study of the pertinency of pressure in liquid chromatography iii. A practical method for choosing the experimental conditions in liquid chromatography, Journal of Chromatography A, 110 (1975) 213-232.

[172] G. Guiochon, Optimization in liquid chromatography, in: High-performance liquid chromatography, Elsevier, 1980, pp. 1-56.

[173] H. Poppe, Some reflections on speed and efficiency of modern chromatographic methods, Journal of Chromatography A, 778 (1997) 3-21.

[174] K. Broeckhoven, D. Cabooter, S. Eeltink, G. Desmet, Kinetic plot based comparison of the efficiency and peak capacity of high-performance liquid chromatography columns: Theoretical background and selected examples, Journal of Chromatography A, 1228 (2012) 20-30.

[175] T.J. Causon, K. Broeckhoven, E.F. Hilder, R.A. Shellie, G. Desmet, S. Eeltink, Kinetic performance optimisation for liquid chromatography: Principles and practice, Journal of Separation Science, 34 (2011) 877-887.

[176] S. Eeltink, W.M.C. Decrop, F. Steiner, M. Ursem, D. Cabooter, G. Desmet, W.T. Kok, Use of kinetic plots for the optimization of the separation time in ultra-high-pressure lc, Journal of Separation Science, 33 (2010) 2629-2635.

[177] D. Cabooter, F. Lestremau, A. de Villiers, K. Broeckhoven, F. Lynen, P. Sandra, G. Desmet, Investigation of the validity of the kinetic plot method to predict the performance of coupled column systems operated at very high pressures under different thermal conditions, Journal of Chromatography A, 1216 (2009) 3895-3903.

[178] S. Heinisch, G. Desmet, D. Clicq, J.-L. Rocca, Kinetic plot equations for evaluating the real performance of the combined use of high temperature and ultra-high pressure in liquid chromatography, Journal of Chromatography A, 1203 (2008) 124-136.

[179] D. Cabooter, F. Lestremau, F. Lynen, P. Sandra, G. Desmet, Kinetic plot method as a tool to design coupled column systems producing 100,000 theoretical plates in the shortest possible time, Journal of Chromatography A, 1212 (2008) 23-34.

[180] D. Clicq, S. Heinisch, J.L. Rocca, D. Cabooter, P. Gzil, G. Desmet, Use of the kinetic plot method to analyze commercial high-temperature liquid chromatography systems, Journal of Chromatography A, 1146 (2007) 193-201.

[181] D. Cabooter, S. Heinisch, J.L. Rocca, D. Clicq, G. Desmet, Use of the kinetic plot method to analyze commercial high-temperature liquid chromatography systems, Journal of Chromatography A, 1143 (2007) 121-133.

[182] G. Desmet, D. Clicq, D.T.T. Nguyen, D. Guillarme, S. Rudaz, J.-L. Veuthey, N. Vervoort, G. Torok, D. Cabooter, P. Gzil, Practical constraints in the kinetic plot representation of chromatographic performance data: Theory and application to experimental data, Analytical Chemistry, 78 (2006) 2150-2162.

[183] G. Desmet, D. Clicq, P. Gzil, Geometry-independent plate height representation methods for the direct comparison of the kinetic performance of lc supports with a different size or morphology, Analytical Chemistry, 77 (2005) 4058-4070.

[184] P.A. Bristow, J.H. Knox, Standardization of test conditions for high performance liquid chromatography columns, Chromatographia, 10 (1977) 279-289.

[185] X. Wang, D.R. Stoll, P.W. Carr, P.J. Schoenmakers, A graphical method for understanding the kinetics of peak capacity production in gradient elution liquid chromatography, Journal of Chromatography A, 1125 (2006) 177-181.

[186] I. Halász, G. Görlitz, Optimale parameter in der schnellen flüssigkeitschromatographie (hplc), Angewandte Chemie, 94 (1982) 50-62.

[187] H. Chen, C. Horváth, High-speed high-performance liquid chromatography of peptides and proteins, Journal of Chromatography A, 705 (1995) 3-20.

[188] V.R. Meyer, The 1000 bar and 24 hour limits of one-dimensional hplc – graphical representations, Analytical and Bioanalytical Chemistry, 396 (2010) 1633-1640.

[189] V.R. Meyer, How to generate peak capacity in column liquid chromatography: The halasz nomograms revised, Journal of Chromatography A, 1187 (2008) 138-144.

[190] G. Gerhardt, R.N. Adams, Determination of diffusion coefficients by flow injection analysis, Analytical Chemistry, 54 (1982) 2618-2620.

[191] A.J. Matula, P.W. Carr, Separation speed and power in isocratic liquid chromatography: Loss in performance of poppe vs knox-saleem optimization, Analytical Chemistry, 87 (2015) 6578-6583.

[192] H. Gu, E.L. Varner, S.R. Groskreutz, A.C. Michael, S.G. Weber, In vivo monitoring of dopamine by microdialysis with 1 min temporal resolution using online capillary liquid chromatography with electrochemical detection, Analytical Chemistry, 87 (2015) 6088-6094.

[193] S.R. Groskreutz, S.G. Weber, Quantitative evaluation of models for solvent-based, on-column focusing in liquid chromatography, J. Chromatogr. A, 1409 (2015) 116-124.

[194] S.O. Ögren, E. Kuteeva, E. Elvander-Tottie, T. Hökfelt, Neuropeptides in learning and memory processes with focus on galanin, European Journal of Pharmacology, 626 (2010) 9-17.

[195] A.E. Rupert, Y. Ou, M. Sandberg, S.G. Weber, Electroosmotic push-pull perfusion: Description and application to qualitative analysis of the hydrolysis of exogenous galanin in organotypic hippocampal slice cultures, ACS Chem. Neurosci., 4 (2013) 838-848.

[196] H. Xu, Y. Guy, A. Hamsher, G. Shi, M. Sandberg, S.G. Weber, Electroosmotic sampling. Application to determination of ectopeptidase activity in organotypic hippocampal slice cultures, Anal. Chem. (Washington, DC, U. S.), 82 (2010) 6377-6383.

[197] X. Wang, D.R. Stoll, A.P. Schellinger, P.W. Carr, Peak capacity optimization of peptide separations in reversed-phase gradient elution chromatography: Fixed column format, Analytical Chemistry, 78 (2006) 3406-3416.

[198] J.M. Davis, J.C. Giddings, Statistical theory of component overlap in multicomponent chromatograms, Analytical Chemistry, 55 (1983) 418-424.

[199] T. Seki, J. Mochida, M. Okamoto, O. Hosoya, K. Juni, K. Morimoto, Measurement of diffusion coefficients of parabens and steroids in water and 1-octanol, Chemical & Pharamaceutical Bulletin, 51 (2003) 734-736.